1969

Application of fracture mechanics to bridges

R. B. Madison

LEHIGH UNIVERSITY INSTITUTE OF RESEARCH

APPLICATION OF FRACTURE MECHANICS TO BRIDGES

by
Ronald B. Madison

June 1969

Fritz Engineering Laboratory Report No. 335.2

APPLICATION OF FRACTURE MECHANICS TO BRIDGES

by

Ronald B. Madison

Fritz Engineering Laboratory
Department of Civil Engineering
Lehigh University
Bethlehem, Pa.

June 1969

Fritz Engineering Laboratory Report No. 335.2

ACKNOWLEDGMENTS

The research of this dissertation was conducted at Fritz Engineering Laboratory, Lehigh University, under the sponsorship of The Bethlehem Steel Corporation.

The author wishes to gratefully acknowledge the help of Dr. G. R. Irwin, Boeing University Professor, his thesis adviser, who developed the theories upon which this work is based.

Sincere thanks to Dr. J. M. Krafft of the Naval Research Laboratory and member of the author's committee, who helped obtain the dynamic test data used in this work; to Dr. P. C. Paris, former thesis adviser and member of the author's committee, who introduced the author to fracture mechanics; to T. E. Dalby, a friend, whose interest in this work gave the author courage to attempt it; to W. J. Eney, who helped the author arrange the academic program so necessary to accomplish this work; to G. F. Melloy of Homer Research Laboratories and member of the author's committee, who arranged for the rolling of the steel; to J. D. Scott and to others from Homer Research Laboratories who were so helpful; to M. A. Macías Rendón, former graduate student, who made a model study of Kings Bridge; to C. S. Lin, a graduate student, who made a Guyon-Massonnet analysis of Kings Bridge; and to Zung-An Lu, a graduate student, who helped with the calculations.

The guidance of Professors L. S. Beedle, L. Tall, and A. W. Pense, members of the author's Committee, and to D. A. VanHorn, Head of the Department of Civil Engineering, is gratefully acknowledged.

Special thanks go to D. E. Luft, former graduate student, who worked closely with the author in developing the fracture testing program, and to Dorothy Fielding, an extraordinary secretary and typist.

Appreciation is expressed to the staff at Fritz Engineering Laboratory; namely, H. T. Sutherland, Instruments Associate, who helped with the instrumentation; I. J. Taylor, former Instruments Associate, who helped design the test setup; to K. R. Harpel, General Foreman of Fritz Engineering Laboratory and his staff; to John Gera and Sharon Balogh, draftsmen; and to R. N. Sopko, photographer. Special thanks to M. L. Prior of Tektronix, who helped with the instrumentation.

The author wishes to express his sincere appreciation and gratitude to his wife and children for their loving patience and understanding.

TABLE OF CONTENTS

LIST OF TABLES

LIST OF FIGURES

Figures

ABSTRACT

This report presents a simplified fracture control plan for steel bridges based upon the concepts of fracture mechanics.

Fracture mechanics relates the crack tip stress intensity, K, to the nominal tensile stress (assuming no crack) and to the crack length. Fracture occurs when the crack tip stress intensity reaches a critical level, K_c, which is a measure of the fracture toughness of the steel. Plastic deformation at the tip of the crack is accounted for in the computation by adding a plasticity adjustment factor, r_Y, to the crack length.

The fracture control plan requires a knowledge of K_c values and fatigue crack growth rates for structural steels. In addition, the relationship between K and the nominal tensile stress (assuming no crack) must be known for cracked members typical in bridges.

A method is presented for obtaining K_c data for structural steels. Included is a collection of K_c data for a heat of ASTM A441 steel in thicknesses of 1/2 inch, 1 inch, and 2 inch for temperatures from -120^{o} to 80^{o} F and at loading rates from static to those typical of Charpy impact tests. K_c was found to decrease (that is, the material becomes less tough) as thickness increases, as loading rate increases, and as temperature decreases. K_c values could not be obtained

when general yielding occurred across the net section of the specimen. For the specimen tested, this condition occurred when r_Y was greater than 1/4 inch.

A limited amount of fatigue crack growth data is presented for the same steel.

An iterative solution for the three ended crack, typical of a crack which extends through the center of a girder flange and into the web, is presented. The flange and web cracks are treated as separate problems with known solutions. The solution of the three-ended crack is obtained from the compatibility of displacements of the flange and the web cracks.

The technique of applying fracture mechanics to bridges is demonstrated with a fracture analysis of the Kings Bridge, Australia, which failed from brittle fracture on July 11, 1962.

INTRODUCTION

The primary objective of this dissertation is to establish the feasibility of applying fracture mechanics to fracture control in steel bridges. The report is presented in three major parts.

Part I contains a shortened and simplified version of the entire work and includes a simplified fracture control plan for steel bridges. Part I begins with a brief description of the problem of brittle fracture in bridges and a rather concise introduction to fracture mechanics. It concludes by demonstrating the technique of applying fracture mechanics to bridges by summarizing the results of a fracture analysis of the Kings Bridge, Australia, which failed from brittle fracture on July 11, 1962.

Part II contains a review of those theoretical concepts of fracture mechanics that are basic to this work. The chief novelty of Part II is the discussion and analysis of a cracking pattern termed a three-ended crack (a crack which extends through the center of a girder flange and into the web). This is the cracking pattern which initiated the final failure of the Kings Bridge.

Part III presents a study of the crack toughness of A441 steel. The impact methods of crack toughness evaluation employed possess certain advantages over impact toughness measurement procedures which

were developed over the same time period at other laboratories. Part III includes a comparison of the results of fracture tests under impact loading to those under static loading. The results of these fracture tests are compared to the plasticity properties of the material.

Part III is followed by a Summary and Conclusions. Details of the stress analysis and the fracture analysis of Kings Bridge are presented as Appendixes.

I APPLICATION OF FRACTURE MECHANICS TO BRIDGES

1. The Risk of Brittle Fracture in Bridges

Today there is no way for a design engineer to "solve" in a quantitative manner the problem of brittle fracture in a bridge. Using the results of transition temperature testing, he can compare the fracture toughness of one steel to another, but there is no way of relating such relative values to design conditions. There is no way short of actual failure experience to determine whether the use of a more expensive, tougher steel is justified. And fortunately fracture failures of bridges are quite rare.

A method of fracture-safe design was accomplished for ship steels after a series of disastrous fractures during and following World War II. Reduction of local stresses by design improvements and a minimum toughness quality in terms of a V-notch Charpy transition temperature requirement reduced the incidence of ship fractures to a tolerable level. But attempts to generalize the ship steel findings to a wide range of structures and conditions have not been successful, despite widespread efforts to do so.

Furthermore, attempts to predict the fracture behavior of bridges based upon the techniques of transition-temperature testing, as was used for the ship steels, result in answers that are much too conservative and therefore not consistent with experience.

It is not surprising that bridge designers have relied quite heavily on their favorable experience with regard to fracture. There have been very few brittle fractures in bridges, and these have been clearly associated with combinations of poor steel, poor fabrication, and poor design.

Nevertheless, a latent fear of brittle fracture prevents many bridge designers from taking full advantage of the improvements that are taking place with respect to design methods, ferrous metallurgy, and fabrication techniques. Is this latent fear justified?

The answer is a simple "no" for structures similar to those that have served so well in the past, and where the steel used is similar to that used in the past. Here the proof is in the service record. Indeed, the service record being generated for the 50,000 psi yield steels indicates that these steels too can be used with confidence in bridges.

But when the designer departs from standard designs and steels, when he begins to think of taking that bold step forward, the possibility of brittle fracture must be estimated in advance without the assistance of prior experience. Therefore he will rely substantially on such understanding as current fracture theory is able to provide.

Any theory which purports to assist the bridge designer must offer the following:

1. It must explain why past fracture failures of bridges have been so rare.

2. It must provide a reasonable means of estimating the risk of brittle fracture.
3. It must indicate possible alternatives in design when the risk of brittle fracture is significant.

The following pages present an approach to the understanding and control of brittle fracture in steel bridge structures. It is an approach based upon fracture mechanics. The method is simple in terms of concept. However, there is much to be learned and a great deal of work to be done before fracture mechanics becomes a conventional bridge design tool.

2. Introduction to Fracture Mechanics

Consider a body with a crack, as in Fig. 1, and designate an element close to the leading edge of this crack by the polar coordinates r and θ. A complex variable method of stress analysis was used by Irwin to solve this problem[1,2] and results in the following equations for stress:

$$\sigma_y = \frac{K}{\sqrt{2\pi r}} \cos\frac{\theta}{2}\left(1 + \sin\frac{\theta}{2}\sin\frac{3\theta}{2}\right) \qquad (1.a)$$

$$\sigma_x = \frac{K}{\sqrt{2\pi r}} \cos\frac{\theta}{2}\left(1 - \sin\frac{\theta}{2}\sin\frac{3\theta}{2}\right. \qquad (1.b)$$

$$\tau_{xy} = \frac{K}{\sqrt{2\pi r}} \sin\frac{\theta}{2}\cos\frac{\theta}{2}\cos\frac{3\theta}{2} \qquad (1.c)$$

$$\sigma_z = 0 \quad \text{for plane stress}$$
$$\sigma_z = \nu(\sigma_x + \sigma_y) \quad \text{for plane strain} \qquad (1.d)$$

The stress at any point near the tip of the crack is dependent only upon the polar coordinates of the point and upon the constant K, termed the stress-intensity factor. K is really a one-parameter measure of the tensile stress near the leading edge of a crack. Of particular interest is the tensile stress in the y-direction for points on the x-axis immediately in front of the crack. With θ equal to zero in Eq. 1.a the expression for σ_y becomes

$$\sigma_y = \frac{K}{\sqrt{2\pi r}} \qquad (2)$$

Given any valid stress analysis solution for σ_y, the value of K can be determined from Eq. 2. Although the stress analysis of a cracked body is difficult, solutions to a great many two-dimensional crack problems have been accomplished and are available.[3]

The simplest and best known solution of a crack problem is the case of an infinite plate subjected to an in-plane uniform stress perpendicular to a through crack of length $2a$, see Fig. 2. The solution is

$$K = \sigma \sqrt{\pi a} \qquad (3)$$

Note that the stress-intensity factor K is proportional to the uniform stress σ some distance from and normal to the crack, and to the square root of the crack length a. The customary units for stress-intensity K are ksi $\sqrt{\text{in}}$.

When the stress-intensity factor reaches a certain limiting value for a given material, the crack becomes unstable and fracture

takes place.[1,4] This limiting value of K is termed the critical stress-intensity factor K_c.

To help clarify the phenomenon of fracture instability, it is helpful to review the more familiar phenomenon of column instability, see Fig. 3a. It is well-known that for a slender column under axial load, the compressive stress at column instability for large values of L/r can be derived from the equation suggested by Leonard Euler in 1744. However, as the L/r ratio of a column is reduced, the column strength falls increasingly below the value predicted by the Euler equation and plastic analysis must be introduced to explain the results. The strength finally approaches the yield strength as a limit, as illustrated by the column strength curve of the Column Research Council[5] (Fig. 3a).

Crack instability can be understood in a manner similar to column instability. Figure 3b is a plot of nominal fracture stress versus crack length for a finite-width plate with a center crack. The tensile stress at crack instability for a large crack length can be derived from Eq. 3 assuming K has a constant value, K_c. However, if the crack size is small a condition of yielding occurs near the crack prior to instability and the elastic equations are inaccurate. Design curves for relatively small crack sizes must include an adjustment for the plasticity at the tip of the crack. The actual strength in the limit of small enough crack size is determined by a plastic instability. Thus the "crack strength" shown in Fig. 3b follows the same pattern as the column strength shown in Fig. 3a.

In most applications of structural interest there is plasticity at the tip of the crack. This plasticity can be included in the elastic fracture mechanics equations in a relatively simple manner, as proposed by Irwin.[6] The method consists of approximating the area of plastic deformation at the tip of the crack as a circle of radius r_Y, as shown in Fig. 4. The linear elastic stress equations, Eq. 1, are an approximation of the stress state for the crack of Fig. 4 if the center of the plastic zone is considered to be the effective leading edge of the crack. This is equivalent to taking the effective length of the crack as $(a + r_Y)$. Tests have indicated that whatever the actual shape of the plastic zone, so long as it is not too large, its influence is well represented by this plastic zone assumption.[7]

In order to apply the r_Y correction to the crack length, one must be able to determine the size of r_Y. This turns out to be a fairly simple task. r_Y can be found from the basic equations of fracture mechanics, and it takes the form

$$r_Y = \frac{1}{2\pi} \left(\frac{K}{\sigma_{YS}} \right)^2 \qquad (5)$$

where σ_{YS} is the yield stress of the material at the temperature and loading rate of interest.

If Eq. 3 is solved for σ using the plasticity adjustment and a generalizing function C, the equation for the nominal critical stress becomes

$$\sigma_c = \frac{K_c}{C\sqrt{\pi(a + r_Y)}} \qquad (6)$$

Whether or not the nominal critical stress σ_c reaches the yield stress prior to instability in a cracked plate depends upon the value of the critical stress intensity factor K_c, the crack length a, and the size of the plasticity adjustment r_Y.

The function C in Eq. 6 is an adjustment factor which is dependent upon the geometry of the cracked structural member. For example, in the finite-width plate shown in Fig. 5, C is a function of the effective crack length $(a + r_Y)$ and the plate width W.

$$K = C \sigma \sqrt{\pi(a + r_Y)} \tag{7}$$

where

$$C^2 = \sec \frac{\pi(a + r_Y)}{W}$$

In reading the following material dealing with fracture mechanics, the reader should remember the following concepts:

K - The Stress-Intensity Factor:
K is geometry dependent. It is a measure of the tensile stress near the tip of a crack. Values of K are determined from stress analysis.

K_c - The Critical Stress-Intensity Factor:
K_c is material dependent. It is a measure of fracture toughness. When K reaches K_c fracture occurs. Values of K_c are determined from fracture tests.

r_Y - The Plasticity Adjustment Factor:
r_Y is dependent upon the level of K and upon the yield strength of the material. It is

a correction in the length of the crack to account for the plastic deformation near the tip of the crack.

3. Fracture Mechanics as an Aid in Bridge Design

Relative to fracture control in steel bridges, a suitable version of the procedure suggested by Irwin and Kies in 1954* consists of four steps as follows

#1 - Determine the critical crack length, a_c.

#2 - Determine the tolerable flaw size, a_T.

#3 - Compare a_T to the flaw size that can be detected.

#4 - Re-design if necessary.

These are accomplished in the following manner.

Step #1 - Determine the critical crack length a_c:

The critical crack length is dependent upon the geometry of the structural member, the nominal stress level, and the fracture toughness of the material. The procedure for determining a_c consists of the following five steps:

a. Determine K_c: K_c is determined from fracture tests of the material under the most severe conditions of temperature and loading rate expected.

*G. R. Irwin and J. S. Kies (1954) Welding Journal, Res. Suppl., Vol. 33, p. 193S

b. Determine σ: The nominal stress σ is determined from stress analysis.

c. Solve for $(a + r_Y)$: The effective crack length $(a + r_Y)$ is found from an expression or a combination of expressions which adequately describes the stress intensity factor at the tip of a crack for the structural member of interest, an expression such as Eq. 7.

$$K_c = C \sigma \sqrt{\pi (a + r_Y)}$$

d. Determine r_Y: The plasticity adjustment factor r_Y is found from Eq. 5:

$$r_Y = \frac{1}{2\pi} \left(\frac{K_c}{\sigma_{YS}}\right)^2$$

A value consistent with the most severe temperature and loading rate expected in the structural member should be used for σ_{YS}.

e. Determine the critical crack length a_c: The critical crack length a_c is simply the effective critical crack length less the radius of the plastic zone:

$$a_c = (a + r_Y) - r_Y \qquad (8)$$

Step #2 - Determine the tolerable flaw size, a_T:

It is well-known that cracks grow under fatigue loading. This growth must be accounted for in the analysis.

a. Predict the total stable crack growth Δa: For medium and low strength steels in fatigue, an

empirical equation suggested for crack growth rate is (see Fig. 34 and Refs. 8,9, 10)

$$\frac{da}{dN} = 2.0 \times 10^{-12} (\Delta K)^4 \qquad (9)$$

where $\frac{da}{dN}$ is the crack growth in inches per cycle of load and ΔK (in ksi $\sqrt{in.}$) is the difference between the maximum and the minimum K resulting from the fluctuation of load. The total crack growth, when Δa is small compared to a_c, can be estimated from

$$\Delta a = N\left(\frac{da}{dN}\right)_{ave.} \qquad (10)$$

where N is the number of cycles expected in the life of the structure, or between inspection periods. When Δa is comparable to or larger than a_c, use can be made of the equation

$$N = \int_{a_c - \Delta a}^{a_c} da / \left(\frac{da}{dN}\right)$$

where $\frac{da}{dN}$ is given by Eq. 9.

b. Determine the tolerable flaw size a_T: The tolerable flaw size is the difference between the critical crack length and the expected total stable crack growth

$$a_T = a_c - \Delta a \qquad (11)$$

a_T represents the maximum size flaw that can be safely allowed to pass at the time the member is inspected.

Step #3 - Compare a_T to the flaw size that can be detected:

The tolerable flaw size a_T must be compared to the flaw size that can be effectively revealed by the inspection methods to be used, such as visual, magnaflux, sonic, x-ray, or any other. In effect, the tolerable flaw size determines the type of inspection required.

Step #4 - Redesign if necessary:

If the tolerable flaw size is so small that a significant risk of brittle fracture exists, the structure should be made sufficiently redundant to survive fracture of the member under consideration. If the structure is not sufficiently redundant to survive such a fracture or if the subsequent life after such a fracture is not sufficient to allow necessary repairs, then a redesign is needed. In either case, fracture mechanics analysis methods are helpful. For example, consider Eq. 3

$$K = \sigma \sqrt{\pi a}$$

Suppose that for a given σ and for the size of flaw that can be effectively detected, K is larger than K_c. To eliminate the risk of fracture a tougher steel might be selected having a K_c enough greater than K so that the possible development of a crack large enough for fracture could be regarded as a negligible risk. Alternately the stress level σ might be decreased.

Thus fracture mechanics can be used to relate material toughness to stress level and to inspection requirements. Furthermore, one can note that avoidance of fracture requires coordinated planning by the metallurgist, designer, fabricator, and inspector.

4. Effects of Thickness, Temperarure, Loading Rate on K_c

K_c was defined in Section 2 as the critical value of the stress-intensity factor: when K increases to K_c, fracture occurs.

K_c is a material property, just as yield strength is a material property. K_c depends upon such factors as thickness, temperature, and loading rate just as yield strength does. However, the variation of K_c with these factors is far more complex than is the variation of yield strength. It is sufficient for most bridge design purposes to use a value for the yield strength as determined from simple, slow, room temperature tests of small samples. But simple, slow, room temperature K_c tests of small samples are inadequate for bridge steels, as will become evident from the following discussion.

Figure 6 shows schematically the variation of K_c with thickness.[11] K_c is theoretically zero for zero thickness, but it quickly increases to a maximum for relatively thin plates, then drops off to a constant, minimum value characteristic of thick material. The value of K_c for thick plates is called K_{Ic} and has a

significant meaning: K_{Ic} is the smallest value of K_c that can be obtained as a result of thickness variation, ignoring of course the case of near zero thickness.

Figure 60 indicates the effect on K_c of both thickness and temperature for an ASTM A441 plate tested at Lehigh. Note that as thickness increases for a given temperature or as temperature decreases for a given thickness, the value of K_c decreases. Toughness decreases as thickness increases or as temperature decreases; a well-known fact for structural steels.

Figure 7 shows schematically how K_c varies with loading rate for structural steels.[12] $\dot{K}$, the rate of change of K with time, provides a convenient means of expressing loading rate for this purpose. The diagram shows $\dot{K}$ on a log plot and covers some eight orders of magnitude of loading rate. Rates comparable to static loading are shown at the far left; rates comparable to Charpy tests, near the center; and rates that are developed at the tips of fast moving cracks, at the far right. Note that as the loading rate is increased, K_c decreases and reaches a minimum value at a loading rate comparable to Charpy tests or to slow moving cracks. The value of K_c rises very rapidly when crack velocity becomes quite fast.

If a real structure is loaded at a slow loading rate, as shown by the dotted line in Fig. 7, the crack will run quite suddenly when K reaches K_c and will quickly reach a crack velocity that is in equilibrium with that same value for K for rapid

fracturing. The crack speed thus established may be over 1000 feet per second.

Because of rate sensitivity, the collection of K_c data for bridge steels is difficult. To obtain loading rates comparable to Charpy tests in large structures, a testing machine was built at Lehigh (see Fig. 8). The testing device provides an accurately aligned and instrumented falling weight as well as appropriate supports for mounting test specimens.[13] Tests made with this machine are termed "Lehigh Impact Tests".

The specimen, shown in Fig. 9, consists of a bar 3 inches deep, 12 inches long, and the full thickness of the plate to be tested. It contains a fatigue crack and is loaded in three-point bending by a striking tup mounted in the weight and instrumented to read the applied load.[13]

The results of the Lehigh Impact Tests on an A441 steel are shown in Fig. 62. These impact values of K_c are less than the static values shown in Fig. 60.

Figure 39 shows the effect of loading rate on K_{Ic} for a one inch thick A441 steel plate tested at minus 40° F. Note that $\dot{K}$ is plotted on a log scale. The plot covers the range from static tests on the left to rates comparable to Charpy loading on the right.

The fastest loading rate that we have seen reported for the bottom flange of a steel girder is equivalent to a $\dot{K}$ of about 75 ksi $\sqrt{\text{in}}$ per second (see Section 14, Part II). This is twice the rate at which the so-called "static tests" were run at Lehigh. Although

there is more scatter at the higher loading rates, the data of Fig. 39 indicates that the value of K_{Ic} for loading rates as high as $\dot{K}$ = 1000 ksi $\sqrt{in}$ sec^{-1} is substantially the same as for a true static with a loading rate of say $\dot{K}$ = 1 ksi $\sqrt{in}$ sec^{-1}.

It would seem that so far as fracture is concerned, the fastest loading rates in a bridge may be no worse than static loading rates. Such rates are smaller than the loading rates typical of Charpy or drop weight tests by a factor of 10^3. If it could be shown that potential bridge fractures will not occur under loading rate conditions comparable to impact tests, the collection of K_c data for bridge steels would be greatly simplified.

5. The Kings Bridge Failure

In the previous section K_c was shown to vary in a rather complicated but predictable manner with thickness, temperature, and loading rate. It would be interesting at this point to indicate how fracture mechanics can help to understand the part that these factors played in a specific case, such as the Kings Bridge, which failed in 1962 from a brittle fracture.

Kings Brige was the longest bridge in Melbourne, Australia: 2290 foot long elevated four lane freeway, which carried 45,000 vehicles daily for fifteen months. Then on July 11, 1962, a rather cold winter morning for Melbourne with a temperature of 40^o Fahrenheit, a truck hauling a mechanical shovel crossed the bridge. The driver of the truck described what happened.[14]

> "I had traveled about 50 yards onto the city side of the bridge when I felt something--I thought the load had shifted. Then I heard a loud noise. I stopped, saw a dip in the bridge, then jumped back in the truck and kept going. I thought the whole thing might collapse."

The failed span of Kings Bridge consisted of a four girder bridge carrying two lanes of a dual highway, see Fig. 10. One of the four girders, the left center girder, was cracked to within a few inches of the top flange long before the day the bridge collapsed. Collapse occurred when the remaining three girders broke. Fortunately, concrete sidewalls beneath the failed span caught the bridge deck and prevented complete collapse when the bridge had fallen only 18 inches.

All of the girder fractures initiated at existing cracks at the ends of the cover plates.

A team of experts assigned to the task of determining cause of the failure found that the first fracture of these girders took place while the girders were still in the shop.[15]

Subsequent welding tests[16] of the Kings Bridge girder flange have shown that the combined effects of poor detail design, poor weldability of the steel, and poor welding procedure, including the failure to properly dry low-hydrogen electrodes, resulted in the formation of shrinkage cracks at the toe of the transverse weld at the ends of the cover plates. Granting that the probability of all those factors occurring at the same time is very small, it is not zero. Such cracks can be expected to occur occasionally.

In the Kings Bridge, shrinkage cracks occurred in over half of the hundred or more girders fabricated for the bridge. Although most of these cracks were about 1/8 inch deep by three inches long, three in the failed span developed into 5 inch cracks that penetrated the flange, see Fig. 11.

Girder W14-2 failed during the first winter the bridge was opened to traffic, but the failure was not detected. The crack in Girder W14-3 extended a slight amount at the time of this failure, but did not become unstable as did the crack in W14-2. W14-3 held, and the bridge showed no outward signs of distress.

During the following twelve months, the web crack in Girder W14-3 grew from fatigue until, during the second winter, the disastrous combination of crack length, temperature, and load was met.

On July 11, 1962, the crack in Girder W14-3 became unstable, the girder suffered a brittle fracture, and the bridge failed, with the remaining two girders also failing in a brittle manner. Only the top flange of Girder W14-4 remained intact.

Results of Charpy tests for the girder flange steel[15] are shown in Fig. 12, as well as the results of Charpy tests for the A441 steel tested at Lehigh. K_c data is not available for the Kings Bridge girder steel. However, V-notch Charpy data is available. A comparison of the steels using Charpy data provides a convenient method of estimating K_c for the Kings Bridge girder steel. According to this comparison, the steel in the Kings Bridge girder flange, which was

3/4 inch thick, had a fracture toughness midway between that of the 1 inch and the 2 inch A441 plate tested at Lehigh.

A stress analysis of the girder (see Appendix A) indicates that at the time of fracture, the total stress in the flange of girder W14-3 from bending was only 20 ksi, see Fig. 13.

A fracture analysis of Girder W14-3 (see Section 15, Part II) indicates that the K value at fracture was probably between 67 ksi $\sqrt{in}$ and 98 ksi $\sqrt{in}$ depending upon the level of the residual stress in the girder flange at the time of fracture, and depending upon whether fracture initiated from a static, high level of K_c or an impact, low level of K_c.

Comparing these values with the static and impact fracture data of Figs. 60 and 62 indicates that fracture probably initiated in an impact mode under the influence of the residual stresses introduced in the girder during welding. This is discussed in more detail in Section 15, Part II.

From the Kings Bridge fracture failure several conclusions can be noted at this point. The advantage of conservative design and redundant load paths is quite evident. The loss from fracture of one of the four girders did not prevent one year of additional use of the bridge. With regard to whether the resistance to fracture should be estimated on the basis of static or rapid-load K_c values, calculations (discussed later in detail) indicate that the most probable relationship between K_c, flaw size, and stresses for the

final instability corresponds to a rapid-load rather than a static value of K_c. This is not unexpected since material cracks tend to be rough in contour and to extend in abrupt increments. An abrupt local extension of substantial size might provide the required element of high strain rate loading. In this way we conclude that a relationship of the customary fracture mechanics type between loads, crack size, and fracture toughness can be assumed to have been applicable to the Kings Bridge fracture failure.

II FRACTURE MECHANICS CONCEPTS

1. The Three Modes of Fracture

So far in this report fracture has been referred to as though it occurs in only one mode, the tensile opening mode. There are, however, three possible modes of fracture.

The most common mode of fracture is the tensile opening mode shown in Fig. 1 and in Fig. 14a. In this mode the crack is positioned transverse to a tensile stress which causes the crack to open in the direction of the stress. The crack propagates in a direction perpendicular to the stress. The stress equations for this mode of fracture, which is called Mode I fracture are given by Eqs. 1a to 1d of Section I and are repeated here for easy reference.

$$\sigma_x = \frac{K_I}{\sqrt{2\pi r}} \cos\frac{\theta}{2}\left[1 - \sin\frac{\theta}{2}\sin\frac{3\theta}{2}\right]$$

$$\sigma_y = \frac{K_I}{\sqrt{2\pi r}} \cos\frac{\theta}{2}\left[1 + \sin\frac{\theta}{2}\sin\frac{3\theta}{2}\right]$$

$$\tau_{xy} = \frac{K_I}{\sqrt{2\pi r}} \sin\frac{\theta}{2}\cos\frac{\theta}{2}\cos\frac{3\theta}{2}$$

$$\sigma_z = \nu(\sigma_x + \sigma_y) \quad \text{for plane stress}$$

$$\sigma_z = 0 \quad \text{for plane strain}$$

If the crack is subjected to shear stresses parallel to the plane of the plate, it will have a tendency to open in the manner shown in Fig. 14b. The equations for this mode of Fracture, Mode II fracture, are given by[3]

$$\sigma_x = -\frac{K_{II}}{\sqrt{2\pi r}} \sin\frac{\theta}{2}\left[2 + \cos\frac{\theta}{2}\cos\frac{3\theta}{2}\right]$$

$$\sigma_y = \frac{K_{II}}{\sqrt{2\pi r}} \sin\frac{\theta}{2}\cos\frac{\theta}{2}\cos\frac{3\theta}{2}$$

$$\tau_{xy} = \frac{K_{II}}{\sqrt{2\pi r}} \cos\frac{\theta}{2}\left[1 - \sin\frac{\theta}{2}\sin\frac{3\theta}{2}\right] \qquad (12)$$

$$\sigma_z = \nu(\sigma_x + \sigma_y) \quad \text{for plane strain}$$

$$\sigma_z = 0 \quad \text{for plane stress}$$

If the crack is subject to shear stress perpendicular to the plate, the crack will open in the manner shown in Fig. 14c. Equations for this mode of fracture, Mode III fracture, are given by[3]

$$\tau_{xz} = \frac{K_{III}}{\sqrt{2\pi r}} \sin\frac{\theta}{2}$$

$$\tau_{yz} = \frac{K_{III}}{\sqrt{2\pi r}} \cos\frac{\theta}{2} \qquad (13)$$

$$\sigma_x = \sigma_y = \sigma_z = \tau_{xy} = 0$$

Since real fractures are rough and irregular on a fine scale, they could be regarded as corresponding to combinations of the three

fracture modes. However, the linear-elastic analysis model ignores details smaller in size than the plastic zone. Thus a Mode I analysis is used whenever the crack is normal to the principal tension.

For bridges, transverse cracks in the tensile flange of a girder are of primary importance. For this situation the first mode predominates and the effect of the other two modes can be neglected.

This report is concerned only with the first or tensile fracture mode.

2. Plane Stress Versus Plane Strain

At the present time no methods are available for handling the general three-eimensional case of a crack in a body. The equations given in the preceding sections were based on one of two assumptions:

> Assumption of Plane Stress - The plate is infinitely thin so that no stress can be developed in the thickness direction. This assumption reduces the three-dimensional crack problem to a two-dimensional problem in terms of the two principal stresses. The third principal stress, the one in the thickness direction, is zero.
>
> Assumption of Plane Strain - The plate is infinitely thick so that no strain can be developed in the thickness direction. This assumption reduces the three-dimensional crack problem to a two-dimensional problem in terms of the two principal strains. The third principal strain, the one in the thickness direction, is zero.

The equations for the stresses (see Eq. 1) are the same for plane stress and plane strain, except for the value of σ_z. The expressions for K are identical in form. For example, for a through crack in an infinite plate:

$$K = \sigma \sqrt{\pi a}$$

for both plane stress and plane strain.

The only three-dimensional solution available for a crack is Sneddon and Green's solution[19] for a flat elliptical crack in an infinite body subjected to uniform tension (see Fig. 15) which can be presented in the form:[3]

$$K_I = \frac{\sigma\sqrt{\pi a}}{\Phi_o} \left(\sin^2 \beta + \frac{a^2}{b^2} \cos^2 \beta\right)^{1/4}$$

where Φ_o is the complete elliptical integral

$$\Phi_o = \int_o^{\pi/2} \left[1 - \left(\frac{b^2 - a^2}{b^2}\right) \sin^2 \theta\right]^{1/2} d\theta$$

the value of which can be found in mathematical tables.*

This three-dimensional solution reduces to a two-dimensional form only for an infinitely small region near the leading edge of the crack where the stress equations correspond to plane-strain. This is the same leading edge region for which Eqs. 1 are considered to be applicable.

---

* β is the phase angle for the customary parametric form of the Cartesian coordinates of an ellipse.

Two methods of analysis of crack problems are available:

Generalized Plane Stress assumes that the stress-strain state on the average through the thickness of the plate corresponds to plane stress. This assumption is used for the solution of many crack problems. It is used, for instance, for K_c and K_{Ic} measurements from laboratory tests using through-the-thickness cracks. As a result the value of K_c and K_{Ic} found corresponds to an averaging of the stress state across the crack front.

Plane Strain is applicable only with reference to a region near the crack tip which is small relative to the section thickness and thus requires a correspondingly small plastic zone.

Whatever assumption is made for an analysis, plane stress or plane strain, it is important that the assumption be carried through consistently. It makes little sense, for instance, to assume a plane stress analysis and then use a plastic zone correction based upon plane strain, even though the specimen may be thick enough to result in a valid K_{Ic} test. It is customary for thick plates, where K_c is at the low level indicated in Fig. 6, to refer to K_c as the plane strain value K_{Ic} even though the specimen is analyzed using a plane stress assumption.

3. Derivation of the Fracture Mechanics Equations

In order that the reader have some idea of how the equations of fracture mechanics were developed, the following is a rather brief outline of the derivation.

The derivation of the fracture mechanics equations begins with the equations of equilibrium for elastic isotropic solids:

$$\frac{\partial \sigma_x}{\partial x} + \frac{\partial \tau_{xy}}{\partial y} = 0$$

$$\frac{\partial \tau_{yx}}{\partial x} + \frac{\partial \sigma_y}{\partial y} = 0 \qquad (16)$$

$$\tau_{xy} = \tau_{yx}$$

These are satisfied by the following expressions for the stress:

$$\sigma_x = \frac{\partial^2 F}{\partial y^2}$$

$$\sigma_y = \frac{\partial^2 F}{\partial x^2} \qquad (17)$$

$$\tau_{xy} = -\frac{\partial^2 F}{\partial x \, \partial y}$$

where the function F is called the Airy stress function.

For strain compatibility:

$$\frac{\partial^2 \epsilon_x}{\partial y^2} + \frac{\partial^2 \epsilon_y}{\partial x^2} = \frac{\partial^2 \gamma_{xy}}{\partial x \, \partial y} \tag{18}$$

From Hook's Law for plane stress:

$$\epsilon_x = \frac{1}{E} [\sigma_x - \nu \sigma_y]$$

$$\epsilon_y = \frac{1}{E} [\sigma_y - \nu \sigma_x] \tag{19}$$

Equations 16, 18, and 19 are basic to the theory of elasticity; their derivations can be found in any elementary test of that subject.

When Eq. 17 is substituted into Eq. 19 and then into Eq. 18, the following expression, which is called Airy's equation, is found to be a solution to the problem:

$$\nabla^2 (\nabla^2 F) = 0 \tag{20}$$

where

$$\nabla^2 = (\frac{\partial^2}{\partial x} + \frac{\partial^2}{\partial y})$$

Any function F which satisfies Eq. 20 will also satisfy the equations of stress equilibrium and the requirement of strain compatibility as well as Hooke's Law. To solve a specific problem, the trick is to find a function F that satisfies Eq. 20 as well as the boundary conditions of the problem.

Westergaard showed that when the external loads are placed symmetrically relative to the x-axis, along which a crack is located, (see Fig. 16) a number of crack problems can be solved by assuming

$$F = \text{Re } \bar{\bar{Z}} + y \text{ Im } \bar{Z} \tag{21}$$

where Z is a function of a complex variable z; the integral of Z is $\bar{Z}$; and the integral of $\bar{Z}$ is $\bar{\bar{Z}}$.

Using Eq. 21 for F, the stresses are (from Eq. 17):

$$\begin{aligned} \sigma_x &= \text{Re } Z - y \text{ Im } Z' \\ \sigma_y &= \text{Re } Z + r \text{ Im } Z' \\ \tau_{xy} &= -y \text{ Re } Z' \qquad \text{for } y \neq 0 \\ \tau_{xy} &= 0 \qquad \text{for } y = 0 \end{aligned} \tag{22}$$

where Z' is the derivative of Z.

If a function Z can be found such that σ_x, σ_y, and τ_{xy} from Eqs. 22 satisfy the boundary conditions of the problem, then Z is a solution to the problem because the conditions of equilibrium and compatability within the body will be automatically satisfied from Eq. 20.

By proper choice of the function Z, Westergaard was able to develop solutions for a variety of situations. For example, for a central crack of length $2a$ along the x-axis in an infinite plate with a tension σ at a large distance from the crack (see Fig. 16),

Westergaard found the following expression for Z:

$$Z = \frac{\sigma}{[1 + (\frac{a}{z})^2]^{1/2}} \tag{23}$$

where z is the complex variable x + iy; and x and y are the rectilinear coordinates of the point.

The complex coordinate z is measured from the center of the symmetric crack. Irwin[20] replaced z with $a + z_1$, where a is the half-length of the crack and z_1 is the complex coordinate measured from the tip of the crack (see Fig. 16). When this is done and the limit is taken as z_1 approaches zero, the Z functions representing various crack solutions, such as Eq. 23, take the following form:

$$\lim_{z_1 \to 0} (Z) = \frac{K}{\sqrt{2\pi z_1}} \tag{24}$$

In other words, the function for the stresses near the tip of a crack is:

$$Z = \frac{K}{\sqrt{2\pi z_1}} \tag{25}$$

The constant K in this expression is termed the "stress-intensity factor".

Once the function Z for the stresses near the tip of the crack is known, it is a relatively simple matter to determine the crack tip stress field. Substituting Eq. 25 into Eq. 22 and using an

equivalent expression ($z_1 = re^{i\theta}$) for the complex variable z_1, results in Eqs. 1.

In the same paper[20] a relationship is developed between the stress-intensity factor K and the strain energy release rate $\mathcal{G}$ proposed by Griffith in 1920.[22] For plane stress:

$$\mathcal{G} = \frac{K^2}{E} \tag{26}$$

The general proof of Eq. 26 is not simple and will not be included here. By considering the specific example of the crack of Fig. 16 and Eq. 23, Eq. 26 can be shown to be valid using a method suggested by Paris (Mech.413 Lectures).

The strain in the y-direction is, from basic theory of elasticity:

$$\epsilon_y = \frac{\sigma_y}{E} - \frac{\nu}{E}(\sigma_x + \sigma_z) \tag{27}$$

Substituting Eqs. 22 into 27, setting $\sigma_z = 0$, and integrating yields the y-direction displacements near the tip of the crack for plane stress:

$$v = \frac{2}{E} \operatorname{Im} \bar{Z} - \frac{1+\nu}{E} y \operatorname{Re} Z \tag{28}$$

where v is the displacement in the y-direction.

Substituting Eq. 23 into Eq. 28 for y = 0, the elastic shape of the crack of Fig. 16 is given by

$$v = \frac{2}{E} \sigma \sqrt{a^2 - x^2} \tag{29}$$

which is the equation of an ellipse with large semi-axis a and small semi-axis $2a\ \sigma/E$. The area of the crack opening is the area of the ellipse:

$$\pi(a)\ (\frac{2\ a\ \sigma}{E}) = \frac{2\pi\ a^2\ \sigma}{E}$$

If a stress of $\sigma_y = \sigma$ is applied to the surface of the crack of Fig. 16, the crack will close and the energy required to close the crack will be equal to the strain energy released when the crack formed. If the σ_y stress on the crack surface is zero, the crack opening displacement is v; if the σ_y stress is σ, the crack opening displacement is zero. The work required to close each element of the crack surface is then

$$dW = \frac{1}{2} \sigma\ v\ dx$$

and the total work required to close the crack is

$$W = 4 \int_0^a \frac{1}{2} \sigma\ v\ dx$$

$$= \frac{1}{2} \sigma \times \text{area of the crack opening}$$

$$= \frac{\pi\ a^2\ \sigma^2}{E}$$

The closure work per unit area of the crack surface is:

$$\frac{\partial W}{\partial(2a)} = \frac{\sigma^2 \pi a}{E}$$

and therefore is equal to K^2/E. Since the work required to close the crack is equal to the strain energy released when the crack formed:

$$\mathcal{G} = \frac{K^2}{E}.$$

4. Derivation of the Plasticity Adjustment Factor, r_Y

The plasticity adjustment factor r_Y is a useful tool in treating crack problems in which the plasticity at the tip of the crack is not negligible. All of the data presented in this report includes an r_Y adjustment to the crack length.

The concept assumes a circular configuration to the plastic zone, as shown in Fig. 4. The radius of this zone is taken as r_Y and the diameter as $2r_Y$. The origin of the coordinate axes is placed at the center of the plastic zone, so that the effective crack length is $(a + r_Y)$. The elastic stress distribution in front of the crack along the y-axis is shown in Fig. 17. σ_y for a point at the forward edge of the plastic zone on the y-axis is, from Eq. 1a:

$$\sigma_{ys} = \frac{K}{\sqrt{2\pi\, r_Y}}$$

Solving for r_Y:

$$r_Y = \frac{1}{2\pi} \left(\frac{K}{\sigma_{ys}}\right)^2$$

If the plastic zone correction is valid, then area I of Fig. 16, which represents the load-carrying capacity lost across the section because of yielding, should be equal to area II, which represents the additional load-carrying capacity provide by the yielded material between the crack front and the stress singularity.

The load represented by the area under the elastic curve from the origin to the forward edge of the plastic zone is:

$$\int_0^{r_Y} \sigma_y \, ds = \int_0^{r_Y} \frac{K}{\sqrt{2\pi\, r}} \, ds = \frac{K}{\pi}\sqrt{2\pi\, r_Y}$$

Substituting K in the above equation from Eq. 5

$$\int_0^{r_Y} \sigma_y \, ds = 2\, r_Y\, \sigma_{YS}$$

The load represented by area I is

$$2r_Y\, \sigma_{YS} - r_Y\, \sigma_{YS} = r_Y\, \sigma_{YS}$$

The load represented by area II is, of course, $r_Y\, \sigma_{YS}$, which is the same as the load represented by area I. This strength of materials viewpoint was first suggested in short course lectures by A. A. Wells.

It is known, of course, that the plastic zone in front of the crack is not a circle.[6] However, the r_Y adjustment to the crack length, although a simple estimate for a difficult elasto-plastic problem, is a successful approximation. The adjustment has been found to eliminate a trend in $\mathcal{G}_c$ values which otherwise occurs as the stress approaches general yield conditions.[7]

5. General Yielding of a Beam Specimen

General yielding of a beam specimen is not so readily defined as it is for a tensile specimen. For simple tensile loading, general yielding occurs when the nominal stress across the net section, $w - 2a$ of Fig. 5, is equal to the yield stress. Rewriting Eq. 7 in the form:

$$K^2 = \sigma^2 \, \pi(a + r_Y) \, \sec \frac{\pi(a + r_Y)}{W}$$

and using Eq. 5 for r_Y, leads to:

$$r_Y = \frac{1}{2}\left(\frac{\sigma}{\sigma_{YS}}\right)^2 (a + r_Y) \, \sec \frac{\pi(a + r_Y)}{W} \qquad (30)$$

If there is general yielding across the net section of a tensile specimen having a crack length of one-fourth of the width of the plate, then

$$\frac{2a}{W} = \frac{1}{4}$$

$$\sigma = \frac{3}{4} \sigma_{YS}$$

Solving Eq. 30 for this general yield condition results in a ratio of the plastic zone size to the net section of:

$$\frac{2\ r_Y}{W-2a} = 0.345$$

If the same computation is made for a tensile specimen having a crack length of one-third the width of the plate, the following results:

$$\frac{2a}{W} = \frac{1}{3}$$

$$\sigma = \frac{2}{2}\ \sigma_{YS}$$

$$\frac{2\ r_Y}{W-2a} = 0.433.$$

If the computation is made for a tensile specimen having a crack length of one-half the width of the plate

$$\frac{2a}{W} = \frac{1}{2}$$

$$\sigma = \frac{1}{2}\ \sigma_{YS}$$

$$\frac{2\ r_Y}{W-2a} = 0.663$$

Thus in a tensile specimen, the nominal plastic zone will exceed 40 percent of the net section for general yielding when

$$\frac{2a}{W} = \geq \frac{1}{3}.$$

In a bend specimen with a crack length of $a/W = 1/3$ (which corresponds to $2a/W = 1/3$ for the tensile specimen), one would expect general yielding to occur when $2r_Y/(W - a)$ is in the range of 0.2 to 0.43 (probably closer to 0.2 because half of the specimen is in compression). Examination of the computations of K for bend specimens with $a/W = 1/3$ shows that the computation tends to diverge and become indeterminant when $2r_Y/(W - a)$ is larger than 0.25. It seems therefore reasonable to regard the indeterminate region of the computation as indicative of a close approach to general yielding.

In this report, general yielding of the beam specimens is taken as the point at which the solution for K, with the plasticity adjustment, does not converge to a finite value for K. Such points are indicated in the data presented herein as minimum points with arrows fixed atop them.

6. The Variation of K with Geometry

Through the judicious use of available solutions for K (see Ref. 3) many problems of engineering importance can be solved. In Section 15 of Part II, for example, several such solutions are combined for the fracture analysis of Kings Bridge.

Of particular interest to bridge engineers are the solutions for through cracks in a plate subjected to a uniform tensile field. The following three solutions provide examples of how K is dependent upon geometry, see Fig. 18:

$$K = C\,\sigma\,\sqrt{\pi\,(a + r_Y)}$$

1. For a center crack in a finite-width plate:

$$C^2 = \sec \frac{\pi (a + r_Y)}{W} \tag{31}$$

2. For a single-edge crack in a finite-width plate:

$$C \text{ is a function of } \frac{a + r_Y}{W} \text{ (see Ref. 3)} \tag{32}$$

3. For a double-edge crack in a finite-width plate:

$$C^2 = \frac{2b}{\pi a} \left(\tan \frac{\pi a}{2b} + 0.1 \sin \frac{\pi a}{b}\right) \tag{33}$$

7. The Three-Ended Crack

The most serious crack flaws in the Kings Bridge were three-ended cracks. They were through-cracks in the center of the flange which also progressed into the web, as in Fig. 19. At the time of fracture, three crack tips were involved in the instability.

If the web crack is long and offers little resistance to the opening of the flange crack, an estimate of K for the flange crack can be made using the equation for a center crack in a finite-width plate (Eq. 31). For a more accurate analysis, the effect of the interaction of the web crack and flange crack should be considered.

The web crack is treated as half of a centrally cracked sheet with the flange on the bisecting centerline of the sheet. The effect of curvature of this line due to beam bending is considered negligible. The presence of a cover plate on the flange ending near the crack means there would be a small interlaminar shear force between

web and flange due to this change of flange stiffness. However, these forces would tend to displace rather than to open the cracks.

The principal interaction is due to the requirement that displacements in the flange normal to the plane of the two cracks must be equal (aside from small three-dimensional adjustments within the flange). A complete matching of web and flange displacements along the interaction centerline is feasible in terms of known computational methods. However, the complexity of this calculation would make it inappropriate.

In this treatment the interaction force is considered localized at the plane of the cracks. To avoid infinite displacements the force is spread out across a one inch span for each crack and the displacement is taken at the center of this span. The magnitude of the interaction force is adjusted to make this center point displacement the same for the web crack and the flange crack.

This practice is believed to furnish a good first approximation of the interaction influence. Equality of displacements at the crack plane does not mean that the displacements elsewhere along the intersection centerline are equal. An additional set of interaction forces, some directed toward the crack, others away from the cracks, would be required to establish a complete matching of the flange and web displacements. However, it is considered these forces would be smaller than the single interaction force used in the first approximation, would be partially self-canceling in their effect on

the K values and would have a reduced influence on the K values due to their greater separation from the cracks.

Thus, the flange crack and web cracks, for which approximate solutions are known, are considered as separate problems. An unknown central closing force is added to one crack and the same force, as an opening force, is added to the other crack. The two problems are then solved in an iterative manner, increasing the unknown force with each iteration until the center displacement of the flange crack is the same as the opening of the web crack.

From Eq. 28 the crack opening displacement is given by:

$$Ev = 2 \text{ Im } \overline{Z} - (1 + \nu) y \text{ Re } Z$$

From Eq. 29, the crack opening displacement for a center crack in an infinite plate under a uniform tensile field is:

$$Ev = 2 \sigma \sqrt{a^2 - x^2}$$

At the center of the crack, x = 0 and

$$v = \frac{2}{E} \sigma a \qquad (34)$$

From Eq. 7, the K value for a center crack in a finite plate subject to uniform tension is:

$$K = \sigma \sqrt{\pi a} \quad \sqrt{\sec \frac{\pi a}{W}}$$

The crack opening due to the partial loading of the crack can be found as follows. The Z function for two pairs of forces

acting on the crack surface in the manner shown in Fig. 20a is[20]

$$Z = \frac{2\,P\,z\sqrt{a^2 - b^2}}{\pi(z^2 - b^2)\sqrt{z^2 - a^2}} \tag{35}$$

For $y = 0$ and $x < a$

$$\text{Re } Z = 0 \tag{36}$$

For $y = 0$ and $b < x < a$, the integral of Eq. 35 is:

$$\bar{Z} = \frac{2P}{\pi}\, i \tanh^{-1}\sqrt{\frac{a^2 - x^2}{a^2 - b^2}}$$

and

$$\text{Im } \bar{Z} = \frac{2P}{\pi} \tanh^{-1}\sqrt{\frac{a^2 - x^2}{a^2 - b^2}} \tag{37}$$

For $y = 0$ and $0 \leq x < b$, the integral of Eq. 35 is:

$$\bar{Z} = \frac{2P}{\pi}\left\{\frac{\pi}{2} + i \coth^{-1}\sqrt{\frac{a^2 - x^2}{a^2 - b^2}}\right\}$$

and

$$\text{Im } \bar{Z} = \frac{2P}{\pi} \coth^{-1}\sqrt{\frac{a^2 - x^2}{a^2 - b^2}} \tag{38}$$

For $y = 0$ and $x = b$, $\bar{Z}$ is not defined.

Substituting Eqs. 36, 37, and 38 into 28, the crack opening displacement is:

$$\text{For} \quad b < x < a \qquad v = \frac{4P}{E\pi} \tanh^{-1}\sqrt{\frac{a^2 - x^2}{a^2 - b^2}}$$

$$\text{For} \quad 0 \leq x < b \qquad v = \frac{4P}{E\pi} \coth^{-1}\sqrt{\frac{a^2 - x^2}{a^2 - b^2}} \tag{39}$$

$$\text{For} \quad x = b \qquad v \text{ is not defined.}$$

The crack opening displacement for the partially loaded crack of Fig. 20b can be found from Eq. 39 by setting

$$P = \sigma \, db$$

and integrating from b = 0 to b = c. The result is:

$$\text{for } x < c \quad v = \frac{4\sigma}{E\pi}\left\{\sqrt{a^2 - x^2}\,\sin^{-1}\frac{c}{a} + c\,\coth^{-1}\sqrt{\frac{a^2 - x^2}{a^2 - c^2}} - x\,\coth^{-1}\frac{c}{x}\sqrt{\frac{a^2 - x^2}{a^2 - c^2}}\right\}$$

$$\text{for } x > c \quad v = \frac{4\sigma}{E\pi}\left\{\sqrt{a^2 - x^2}\,\sin^{-1}\frac{c}{a} + c\,\tanh^{-1}\sqrt{\frac{a^2 - x^2}{a^2 - c^2}} - x\,\tanh^{-1}\frac{c}{x}\sqrt{\frac{a^2 - x^2}{a^2 - c^2}}\right\} \qquad (40)$$

for x = c, v is not defined.

For x = 0

$$v = \frac{4\sigma}{E\pi}\left[a\,\sin^{-1}\frac{c}{a} + c\,\tanh^{-1}\left(1 - \frac{c^2}{a^2}\right)^{-1/2}\right] \qquad (41)$$

An expression for the stress-intensity for the partial loading of Fig. 19b can be found as follows. From Eq. 35, the Z function for the loading of Fig. 20a is:

$$Z = \frac{2\,P\,z\sqrt{a^2 - b^2}}{\pi(z^2 - b^2)\sqrt{z^2 - a^2}}$$

Setting $z = a + z_1 = a + re^{i\theta}$, the tensile stress σ_y along the x-axis is, from Eqs. 1a and 22:

$$\sigma_y \Big|_{y=0} = \lim_{r \to o} \text{Re } Z = \frac{K}{\sqrt{2\pi r}}$$

and from Eq. 35

$$K = 2 \frac{P \sqrt{\pi a}}{\pi \sqrt{a^2 - b^2}}$$

Letting $P = \sigma \, db$ and integrating results in the expression for K for the loading of Fig. 20b:

$$K = \int_o^c \frac{2 \sigma \, db \sqrt{\pi a}}{\pi \sqrt{a^2 - b^2}}$$

$$K = \sigma \sqrt{\pi a} \left(\frac{2}{\pi} \sin^{-1} \frac{c}{a}\right) \qquad (42)$$

The web crack can be analyzed in a similar manner, see Fig. 20c. If the crack is small compared to the distance to the neutral axis, the analysis can be simplified to that of an edge crack in an infinite plate. This can be further approximated as half of a through crack in an infinite plate.

For the bending stress in the web K can be found from Eq. 3 and v can be found from Eq. 34:

$$K = \sigma_1 \sqrt{\pi a}$$

$$v = \frac{2}{E} \sigma_1 a$$

Equations 41 and 42 can be used to determine the K and v values from a partial load on the web crack.

Now that the required equations for K and v are known, the computation proceeds as follows:

1. Approximate the stress over the cracked sections as the sum of several loadings on each crack: A uniform stress across the entire section and one or more stress levels over one or more parts of the crack. This was done for Kings Bridge in Fig. 13d.

2. Determine the total K and v values of the flange using Eqs. 7 and 34 for the uniform stress over the entire section and Eqs. 42 and 41 for the partial loading:

$$K_1 = K_{11} + K_{12} + K_{13} + \cdots$$

$$K_{11} = \sigma_{11} \sqrt{\pi a_1} \sqrt{\sec \frac{\pi a_1}{W}}$$

$$K_{12} = \sigma_{12} \sqrt{\pi a_1} \left[\frac{2}{\pi} \sin^{-1} \frac{c_{12}}{a_1} \right]$$

$$K_{13} = \sigma_{13} \sqrt{\pi a_1} \left[\frac{2}{\pi} \sin^{-1} \frac{c_{13}}{a_1} \right]$$

etc.

$$v_1 = v_{11} + v_{12} + v_{13} + \cdots$$

$$v_{11} = \frac{2}{E} \sigma_{11} a_1$$

$$v_{12} = \frac{4 \sigma_{12}}{\pi E} \left[a_1 \sin^{-1} \frac{c_{12}}{a_1} + c_{12} \coth^{-1} \left(1 - \frac{c_{12}}{a_1}\right)^{-1/2} \right]$$

$$v_{13} = \frac{4 \sigma_{13}}{\pi E} \left[a_1 \sin^{-1} \frac{c_{13}}{a_1} + C_{13} \coth^{-1} \left(1 - \frac{c_{13}}{a_1}\right)^{-1/2} \right]$$

etc.

3. Determine the total K and v values of the web using Eqs. 3 and 34 for the uniform stress over the entire section and Eqs. 41 and 42 for the partial loading.

$$K_2 = K_{21} + K_{22} + \ldots$$

$$K_{21} = \sigma_{21}\sqrt{\pi\, a_2}$$

$$K_{22} = \sigma_{22}\sqrt{\pi\, a_2}\left[\frac{2}{\pi}\sin^{-1}\frac{c_{22}}{a_2}\right]$$

etc.

$$v_2 = v_{21} + v_{22} + \ldots$$

$$v_{21} = \frac{2}{E}\sigma_{21}\, a$$

$$v_{22} = \frac{4\,\sigma_{22}}{E\,\pi}\left[a_2 \sin^{-1}\frac{c_{22}}{a_2} + c_{22}\coth^{-1}\left(1-\frac{c_{22}}{a_2}\right)^{-1/2}\right]$$

4. Apply equal and opposite forces to the flange and web cracks to make $v_1 = v_2$. These forces must be treated as stresses over part of the crack because the crack opening displacement immediately beneath a point load is infinite. This part of the computation can best be done by iteration, starting with a zero force and increasing it by steps until $v_1 = v_2$.

5. From the last value of K_1 and K_2, compute the plasticity adjustment factor r_Y for the flange crack and for the web crack.

6. Repeat the above computations using $a + r_Y$ for the half crack length and continue the procedure until K_1 and K_2 are obtained to the desired accuracy.

The preceding method is applied to the three-cornered crack of the Kings Bridge in Appendix B.

8. Elevation of Yield due to Loading Rate and Temperature

When computing an r_Y correction for the plasticity at the tip of the crack, the value of the yield strength used in the computation should be the value of the yield strength at the loading rate and at the temperature of interest. Since all the tests conducted at Lehigh, even the "static" tests, were run at loading rates considerably greater than for the standard tensile test, an appropriately increased value of the yield stress was used. Similarly, the decrease in temperature, as opposed to room temperature, caused an increase in the yield stress.

The following empirical equation[10] can be used to estimate this increase in yield

$$\sigma_{YS}\Big|_{at(T,t)} = \sigma_{YS}\Big|_{at(T_o,t_o)} + \frac{174{,}000}{\log(2\times10^{10}t)\,(T+459)} - 27.4 \qquad (43)$$

where T = specimen temperature in degrees Fahrenheit

t = load rise time for the specimen

T_o = test temperature for the standard tensile test (75^o F)

t_o = load rise time for the standard tensile test (50 seconds)

In Fig. 40, Eq. 43 is compared to the yield strength of 1 inch thick A441 plate tested at minus 40^{o} F over several orders of magnitude of loading rate. The comparison is quite good.

9. Fatigue Crack Growth Rates

Paris[8] found that the growth rate of fatigue cracks for a high strength aluminum alloy was a function of the applied ΔK and was nearly proportional to $(\Delta K)^4$, see Fig. 21. Subsequent tests on other aluminum alloys, molybdenum, and steel by Paris and Erdogan,[23] indicate that the fourth power dependency holds for these materials as well. Fatigue data for four types of steels[9,24,25,26] indicate that the fourth power law can be used without serious inaccuracy for steels generally.

The fourth power hypothesis in equation form for steels is[10]

$$\frac{da}{dN} = c(\Delta K)^4 \qquad (44)$$

where

$c = 1.0 \times 10^{-12}$ (for mean data on medium and low strength steel)

$c = 1.6 \times 10^{-12}$ (for mean data on all steel)

$c = 2.0 \times 10^{-12}$ (for conservative estimating of fastest rates on all steels)

$\frac{da}{dN}$ = inch/cycle,

and ΔK is in units of ksi $\sqrt{\text{in.}}$

"Equation 44 gives a reasonable estimate for growth rates from 10^{-6} in./cycle up to final failure, provided the cyclic K stays below K_{Ic} for the material and the cyclic nominal stress is below the static yield point.

However, Eq. 44 is not recommended for estimates of fatigue life [under abnormal conditions and over a wide range of ΔK]. By itself it is too crude an empirical relationship for this purpose. It does not contain the effects of mean load, frequency, environment, or temperature, which surely play a role in the flaw growth".[10]

Although the crack growth rate does depend primarily on the stress intensity range ΔK there is no question that other factors, such as mean load (mean K), maximum load (max. K), frequency of loading, thickness, and material processing do effect the growth rate, but in a secondary manner. Other theories of fatigue crack growth attempt to account for these variables.[27] For certain materials environment and temperature can have a dramatic effect on crack growth. This is the case, for example, with high strength steels (200,000 psi yield) in the presence of moisture.[28]

The data reported in Part III, Section 9, and shown in Fig. 34 indicates that the crack growth rate for the A441 steel tested at Lehigh can be approximated by the equation

$$\frac{da}{dN} = 2.0 \times 10^{-12} (\Delta K)^4 \qquad (45)$$

where

$\frac{da}{dN}$ = inches per cycle

and

ΔK = ksi $\sqrt{in}$

Verification of the fourth power law was found. The fact that the crack growth rate was about twice that suggested by Paris is not very significant since this difference is within the expected uncertainty of Paris' suggestions.

10. Correlation of K_{Ic} to Critical Strain

Krafft found a correlation between the critical plain-strain value of the stress intensity factor K_{Ic} and the failure strain of a simple static test.[12] The correlation is based upon Krafft's theory that fracture occurs when small ligaments along the crack front become unstable, see Fig. 22. When the leading edge of the crack is loaded, the ligament is regarded as loaded in the same manner as a simple tensile specimen. Krafft calls the diameter of this ligament the "process zone size" and has designated it d_T.

The correlation involves the matching of two sets of data: (1) showing ε_c versus $\dot{\varepsilon}$ and (2) showing K_{Ic} versus $\dot{K}$. The details of the match can best be presented as an example, see Section 15 of Part III. The theory is as follows.

Krafft found[29] that the total elastic plus plastic strain of the ligament at instability can be approximated by:

$$\varepsilon_c = \frac{K_{Ic}}{\sqrt{2\pi\, d_T}} \tag{46}$$

The strain rate, assuming the crack has not moved, is the derivative with respect to time of Eq. 45:

$$\dot{\epsilon} = \frac{\dot{K}}{E\sqrt{2\pi\, d_T}}$$

From the above two equations:

$$\frac{\dot{K}}{\dot{\epsilon}} = \frac{K_{Ic}}{\epsilon_c} \tag{47}$$

If two sets of data points are available, one relating ϵ_c to $\dot{\epsilon}$ and one relating K_{Ic} to $\dot{K}$, and if both sets of data are plotted to the same scales, the ratio of K_{Ic}/ϵ_c can be found by matching the data points from the two sets. The process zone size d_T, a material constant, can then be computed from Eq. 46 rearranged as follows:

$$d_T = \frac{1}{2\pi E^2}\left(\frac{K_{Ic}}{\epsilon_c}\right) \tag{48}$$

In Section 15, Part III, the correlation of K_{Ic} and ϵ_c is used to determine dynamic K_{Ic} values for A441 steel.

11. Computation of K_c for the Lehigh Test Specimen

An expression for K for the single-edge cracked plate subjected to three-point bending, a popular fracture specimen configuration and the one used for the Lehigh fracture tests, was developed by Gross and Srawley using a boundary collocation method.[30] The K calibration is represented by a fourth-degree polynomial, which is within 0.2 percent for all values of a/W up to 0.6:

$$Y = \frac{K\, B\sqrt{W}}{6\, M\frac{a}{W}} = A_o + A_1\left(\frac{a}{W}\right) + A_2\left(\frac{a}{W}\right)^2 + A_3\left(\frac{a}{W}\right)^3 + A_4\left(\frac{a}{W}\right)^4 \tag{49}$$

where M is the applied bending moment, and the coefficients A have the following values.

	A_o	A_1	A_2	A_3	A_4
Pure bending	+ 1.99	- 2.47	+ 12.97	- 23.17	+ 24.80
Three-point:					
S/W = 8	+ 1.96	- 2.75	+ 13.66	- 23.98	+ 25.22
S/W = 4	+ 1.93	- 3.07	+ 14.53	- 25.11	+ 25.80
S/W = 3.33	+ 1.93	- 3.12	+ 14.68	- 25.30	+ 25.90

where S/W is the span-to-depth ratio of the specimen. The values shown above for S/W of 3.33 are a linear extension of the values recommended by Srawley and Brown for S/W of 8 and 4. The S/W of the Lehigh specimen is 3.33.

The supports of the Lehigh specimen were not free to move horizontally, as are the supports of the Srawley-Brown calibration. However, an experimental compliance calibration of the Lehigh specimen[13] showed that the above extrapolation of the Srawley-Brown calibration is valid for the Lehigh specimen and the Srawley-Brown calibration was the basis of the computation of K for these tests.

Most of the K_c computations for the data presented in this dissertation were done with the aid of a computer. The program was written to include a plastic zone correction and an elevation of the yield strength resulting from the loading rate and the low temperature. The computer program is discussed in detail in Ref. 13. The following is an outline of the steps in computing K_c.

1. Compute σ_{YS} for the test temperature and loading rate of the specimen from Eq. 43:

$$\sigma_{YS} = \sigma_{YS}\Big|_{T_o,t_o} + \frac{174{,}000 \text{ ksi}}{\log(2\times10^{10}t)(T + 459)} - 27.4 \text{ ksi}$$

where

$\sigma_{YS}\Big|_{T_o,t_o}$ = 56.9 for the 1/2 inch plate

$\sigma_{YS}\Big|_{T_o,t_o}$ = 55.5 ksi for the 1 inch plate

$\sigma_{YS}\Big|_{T_o,t_o}$ = 54.0 ksi for the 2 inch plate

T = test temperature in degrees Fahrenheit

t = loading time in seconds.

2. Compute K from Eq. 49 using a span length of 10 inches.

$$K = \frac{60P}{B\sqrt{W}} \frac{a}{W}\left[1.93 - 3.12\left(\frac{a}{W}\right) + 14.68\left(\frac{a}{W}\right)^2 - 25.3\left(\frac{a}{W}\right)^3 + 29.9\left(\frac{a}{W}\right)^4\right] \quad (50)$$

where

P = fracture load

a = crack length at fracture

W = specimen depth

B = specimen thickness

3. Compute r_Y from Eq. 5:

$$r_Y = \frac{1}{2\pi}\left(\frac{K}{\sigma_{YS}}\right)^2$$

4. Compute the effective crack length from

$$a = a_o + r_Y \tag{51}$$

5. Compute a revised K from Eq. 50 using

$$a = a_o + r_Y$$

6. Continue the iteration until the change in r_Y from one iteration to the next is less than .0005 inches.

If the program converges on a value of K, that value is K_c, the critical stress-intensity factor of the material at the loading rate and temperature of the test.

If the program does not converge on a finite value of K but goes toward infinity, then gross yielding has taken place beyond the tip of the crack (see Section 5) and the linear elastic fracture mechanics equations and the plasticity correction factor are not accurate. In this case a lower bound to K_c can be estimated using a graphical procedure suggested by Irwin.

From Eq. 49

$$K^2 = \frac{36\ M^2\ a}{B\ W^4}\ Y^2 \tag{52}$$

From Eqs. 5, 51, and 52

$$r_Y = A \cdot f(\frac{a}{W})$$

where

$$A = \frac{36\ M^2}{2\pi\ \sigma_{YS}^{\ 2}\ B^2\ W^2}$$

$$f(\frac{a}{W}) = \frac{a}{W}\ [1.93 - 3.12\ \frac{a}{W} + 14.68\ (\frac{a}{W})^2 - 25.3\ (\frac{a}{W})^3 + 29.9\ (\frac{a}{W})^4$$

$$a = a_o + r_y$$

1. Plot $f(\frac{a}{W})$ as in Figure 23.

2. Extend a vertical line at $\frac{a_o}{W}$.

3. At $f(\frac{a}{W}) = 4$ plot a point a distance of $4\ \frac{A}{W}$ horizontally from the vertical line at $\frac{a_o}{W}$.

4. Draw a line from the point of step 3 to the point $(f = 0, \frac{a}{W} = \frac{a_o}{W})$.

5. The intercept of the line of step 4 with the $f(\frac{a}{W})$ curve is the value of $(a_o + r_Y)/W$.

The proof is rather simple:

$$r_Y = Af$$

$$\frac{r_Y}{W} = \frac{A}{W}\ f$$

$$\frac{r_Y}{W} \div f = \frac{A}{W} = \frac{4\ \frac{A}{W}}{4}$$

If gross yielding takes place at the crack tip, the construction line of step 4 will not intersect the curve of $f(\frac{a}{W})$. In this case draw a tangent to the curve parallel to the construction line of step 4. A lower bound on r_Y/W is taken as the distance from the vertical line of step 2 to the construction line of step 4, the distance being measured through the point of tangency to $f(\frac{a}{W})$.

Once K_c is known, an estimate of K_{Ic} can be made using an empirical formula suggested by Irwin[10]

$$K_{Ic}^2 = \frac{K_c^2}{1 + 0.5\,\beta_c} \tag{54}$$

where

$$\beta_c = \frac{1}{B}\left(\frac{K_c}{\sigma_{YS}}\right)^2$$

Equation 54 is not valid if the plastic zone size $2r_Y$ is greater than the thickness of the plate.

12. Recommendations of ASTM Committee E24 for Fracture Testing

Committee E24, the Committee on Fracture of the American Society for Testing and Materials, has established a tentative standard for K_{Ic} testing of high strength metallic materials,[31] primarily intended for steels having yield strengths in excess of 200,000 psi. Such materials do not usually have a significant plastic zone at crack instability. In fact, the standards are set up so as to preclude the formation of a significant plastic zone, and no attempt is made in the standards to include a plasticity adjustment

to the computations. The standards are an attempt to ensure valid and standardized K_{Ic} testing of the materials for which they were written.

The problem of standardized testing of lower strength metals is still under study by Committee E24. There is no general agreement as yet on what testing standards would be best for the lower strength metals. The tentative standards for high strength materials require:

A specimen thickness of $$B \geq 2.5 \left(\frac{K_{Ic}}{\sigma_{YS}}\right)^2 \quad (55)$$

A crack length of $$a_o \geq 2.5 \left(\frac{K_{Ic}}{\sigma_{YS}}\right)^2 \quad (56)$$

A ligament length of $$W - a_o \geq 2.5 \left(\frac{K_{Ic}}{\sigma_{YS}}\right)^2 \quad (57)$$

For the Lehigh tests only the 2 inch dynamic tests meet these limitations because:

For the 1/2" static tests, specimen thickness controls and none of the data meets the standard.

For the 1/2" dynamic tests, specimen thickness controls and only tests below -80° meet the standard.

For the 1" static tests, specimen thickness controls and only tests below -90° meet the standard.

For the 1" dynamic tests, specimen thickness controls and only tests below -10° meet the standard.

For the 2" static tests, crack length controls and only tests below -70° meet the standard.

For the 2" dynamic tests, crack length controls and all tests below 40° meet the standard.

The Lehigh tests were concerned with obtaining useful fracture data for a specific application--plates between 1/2" and 2" thick tested at temperatures between -40^{o} and $+40^{o}$ Fahrenheit. These objectives cannot be accomplished within the limitations of the tentative E24 standards. Consequently practices customary before the development of the Standards for high strength materials were used in these tests. These practices, as in the past, appear to give useful results.

13. The Validity of Impact K_c Tests

There is some question as to whether the static, equilibrium solutions of the three-point bend specimen can realistically be used for computing K_c values from impact testing. Even if the applied load can be determined accurately (a major undertaking in itself) the question remains as to whether the stress state at the crack tip for such high loading rates is the same as the stress state for the same load under static conditions.

Surely, if the loading time is sufficiently long that the shock wave can traverse the specimen from load point to support many times, then the static equations are valid approximations of the physical event. If the specimen breaks before the shock wave can travel to the support and back to the load point, then the static equations cannot possibly be a valid approximation of the physical event.

In the Lehigh impact tests, the distance from the load point to the support is 5-1/2 inches. Since the load wave travels at nearly the shear wave velocity in steel, 10,000 ft. per second, the load will travel the distance from load point to support and back again five times in the .5 millisecond that it takes to break the specimen.

Is five times enough to assure the validity of the steady state equations? An affirmative answer can be found by comparison of the Lehigh tests to analysis studies at the Naval Research Laboratory. A general analysis of the impact problem in the drop-weight test is being developed by Nash at the Naval Research Laboratory.[32] Nash offers the following comments in the introduction to his work:

> "... The approach used parallels the standard method for treating transverse impact problems;[33] however, there are several important differences...
>
> In this investigation, a refined one dimensional bending theory is devised using a variational principle proposed by Gurtin.[34] Using these results, an integral equation is derived for the hammer force as a function of time and solved in closed form by Laplace transforms. The closed form solution, however, requires the assumption of a single active bending mode. The influence of the higher modes is evaluated subsequently and an iterative procedure is described with which the hammer force can be obtained to any degree of precision desired. ... The effects of localized plasticity at the contact point and gross yielding of the specimen are neglected. The analysis

is thus limited to relatively brittle materials at this time."

Nash found that the force acting on the specimen from contact to initiation of fracture can be approximated by:

$$F(t) = \frac{(V_{o1} - V_{o2})K_4}{\alpha\,\beta(\alpha^2 - \beta^2)}\,[\alpha(\omega_1^2 - \beta^2)\,\sin\beta t + \beta(\alpha^2 - \omega_1^2)\,\sin\alpha t] \tag{58}$$

where

$F(t)$ = tup force as a function of time

V_{o1} = initial velocity of the tup

V_{o2} = initial velocity of the beam

K_4 = constant of the contact theory

α and β = functions of the eigenvalues of the beam equations, the mass of the beam, and the load and the contact theory constants.

ω_1 = fundamental frequency of the beam

A plot (Eq. 58) is compared to the actual load-time record for Nash's specimen in Fig. 24. The specimen is a brittle steel bar 5/8 inch thick, 1-5/8 inches deep, and 7 inches long. Note the excellent agreement between the experimental and theoretical curves.

Nash approximates the bending moment of the beam by:

$$M(\xi, t) = P\left[\frac{(\omega_1^2 - \beta^2)}{\beta}\right]^{1/2} \sum_{i=1,3,5..}^{\infty} \frac{\beta_o \sin(\omega_i t) - \omega_i \sin\beta_t}{(\beta^2 - \omega_1^2)^{1/2}}$$

$$\sin\left(\frac{i\pi}{2}\right) \sin(i\pi\xi) + \frac{(\alpha^2 - \omega_i^2)}{\alpha}$$

$$\sum_{i=1,3,5..}^{\infty} \frac{\alpha \sin(\omega_i t) - \omega_1 \sin \alpha t}{(\alpha^2 - \omega_i^2)} \sin\left(\frac{i\pi}{2}\right) \sin(i \pi \xi)] \qquad (59)$$

where

$$P = \frac{2K_4 \omega_i L(V_{o1} - V_{o2})}{\pi^2 (\alpha^2 - \beta^2)}$$

$\xi = \frac{x}{L}$ where x is measured from the center of the span along the beam axis.

Figure 25 shows a plot of the bending moment at mid-span as a function of time, from Eq. 59. Also shown is the bending moment at the mid-span predicted from the static equation $M = \frac{FL}{4}$. Note that after 200 μ sec, the difference between the static and dynamic bending moments is relatively minor. According to Nash, the actual difference is even less than that indicated in Fig. 25 because of damping effects which are not accounted for in the analysis.

In the Lehigh impact tests, the specimens were fractured at loading rates of from 300 to 500 μ sec.

It is interesting to note that when loading rates less than that of Fig. 24 are used, Eq. 58 predicts a decrease in the peak load and the appearance of a second peak. Further decrease of the load rate reduces the first peak, but the second peak remains constant. This same effect was found experimentally in the Lehigh tests,[13] see

Fig. 26. The load curve predicted from Eq. 58 by Nash for a loading velocity of 10 ft. per second is shown in Fig. 27. It is remarkably like that of the Lehigh impact tests for a 1 foot drop, which corresponds to a tup speed of 8 ft. per second.

Three experimental variations were used in the Lehigh impact tests: padded tests, unpadded tests, and gaged specimen tests.

Padded Tests - a small aluminum pad was placed on the test specimen at the point of contact of the tup to slow the loading rate to about one-fifth the loading rate when struck directly. The maximum load measured at the striking tup was taken as the fracture load.

Unpadded Tests - the drop height was lowered to 6 inches so that just enough energy was applied to the specimen to fracture it. The load curve at the tup exhibited a characteristic double peak. The maximum value of the second peak was taken as the fracture load.

Gaged Specimen Tests - strain gages were mounted on the test specimen to record the bending moment in the specimen. The maximum load was taken as the fracture load.

Except for the beam record of the 2 inch thick specimen (see Fig. 57) the K_c values computed from the three methods fall within an assuringly narrow band when plotted, see Figs. 45 and 51. The consistency of the results gives credence to the fact that the use of static equations for the bending moment at fracture is valid.

14. Loading Rates in Bridges

Since fracture toughness is dependent upon loading rate, see Fig. 7, some idea of the loading rates that are likely to prevail in bridges must be determined so that K_c values for these loading rates can be estimated.

Although many researchers have instrumented bridge beams and recorded deflections under load, there is surprising little data in the literature from which loading rates can be determined.

Figure 28 shows a strain-time curve taken from the AASHO Road Tests.[35] The maximum loading rate for the vehicle traveling at 30 mph is (Fig. 28) 1.27×10^{-3} in./in. per second. It is not likely that loading rates in bridges would exceed this value. The AASHO test bridge was relatively small (50 foot span) and the loading was relatively large (36 ksi max. stress under load).

The total time required to load the AASHO test bridge from zero to maximum load was one second. The Lehigh "static" tests had a total loading time of two seconds. Thus the Lehigh "static" tests were comparable to the fastest loading time one might expect to find in a bridge.

For a stationary crack front, the time rate of increase of K can be found from Eq. 3 as follows:

$$K = \sigma \sqrt{\pi a}$$

$$\dot{K} = \frac{dK}{dt} = \dot{\sigma} \sqrt{\pi a}$$

$$\dot{K} = E \dot{\epsilon} \sqrt{\pi a} \qquad (60)$$

Assuming a 1 inch crack and an $\dot{\epsilon}$ of 1.27×10^{-3} in./in. per sec.:

$$\dot{K} = 67.5 \text{ ksi } \sqrt{\text{in}} \text{ sec}^{-1}$$

The Lehigh "static" tests were run at a $\dot{K}$ of 31.5 ksi $\sqrt{\text{in}}$ or one-half as fast.

The data of Fig. 39 indicates that even at a loading rate of $\dot{K}$ = 1000 ksi $\sqrt{\text{in}}$ sec^{-1}, the $\dot{K}_{Ic}$ level is nearly the same as for a slow static test, with a $\dot{K}$ equal to 1.0 ksi $\sqrt{\text{in}}$ sec^{-1} or less. One might conclude from this that it may be sufficient for bridge structures to determine the appropriate K_c from static rather than from impact tests.

On the other hand, it can also be argued that instability of a broad crack front may be initiated by some stable (or localized unstable) movement at selected portions of the crack front. Instability of the broad crack front would then occur only after some slight stable movement of the crack takes place. This slight stable movement of the crack might reduce K_c to the low levels typical of slow moving cracks, see Fig. 7.

A discussion of crack toughness results is given in Part III.

15. A Fracture Analysis of Kings Bridge

It is not known how bridge fractures, if they occur, are likely to be initiated: from a stationary crack becoming unstable under a dynamic load at a high, nearly static K_c level; or from a

slow moving crack becoming unstable at a relatively low, impact K_c level. Nor is it known with high accuracy to what extent weld residual stresses currently present in structural steel bridges assist fracturing.

A study of the Kings Bridge failure (Melbourne, 1962) was made because the crack extensions contributing to this bridge failure were reported, thus providing an opportunity to look for a specific illustration of these uncertainities. Fortunately the large cracks present in the Kings Bridge prior to final failure are not typical. Nevertheless the fracture analysis of Kings Bridge provides a realistic bridge structure example illustrative of the use of fracture mechanics and is therefore of special interest.

In making the stress analysis, presented in Appendix A, several assumptions had to be made regarding the loading conditions at the time of fracture. For this reason, we cannot be certain that the results provide an accurate indication of what happened at failure. However, it is considered that the procedures followed are appropriate and permit a reasonable estimate of what happened. At the time of fracture only three of the four girders were acting, which greatly complicated the problem. However, only a simplified analysis was attempted and this proved to be a less formidable task than had been expected. The problem of determining the load distribution to each girder was adjusted so as to provide an estimate of the dead and live load stress in Girder W14-3 at the time of failure. The upper and lower bounds obtained for the load carried by Girder W14-3 were surprisingly close. The residual stress proved more

troublesome. The residual stress pattern assumed in the analysis can, however, be justified as highly plausible. The results of the stress analysis of the bottom flange of Girder W14-3 at failure are shown in Fig. 13. From Fig. 13d, the total stress in the bottom flange of Girder W14-3 can be approximated as a uniform stress of 12 ksi across the entire flange plus a uniform stress of 38 ksi across a four inch portion of the center of the crack. This was arrived at as follows:

1. The total live and dead load stress at the cracked section, see Fig. 13a, was found to be 20 ksi (14 ksi from dead load and 6 ksi from live load).

2. The residual stress pattern at the cracked section after making the flange to web welds and the cover plate welds, see the dashed lines in Fig. 13b, was found to be a tensile stress of 53 ksi (the yield strength of the steel) at the center of the flange balanced by a 24 ksi compressive stress over the rest of the flange.

3. If the residual stress is added to the dead load plus a live load 50% greater than that of Fig. 13a (since it is quite likely that a load heavier than the actual failure load occurred sometime during the year of service of the bridge at a warmer and less brittle temperature) the overall load in the girder will be increased. But since the yield stress cannot be exceeded, the stress at the center of the flange remains at 53 ksi.

If we now remove the dead plus live load, the residual tensile stress must be reduced elastically to 30 ksi and the balancing residual compressive stress must be reduced a comparable amount. The result of this loading stress relief is a residual stress of 30 ksi tension and a balancing compressive stress of 11 ksi, as shown in Fig. 13b.

4. The stress pattern at failure was the total bending stress (Fig. 13a) plus the residual stress (Fig. 13b) as shown in Fig. 13c. The stress pattern of Fig. 13c can be approximated as two uniform stresses; 12 ksi across the entire flange and 38 ksi across the central four inches of the flange (see Fig. 13d). This is the stress pattern used in the following computations for K.

The fracture analysis was done in four ways:

1. Finite-plate analysis, no residual stress
2. Finite-plate analysis, with residual stress
3. Three-ended crack analysis, no residual stress
4. Three-ended crack analysis, with residual stress

The results of these four analyses are summarized at the end of this chapter. The finite-plate analysis with residual stress included, is presented here in detail to illustrate the fracture mechanics method. The three-ended crack analysis, which required a computer analysis is presented in Appendix B.

In the computations that follow, the approximate estimates of K (assuming $r_Y = 0$) are shown and are used to exhibit an initial estimate of r_Y. This is followed by presentation of the results from enough r_Y trials to obtain convergence to final values of K.

1. Uniform Stress Across the Flange (see Fig. 29a):

From Eq. 7:

$$K = C\,\sigma\sqrt{\pi\,(a_o + r_Y)}$$

where

$$C^2 = \sec\frac{\pi\,(a_o + r_Y)}{W}$$

For Girder W14-3:

$$W = 16", \quad \sigma = 12.0 \text{ ksi}, \quad a_o = 2.5"$$

For $r_Y = 0$

$$K_1 = 1.065 \times 12.0 \times 2.802 = 35.85 \text{ ksi } \sqrt{\text{in}}$$

2. Uniform Stress Across the Central 4" (see Fig. 29b)

From Eq. 42:

$$K = C\,\sigma\sqrt{\pi\,(a_o + r_Y)}$$

where

$$C = \frac{2}{\pi}\sin^{-1}\frac{c}{(a_o + r_Y)}$$

For Girder W14-3

$$\sigma = 38.0 \text{ ksi}, \quad a_o = 2.5", \quad c = 2.0"$$

For $r_Y = 0$

$$K_2 = 0.590 \times 38.0 \times 2.802 = 62.9 \text{ ksi } \sqrt{\text{in}}$$

3. Transfer Load from the Cover Plate (see Fig. 29c)

Since the end of the cover plate is welded, there will be a transfer of load from the end of the cover plate to the flange plat

Since this load is transferred across the crack, it should be considered in computing K, and its effect is approximately as follows.

The load transferred across the crack is that part of the bending stress which is carried by the 3 inch end of the cover plate. The nominal stress just inboard of the crack (toward the support) is the 20 ksi, live load and dead load stress from bending (see Fig. 13a). Since the distance to the neutral axis is large (49") and assuming there is little shift of the neutral axis across the crack, the bending stress just outboard of the crack (toward the center span) is (see Fig. 29c)

$$\sigma_b \approx \sigma_a \frac{A_a}{A_b} = \sigma_a \times \frac{16 \times \frac{3}{4}}{16 \times \frac{3}{4} + 3 \times \frac{1}{2}} = \frac{8}{9} \sigma_a$$

The load transferred from the end of the cover plate is the stress times the area of the end of the cover plate.

$$P = \sigma_b \times \frac{1}{2} \times 3 = \frac{3}{2} \sigma_b = \frac{4}{3} \sigma_a$$

The stress acting on the crack face is the load divided by the area over which the force acts. Assume the effective area is 4 inches times the thickness of the plate.

$$\sigma_c = \frac{P}{4 \times \frac{3}{4}} = \frac{1}{3} P = \frac{1}{3} \times \frac{4}{3} \sigma_a = \frac{4}{9} \sigma_a$$

The crack loading of Fig. 29c is half that of 29b. Thus, from Eq. 42

$$K_{31} = C\,\sigma_3\sqrt{\pi\,(a_o + r_Y)}$$

where

$$C = \frac{1}{\pi}\sin^{-1}\frac{C}{a_o + r_Y}$$

For Girder W14-3

$$\sigma = \frac{4}{9} \times 20.0 \text{ ksi}, \quad a_o = 2.5, \quad c = 2.0$$

For $r_Y = 0$

$$K_{31} = 0.295 \times 8.9 \times 2.802 = 7.36 \text{ ksi } \sqrt{\text{in}}$$

If the load P is transferred across the crack as computed above, an equivalent uniform stress must be subtracted from the value of K_1 previously computed, or the effect of P will be counted twice. The stress is P divided by the area of the flange.

$$\sigma_d = -\frac{P}{16 \times \frac{3}{4}} = -\frac{P}{12} = \frac{\frac{4}{3}\sigma_a}{12} = -\frac{1}{9}\sigma_a$$

From Eq. 7

$$K = C\,\sigma\sqrt{\pi(a_o + r_Y)}$$

where

$$C^2 = \sec\frac{\pi\,(a_o + r_Y)}{W}$$

For Girder W14-3

$$W = 16, \quad \sigma = -\frac{1}{9} \times 12.0, \quad a_o = 2.5$$

For $r_Y = 0$

$$K_{32} = 1.065 \times (-1.333) \times 2.802 = -3.99 \text{ ksi } \sqrt{\text{in}}$$

The net effect is

$$K_3 = K_{31} + K_{32} = 3.37 \text{ ksi } \sqrt{\text{in}}$$

The total K for $r_Y = 0$ is

$$K = K_1 + K_2 + K_3 = 35.85 + 62.9 + 3.37$$

$$K = 102.12 \text{ ksi } \sqrt{\text{in}}$$

Compute the r_Y correction (from Eq. 5)

$$r_Y = \frac{1}{2\pi}\left(\frac{K}{53}\right)^2 = 0.590" \text{ for static mode fracture}$$

For an impact mode failure, σ_{YS} must be increased. From Eq. 43:

$$\sigma_{YS} = 53 + \frac{174{,}000}{\log(2 \times 10^{10}\ t)(T + 459)} - 27.4 = 80 \text{ ksi}$$

where

$$t = 1/2 \times 10^{-3} \text{ sec}$$

$$T = 40^{\circ} \text{ F}$$

and

$$r_Y = \frac{1}{2\pi}\left(\frac{K}{80}\right)^2 = 0.258" \text{ for impact mode fracture.}$$

Continue the calculation, using $a_o + r_Y$ for the crack length. Until the computations converge to K. The results are:

For Static Mode Fracture $K = 95.8 \text{ ksi } \sqrt{\text{in}}$

$r_Y = 0.524"$

For Dynamic Mode Fracture $K = 98.6 \text{ ksi } \sqrt{\text{in}}$

$r_Y = 0.240"$

The following is a summary of the finite-plate and three-ended crack analyses of the Kings Bridge. See Appendix B for the three-ended crack analysis.

	Finite-Plate Analysis K	Three-Ended Crack Analysis K
Static Mode Fracture (σ_{YS} = 53 ksi)		
No Residual Stress	63 ksi $\sqrt{in}$	69 ksi $\sqrt{in}$
Residual Stress Incl.	96	97
Impact Mode Fracture (σ_{YS} = 80 ksi)		
No Residual Stress	60	67
Residual Stress Incl.	99	98

Note that there is little difference in the results from the finite-plate analysis and the three-ended crack analysis for the case including residual stress. When the residual stress is neglected, the results are within 12%. The result suggests that for long web cracks in webs that are relatively thin compared to the flange, the finite-plate analysis provides a good estimate of the K level of the flange crack.

Both for the static and the dynamic calculation, the web and flange crack openings, without interaction, differed by 2.2×10^{-3} inches. This resulted in an interaction force of approximately 4 kips which tended to restrict the opening of the flange crack and reduced the flange crack K value by nearly 2 ksi $\sqrt{in}$. Presumably if the calculation had included the estimated effect of load transfer

from the cover plate, the web and flange crack openings would have been nearly equal and the interaction force nearly zero. Regardless of whether or not the cover plate load transfer is taken into account, the three-ended crack calculations show that the last 1.5 inches of web crack extension caused nearly a 2 ksi $\sqrt{in}$ increase of the flange crack K value.

The Charpy data of Fig. 12 indicates that the fracture toughness of the bottom flange of Girder W14-3 at 40^{o} F was about midway between that of the 1" and 2" A441 plate tested at Lehigh. The fracture data for "static" testing, shown in Fig. 60, indicates that even at a K level of 97 ksi $\sqrt{in}$, fracture is not likely. On the other hand, the fracture data for impact testing, shown in Fig. 62, indicates that a K level of 68 ksi $\sqrt{in}$ may have been sufficient to initiate fracture. Certainly, a K level of 94 ksi $\sqrt{in}$ would have been sufficient to maintain fracturing after some crack motion at the leading edge had produced an increase of the strain rate.

Thus it seems probable that the Kings Bridge fracture was initiated in a high strain rate or impact mode, and that the presence of residual stresses in the girder flange were a large contributing factor.

III FRACTURE DATA FOR A 50,000 PSI YIELD BRIDGE STEEL - ASTM A441

1. Introduction

In 1966 when this work was begun, an extensive program of fracture testing was in progress for steels used in gas transmission pipelines. These steels are quite similar to the steels used in bridges, particularly ASTM A441. The fracture test adopted by the line-pipe industry is the Battelle version of the Drop Weight Tear Test,[36] a test originally developed by Pellini at the Naval Research Lab.[37] The philosophy of the test program is to develop a statistical history from the laboratory tests and compare that history with full size test specimens, sections of line-pipe that contain flaws and are pressurized until fracture occurs, often with the aid of a small explosive charge.

A correlation was found between the temperature at which the fracture surface of the specimens exhibited a 50 percent shear - 50 percent cleavage appearance and the temperature at which the crack velocity of the prototype tests changed from a slow to a fast propagation rate of over 1500 feet per second. This temperature is called the 50 percent FATT (fracture appearance transition temperature). The catastrophic failure of a pipeline can occur only when the propagation rate of the crack is faster than the decompression wave of the gas pressurizing the pipe. Otherwise, the gas will escape

and the pipeline will unload before the crack has a change to run very far. If the steel in a pressurized line has a 50 percent FATT comfortably below the operating temperature of the line, any failure that occurs should be a local rupture rather than a propagating fracture involving long lengths of pipe.

The line-pipe studies depend upon a correlation between a laboratory test and a fracture history. Once found, the correlation provides some assurance that by meeting the standards of the laboratory test, service failures can be avoided. But the results are limited to a particular type of steel and a particular application.

The original intent of the work presented here was to instrument the Battelle Drop Weight Tear Test, use fracture mechanics to extend the usefulness of the results, and see if the results would be helpful in predicting the likelihood of fracture in bridges.

It was found, however, that the fracture records from the Battelle type test were inadequate for existing means of analysis unless the notch configuration was significantly altered and the energy input greatly reduced. Therefore, fatigue cracks were used instead of the pressed notch of the Battelle test, and the energy applied was kept as low as possible while still sufficient to break the specimen.

The original objective of attempting to analyze the Battelle test was dropped in favor of the more useful objective of obtaining direct K_c data for temperatures, loading rates, and thicknesses typical of bridge structures.

2. Comparison of the Lehigh Method to Other Methods for Impact K_c and K_{Ic} Testing

The impact methods of crack toughness employed at Lehigh possess certain advantages over impact toughness measurement procedures which were developed over the same time period at other laboratories.

Ripling[38] uses a double cantilever beam and applies the load by dropping a weight on a loading bar. The specimen is tapered to produce a constant value of K as the crack propagates. The maximum loading time that can be applied without ringing in the loading system is about 2×10^{-3} sec. Load is measured from a load cell. The advantages of the Lehigh method are a less complicated loading system, less complicated specimen, and the ability to load at a rate four times as fast.

Rolfe and Shoemaker[39] use a loading system and specimen similar to that used at Lehigh. The loads are recorded from gages mounted directly on the specimen. They have emphasized K_{Ic} testing using thicker specimens and colder temperatures than those used in the Lehigh K_c tests. Advantages of the Lehigh method are the elimination of gages on the specimens (except for a few comparative tests) which results in a more economical test. Furthermore, the Lehigh method includes a plasticity correction which makes it possible to derive results applicable to the temperatures and to the thicknesses expected in many prototype structures.

3. The Lehigh Impact Test Machine

The Lehigh Impact Test Machine (see Fig. 8) consists of a 200-pound free-falling weight carefully guided so that its point of contact with the specimen is accurate within 1/16 inch. The striking tup of the weight is instrumented to record load versus time during the fracture event.

The machine, which is mounted on the foundation of the 5,000,000 pound Universal Testing Machine at Fritz Engineering Laboratory, was built heavy and stiff so that the falling weight would not introduce vibrations into the framework of the machine that might distort the load record. The main uprights of the machine are 12W85 sections with "T"-shaped guide tracks bolt-mounted for easy alignment. The base anvil is a 6 inch thick steel block mounted on a large weldment, which is anchored to the test bed of the 5,000,000 pound testing machine with two 3-1/2 inch diameter bolts under tension.

The 200 pound loading weight can be dropped from any height up to 20 feet. The close tolerance of 1/16 inch between the weight and each guide track results in an impact load virtually free of a lateral component, which might introduce random stress waves in the specimen. The removable impacting tup of the weight, shown in the top of Fig. 9, is machined from 4340 steel heat-treated to Rc 50 (200 ksi yield). To insure elastic behavior of the tup during impact, the nominal stress in the tup was kept low (less than 10 ksi). The fixture supporting the specimen, see Fig. 9, was fabricated from heat-treated tool steel and is bolted securely to the base anvil. The

weight is supported by an electromagnetic release mechanism, which is raised and lowered by an overhead crane. The falling weight is stopped by two 2-inch wide by 12-inch deep oak blocks, each topped by a 1-3/4 inch thick steel laminated elastomeric bridge bearing pad.

4. Instrumentation

To calculate K_c at fracture, the value of the load at the instant of crack instability must be known. In the Lehigh impact tests the load time record of the fracture event was obtained by loading the specimen through a striking tup on which was mounted a temperature compensating four-arm bridge of electrical resistance strain gages. The voltage across the bridge controlled the vertical deflection of an oscilloscope trace.

The oscilloscope used is a Tektronix Model 549 with a Type 1A1 dual trace vertical amplifier. The system has a rise time of 16 ns (16×10^{-9} sec). Since the load record has a rise time of 80 μs (80×10^{-6} sec) or 5,000 times that of the oscilloscope, the response rate of the scope is more than sufficient to accurately record the load.

The scope provides dual trace capability with a chop rate fast enough that a chop influence is not evident at sweep speeds above 20 μs, or ter times faster than the fastest sweep speed used in the records presented here. There is therefore no evidence of chop in the dual trace records presented in this report.

The load-recording system was calibrated experimentally on a static test machine. The voltage was adjusted prior to each test so that a one centimeter deflection of the trace corresponds to a ten-kip load.

All electrical systems were carefully grounded to prevent spurious electronic noise from being picked up on the load signal. Twelve-volt wet cell batteries were used to provide a steady power supply, unaffected by variations in the normal AC power supply. In addition to these precautions, it was necessary to avoid making a test record when electronic switches were in operation in the lab, such as those in the overhead cranes and in a large digital strain-gage recorder used for other tests. Occasionally an unknown and rather strong source of electrical noise was encountered. No test was made when this noise was present.

A vacuum tube photocell, which was activated by the falling weight several milliseconds before impact was used to trigger the sweep of the scope. By triggering prior to impact, any spurious signal that might override or distort the load signal was revealed during the several millisecond lead of the trace prior to impact.

The result of these precautions was oscilloscope traces that appear free of external electrical noise and external vibrations in the testing machine, at least until after fracture. The instrumentation, including schematic diagrams of the circuits, is described in Ref. 13.

5. Temperature Control During Testing

Prior to fracture, the specimens were cooled to the desired test temperature. The 1 inch and 2 inch specimens were packed in dry ice for at least one hour. They were then quickly placed into the test fixture. When the specimen temperature near the crack tip had warmed to the desired test temperature, the specimens were fractured and the temperature at fracture recorded. Temperature was monitered with an iron-constantine thermocouple mounted in a 3/32 inch hole drilled approximately one inch deep in the top center of the specimen 1 inch from the center of the span. The hole was filled with a silicone gel to ensure good thermal contact and at the same time prevent electrical contact. The calibration of the thermocouples was periodically checked against three standards: liquid nitrogen, ice water, and boiling water. The temperature measurement was found to be accurate within 2^{o} F.

Because of the smaller mass of the 1/2 inch specimens, a more elaborate method of cooling was used to minimize temperature gradients between the crack tip and the measurement point. The 1/2 inch specimens were placed in a cooling box designed to cool the air surrounding the specimen to the desired test temperature. This system was effective to minus 40^{o} F. It is described in Ref. 13. The specimen was held at the test temperature for at least 20 minutes prior to fracture. Temperature monitoring was obtained with an electrical resistance temperature gage mounted on an aluminum carrier placed near the crack tip, taped to the specimen, and insulated with 1/2 inch glass wool. A layer of silicone gel between steel and aluminum insured good thermal conduct.

This system was found to be accurate within 5^{o} F. Specimens tested below minus 40^{o} F were cooled by packing in dry ice and tested in the same manner as the 1 inch and 2 inch specimens.

6. The Specimen

The specimen (see Fig. 9) consisted of a bar three inches deep, twelve inches long, and the thickness of the plate to be tested. It was loaded in three-point bending on a ten inch span. Fracture initiated at a fatigue crack approximately one inch long on the bottom side of the specimen in the center of the span opposite the loading tup.

The surfaces of the specimen were as-rolled and contained moderate, typical amounts of mill scale. The mill scale was, however, removed from the area of the fatigue crack on one side so that the growth of the crack could be monitored during fatiguing.

The edges of the 3 inch specimen were either mill edge, burned, or saw cut depending on the location of the sample in the plate. Fatigue cracks were not grown on a mill edge or a burned edge. The 12 inch top and bottom edges of the specimen had to be square to facilitate fatigue crack growth. Saw cuts, if square, were satisfactory. But mill edges, burned edges, and unsquare saw cuts had to be milled square to prevent lateral movement of the specimen during fatigue crack growth. Such movement would produce a crooked crack.

For the dynamic tests, the top edge of the specimen was milled to remove the fatigue pressure indent at the center load point. If

this indent was not removed, the load record exhibited a series of small spikes caused by crushing or slipping at this point. Such spikes would cause the entire record to be questionable. The indents at the bottom of the specimen caused no problem because the load spans were different for loading than for fatiguing.

Specimens were cut from plates according to the patterns shown in Fig. 30a. Specimens having a length parallel to the rolling direction and a crack perpendicular to the rolling direction were called "longitudinal" specimens. Specimens having a length perpendicular to the rolling direction were called "transverse" specimens.

7. The Material

The plates tested were rolled from four slabs of manganese vanadium ASTM A441 silicon killed steel (Heat No. 482T0241) on the 60 inch Universal Rolling Mill at the Sparrows Point Plant of the Bethlehem Steel Corporation. There was no cross rolling.

The ladle analysis of Heat No. 482T0241 was:

C	Mn	P	S	Si	Cu	Cr	Ni	Mo	V
.20	1.08	.017	.025	.21	.23	.03	.02	.002	.051

A total of 15 ingots were teemed from this heat and ingots 9, 10, and 11 were used for this rolling. Ingots 8 and 10 were 26" x 50" in size; ingot 11 was 23" x 41". All three had tiger hot tops.

All three plates were 36 inches wide and were roller leveled. The 1/2 inch and 1 inch plates were sheared to 6 feet lengths; the 2

inch plates were burned to 6 feet lengths. The cut plates were identified according to the sketch shown in Fig. 30b.

Tensile properties of the plates are shown in Table 1. The 1/2 inch plate was found to have a 50 percent FATT (fracture appearance transition temperature) of 80^{o} F, as indicated by the drop weight tear data of Fig. 31. This data was obtained using the Battelle DWTT test testing procedure and an industrial drop weight machine at the Homer Research Laboratories of the Bethlehem Steel Corporation. Transverse and longitudinal Charpy v-notch data for the 1/2 inch plate is shown in Fig. 32. Results of longitudinal Charpy v-notch tests for all three plate thicknesses are shown in Fig. 12.

8. Rolling Practice and Micro-structure

The toughness testing of steel plate using thickness as a variable presents a problem. Fracture toughness is dependent upon thickness, as was pointed out in Part I and in Fig. 6. But it is also dependent upon microstructure, and microstructure is dependent to some degree on thickness and to a greater degree on rolling practice.

It is difficult to eliminate the effect of microstructure so that the effect of thickness can be isolated. The best approach would be to cut the 1/2 inch specimen, the 1 inch specimen, and the 2 inch specimen from a single 3-1/2 inch thickness. However, this is somewhat impractical for a large testing program. Even if this is done there may still exist a slight difference in microstructure because of the difference in cooling rate through the thickness of the 3-1/2 inch plate.

In the Lehigh tests the effect of thickness was considered as a single variable to include the effect of grain size coincident with the normal cooling rate of the plate after rolling to that particular thickness. The rolling practice was carefully controlled to eliminate variations in microstructure other than that due to cooling rate.

The three slabs were charged into the same furnace several hours prior to rolling and were brought to a uniform temperature, which varied between 2350 and 2400° F during the holding time. The slabs were then rolled into the finished plate in eleven drafts taking a total of 120 to 125 seconds from furnace to completion of the last pass. The finishing temperature at the surface varied from 1850° F for the 1/2 inch plate to 1940° F for the 2 inch plate. The rolling schedule is shown in Table 2.

The resulting grain structure for the three plates is quite similar, see Fig. 33. The ferritic grain size varies from 8 for the 1/2 inch plate to 6-1/2 for the center of the 2 inch plate. The grain size of the 1 inch plate varies from 7 at the center to 7-1/2 at the edge. Longitudinal and transverse grain size are the same in each plate.

9. Fatigue Crack Growth

Initial attempts at fatigue cracking indicated that unless a successful method of pre-cracking the specimens was found, the time required to grow the cracks would be too long to allow the testing of very many specimens. By using the following method of pre-cracking, fatigue cracks were grown within 1/2 to 1 hour of total fatiguing time.

A dab of sulfur and water paste was placed on the bottom center of the specimen. A 1/8 inch diameter stud was then resistance welded to the spot, taking care to weld through the sulfur-water paste. The resulting weld was so poor that the stud could usually be removed by tapping lightly with a hammer. When necessary, the studs were removed with a cold chisel.

Saw cuts were made on each side of the welds to produce a minimum section at the weld. These saw cuts are clearly evident in Fig. 67. The point of the saw cut was located at the fusion line of the weld, the point at which the largest weld micro-cracks might be found.

The specimens were placed in a 10 ton Amsler Vibrophore, a high frequency fatigue testing machine, and fatigued in three-point bending at a cycling rate of 10,000 cycles per minute. Two stages of fatiguing were used: crack start and crack growth. The crack starting stage was simply to develop a growing crack. The only limitation was the capacity of the machine or the crack growth rate which could be controlled. In the subsequent crack growth stage the loading was controlled to provide a crack growth rate equal to that suggested by ASTM Committee E24, a rate of .050 inch in 50,000 cycles.[30] This rate was usually maintained for the last 1/4 inch of crack growth.

The loads, span lengths, crack growth rates, and the maximum K value for the last few cycles of crack growth are shown in Table 3 for each specimen tested. All fatiguing was done at room temperature.

Even though the crack growth rate was within the .050 inch in 50,000 cycles recommended for high strength steels (200 ksi yield or greater), the maximum level of K in the last stage of crack growth was higher than the test value of K_c for the specimens broken at the lowest temperatures. Although it is preferable to fatigue at a K level greater than K_c of the test, the results do not seem to have been adversely affected by this expedient.

10. Fatigue Crack Growth Rate

Fatigue crack growth rate of steels was discussed in Section 9, Part II. Crack growth of a few specimens was monitored during fatiguing to determine if the growth rate could be estimated by the $(\Delta K)^4$ rule.[8]

The crack growth was averaged over 1/16 inch intervals and the maximum and minimum value of K for the average crack length of the interval were used to determine ΔK. K was calculated in the usual manner, including a plasticity adjustment factor in the effective length of the crack. The crack growth data is presented in Table 4.

The results, which are plotted in Fig. 34, indicate that the fatigue crack growth rate of this steel can be represented by the expression:

$$\frac{da}{dN} = 2 \times 10^{-12} (\Delta K)^4$$

where $\frac{da}{dN}$ is the crack growth per cycle in inches, and ΔK is the difference between the maximum and the minimum K in units of ksi $\sqrt{in}$.

11. Impact K_c from Unpadded Specimens

Initial attempts at determining K_c from impact tests consisted of dropping the weight from ten feet, as is common for drop weight tear testing. Although the load records looked good, showing a single large spike at the point of fracture (see Fig. 26) K_c values computed from these tests were far too high. When the drop height was lowered, the apparent value of the maximum load decreased and a second, lower peak was revealed (see Fig. 26). Further reduction of the drop height decreased the first peak but did not alter the second peak. This indicated that the first peak was primarily the result of inertia and did not represent the load felt by the specimen. The second peak, because of its constant nature, was taken to be indicative of the load in the specimen and the maximum value of the second peak was taken as the fracture load.

The height of the drop was kept as low as possible and still be sufficient to break the specimen. A 6 inch drop was usually sufficient.

Data for these tests is presented in Table 5. The load records can be seen in Fig. 41. The resulting K_c, K_{Ic}, and r_Y values are plotted in Figs. 45, 46, and 47 for the 1/2 inch specimens and in Figs. 51, 52, and 53 for the 1 inch specimens.

12. Impact K_c from Padded Specimens

By placing an aluminum pad on the specimen at the point of contact with the loading tup, the loading rate was slowed sufficiently to produce a smooth loading record apparently free of inertia effects (see p. 174). These loading rates were about one-fifth as fast as for the unpadded tests. Because of inertia effects in the unpadded tests, the rate of application of bending moment in the padded tests was about 2/3 that of the unpadded tests.

A 1/4 inch high half-round aluminum pad cut from a 1/2 inch round bar was used as the pad. The grade of aluminum was usually 6061-T6, but at warmer temperatures 6061-T6 became too soft and the tup bottomed out before fracture, making the load record difficult to interpret. For these higher temperatures 2024-T6 aluminum was used. For the high fracture loads of the 2 inch specimens at warm temperatures, it was necessary to use 7075-T6 aluminum. The harder 7075 alloy did not provide as smooth a record as the others because it tended to fracture during load.

Drop heights of one to four feet were used for the padded tests. Data for these tests is presented in Table 5. The load records can be seen in Fig. 41. The resulting K_c, K_{Ic}, and r_Y values are plotted in Figs. 45, 46, and 47 for the 1/2 inch specimens, in Figs. 51, 52, and 53 for the 1 inch specimens, and in Figs. 57, 58, and 59 for the 2 inch specimens.

13. Impact K_c from Instrumented Specimens

The load that is of interest in computing K_c is the load that the specimen feels at crack instability. At high loading rates, this may not be the same, at the instant of fracture, as the load recorded by the tup. To determine whether or not the tup record provides an adequate estimate of the load at fracture, a few specimens were gaged (see Fig. 35) and calibrated prior to testing. The gages were located far enough from the crack that the stress across the specimen was triangular and not effected by the discontinuity of the notch. Experimental calibration of these specimens indicated that normal beam theory could be used to determine the load from the strains recorded by the gages. The gages were mounted two in compression and two in tension, so that thermal stresses were self-compensating.

The dual trace capability of the scope was used to simultaneously record the load signal from the specimen gages and from the tup gages. K_c values were computed independently for the two records and compared. Data from these tests is presented in Table 5. The load records can be seen in Fig. 41. The resulting K_c, K_{Ic}, and r_Y values are plotted in Figs. 45, 46, and 47 for the 1/2 inch specimens, in Figs. 51, 52, and 53 for the 1 inch specimens, and in Figs. 57, 58, and 59 for the 2 inch specimens.

14. Static K_c Tests

In order to determine values of K_c for loading rates comparable to those that might be expected in bridge structures, a series

of tests were conducted on a standard tensile testing machine at Lehigh, a 120 kip Tinius-Olsen hydraulic testing machine, at a crosshead speed of 1 inch per minute.

Pops were occasionally noted in these load records (see Fig. 41). Since the specimens do not meet the requirements of ASTM E24 for plane strain testing, such pops do not necessarily indicate a plane strain movement of the crack front. For consistency in plotting the data, such records were considered to be K_c tests, but they may have been indicative of a plane strain rather than a plane stress behavior.

The same instrumentation was used to record load for the static tests as for the impact tests. The instrumented tup was mounted in the head of the testing machine and the load record was taken from the oscilloscope trace. Data for the static tests is presented in Table 5. The load records can be seen in Fig. 41. The resulting K_c, K_{Ic}, and r_Y values are plotted in Figs. 42, 43, and 44 for the 1/2 inch specimens, in Figs. 48, 49, and 50 for the 1 inch specimens, and in Figs. 54, 55, and 56 for the 2 inch specimens.

15. Dynamic K_{Ic} from Compression Tests

The static and impact Lehigh tests provide K_c values at two extremes of loading rate. To provide fracture data for intermediate loading rates, an indirect method was used based upon the relationship between K_{Ic} and ϵ_c developed by Krafft (see Part II, Section 10) A convenient way of obtaining ϵ_c versus $\dot{\epsilon}$ data is from simple tensile

or compression tests. The plastic region of the true stress versus true strain curve ($\bar{\sigma}$ versus $\bar{\epsilon}$) for steel can be approximated by a power function.[40]

$$\bar{\sigma} = A(\bar{\epsilon})^n \tag{61}$$

where A and n are material constants. n is called the strain hardening exponent. Taking the log of both sides and differentiating

$$\frac{d\bar{\sigma}}{\bar{\sigma}} = n \frac{d\bar{\epsilon}}{\bar{\epsilon}}$$

or

$$\bar{\theta} = \frac{d\bar{\sigma}}{d\bar{\epsilon}} = \frac{n\bar{\sigma}}{\bar{\epsilon}} \tag{62}$$

$\bar{\theta}$ is called the strain hardening rate.

At the instant of instability in a simple tensile specimen,

$$d F = 0$$

where F is the applied force. Then,

$$d F = d(A \bar{\sigma}) = A\, d \bar{\sigma} + \sigma\, d A = 0$$

where A is the cross sectional area. Thus

$$A\, d \bar{\sigma} = - \bar{\sigma}\, d A$$

$$\frac{d \bar{\sigma}}{\bar{\sigma}} = - \frac{d A}{A} \tag{63}$$

The true strain is

$$\bar{\epsilon} = \int_{\ell_o}^{\ell} \frac{d \ell}{\ell} = \ln \frac{\ell}{\ell_o} \tag{64}$$

Assuming constant volume:

$$A \ell = A_o \ell_o$$

or

$$\bar{\epsilon} = \ln \frac{A_o}{A}$$

differentiating,

$$d\,\bar{\epsilon} = - \frac{d\,A}{A} \tag{65}$$

From Eqs. 62, 63, and 65:

$$\bar{\theta} = \frac{d\,\bar{\sigma}}{d\,\bar{\epsilon}} = \bar{\sigma} \tag{66}$$

Thus, in a simple tensile test the critical strain $\bar{\epsilon}_c$ is the strain of the true stress-true strain curve where the slope

$$\bar{\theta} = \frac{d\,\bar{\sigma}}{d\,\bar{\epsilon}}$$

is equal to the true stress.

If one assumes that the shape of the true stress-true strain curve is the same from compression tests as from tension tests (except for the influence of local necking after $\bar{\epsilon}_c$ in the tensile test), the value of $\bar{\epsilon}_c$ for ligament fracturing can be determined from compression tests, which are more convenient for this purpose than tensile tests.

Small (1/2 inch diameter by 7/16 inch long) compression specimens were tested in an NRL dynamic universal testing machine at strain rates varying from 1×10^{-3} in./in. per second to 100 in./in. per second. The NRL dynamic universal testing machine is designed for the testing of small samples at high speed and constant loading rates. The machine and the test method is described in Ref. 41.

For a stable crack front, elongation of the failure ligament takes place isothermally. That is, the heat generated by the straining of the ligament is dissipated into the neighboring steel fast enough that the straining of the ligament occurs virtually at a constant temperature. This is not true, however, for moving cracks.[12]

To prevent the effect of adiabatic heating of the specimen at high strain rates, the specimens were loaded in a stepwise manner, applying approximately 2% strain in each step. The specimens were recooled to test temperature prior to each straining increment. By connecting the yield points of each loading increment, an isothermal stress-strain curve was produced. A typical oscilloscope record is shown in Fig. 36.

Krafft assumes a parabolic stress-strain curve and determines the critical strain from the value of the stress and strain at 3% strain of the engineering stress-strain curve. When this simplified method was applied to the Lehigh steel, a proper correlation between room temperature compression tests and room temperature tensile tests conducted at the same loading rate could not be obtained. The critical strain for the Lehigh steel was therefore obtained by first plotting the true stress-strain curve from the engineering stress-strain curve for each specimen.

The effect of barreling of the compression specimen was kept to a minimum by lubricating the top and bottom surfaces with a Teflon powder and was neglected in these computations. The method for obtaining the critical strain is shown in Fig. 36 and consists of

the following steps:

1. The engineering stress was converted to true stress. Since the volume remains constant during the test, for a compression test

$$A_o \ \ell_o = A(\ell_o - \Delta\ell)$$

from which

$$A = A_o \left(\frac{1}{1 - \epsilon}\right)$$

To find the true stress:

$$\bar{\sigma} = \frac{P}{A} = \frac{P(1 - \epsilon)}{A_o} = \sigma(1 - \epsilon) \qquad (67)$$

2. The engineering strain was converted to true strain:

$$\bar{\epsilon} = \ln \frac{A}{A_o} = \ln \left(\frac{1}{1 - \epsilon}\right)$$

For small values of the natural log,

$$\ln(1 - \epsilon)^{-1} = (1 + \frac{1}{2} \epsilon)$$

and

$$\bar{\epsilon} = \epsilon(1 + \frac{1}{2} \epsilon) \qquad (68)$$

3. The point on the true-stress true-strain curve where the slope of the curve is equal to the stress is the value of $\bar{\epsilon}_c$ (see Eq. 66)

$$\bar{\epsilon}_c = \bar{\epsilon} \Big|_{\bar{\theta} = \bar{\sigma}}$$

4. The above data was plotted as $\bar{\epsilon}_c$ versus $\dot{\epsilon}$, see Fig. 37. The loading rate was taken as the total strain of the test divided by the time to load:

$$\dot{\epsilon} = \frac{\epsilon_T}{t}$$

5. The results of the Lehigh impact and static tests at minus 40^{o} F were used to plot K_{Ic} versus $\dot{K}$, see Fig. 38. $\dot{K}$ was taken as the value of K at fracture divided by the time to fracture:

$$\dot{K} = \frac{K_c}{t}$$

6. A line was drawn on the curves of 4 and 5 for points where $\bar{\epsilon}_c/\dot{\epsilon} = 1$ and $K_{Ic}/\dot{K} = 1$.

7. The two sets of data were superimposed along the lines of $\bar{\epsilon}_c/\dot{\epsilon} = 1$ and $K_{Ic}/\dot{K} = 1$ until a good fit was obtained between the two. The best fit is obtained when

$$\frac{K_{Ic}}{\epsilon_c} = \frac{\dot{K}}{\dot{\epsilon}} = \frac{57.8 \text{ ksi } \sqrt{\text{in}}}{0.15 \text{ in./in.}} = 3.85 \times 10^2 \text{ ksi } \sqrt{\text{in}}$$

8. All the data points were then plotted as K_{Ic} versus $\dot{K}$, see Fig. 39.

Results of the critical strain tests, as shown in Fig. 39, indicate that testing speeds from static to ten times faster than the two-second loading time for the Lehigh "static" tests would not have caused a significant change in the K_{Ic} values.

The size of Krafft's instability ligament, see Fig. 22, can be determined from Eq. 48:

$$d_T = \frac{1}{2 \pi E^2} \left(\frac{K_{Ic}}{\epsilon_c}\right)^2 = 26.2 \times 10^{-6} \text{ inch}$$

This result is comparable to a d_T of 30.5×10^{-6} in. determined by Krafft for a linepipe steel of similar yield strength.

The compression tests provide an excellent opportunity to check the accuracy of Eq. 43 for estimating the yield strength of the steel at low temperature and high loading rates. The values of the yield stress from compression tests at minus 40^{o} F are compared in Fig. 67 with Eq. 43. The agreement is quite good.

16. Results of the Lehigh Tests

Load time oscilloscope records of the static and impact K_c tests are shown in Fig. 41. Records are presented for each thickness in order of increasing temperature to facilitate locating the corresponding data point in the tables and in the figures. These traces show the load versus time, with the trace moving from left to right. Some of the records show two traces. The second trace is the load recorded from strain gages mounted on the specimen. One of the traces shows a crack-wire record, which is described in Ref. 13.

Results of the static and impact K_c tests are plotted in Figs. 42 through 59. These plots show K_c, K_{Ic}, and r_Y as a function of temperature for the 1/2 inch, 1 inch, and 2 inch thick ASTM A441 steel. $K_c = K_{Ic} = 0$ at absolute 0 was used as an additional data point for plotting the faired curve. The plots of K_c versus temperature (Figs. 42, 45, 48, 51, 54, and 57) indicate additional information useful in interpreting the results:

1. The range of possible experimental error resulting from data measurement is shown as a dashed line above and below the faired curve.

2. The level of stress corresponding to 0.8 times the nominal yield stress and 1.2 times the nominal yield is shown. These are determined from the nominal stress at the notch tip using simple bending theory. The increased value of the yield stress from loading rate and temperature was used.

The results of the K_c and K_{Ic} tests are summarized in Figs. 60 through 63. Figures 60 and 61 show static K_c and K_{Ic} versus temperature. Figures 62 and 63 show impact K_c and K_{Ic} versus temperature.

In Figs. 64, 65, and 66 the static and impact values of r_Y are superimposed for each thickness. r_Y was chosen for this comparison because it is proportional to K_c^2 and thus reflects the fracture transition more sensitively then K_c and K_{Ic}. The temperature shift required to obtain the superposition is noted and was found to be:

60^o F for the 1/2 inch specimens
80^o F for the 1 inch specimens
100^o F for the 2 inch specimens

The results of the study of fatigue crack growth rate are presented in Fig. 34. It was found that the fatigue crack growth rate of the steel can be represented by:

$$\frac{da}{dN} \text{ (in./cycle)} = 2 \times 10^{-12} \left[\Delta K(\text{ksi}\sqrt{\text{in}})\right]^4$$

Figure 39 shows the matching of dynamic compression tests with K_{Ic} tests. The result is a plot of K_{Ic} versus loading rate for some eight orders of magnitude of loading rates.

Data for fatiguing the test specimens is presented in Table 3; data for the fracture tests, in Table 5. The specimens are listed by thickness in order of the temperature at which they were tested, so as to facilitate locating each data point on the corresponding plot.

Table 3, the fatigue crack history, shows mean load and the load range used for the two stages of fatigue crack growth. The growth rate for the last fraction of an inch listed is presented in terms of the average number of cycles to grow the crack 0.050 inches. The maximum value of K for the last few cycles of growth is also shown.

Table 5 lists the measured dimensions of the test sample, the experimental values of the load, loading time, and temperature, as well as the computed values of K_c, K_{Ic}, and r_Y for each specimen tested.

The fracture surface for each specimen is shown in Fig. 67. Clearly evident in these photographs are: the weld bead used to initiate the crack; the saw cut used to intensify the stress at the point of initiation of the crack; and the two stages of fatigue crack growth. Some of the specimens did not break in two. These were removed from the test fixture after the test, cooled to a sufficient temperature, and broken open. Where this has been done, the point of stopping of the crack can be determined by noting the configuration of the shear lips at the edges of the crack.

SUMMARY AND CONCLUSIONS

The objective of this report was to demonstrate the feasibility of applying the methods of fracture mechanics to steel bridges. The lack of well-defined testing standards for the crack toughness of structural steel and the stress analysis complexities of cracks in actual bridge structures were formidable difficulties. However, the progress reported here was enough to permit the desired demonstration.

Crack toughness measurement techniques were developed and used to establish static and impact K_c and K_{Ic} values for a typical 50,000 psi yield bridge steel in three plate thicknesses (ASTM A441 steel in thicknesses of 1/2 inch, 1 inch, and 2 inches). The measurement techniques are valid provided the plastic zone size is not greater than about 1/2 inch for the specimen tested. Above this level the calculation of K_c does not converge and a condition of general yielding exists at the crack front.

Sufficient fracture data is presented for the ASTM A441 plates tested to enable a fracture analysis of any structure built with this plate material, provided the geometry of the structure is such that a calculation of K can be made, provided the loading rate and temperature are known, and provided the crack size is known.

The data indicates that the difference between static and impact tests is equivalent to a temperature shift of

60^{o} F for the 1/2 inch plate
80^{o} F for the 1 inch plate
100^{o} F for the 2 inch plate

The results of the fracture tests compare favorably with the work of others:

1. The A441 plate was found to have an instability ligament size of $d_T = 26.2 \times 10^{-6}$ inch. This compares well with the value of $d_T = 30.5 \times 10^{-6}$ inch that Krafft reports for a 3/8 inch line pipe steel of similar yield strength.[41]

2. The K_c data for the 1/2 inch A441 plate is compared to the drop weight tear test data for the same steel in Ref. 13. The 1/2 inch A441 plate was found to have a 50% FATT (Fracture Appearance Transition Temperature) of 80^{o} F. This is equivalent to an NDT (Nil Ductility Temperature) of 20^{o} F. At this temperature, K_{Ic} can be approximated by

$$K_{Ic} = 0.78 \sqrt{in}\ \sigma_{YS}$$

Since the steel has a yield stress of 81 ksi at a loading time of 0.5 ms and a temperature of 20^{o} F, K_{Ic} can be estimated from the above equation as 63 ksi $\sqrt{in}$. The impact K_c data for the same steel at this temperature indicates a K_{Ic} of 58 ksi $\sqrt{in}$. The moderate difference between the two estimates is not significant in view of the approximate nature of the estimation procedure.

Estimates were developed for the K factor acting to cause unstable crack propagation of the relatively large flange crack in Girder W14-3 of the Kings Bridge at the time of fracture. These estimates were based on both static loading (with and without welding residual stress) and impact loading (with and without welding residual stress). Estimates of the probable crack toughness of the girder flange steel for both static and dynamic conditions were obtained through comparisons of the V-notch Charpy tests of the girder flange steel and the A441 plates used in the Lehigh fracture tests.

The K values calculated for the critical flange crack in the Kings Bridge were

1. Static, no residual stress: $K = 69$ ksi $\sqrt{in}$
2. Impact, no residual stress: $K = 67$ ksi $\sqrt{in}$
3. Static, with residual stress: $K = 97$ ksi $\sqrt{in}$
4. Impact, with residual stress: $K = 98$ ksi $\sqrt{in}$

The K_c estimates of the crack toughness for the temperature at which the bridge failed were:

1. Static $K_c > 125$ ksi $\sqrt{in}$
2. Impact $K_c \approx 70$ ksi $\sqrt{in}$

In view of the roughness of the contour of the leading edge of the flange crack, one would anticipate

a. The fracture roughness of the natural flange would tend to substantially elevate the effective K_c value.

b. Local regions of the leading edge of the flange crack would be expected to fracture abruptly prior to final instability.

From these considerations the K value estimates based upon zero residual stress must be regarded as too small, and the crack toughness assuming static loading must be regarded to too large. It is therefore considered that the sequence of events was as follows. The flange crack remained generally stable until the flange crack K value reached approximately 90 ksi $\sqrt{in}$. Studies of the flange crack and web crack interaction show that fatigue extension of the web crack provided a continuing substantial increase of the flange crack K value for a given live load on the structure. During loadings which were nearly large enough for crack propagation, abrupt crack motions along the irregular leading edge of the flange crack would be expected to occur. Each such event would cause a large increase of strain rate local to the affected region. Due to the increase of the K_c crack toughness by fracture surface roughening, abrupt local crack motions did not initiate general crack propagation until the value of K for the flange crack reached a value of 25 to 30 percent above the estimated dynamic K_c value for the material. This result is quite reasonable since comparable increases of K_c due to fracture surface roughening have been observed in laboratory testing.[42]

Development of a simplified plan for fracture control in structural steel bridges requires an understanding of the various possible mechanisms of fracture failure. The development of such a plan depends upon an ability to ascertain:

1. The fracture toughness K_c of bridge steels.
2. The growth rate of fatigue cracks in bridge steels.
3. A valid stress analysis of bridge members with flaw present.

From the results of this report, the crack toughness measurement problem is found to be relatively straightforward. The remaining uncertainities, such as the influence upon the crack toughness of the bluntness and roughness of real cracks, require realistic approximations.

There is much work to be done regarding the growth of cracks from fatigue and (possibly) from stress corrosion. The growth rate from fatigue of the steel studied in this investigation was found to be representable in an approximate manner by the equation

$$\frac{da}{dN} \text{ (in./cycle)} = 2 \times 10^{-12} \left[\Delta K \text{ (ksi } \sqrt{\text{in}})\right]^4$$

The validity of applying such a simplified approach to fatigue crack growth in real structures deserves additional study and verification.

The complexities of obtaining adequate knowledge of stresses in real structures are indeed formidable. However, the analysis of the three-ended crack studied in this report can be regarded as illustrative and this analysis was successfully accomplished.

This report includes a fracture analysis of the failure due to brittle fracture of the Kings Bridge at Melbourne. A plausible understanding in quantitative terms of the events which led to that fracture was obtained, thus providing assurance that the proposed fracture control plan is a reasonable approach for actual bridge structures.

SYMBOLS

a = crack length

a_c = critical crack length

a_T = tolerable flaw size

d_T = diameter of Krafft instability ligament

n = strain hardening exponent

r = radial polar coordinate from the crack tip

r_Y = plasticity adjustment factor, radius of the plastic zone

v = y-direction displacement

x,y = rectangular coordinates

z = complex coordinate $x + iy$

$\mathcal{G}$ = the Griffith strain energy release rate

K = stress intensity factor

K_c = critical stress intensity factor

K_I, K_{II}, K_{III} = Mode I, II, and III stress intensity factors

K_{Ic} = critical stress intensity factor for a thick plate

ϵ = strain

ϵ_c = critical strain

$\bar{\epsilon}$ = true strain

θ = angular polar coordinate from the crack plane

$\bar{\theta}$ = strain hardening rate

ν = Poisson's ratio

σ = nominal tensile stress

$\bar{\sigma}$ = true stress

σ_c = critical nominal tensile stress

σ_x, σ_y, σ_z = components of stress

σ_{YS} = uniaxial tensile yield stress

τ_{xy}, τ_{yx} = shear stresses

Δa = stable crack growth

ΔK = difference between maximum and minimum K during cyclic loading

$\frac{da}{dN}$ = crack growth per cycle

$(a+r_Y)$ = effective crack length

ms = millisecond, 1×10^{-3} sec

μs = microsecond, 1×10^{-6} sec

ns = nanosecond, 1×10^{-9} sec

FATT = Fracture Appearance Transition Temperature

TABLES AND FIGURES

TABLE 1 SUMMARY OF TENSILE DATA

1/2" Thick Material

Yield* Strength (psi)	Tensile Strength (psi)	% Elongation	Type of Test
59,400	88,000	21.0 in 8"	Mill Test
56,650	83,050	27.2 in 4"	Longitudinal Flat Tensile (ave. of 4 tests)
57,180	82,900	26.6 in 4"	Transverse Flat Tensile (ave. of 4 tests)

56,900 psi yield was used for computation purposes.

1" Thick Material

56,700	82,700	23.0 in 8"	Mill Test
55,900	82,300		Longitudinal .505 Bar (ave. of 4 tests)
55,010	82,200		Transverse .505 Bar (ave. of 4 tests)

55,500 psi yield was used for computation purposes.

2" Thick Material

54,000	81,000	26.0 in 2"	Mill Test
55,000	87,000	29.0 in 2"	Longitudinal .505 Bar (ave. of 2 tests)
49,100	85,600	26.0 in 2"	Transverse .505 Bar (ave. of 2 tests)

54,000 psi yield was used for computation purposes.

*0.2% Offset

TABLE 2 ROLLING SCHEDULE

Rolled - January 25, 1967

Furnace Temperature: 2350° F to 2400° F

Plate	1/2"	1"	2"
Initial Thickness	5"	6"	8"
Slab	11A	10C	9A
Draft #1	4-7/16*	5-1/2*	7-1/2*
#2	4	4-11/16	6-3/4
#3	3-1/2	4	6
#4	3	3-1/2	5-1/4
#5	2-1/2	3	4-1/2
#6	2	2-1/2	3-11/16
#7	1-1/2	2	3-1/8
#8	1-1/8	1-5/8	2-3/4
#9	13/16	1-3/8	2-3/8
#10	5/8	1-3/16	2-1/4
#11	9/16	1-1/8	2-1/8
Final Gage**	.0510	1.020	2.040
(Aim Gage)	.0506	1.015	2.030
Rolling Time*** (min:sec)	2:05	2:05	2:00
Finishing Temp.	1850° F	1900° F	1940° F

*As set in rolls

**As measured

***From furnace to end of last pass

TABLE 3a FATIGUE DATA

1/2" SPECIMENS - STATIC TESTS

Specimens Fatigued in 3-Point Bending, 7" Span

Test Temp.	Spec. Number	Fatigue Date	Mean Load (P) (kips)	Δ P (kips)	Crack Length in.	No. of Cycles x 10^{-3}	Final Ave. Growth Rate Cycles per .050"	Max. K ksi $\sqrt{in.}$
-85	L334-4	1/19/68	9.0	14.0	.625	57		
	Slow Growth →		9.0	4.4	.812	186	Last 1/8 @ 74,500 Last 1/16 @ 67,100	59.9
-61	L114-4	1/16/68	10.9	10.2	.815	(1)		
			8.9	4.7	1.067	114	Last 3/16 @ 30,400	64.0

(1) Counter not working properly.

TABLE 3(b) FATIGUE DATA

1/2" **SPECIMENS** - IMPACT TESTS

Specimens Fatigued in 3-Point Bending, 7" Span

Test Temp.	Spec. Number	Fatigue Date	Mean Load (P) (kips)	Δ P (kips)	Crack Length	No. of Cycles x 10^{-3}	Final Ave. Growth Rate Cycles per .050"	Max. K ksi $\sqrt{in.}$
-122	T121-4	1/18/68	10.9	10.6	.50	127		
	Slow Growth →		9.0	5.0	.775	209	Last 1/4" @ 42,000 Last 1/8" @ 40,000 Last 1/16" @ 45,000	53.9
-92	L622-3	1/18/68	10.9	10.2	.56	216		
			8.9	5.2	.765	427	Last 1/4" @ 85,000	47.6
-90	T211-4	1/17/68	11.1	9.6	.435	137		
			9.0(3)	5.2	.833	346(2)	Last 5/16" @ 55,400	57.2
-85	T611-3	1/18/68	10.9	10.6	.55	166		
			9.0(3)	5.0	.808	306	Last 17/64" @ 58,000	54.8
-40	L112-4	1/16/68	10.9	10.2	.815			
			8.9	4.6	.980	183	Last 5/32" @ 58,500	57.1
-39	L113-4	1/16/68	10.0	10.2	.60	217		
			9.1	5.8	.752	110	Last 9/64" @ 39,000	48.5
-39	L533-4	12/27/67	11.0	10.0	.60	186		
			9.0	5.4	.748	165	Last 3/16" @ 44,000	48.2
-34	T123-4	12/27/67	11.0	10.0	.60	295		
			9.0	5.4	.780	207	Last 5/32" @ 60,000	50.0
-33	T223-4	12/18/67	11.0	7.6	.60	558		
			9.0	5.4	.818	157	Last 5/32" @ 58,200	47.8

TABLE 3(b) FATIGUE DATA (continued)

1/2" SPECIMENS - IMPACT TESTS

Specimens Fatigued in 3-Point Bending, 7" Span

Test Temp.	Spec. Number	Fatigue Date	Mean Load (P) (kips)	Δ P (kips)	Crack Length (in.)	No. of Cycles x 10^{-3}	Final Ave. Growth Rate Cycles per .050"	Max. K ksi √in.
-32	L334-3	1/16/68	11.1	10.0	.545	(1)		
			9.0	4.8	.810	280(2)	Last 1/4" @ 55,000	54.9
-26	T411-4	3/11/68	11.1	9.6	.47	(1)		
			9.0	5.0	.778	235	Last 9/32" @ 42,000	54.0
-25	T213-4	12/2/67	11.0	10.0	.50	353+		
			9.0	5.4	.758	287	Last 1/4" @ 57,400	44.7
-25	T612-3	1/3/69	11.0	10.0	.53	196		
			9.0	5.2	.775	276	Last 13/64" @ 68,000	49.5
0	L333-4	1/16/69	11.1	10.0	.50	159		
			9.0	4.8	.75	352	Last 1/4" @ 70,500	46.3
0	T423-4	1/16/69	11.1	10.0	.485	154		
			9.0	5.0	.818	372	Last 9/32" @ 66,000	52.2
0	L331-4	12/27/68	11.0	10.0	.60	254		
			9.0	5.4	.768	137	Last 5/32" @ 44,000	48.1
2	T613-3	1/3/69	11.0	10.0	.72	152		
			9.0	5.2	.835	85	Last 1/16" @ 68,500	52.7
30	L511-4	1/18/69	11.0	10.0	.625	122		
			9.0(1)	5.0	.763	190	Last 1/8" @ 76,000 Last 1/16" @ 22,000	53.1
32	T433-4	1/16/69	11.1	10.0	.50	143		
			9.0	5.0	.753	305	Last 1/4" @ 61,000	48.8

(1) Counter not working properly.

(2) Counter not working properly; no. of cycles determined from time.

(3) Load point 1/4" off center.

TABLE 3(c) FATIGUE DATA

1" SPECIMENS - STATIC TESTS

Specimens Fatigued in 3-Point Bending, 9-1/2" Span

Test Temp.	Spec. Number	Fatigue Date	Mean Load (P) (kips)	Δ P (kips)	Crack Length (in.)	No. of Cycles x 10^{-3}	Final Ave. Growth Rate Cycles per .050"	Max. K ksi √in.
-112	T224-2	5/8/68	12.0	16.0	.625	262		
	Slow Growth →		12.0	6.0	1.015	868	Last 3/8" @ 115,000 Last 5/16" @ 91,000 Last 1/4" @ 86,500 Last 3/16" @ 82,600 Last 1/8" @ 71,400 Last 1/16" @ 64,900	55.1
-107	L512-3	6/14/68	10.4	19.2	.75	104		
			10.4	5.6(1)	1.037	757	Last 1/4" @ 151,000 Last 1/8" @ 55,500	46.1
-90	L523-2	5/7/68	12.0	16.0	.875	252		
			12.0	6.0	1.018	289	Last 1/8" @ 115,000	55.2
-60	L414-3	6/11/68	10.4	19.2	.75	168		
			10.4	6.8	1.045	307	Last 1/4" @ 61,300 Last 1/8" @ 51,500	52.1
-40	T232-2	1/22/68	12.0	16.0	.75	152		
			12.0	6.0	1.020	374	Last 1/4" @ 74,600 Last 1/32" @ 44,800	57.3
-39	L622-2	2/20/68	12.0	16.0	.935	154		
			12.0	6.0	1.060	172	Last 1/16" @ 57,600	58.1

TABLE 3(c) FATIGUE DATA (continued)

1" SPECIMENS - STATIC TESTS

Specimens Fatigued in 3-Point Bending, 9-1/2" Span

Test Temp.	Number	Fatigue Date	Mean Load (P) (kips)	Δ P (kips)	Crack Length (in.)	No. of Cycles x 10^{-3}	Final Ave. Growth Rate Cycles per .050"	Max. K ksi $\sqrt{in.}$
-20	L624-3	6/10/68	10.4	19.2	.75	146		
			10.4	6.4	1.045	(2)	Last 1/4" slow Last 1/8" @ 60,000(3)	51.2
0	T214-2	5/6/68	12.0	16.0	.875	175		
			12.0	6.0	1.048	196	Last 11/64" @ 56,200	57.3
1	L512-2	2/20/68	12.0	16.0(4)	.75	239		
			12.0	6.0	1.018	626	Last 1/4" @ 79,500 Last 3/16" @ 69,000 Last 1/8" @ 64,300 Last 1/16" @ 58,300	55.5
40	T614-2	5/22/68	12.0	16.0	.875	168		
			12.0	6.0	1.013		Last 1/8" @ 68,700	54.3
76	T434-2	5/8/68	12.0	16.0	.344	284		
	Medium Growth→		12.0	10.0	.813	112		
	Slow Growth→		12.0	6.0	1.015	315	Last 3/16" @ 84,000 Last 1/8" @ 94,500 Last 1/16" @ 84,000	55.1

(1) Raised ΔP to 6.0^k for last 1/8" of crack growth.

(2) Counter not working properly.

(3) Counter not working properly; no. of cycles determined from time.

(4) Load fell to 12^k during run.

TABLE 3(d) FATIGUE DATA

1" SPECIMENS - IMPACT TESTS

Specimens Fatigued in 3-Point Bending, 9-1/2" Span

Test Temp.	Spec. Number	Fatigue Date	Mean Load (P) (kips)	Δ P (kips)	Crack Length (in.)	No. of Cycles x 10^{-3}	Final Ave. Growth Rate Cycles per .050"	Max. K ksi $\sqrt{in.}$
-102	L623-2	2/19/68	12.0	16.0	.75	188		
	Slow Growth→		12.0	5.8	1.043	373	Last 1/4" @ 74,400 Last 3/16" @ 65,500 Last 1/8" @ 57,500 Last 1/16" @ 49,000	56.4
-99	L313-2	2/20/68	12.0	16.0	.75	191		
			12.0	5.8	1.068	219	Last 1/4" @ 40,800 Last 3/16" @ 37,000	58.2
-98	L532-2	5/1/68	12.0	16.0	.75	306		
			12.0	6.0	1.062		Last 1/4" slow Last 1/16" @ 56,000	59.0
-88	L131-2	1/20/68	12.0	16.0	.69	156		
			12.0	6.2	1.018	349	Last 5/16" @ 56,200 Last 3/16" @ 58,500 Last 1/8" @ 59,500 Last 1/16" @ 49,500	57.6
-42	L112-2	1/20/68	12.0	16.0	.75	130		
			12.0	6.8	1.075	250	Last 1/4" @ 50,000 Last 3/32" @ 25,000	62.8
-41	L322-2	1/20/68	12.0	16.0	.78	342		
			12.0	6.0	1.057	393	Last 7/32" @ 89,600	57.9

TABLE 3(d) FATIGUE DATA (continued)

1" SPECIMENS - IMPACT TESTS

Specimens Fatigued in 3-Point Bending, 9-1/2" Span

Test Temp.	Spec. Number	Fatigue Date	Mean Load (P) (kips)	Δ P (kips)	Crack Length (in.)	No. of Cycles x 10^{-3}	Final Ave. Growth Rate Cycles per .050"	Max. K ksi √in.
-40	L534-2	2/20/68	12.0	16.0	.75	220		
			12.0	6.0	1.008	442	Last 1/4" @ 88,500 Last 3/16" @ 75,000 Last 1/8" @ 64,800 Last 1/16" @ 66,500	54.6
-40	L312-2	2/20/68	12.0	16.0	.75	240		
			12.0	5.8	1.025	471	Last 1/4" @ 94,400 Last 3/16" @ 84,400 Last 1/8" @ 92,400 Last 1/16" @ 74,000	55.2
-39	L134-2	1/22/68	12.0	16.0	.655	132		
			12.0	6.0	1.00	507	Last 11/32" @ 67,500 Last 1/4" @ 62,500 Last 1/16" @ 52,800	58.0
-39	T211-3	5/6/68	12.0	16.0	.875	150		
			12.0	6.0	1.092	197	Last 1/8" @ 79,000	60.5
-38	T233-2	1/22/68	12.0	16.0	.75	195		
			12.0	6.0	1.045	336	Last 1/4" @ 67,000 Last 3/16" @ 54,000 Last 1/8" @ 50,000 Last 1/16" @ 46,600	59.1

TABLE 3(d) FATIGUE DATA (continued)

1" SPECIMENS - IMPACT TESTS

Specimens Fatigued in 3-Point Bending, 9-1/2" Span

Test Temp.	Spec. Number	Fatigue Date	Mean Load (P) (kips)	Δ P (kips)	Crack Length (in.)	No. of Cycles x 10^{-3}	Final Ave. Growth Rate Cycles per .050"	Max. K ksi $\sqrt{in.}$
-38	T612-2	5/4/68	12.0	16.0	.875	211		
			12.0	6.0	1.035	293	Last 1/8" @ 117,000	56.4
-37	L514-2	2/19/68	12.0	16.0	.765	160		
			12.0	5.6	1.025	188	Last 1/4" slow Last 1/16" @ 57,500	48.8
-30	T422-2	5/8/68	12.0	16.0	.94	271		
			12.0	6.0	1.08	187	Last 1/16" @ 149,000	57.7
-19	T632-2	5/2/68	12.0	16.0	.81	245		
			12.0	6.0	1.015	368	Last 3/16" @ 95,400 Last 1/8" @ 75,500 Last 1/16" @ 70,500	55.1
0	L524-2	5/6/68	12.0	16.0	.875	248		
			12.0	6.0	1.047	172	Last 1/8" @ 68,600	57.2
0	L624-2	2/20/68	12.0	16.0	.81	171		
			12.0	5.8	1.045	308	Last 3/16" @ 82,300 Last 1/8" @ 70,400 Last 1/16" @ 77,500	56.6
1	L314-2	2/20/68	12.0	16.0	.81	146		
			12.0	5.6	1.003	272	Last 3/16" @ 72,500 Last 1/8" @ 66,000	53.4

TABLE 3(d) FATIGUE DATA (continued)

1" SPECIMENS - IMPACT TESTS

Specimens Fatigued in 3-Point Bending, 9-1/2" Span

Test Temp. °F	Spec. Number	Fatigue Date	Mean Load (P) (kips)	Δ P (kips)	Crack Length (in.)	No. of Cycles x 10^{-3}	Final Ave. Growth Rate Cycles per .050"	Max. K ksi √in.
1	T234-2	1/22/68	12.0	16.0	.75	167		
			12.0	6.0	1.023	303	Last 1/4" @ 60,500 Last 3/16" @ 52,500 Last 1/8" @ 56,000 Last 1/16" @ 52,500	58.2
10	T121-2	1/22/68	12.0	16.0	.685	135		
			12.0	6.0	1.075	419	Last 5/16" @ 67,000 Last 1/4" @ 56,000 Last 3/16" @ 57,000 Last 1/8" @ 51,500 Last 1/16" @ 46,400	61.4
+30	L521-2	2/19/68	12.0	16.0	.75	158		
			12.0	5.8	1.058	253	Last 1/4" @ 50,500 Last 3/16" @ 42,000 Last 1/16" @ 39,200	57.5
+30	L324-2	2/19/68	12.0	16.0	.86	235		
			12.0	5.8	1.085	139	Last 1/8" @ 39,200 Last 1/16" @ 39,200	60.1
+38	L522-2	5/2/68	12.0	16.0	1.125	305		
			12.0	6.0	1.295	125	Last 1/8" @ 50,000	83.3

TABLE 3(d) FATIGUE DATA (continued)

1" SPECIMENS - IMPACT TESTS

Specimens Fatigued in 3-Point Bending, 9-1/2" Span

Test Temp. °F	Spec. Number	Fatigue Date	Mean Load (P) (kips)	Δ P (kips)	Crack Length	No. of Cycles x 10^{-3}	Final Ave. Growth Rate Cycles per .050"	Max. K ksi √in.
+39	T613-2	5/2/68	12.0	16.0	.81	267		
			12.0	6.0	1.018	252	Last 3/16" @ 67,300	55.2
+57	L531-2	5/7/68	12.0	16.0	.875	257		
			12.0	6.0	1.017	201	Last 1/8" @ 80,300	56.5
+58	L513-2	5/4/68	12.0	16.0	.875	242		
			12.0	6.0	1.040	252	Last 1/8" @ 101,000	58.0
+80	T231-2	1/22/68	12.0	16.0	.765	161		
			12.0	6.0	1.065	284	Last 17/64" @ 53,500 Last 3/16" @ 42,600 Last 3/32" @ 36,800	58.5

TABLE 3(e) FATIGUE DATA

2" SPECIMENS - STATIC TESTS

Specimens Fatigued in 3-Point Bending, 11" Span

Test Temp. ^{o}F	Spec. Number	Fatigue Date	Mean Load (P) (kips)	Δ P (kips)	Crack Length (in.)	No. of Cycles x 10^{-3}	Final Ave. Growth Rate Cycles per .050"	Max. K ksi $\sqrt{in.}$
-112	L622-3	5/30/68	11.0	19.2	.75	755		
	Slow Growth→		11.0	12.3	1.080	177	Last 1/4" @ 35,400	34.5
-90	L531-3	5/29/68	11.0	18.0	.875	501		
			11.0	12.2	1.080	34	Last 1/8" @ 13,600	44.5
-40	L522-3	5/27/68	11.0	18.0	.78	1437		
			11.0	11.2	1.060	426	Last 1/4" @ 85,400	33.0
-40	T632-3	5/30/68	11.0	18.0	.81	1035		
			11.0	11.4	1.005	286	Last 3/16" @ 76,400	31.5
-4	L513-3	5/29/68	11.0	18.0	.75	1453		
			11.0	12.4	1.067	205	Last 1/4" @ 41,500	35.8
20	L623-3	5/29/68	11.0	18.0	.75	1175		
			11.0	12.2	.952	455	Last 1/4" @ 91,000	30.7
40	L532-3	5/29/68	11.0	18.0	1.10	1402	No Slow Growth	44.9
82	L624-3	5/30/68	11.0	18.0	1.265	755	No Slow Growth	50.8

TABLE 3(f) FATIGUE DATA

2" SPECIMENS - IMPACT TESTS

Specimens Fatigued in 3-Point Bending, 11" Span

Test Temp. °F	Spec. Number	Fatigue Date	Mean Load (P) (kips)	Δ P (kips)	Crack Length (in.)	No. of Cycles x 10^{-3}	Final Ave. Growth Rate Cycles per .050"	Max. K ksi √in.
-43	T634-3	6/12/68	10.8	20.0	1.125	325	No Slow Growth	54.7
-38	L533-3	5/27/68	11.0	18.0	.69	1143		
	Slow Growth→		11.0	18.0	1.073	114	Last 5/16" @ 18,200	43.5
0	T612-3	5/28/68	11.0	18.0	.75	1175		
			11.0	12.4	1.033	256	Last 1/4" @ 51,300	34.0
39	L511-3	5/31/68	11.0	20.2	.75	1205		
			11.0	11.8	1.062	476	Last 1/4" @ 95,000	29.1
39	T611-3	6/12/68	10.8	18.4	.875	221		
			10.8	11.2	1.391	110	Last 3/8" @ 15,700	54.8
40	T613-3	5/28/68	11.0	18.0	.75	1147		
			11.0	12.0	1.016	409	Last 1/4" @ 82,000	32.0

TABLE 4 FATIGUE CRACK GROWTH RATE DATA

All Specimens are 1" Thick

Specimens Fatigued in 3-Point Bending, 9-1/2" Span

Spec. Number	Ave. Crack Length in 1/64's a	Change in Crack Length in 1/64's Δa	No. of Cycles $\times 10^{-3}$ N	Growth per Cycle in/cycle $\times 10^{7}$ da/dN	Mean Load (kips)	Max. Load (kips)	Spec. Depth (in.)	Max. K ksi $\sqrt{in.}$
T224-2	46.0	4.0	135	4.63	12	15	2.88	16.96
	49.9	3.8	122	4.87	12	15		18.15
	53.8	4.0	135	4.63	12	15		19.46
	57.9	4.2	94	6.98	12	15		20.94
L511-2	48.0	16.0	68.1	36.7	12	18	2.88	35.49
	62.0	4.0	139	4.51	12	15.2		24.19
T434-2	40.0	4.0	9.0	69.4	12	20	2.88	41.60
	50.0	4.0	35	17.87	12	17		30.51
	58.0	4.0	121.4	5.16	12	15		20.96
	61.5	3.0	105.2	4.46	12	15		22.42
T632-2	48.5	7.0	12.7	86.3	12	20	2.88	48.34
	62.5	3.0	113	4.15	12	15		22.89
T411-2	41.0	8.0	32.4	38.6	12	18	2.87	31.78
	58.0	4.0	105.5	5.95	12	15		21.18
	62.0	4.0	95.7	6.53	12	15		22.94

TABLE 5(a) FRACTURE DATA

1/2" SPECIMENS - STATIC TESTS

Item	Symbol	Units		
Temperature	T	^{o}F	-85	-61
Specimen Number	No		L334-4	L114-4
Test Date	Date		7/10/68	7/10/68
Height of Pad	Pad	inch	0	0
Drop Height	Drop	feet	0	0
Specimen Width	B	inch	1/2	1/2
Specimen Depth	W	inch	2.69	2.91
Crack Length	a_o	inch	.812	1.067
Fracture Load	P	kip	8.5	8.3
Dynamic Yield	σ_{YS}	ksi	73.38	70.73
Plastic Zone Radius	r_Y	inch	.128	.152
Fracture Toughness	K_c	ksi $\sqrt{in}$	66.09	69.15
Plane Strain K_c	K_{Ic}	ksi $\sqrt{in}$	49.10	49.45
Remarks (see below)				1

[1] The crack front was at an angle of 70^{o} to the specimen $\mathcal{L}$ (instead of 90^{o}). As a result, the fracture values obtained should be somewhat low for the material.

TABLE 5(b) FRACTURE DATA

1/2" SPECIMENS - IMPACT TESTS

Item	Symbol	Units									
Temperature	T	^{o}F	-112	-92	-90	-85	-40	-39	-39	-34	-33
Specimen Number	No.		T121-4	L622-3	T211-4	T611-3	L112-4	L113-4	L533-4	T123-4	T223-4
Test Date	Date		3/12/68	2/22/68	4/19/68	4/19/68	2/22/68	2/15/68	1/11/68	2/1/68	12/18/67
Height of Pad	Pad	inch	1/4	1/4	0	0	1/4	1/4	0	0	0
Drop Height	Drop	feet	4	4	1/2	1/2	4	4	1	1	1
Specimen Width	B	inch	1/2	1/2	1/2	1/2	1/2	1/2	1/2	1/2	1/2
Specimen Depth	W	inch	2.78	2.90	2.795	2.80	2.915	2.92	2.89	2.885	2.98
Crack Length	a_o	inch	.775	.765	.833	.808	.980	.752	.748	.780	.818
Fracture Load	P	kip	6.70	8.20	7.30	8.00	8.00	8.50	12.00	9.00	9.69
Dynamic Yield	σ_{YS}	ksi	102.15	97.68	98.40	97.47	88.48	88.69	90.03	89.66	88.92
Plastic Zone Radius	r_Y	inch	.0272	.0369	.0382	.0452	.0645	.046	.103	.058	.064
Fracture Toughness	K_c	ksi $\sqrt{in}$	42.33	47.14	48.35	52.11	56.32	47.97	72.62	54.03	56.19
Plane Strain	K_{Ic}	ksi $\sqrt{in}$	39.11	42.45	43.39	45.96	47.54	42.20	56.52	46.28	47.50
Remarks (see below)	Rem		1			2				3	

[1] Temperature was measured from dry ice reference. As a result, temperature accuracy only about $\pm 10^{o}$ F.

[2] Temperature measured from similar test at similar time from dry ice to fracture. Temperature accuracy only about $\pm 5^{o}$ F.

[3] A crack propagation gage was mounted on specimen with the first wire at the tip of the crack.

[4] Strain gages were mounted on the specimen to record bending moment. Values shown under Tup are determined from the loading tup in the normal manner. Values shown under Beam are determined from the gages mounted on the specimen.

[5] Trace did not return to zero, but the zero change probably occurred after fracture.

[6] Fracture was arrested. Specimen was later cooled and broken open.

TABLE 5(b) FRACTURE DATA (continued)

1/2" SPECIMENS - IMPACT TESTS

Symbol										
T	-32	-26	-25	-25	0	0	0	2	30	32
No.	L334-3	T411-4	T213-4	T612-3	L333-4	T423-4	L331-4	T613-3	L511-4	T433-4
Date	3/11/68	3/11/68	12/13/67	2/2/68	2/5/68	2/2/68	2/2/68	2/5/68	2/22/68	2/22/68
Pad	1/4	1/4	0	1/4	1/4	0	0	1/4	3/8	1/2
Drop	4	4	2	4	4	1	1	4	4	4
B	1/2	1/2	1/2	1/2	1/2	1/2	1/2	1/2	1/2	1/2
W	2.79	2.78	2.99	2.88	2.915	2.86	2.915	2.88	2.78	2.86
a_o	.810	.778	.758	.775	.760	.818	.768	.835	.763	.753
	Tup / Beam									
P	7.50 / 8.00	8.00	8.67	10.0	12.5	12.5	13.0	12.0	13.0	14.8
σ_{YS}	86.95 / 89.62	86.27	87.36	84.95	81.07	85.09	85.09	80.91	79.77	79.32
r_Y	.0514 / .0559	.0580	.0451	.0828	.1465	.1678	.1457	.1718	.249	.315
K_c	49.63 / 53.16	52.14	46.65	61.36	77.91	87.46	81.53	84.16	100.20,	111.7
K_{Ic}	43.10 / 45.72	44.62	41.15	49.74	56.17	60.99	58.87	58.32	62.50	64.68
Rem	4								5 & 6	

TABLE 5(c) FRACTURE DATA

1" SPECIMENS - IMPACT TESTS

Symbol	Units											
T	^{o}F	-112	-107	-90	-60	-40	-39	-20	0	1	40	76
No.		T224-2	L512-3	L523-2	L414-3	T232-2	L622-2	L624-3	T214-2	L512-2	T614-2	T434-2
Date		5/21/68	7/10/68	5/22/68	7/10/68	5/22/68	5/22/68	7/10/68	5/22/68	5/22/68	5/22/68	5/22/68
Pad	inch	0	0	0	0	0	0	0	0	0	0	0
Drop	feet	0	0	0	0	0	0	0	0	0	0	0
B	inch	1	1	1	1	1	1	1	1	1	1	1
W	inch	2.88	2.93	2.88	2.87	2.85	2.88	2.87	2.88	2.875	2.89	2.88
a_o	inch	1.015	1.0375	1.018	1.045	1.020	1.060	1.045	1.048	1.018	1.013	1.015
P	kip	12.5	11.7	14.0	15.0	17.0	16.5	20.8	14.5	23.0	19.5	22.0
σ_{YS}	ksi	78.54	74.98	73.13	68.92	67.38	67.67	64.56	63.86	63.55	60.75	58.50
r_Y	inch	.055	.0503	.0852	.1316	.1946	.1810	.449	.1451	.47	.437	.491
K_c	ksi $\sqrt{in}$	46.45	42.33	53.65	62.78	74.56	72.21	109.00	60.32	109.00	105.00	103.00
K_{Ic}	ksi $\sqrt{in}$	42.85	39.31	47.67	52.78	58.72	57.64	55.50	50.16	55.00	52.60	50.90
Rem		1			2			3	4	3	3&4	3,4,5

[1] Temperature measured from similar test at similar time from dry ice to fracture. Temperature accuracy only about $\pm 5^{o}$ F.

[2] Thermocouple was only 1/4" deep. Actual temperature may have been lower.

[3] Value of K_c did not converge. Consequently r_Y, K_c, and K_{Ic} values shown are a lower bound. Actual value is considerably greater.

[4] This was a "pop-in". The K_c value shown may indicative of a K_{Ic} for the material.

[5] This data is not shown on the plots.

TABLE 5(d) FRACTURE DATA

1" SPECIMENS - IMPACT TESTS

Symbol	Units											
T	^{o}F	-102	-99	-98	-88	-42	-41	-40	-40	-39	-39	-38
No.		L623-2	L313-2	L532-2	L131-2	L112-2	L322-2	L534-2	L312-2	L134-2	T211-2	T233-2
Date		4/15/68	4/15/68	6/25/68	4/16/68	4/18/68	6/26/68	4/19/68	4/18/68	4/18/68	6/25/68	4/19/68
Pad	inch	1/4	1/4	1/4	0	1/4	0	0	1/4	3/8	1/4	1/4
Drop	feet	4	4	1	1/2	4	1/2	1/2	2	4	1	1
B	inch	1	1	1	1	1	1	1	1	1	1	1
W	inch	2.88	2.88	2.87	2.85	2.86	2.88	2.88	2.88	2.86	2.88	2.85
a_o	inch	1.043	1.068	1.0625	1.018	1.075	1.0575	1.008	1.025	1.040	1.092	1.045
P	kip	10.5	10.0	10.5	12.3	13.0	13.5	13.7	12.3	13.0	10.0	11.7
σ_{YS}	ksi	96.62	95.73	96.95	96.62	87.54	88.12	88.03	86.77	87.68	87.00	86.34
r_Y	inch	.0258	.0249	.0271	.0362	.0562	.0558	.0517	.0437	.0516	.0320	.0437
K_c	ksi $\sqrt{in}$	38.96	37.95	40.07	46.22	52.07	52.22	50.42	45.65	50.15	39.09	45.41
K_{Ic}	ksi $\sqrt{in}$	37.47	36.54	38.46	43.78	48.00	48.16	46.73	42.78	46.29	37.25	42.56
Rem						1	2				2	

[1] The fatigue crack was grown somewhat fast: 25,000 cycles for the last 1/8". K_c value may be slightly high.

[2] Strain gages were mounted on the specimen to record bending moment. These gages failed prematurely because of a poor bond.

TABLE 5(d) FRACTURE DATA (continued)

1" SPECIMENS - IMPACT TESTS

Symbol	Units									
T	^{o}F	-38	-37	-30	-19	0	0	+1	+1	+10
No.		T612-2	L514-2	T422-2	T632-2	L524-2	L624-2	L314-2	T234-2	T121-2
Date		8/13/68	4/19/68	8/14/68	8/13/68	6/22/68	4/19/68	4/19/68	4/19/68	4/15/68
Pad	inch	0	1/4	1/4	0	0	1/4	1/4	1/4	3/8
Drop	feet	1/2	1	1	1/2	1/2	1	1	1	2
B	inch	1	1	1	1	1	1	1	1	1
W	inch	2.88	2.86	2.88	2.88	2.88	2.88	2.88	2.84	2.88
a_o	inch	1.035	1.025	1.055	1.015	1.047	1.045	1.003	1.023	1.075
				Tup	Beam					
P	kip	12.8	11.5	12.00	13.72	14.5	17.0	15.0	13.75	12.0	16.5
σ_{YS}	ksi	87.53	86.66	84.98	87.35	84.77	82.61	80.83	80.60	80.71	81.85
r_Y	inch	.0477	.0394	.046	.058	.065	.109	.0842	.0643	.0521	.1192
K_c	ksi $\sqrt{in}$	48.12	43.25	45.89	53.09	54.39	68.53	58.90	50.91	46.39	70.92
K_{Ic}	ksi $\sqrt{in}$	44.85	40.75	42.87	48.78	49.53	59.11	52.36	46.49	42.97	60.47
Rem		3	4	5							

[3] Strain gages were mounted on the specimen to record bending moment. The trace is not legible at fracture.

[4] Test specimen was lost. No photo of fracture surface is available.

[5] Strain gages were mounted on the specimen to record bending moment. Values shown under "Tup" are determined from the loading tup in the normal manner. Values shown under "Beam" are determined from the gages mounted on the specimen. The slow crack growth rate was much slower than normal.

TABLE 5(d) FRACTURE DATA (continued)

1" SPECIMENS - IMPACT TESTS

Symbol	Units							
T	^{o}F	+30	+30	+38	+39	+57	+58	+80
No.		L521-2	L324-2	L522-2	T613-2	L531-2	L513-2	T231-2
Date		4/20/68	4/20/68	8/14/68	8/14/68	6/26/68	6/26/68	4/20/68
Pad	inch	1/4	1/4	1/4	1/4	1/4	0	1/4
Drop	feet	1	1	2	2	2	1	1
B	inch	1	1	1	1	1	1	1
W	inch	2.88	2.87	2.89	2.88	2.86	2.86	2.88
a_o	inch	1.058	1.085	1.295	1.018	1.0175	1.040	1.065
P	kip	17.7	17.7	12.7	18.0	23.5	20.5	18.0
σ_{YS}	ksi	76.91	77.07	77.31	76.25	74.82	77.05	72.45
r_Y	inch	.1515	.1672	.1142	.1459	.446	.2193	.2087
K_c	ksi $\sqrt{in}$	75.09	79.10	65.57	73.05	125.30	90.51	83.02
K_{Ic}	ksi $\sqrt{in}$	61.79	64.02	56.23	60.48	64.30	69.62	64.50
Rem		6		7		8	6	9

[6] This was a "pop-in". The K_c value shown mya be indicative of a K_{Ic} for the material.

[7] The crack was 25% longer than normal for a 1" specimen.

[8] Computations done graphically for r_Y, K_c, and K_{Ic} values shown are a lower bound.

[9] This data is not shown on the plots.

TABLE 5(e) FRACTURE DATA

2" SPECIMENS - STATIC TESTS

Symbol	Units								
T	°F	-112	-90	-40		-40	-4	+20	+40	+82
No.		L622-3	L531-3	L522-3		T632-3	L513-3	L623-3	L532-3	L624-3
Date		7/10/68	7/8/68	7/8/68		7/10/68	7/8/68	7/10/68	7/8/68	7/8/68
Pad	inch	0	0	0		0	0	0	0	0
Drop	feet	0	0	0		0	0	0	0	0
B	inch	2	2	2		2	2	2	2	2
W	inch	2.95	2.70	2.94		2.94	2.90	2.94	2.94	2.94
				Pop	Fracture					
a_o	inch	1.08	1.08	0.96	1.06	1.005	1.067	.9525	1.160	1.265
P	kip	22.2	19.8	23.0	34.3	28.5	31.0	41.1	35.5	36.5
σ_{YS}	ksi	73.54	70.96	65.51	64.95	65.26	61.97	59.98	58.68	56.05
r_Y	inch	.0496	.0714	.0596	.2217	.1003	.1922	.3932	.454	.435
K_c	ksi $\sqrt{in}$	41.22	47.61	40.11	76.70	51.94	68.15	94.33	99.20	93.10
K_{Ic}	ksi $\sqrt{in}$	39.68	45.13	38.35	66.04	48.26	59.68	74.15	50.60	48.20
Rem		1		2				3	4	4&5

[1] Temperature measured from similar test at similar time from dry ice to fracture. Temperature accuracy only about ±5° F. There may have been a slight "pop" prior to fracture. It has been ignored in these computations.

[2] This was a "pop-in". The K_c value shown may be indicative of a K_{Ic} for the material. Crack extension from the "pop" is difficult to see on the fracture surface; it appeared to be 0.1 in. max.

[3] Load was corrected for a 7% high voltage reading.

[4] No slow fatigue crack growth, which would cause the value of K_c to be high; but the fatigue crack is at a 5° slant which would cause the value of K_c to be low.

[5] Value of K_c did not converge. Consequently r_Y, K_c, and K_{Ic} values shown are a lower bound.

TABLE 5(f) FRACTURE DATA

2" SPECIMENS - IMPACT TESTS

Symbol	Units							
T	^{o}F	-43		-38	0	+39	+39	+40
No.		T634-3		L533-3	T612-3	L511-3	T611-3	T613-3
Date		8/14/68		8/15/68	8/15/68	9/30/68	9/27/68	9/27/68
Pad	inch	1/4		1/4	1/4	1/4	1/4	1/4
Drop	feet	2		2	2	2	2	2
B	inch	2		2	2	2	2	2
W	inch	2.86		2.88	2.92	3.109	2.828	2.953
a_o	inch	1.208		1.073	1.033	1.0625	1.3910	1.016
			Tup	Beam				
P	kip	18.7	21.4	30.7	28.8	33.0	25.50	31.0
σ_{YS}	ksi	84.88	83.56	84.98	78.16	72.31	74.45	74.22
r_Y	inch	.039	.039	.085	.075	.0913	.2525	.0916
K_c	ksi $\sqrt{in}$	42.18	41.55	62.27	53.80	54.87	93.87	56.41
K_{Ic}	ksi $\sqrt{in}$	40.93	40.32	58.45	50.86	51.28	79.35	52.72
Rem		1&2		3&4			5&6	

[1] Thermocouple only 1/8" deep. Temperature reading may be as much as 10^{o} high.

[2] No slow fatigue crack growth. This should cause the value of K_c to be high.

[3] Strain gages were mounted on specimen to record bending moment. Values under "Tup" determined from the loading tup in the normal manner. Values shown under "Beam" determined from gages mounted on the specimen.

[4] The fatigue crack was grown somewhat fast: 18,000 cycles for the last 5/16". K_c value may be somewhat high.

[5] Fatigue crack is about 30% deeper than normal.

[6] Slow growth rate 3 times faster than normal.

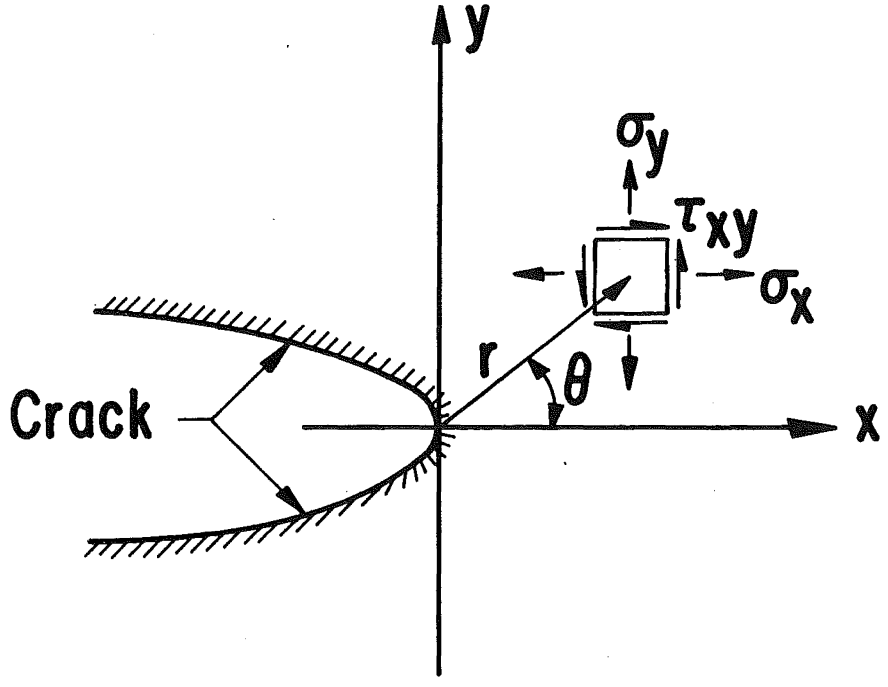

Fig. 1 THE CRACK TIP STRESS FIELD

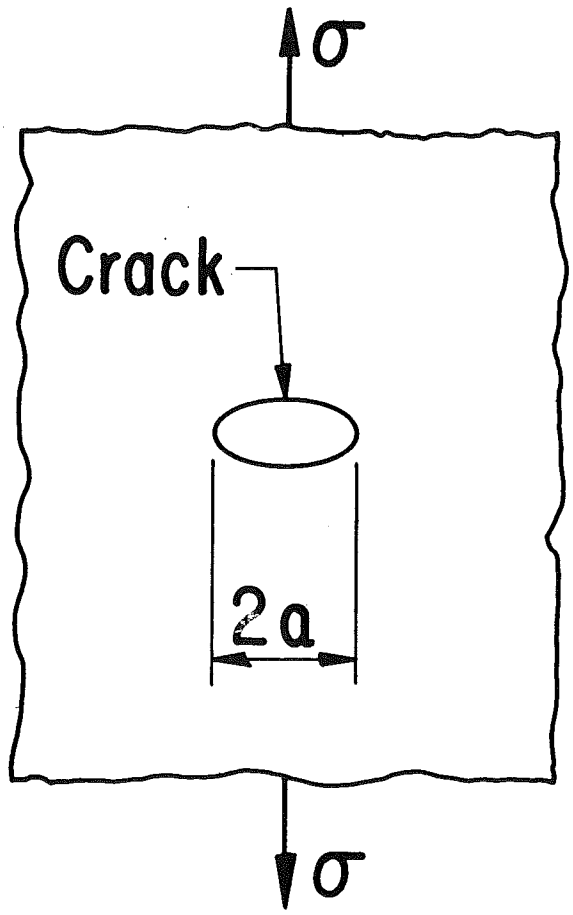

$$K = \sigma \sqrt{\pi a}$$

Fig. 2 CENTER CRACK IN AN INFINITE PLATE

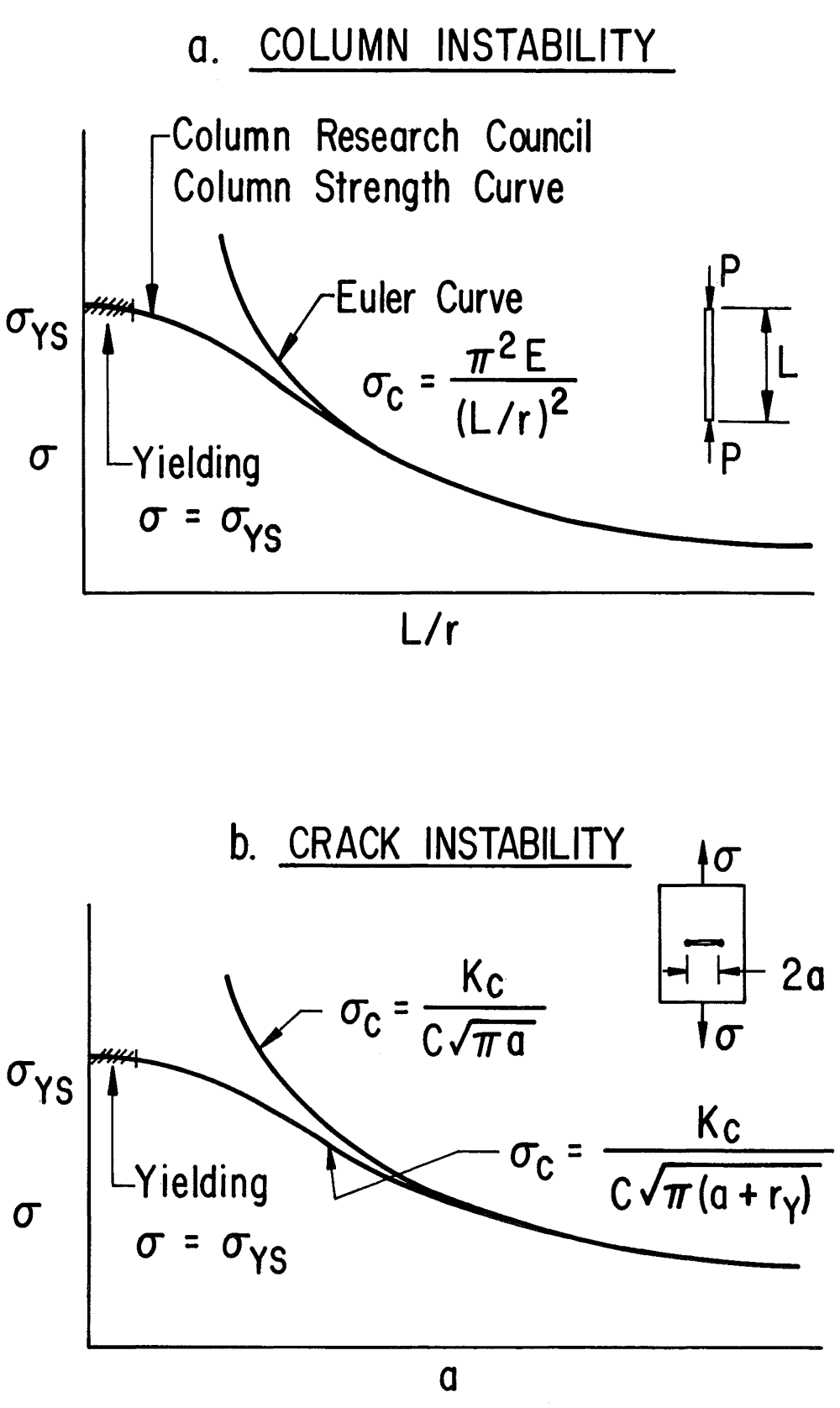

Fig. 3 COLUMN INSTABILITY AND CRACK INSTABILITY

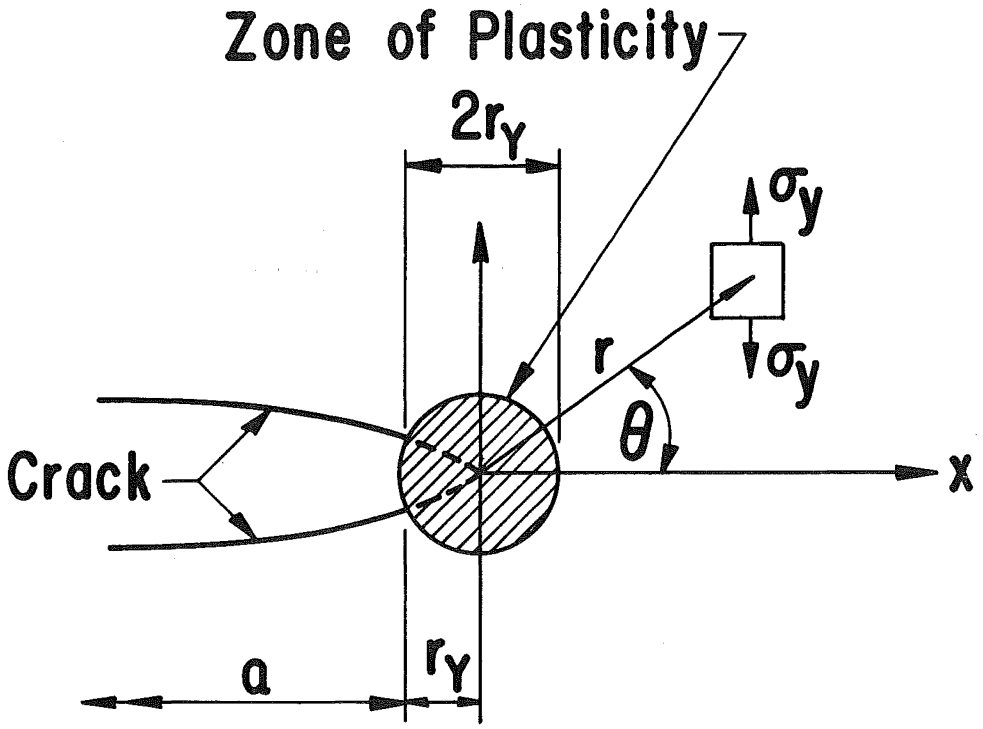

$$r_Y = \frac{1}{2\pi}\left(\frac{K}{\sigma_{YS}}\right)^2$$

Fig. 4 THE ZONE OF PLASTICITY

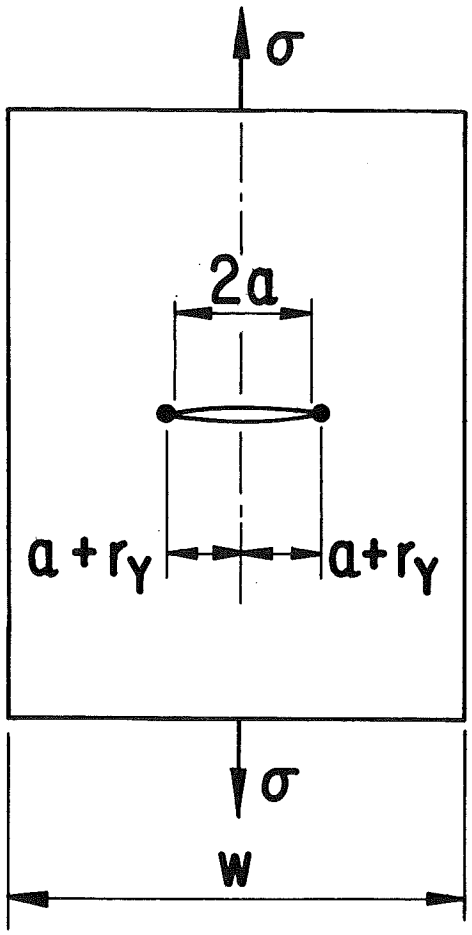

$$K = C\sigma\sqrt{\pi(a + r_Y)}$$

Where:

$$C = \sqrt{\sec\frac{\pi(a + r_Y)}{W}}$$

Fig. 5 CENTER CRACK IN A FINITE-WIDTH PLATE

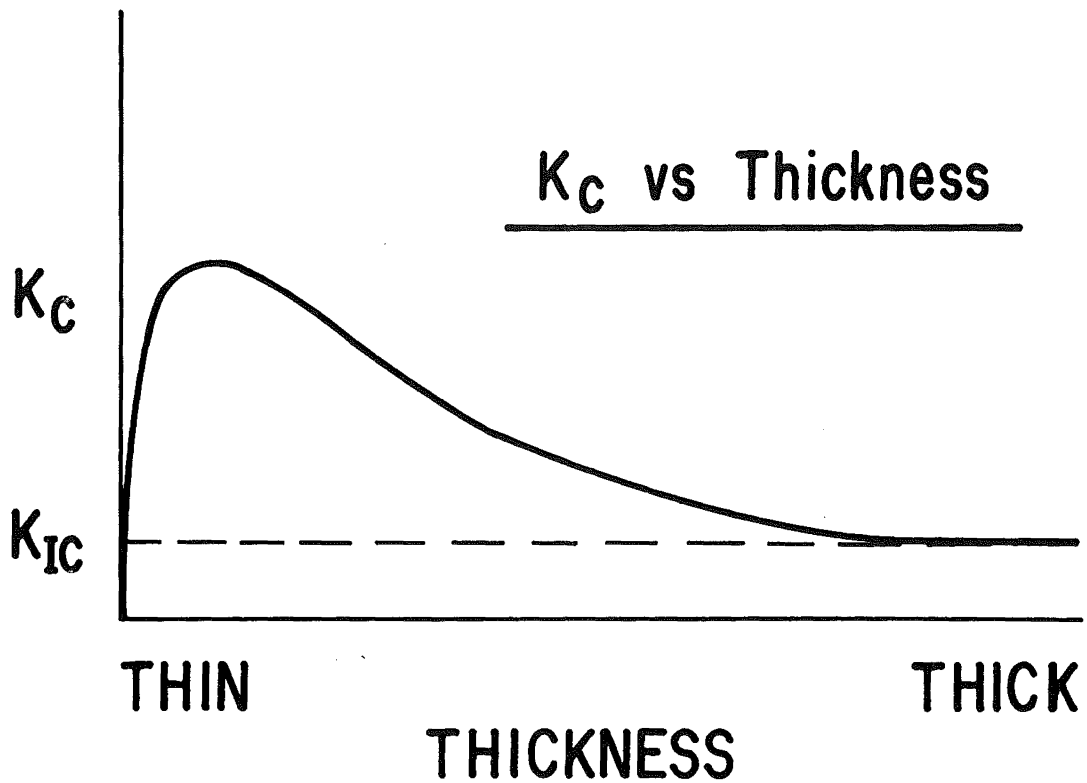

Fig. 6 THE VARIATION OF K_c WITH THICKNESS

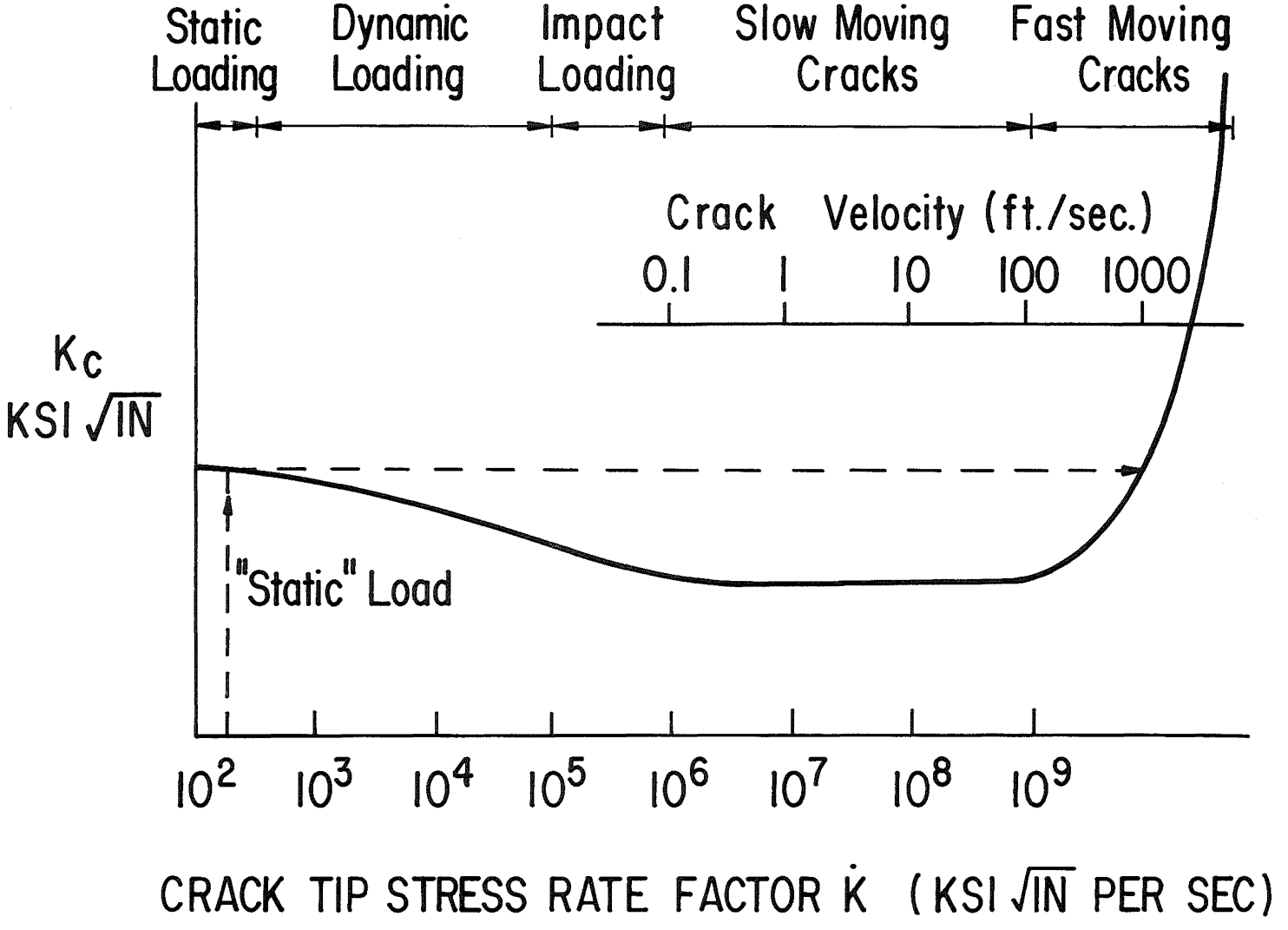

Fig. 7 THE VARIATION OF K_c WITH LOADING RATE

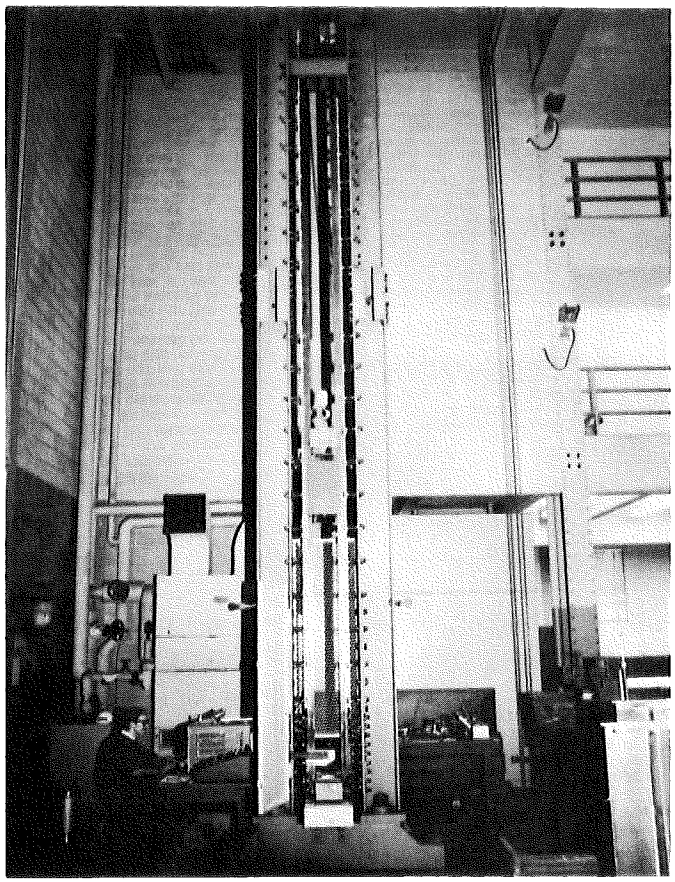

Fig. 8 THE LEHIGH IMPACT TEST MACHINE

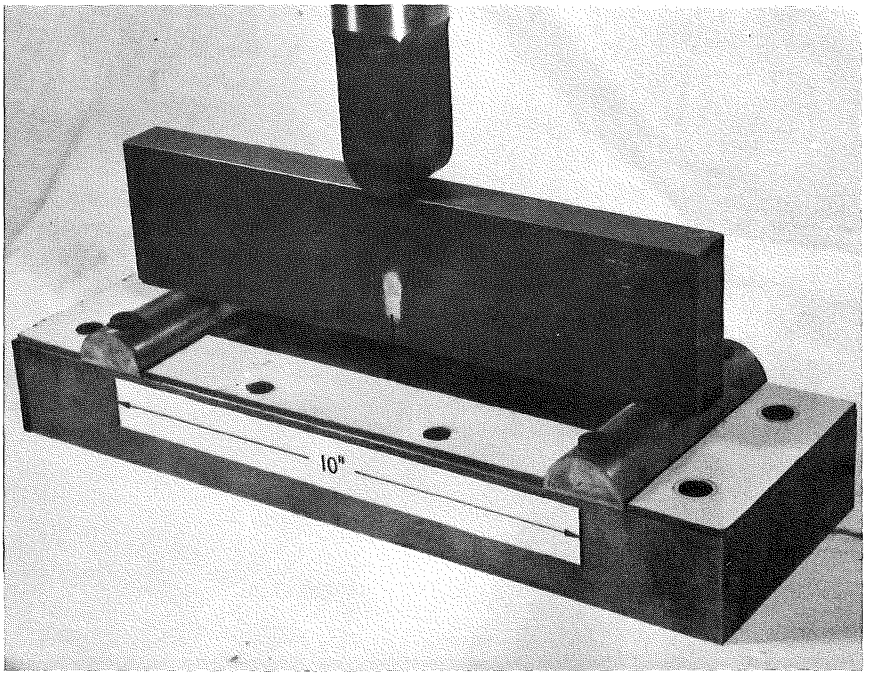

Fig. 9 THE TEST SPECIMEN

CROSS SECTION OF THE
WEST PORTION OF SPAN #14

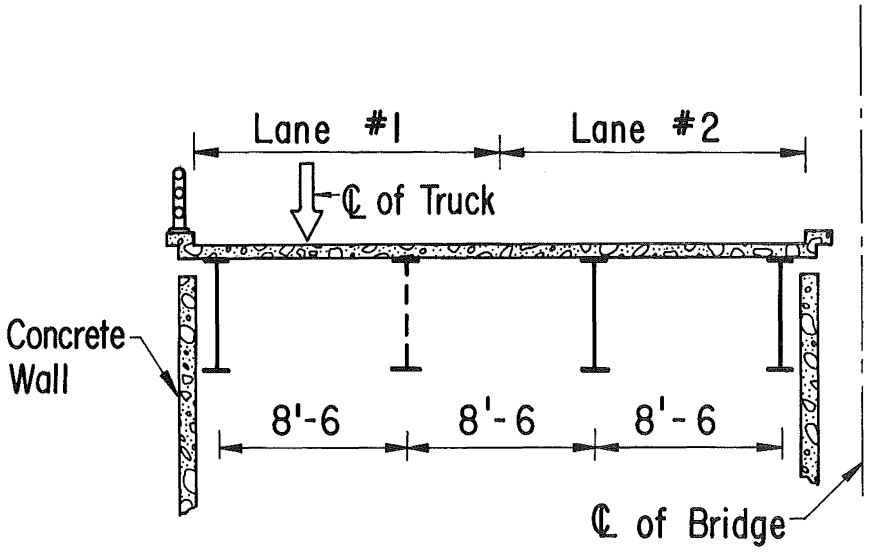

LONGITUDINAL SECTION OF SPAN W14

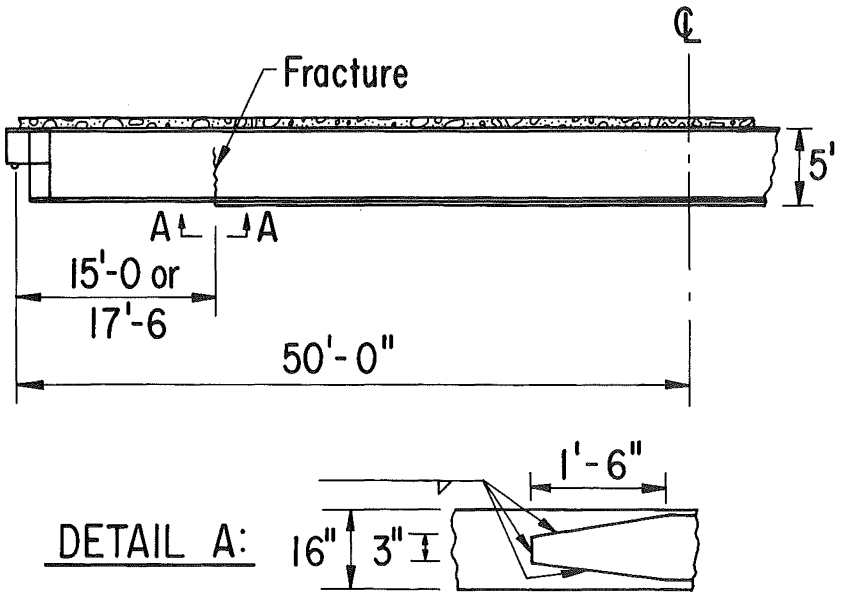

Fig. 10 THE FAILED SPAN OF KINGS BRIDGE

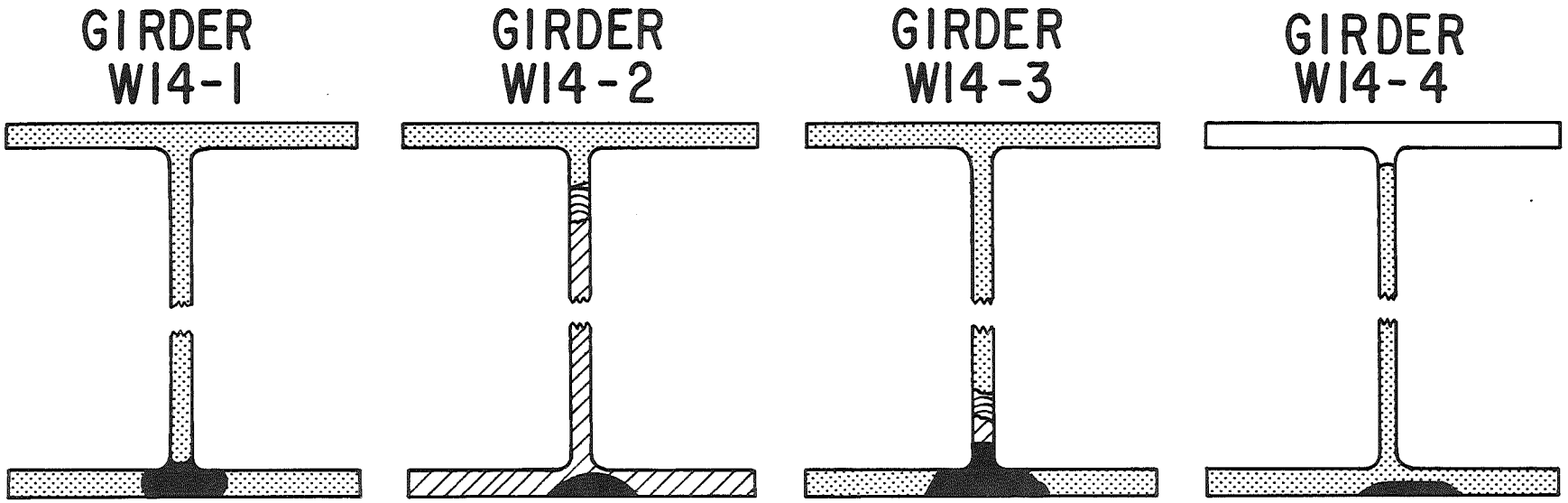

Fig. 11 CONDITION OF THE FAILED GIRDERS OF KINGS BRIDGE

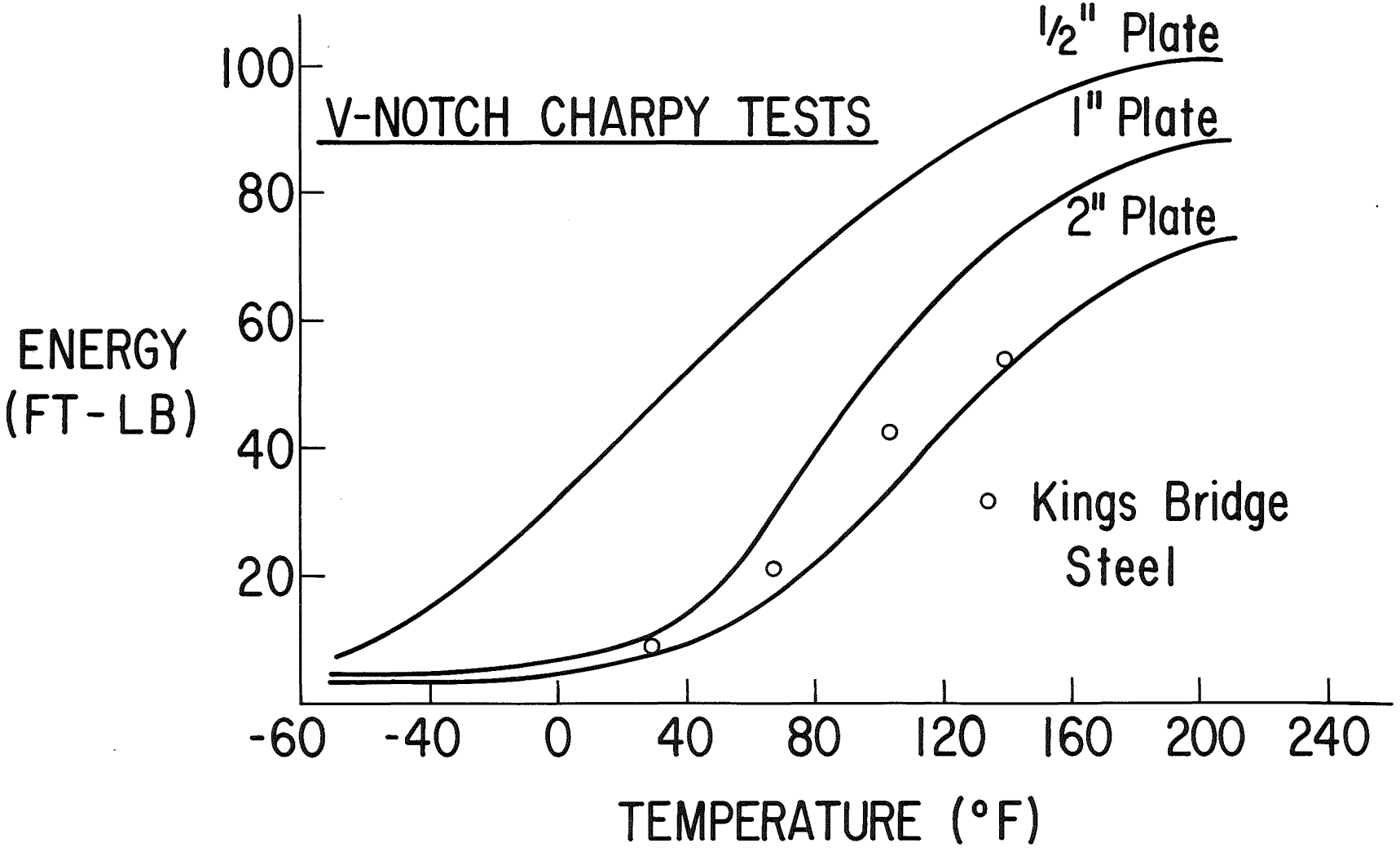

Fig. 12 RESULTS OF LONGITUDINAL CHARPY TESTS

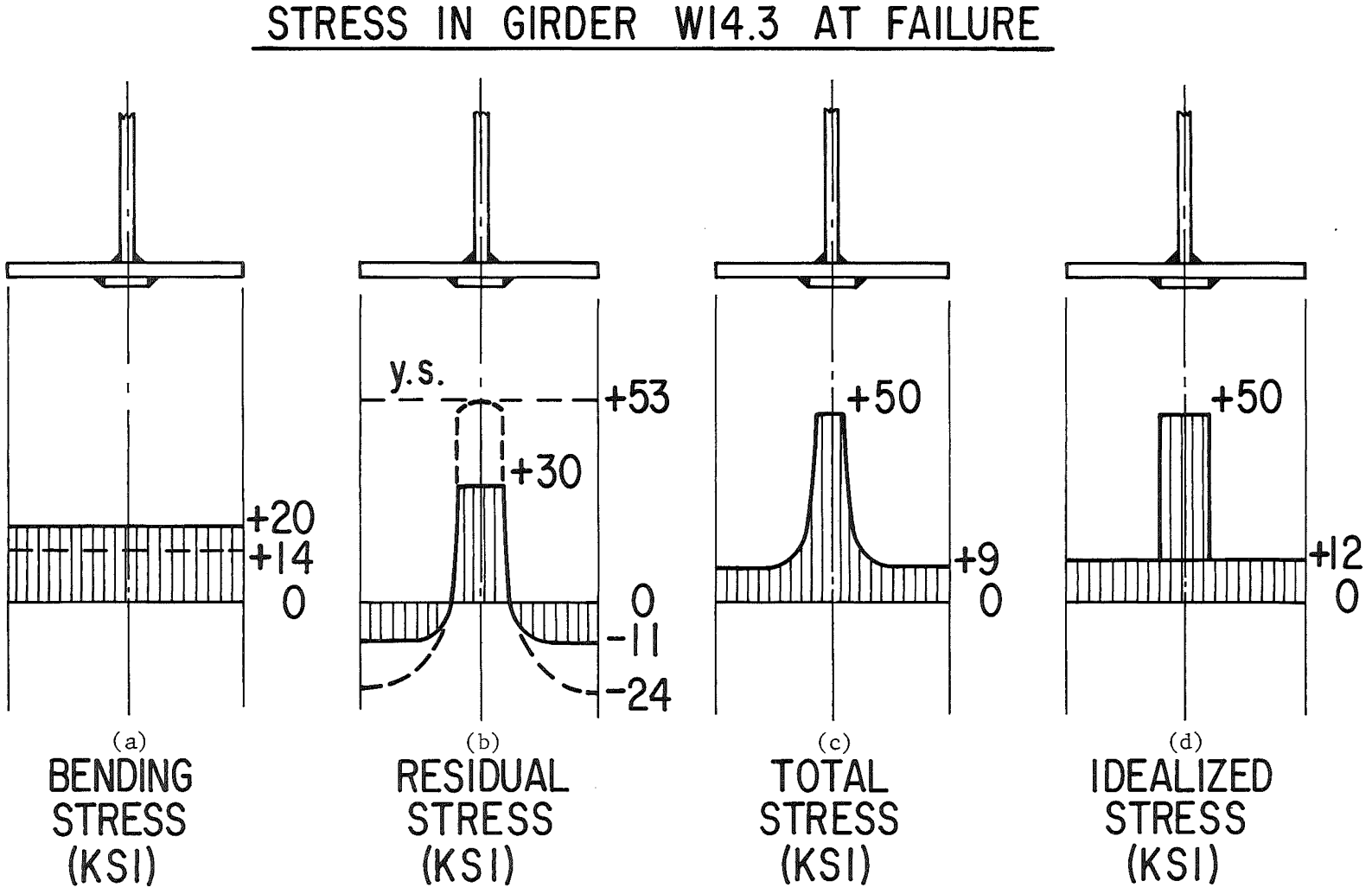

Fig. 13 STRESSES IN THE BOTTOM FLANGE OF GIRDER W14-3 AT THE TIME OF FAILURE

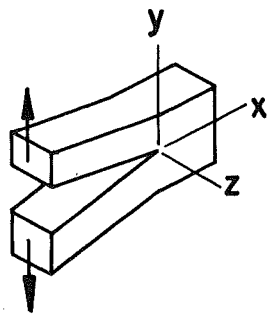

a. Mode I Fracture

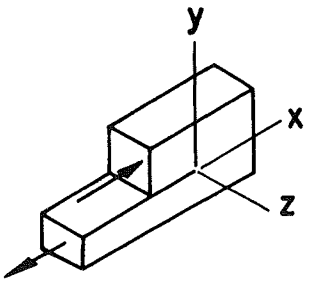

b. Mode II Fracture

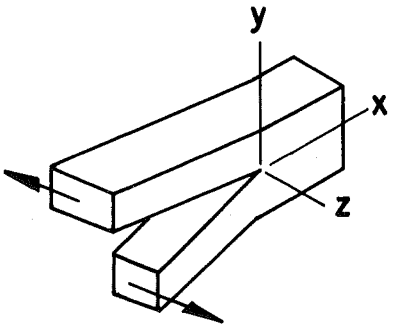

c. Mode III Fracture

Fig. 14 THE THREE BASIC FRACTURE MODES

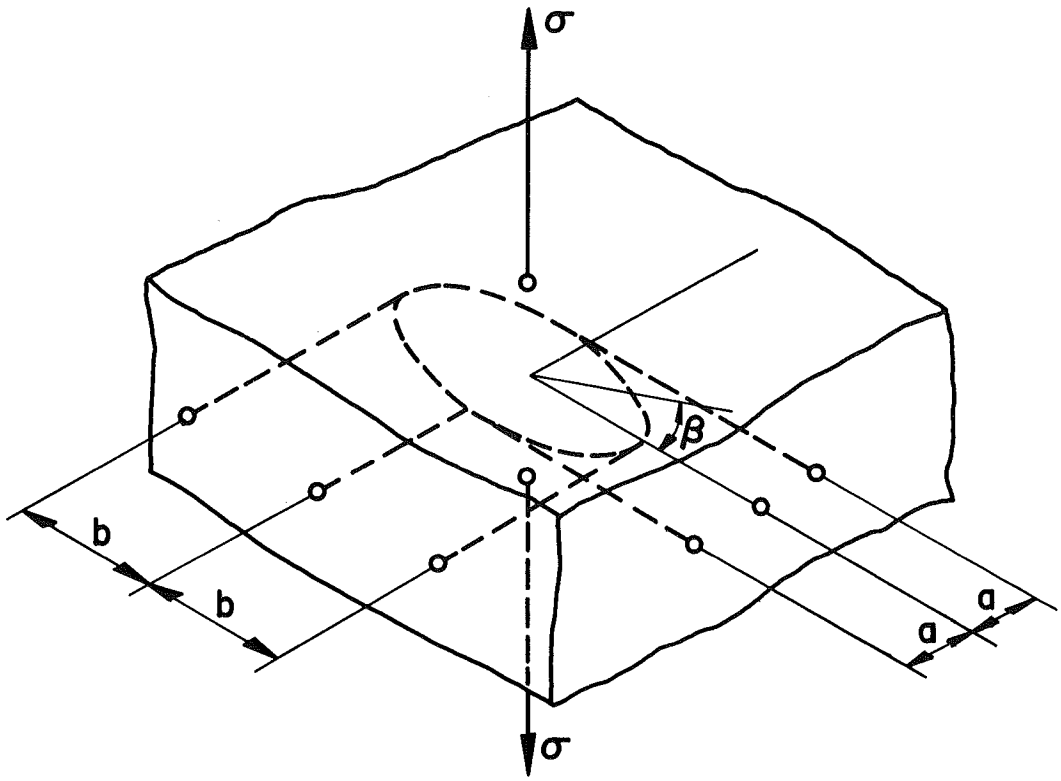

Fig. 15 AN ELLIPTICAL CRACK IN AN INFINITE BODY SUBJECTED TO UNIFORM TENSION

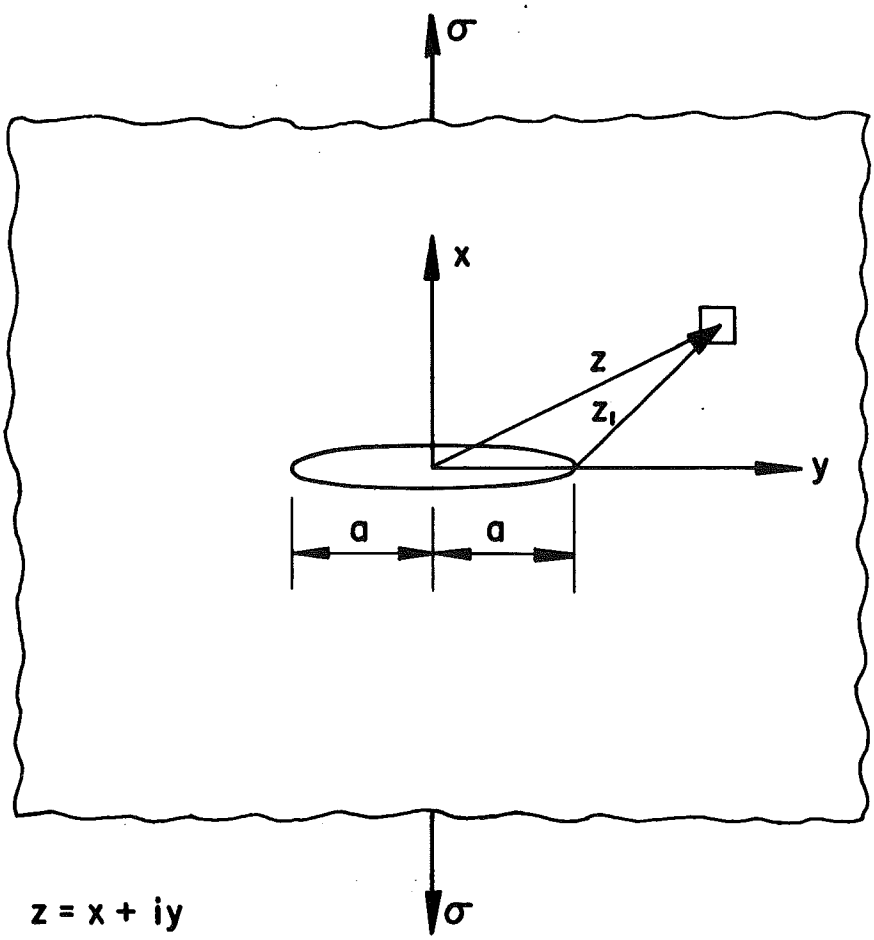

Fig. 16 CENTER CRACK IN AN INFINITE PLATE

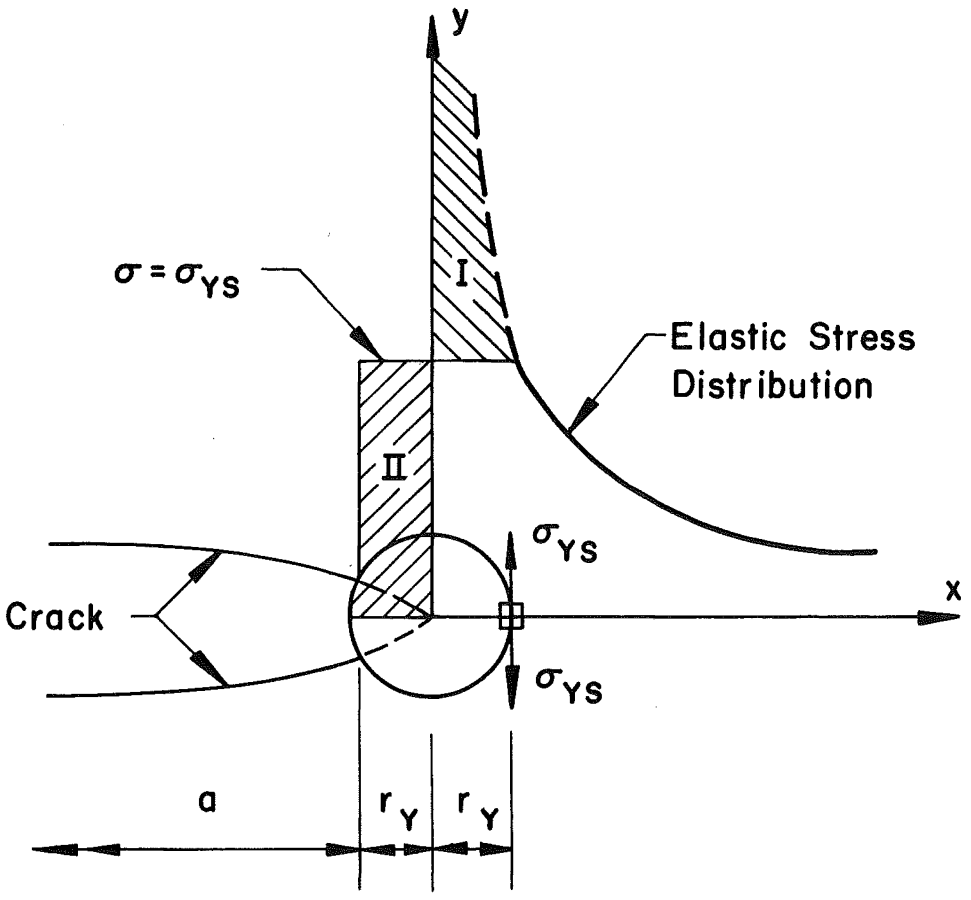

Fig. 17 STRESS DISTRIBUTION AT THE ZONE OF PLASTICITY

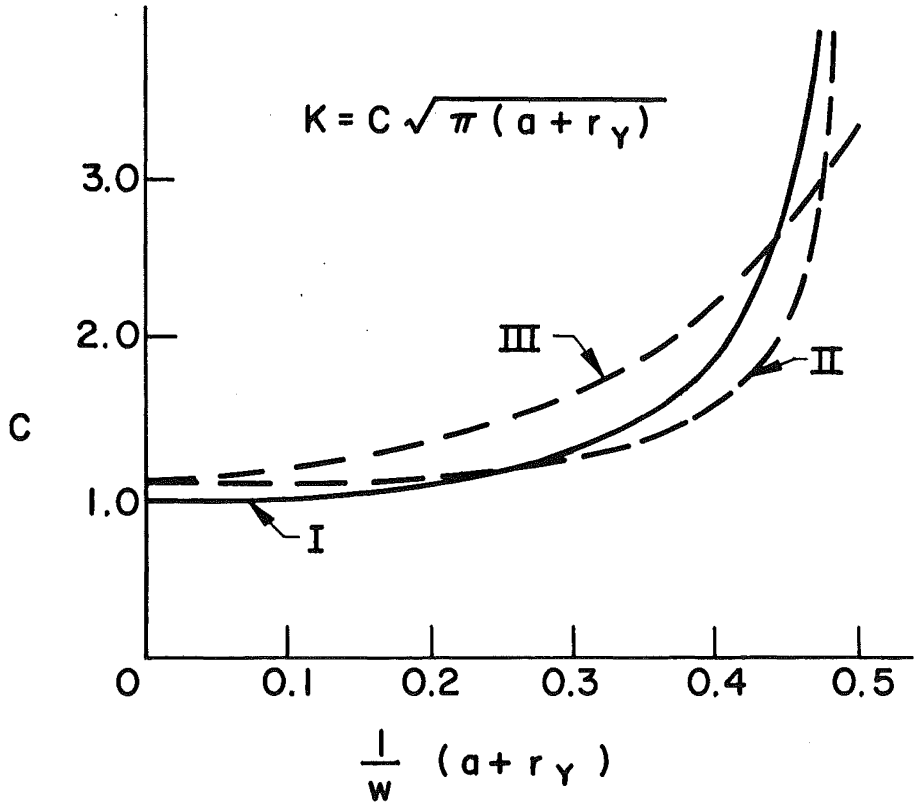

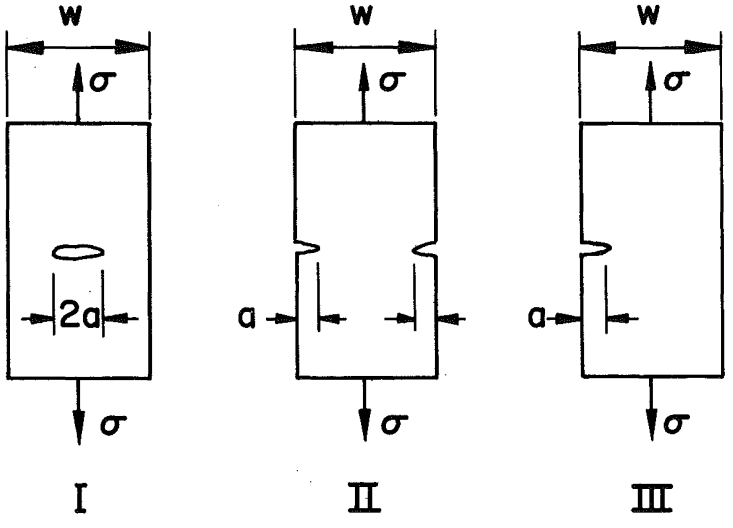

Fig. 18 K FOR THROUGH CRACKS IN A FINITE-WIDTH PLATE

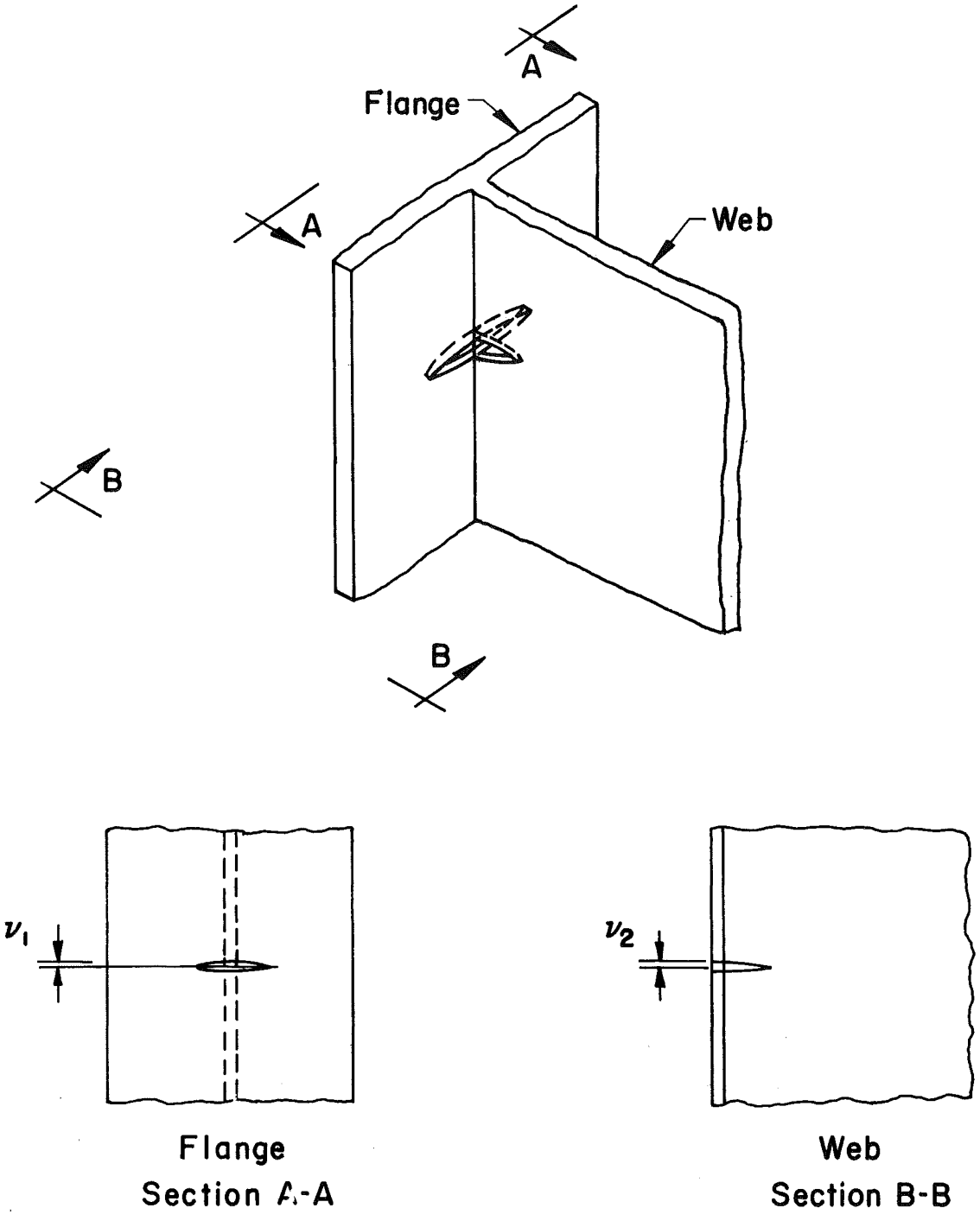

Fig. 19 THE THREE-ENDED CRACK

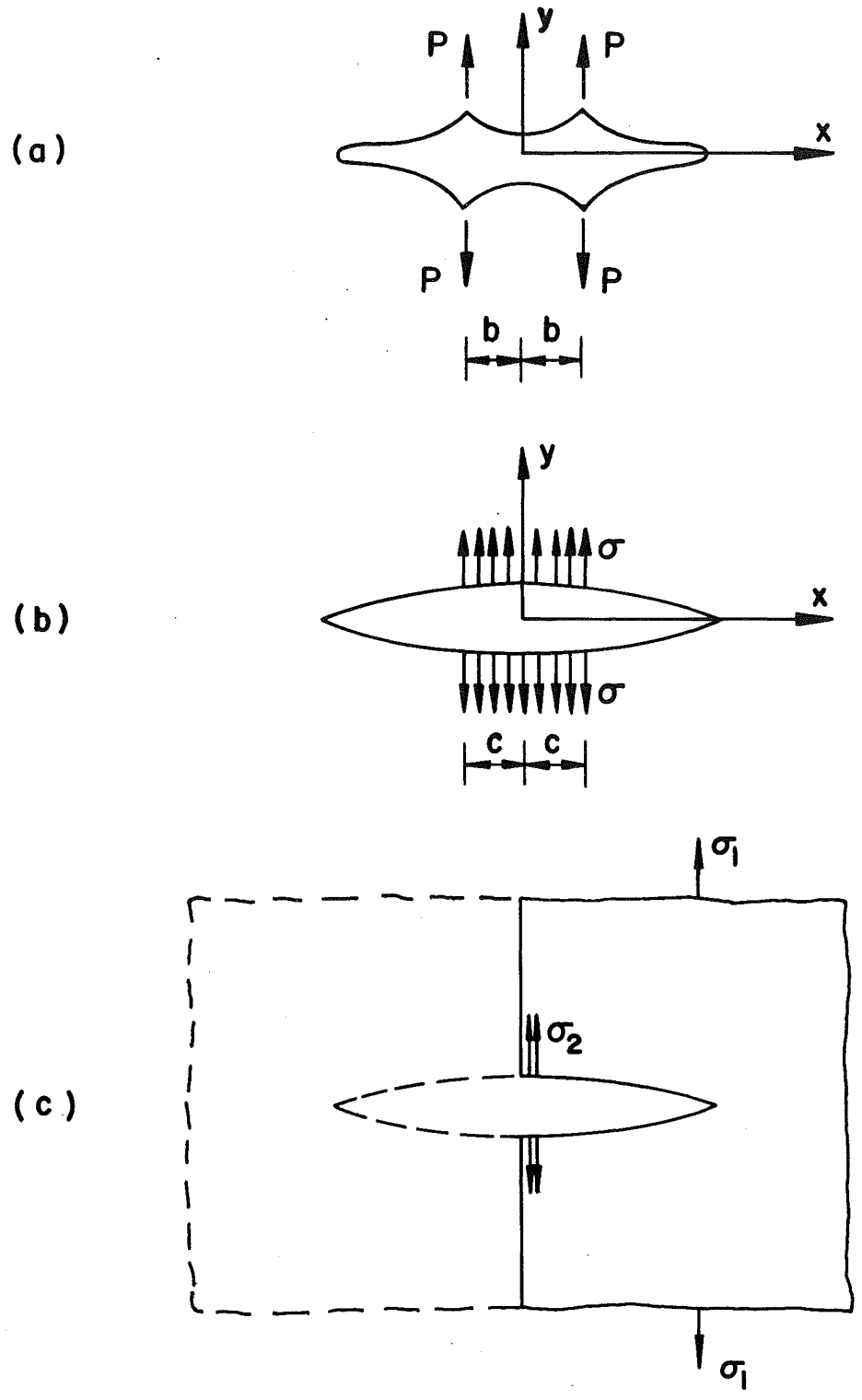

Fig. 20 OPENING OF A CRACK BY WEDGE FORCES

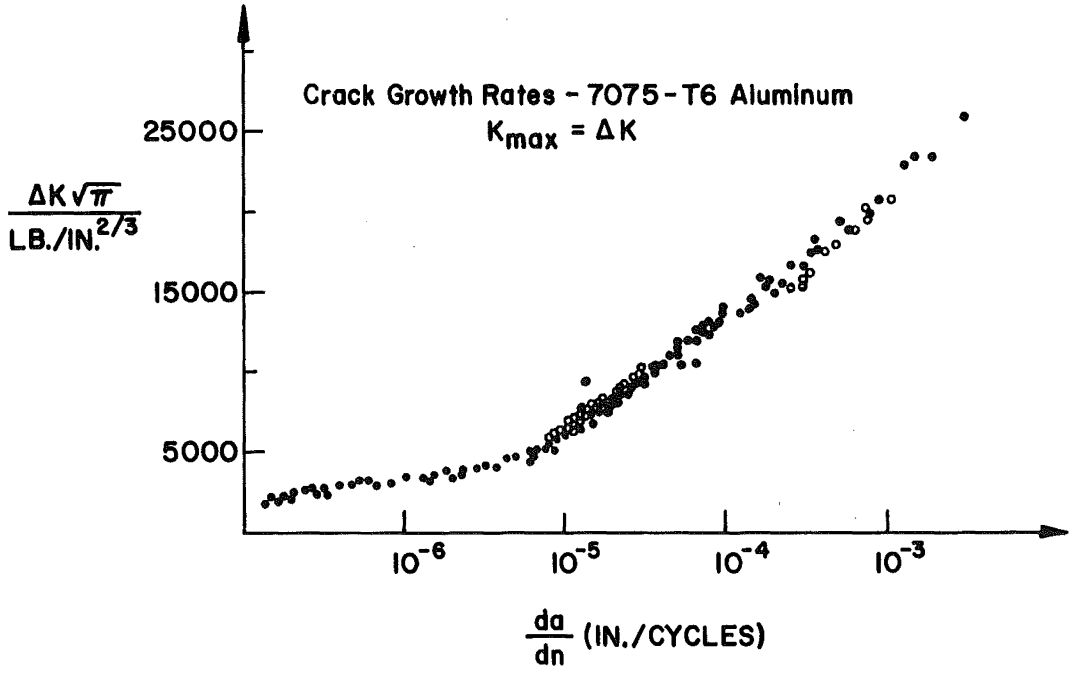

Fig. 21 CRACK GROWTH RATE OF AN ALUMINUM ALLOY (FROM PARIS[8])

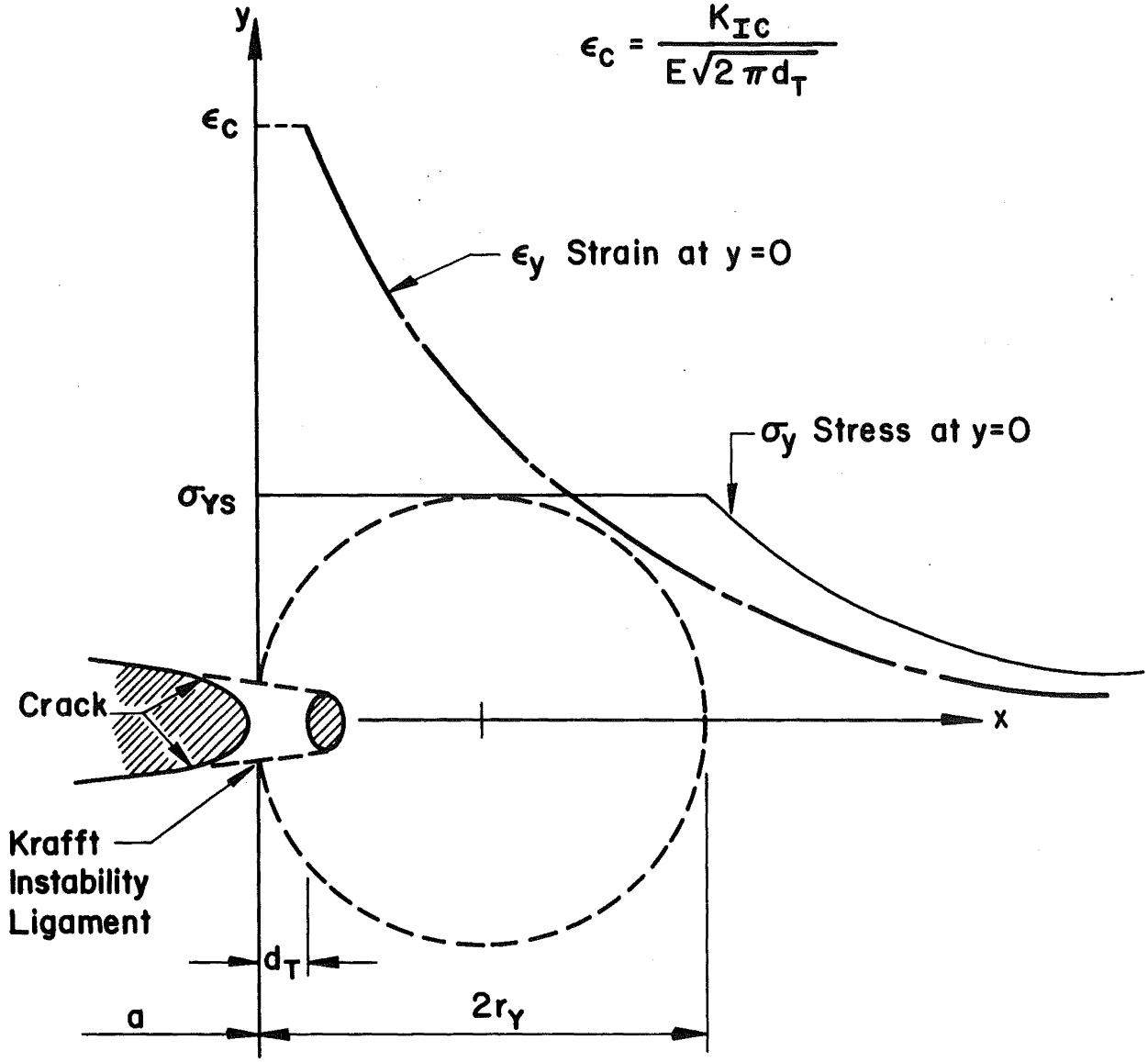

Fig. 22 THE KRAFFT MODEL OF CRACK TIP PLASTIC INSTABILITY

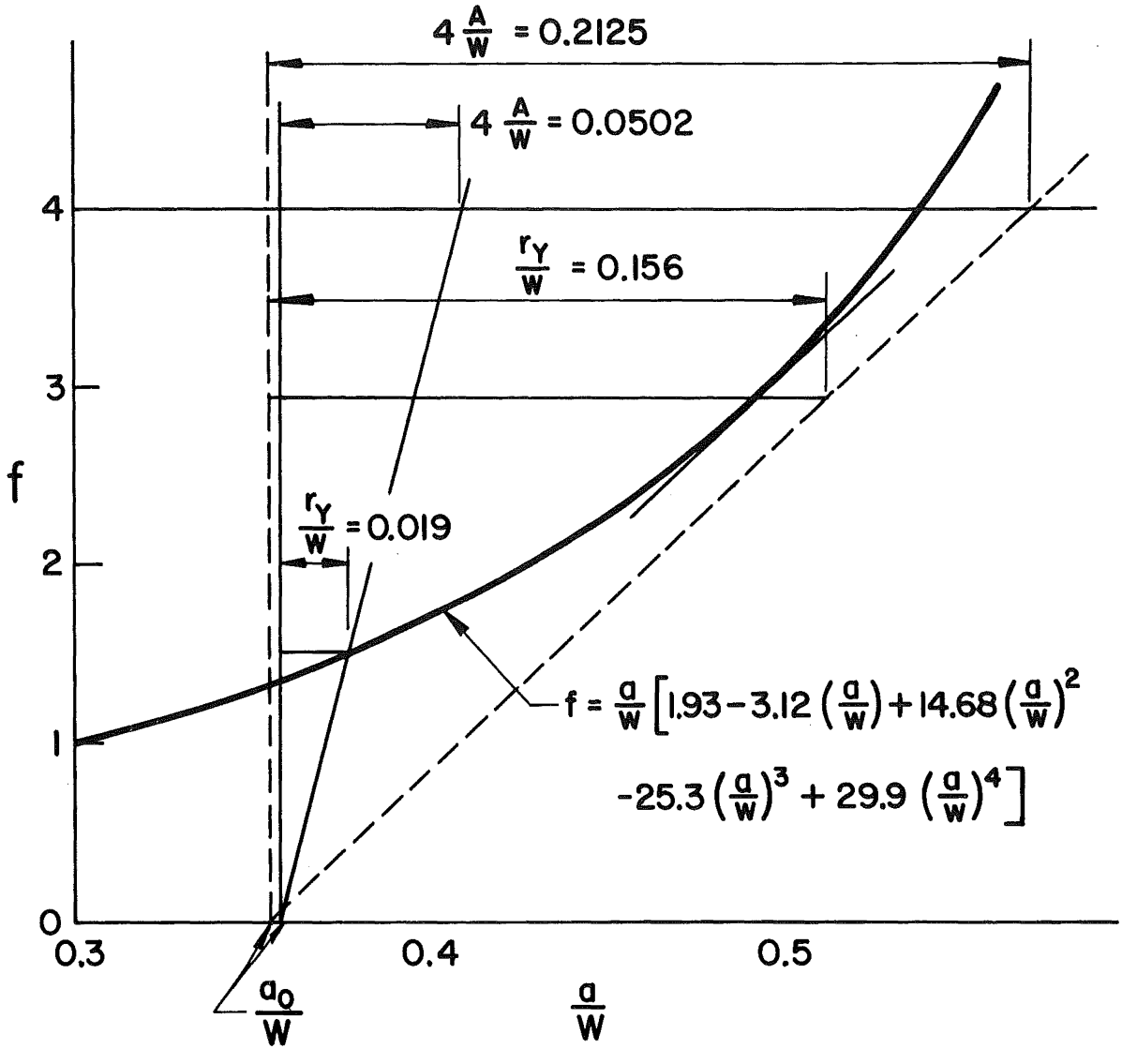

T 234-2-1"	L 531-2-1"
$4\left(\frac{a}{W}\right) = 0.0502$	$4\left(\frac{a}{W}\right) = 0.2125$
$\frac{a_o}{W} = 0.359$	$\frac{a_o}{W} = 0.356$
$\frac{r_Y}{W} = 0.0540$	$\frac{r_Y}{W} > 0.156$
$K_c = 46.9$ ksi $\sqrt{in}$	$K_c > 125.3$ ksi $\sqrt{in}$

Fig. 23 A GRAPHICAL SOLUTION FOR K_c

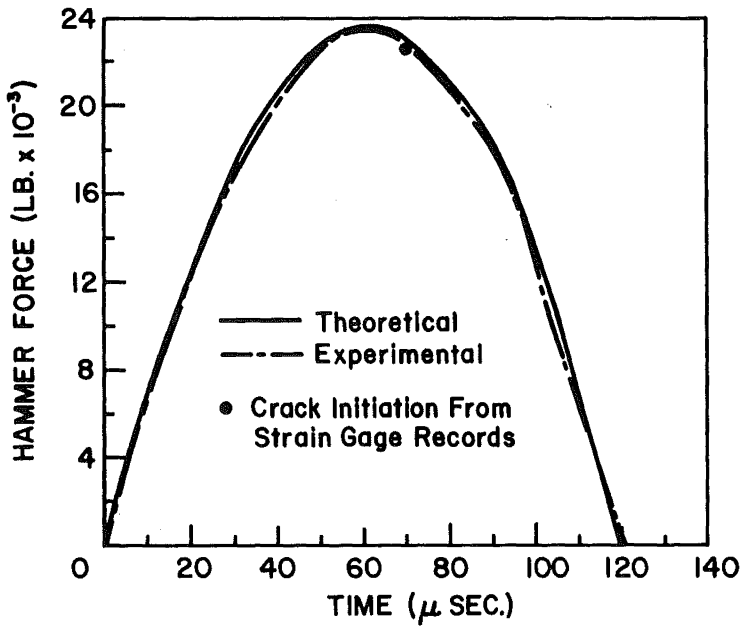

Fig. 24 HAMMER FORCE VERSUS TIME (FROM NASH[32])

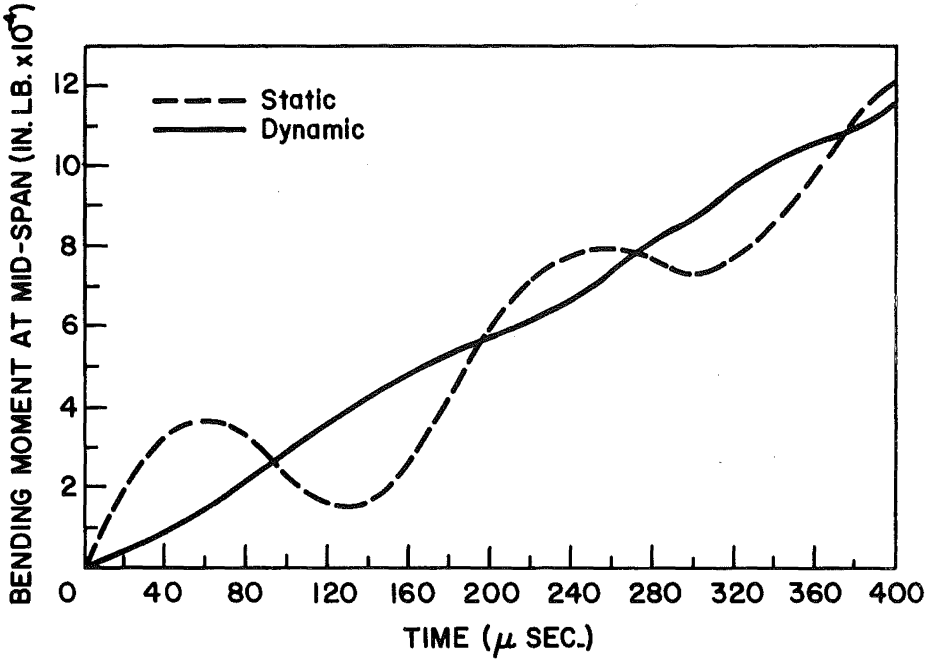

Fig. 25 BENDING MOMENT VERSUS TIME (FROM NASH[32])

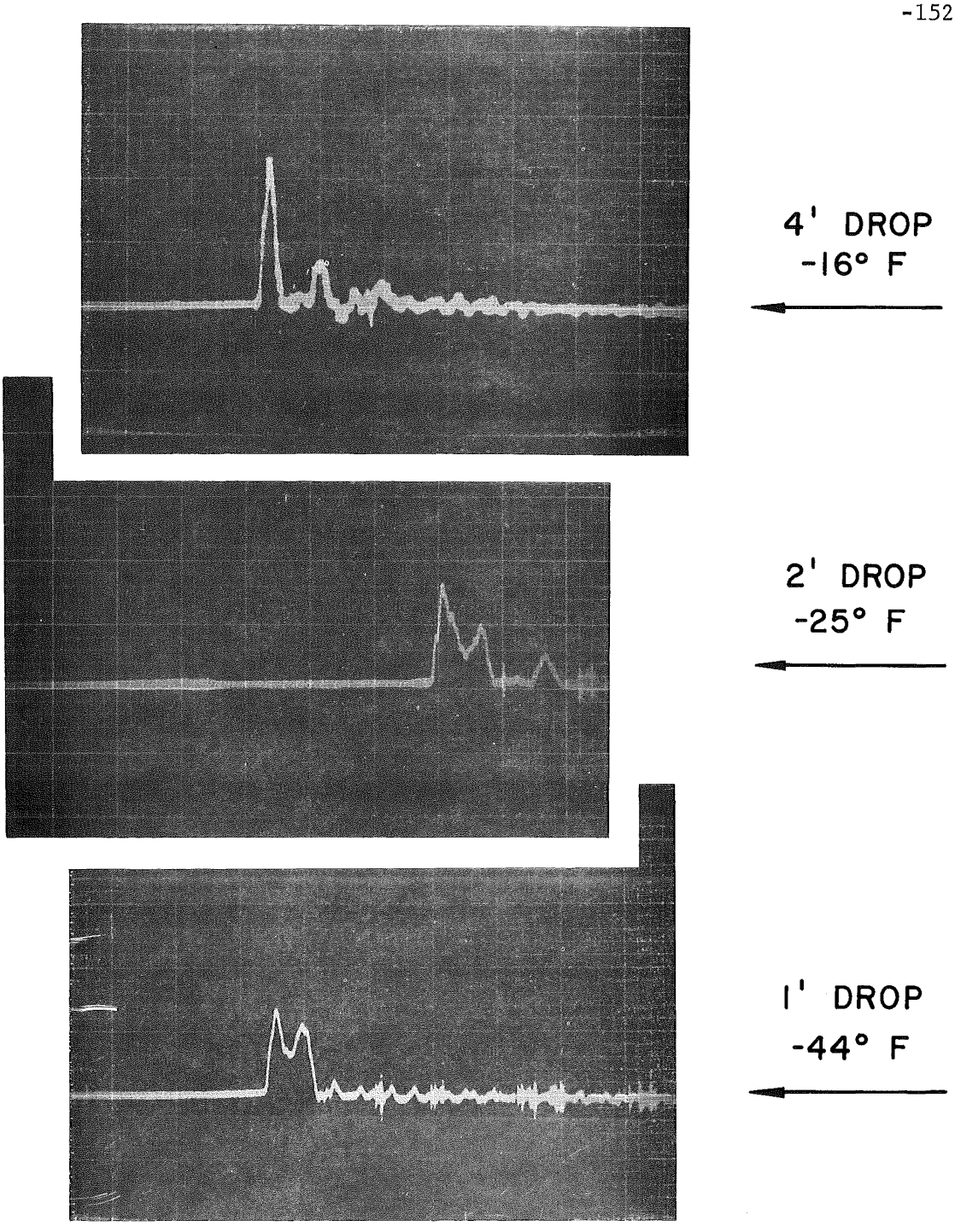

Fig. 26 LOAD RECORDS FOR VARIOUS DROP HEIGHTS

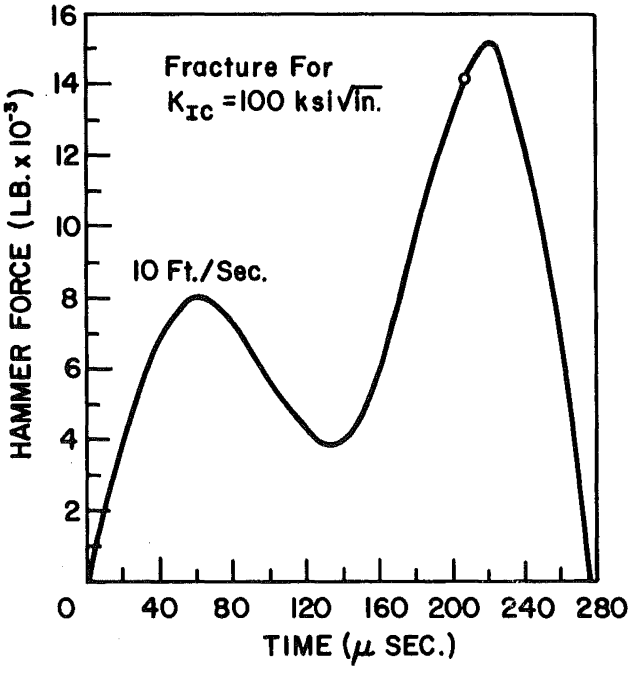

Fig. 27 FORCE-TIME RESPONSE FOR AN INITIAL IMPACT VELOCITY DECREASED FROM THOSE OF Fig. 24 (FROM NASH[32])

BRIDGE IB

Strain vs. Time Record For The Center Beam

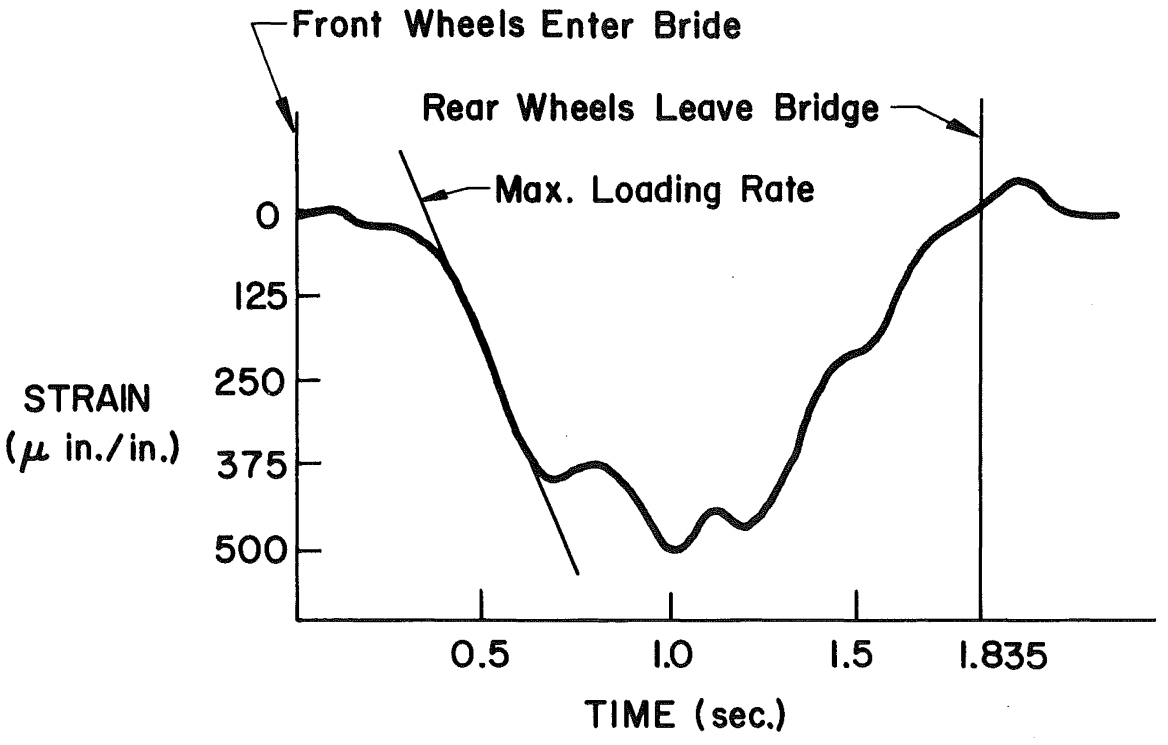

Notes:

1. Vehicle speed: 30 mph.
2. Maximum fiber stress, Dead + Live Loads: 35.4 ksi.
3. Total time to load, zero to maximum: 1 sec.
4. Maximum loading rate: 1.27 in/in per sec.
5. Bridge span: 50 ft.
6. Bridge steel: 18W50, ASTM A7-55T.
7. Slab: 6-1/2 inch thick, noncomposite.
8. Gross vehicle weight: 51,000 lbs.

Fig. 28 STRAIN VERSUS TIME FOR AASHO ROAD TEST BRIDGE[35]

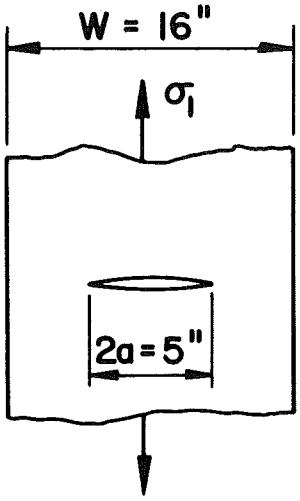

a. Uniform Stress Across the Flange

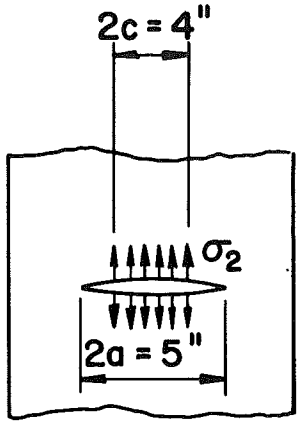

b. Uniform Stress Across the Central 4"

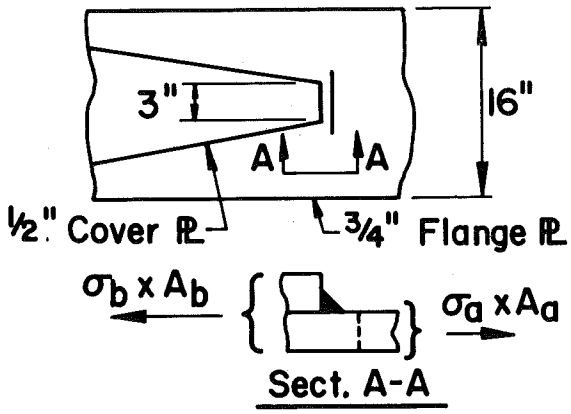

c. Cover Plate Load Transfer

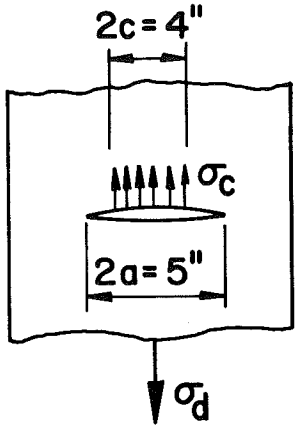

d. Stress From Cover Plate Load Transfer

Fig. 29 CRACK LOADING STRESSES - KINGS BRIDGE

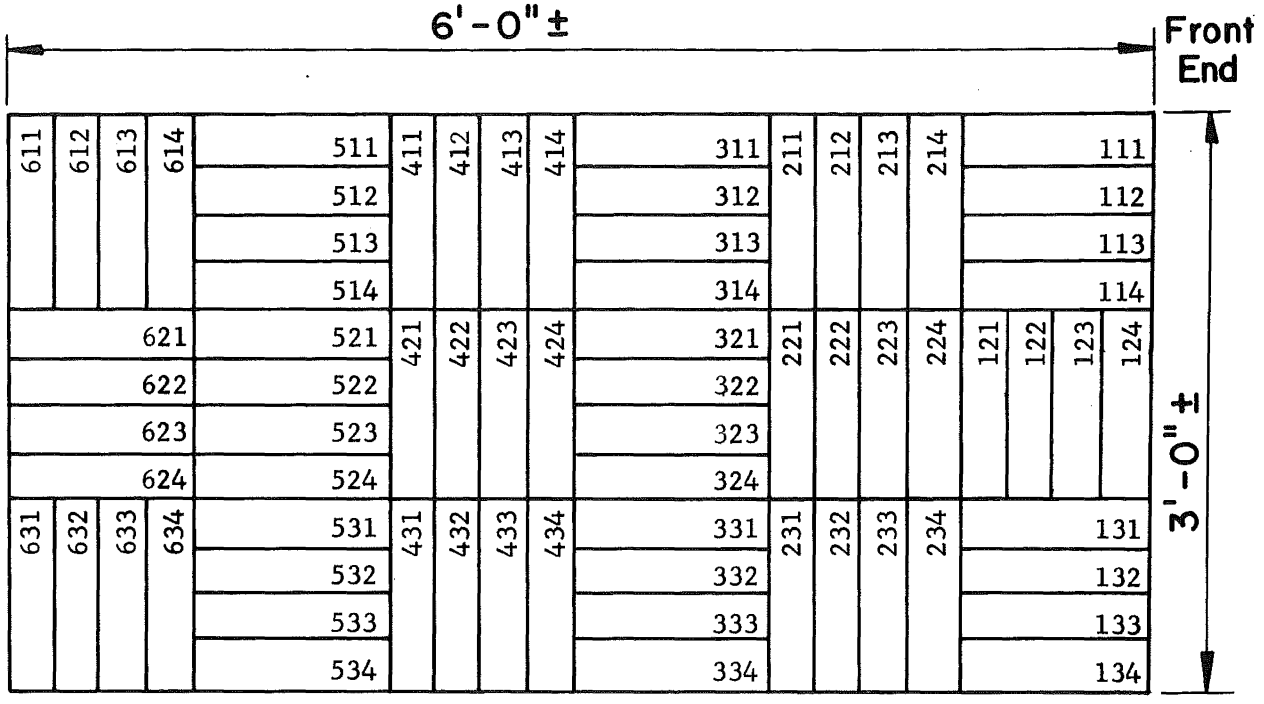

a. Specimen Layout in the Plate

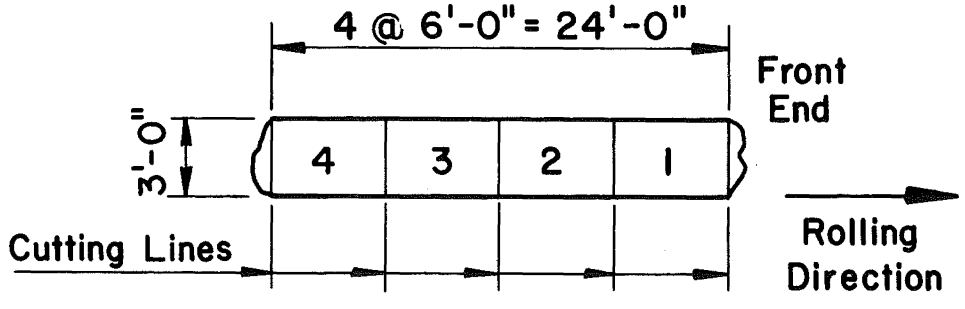

b. Cutting Sequence of Plates

Fig. 30 SPECIMEN LOCATION IN THE TEST PLATES

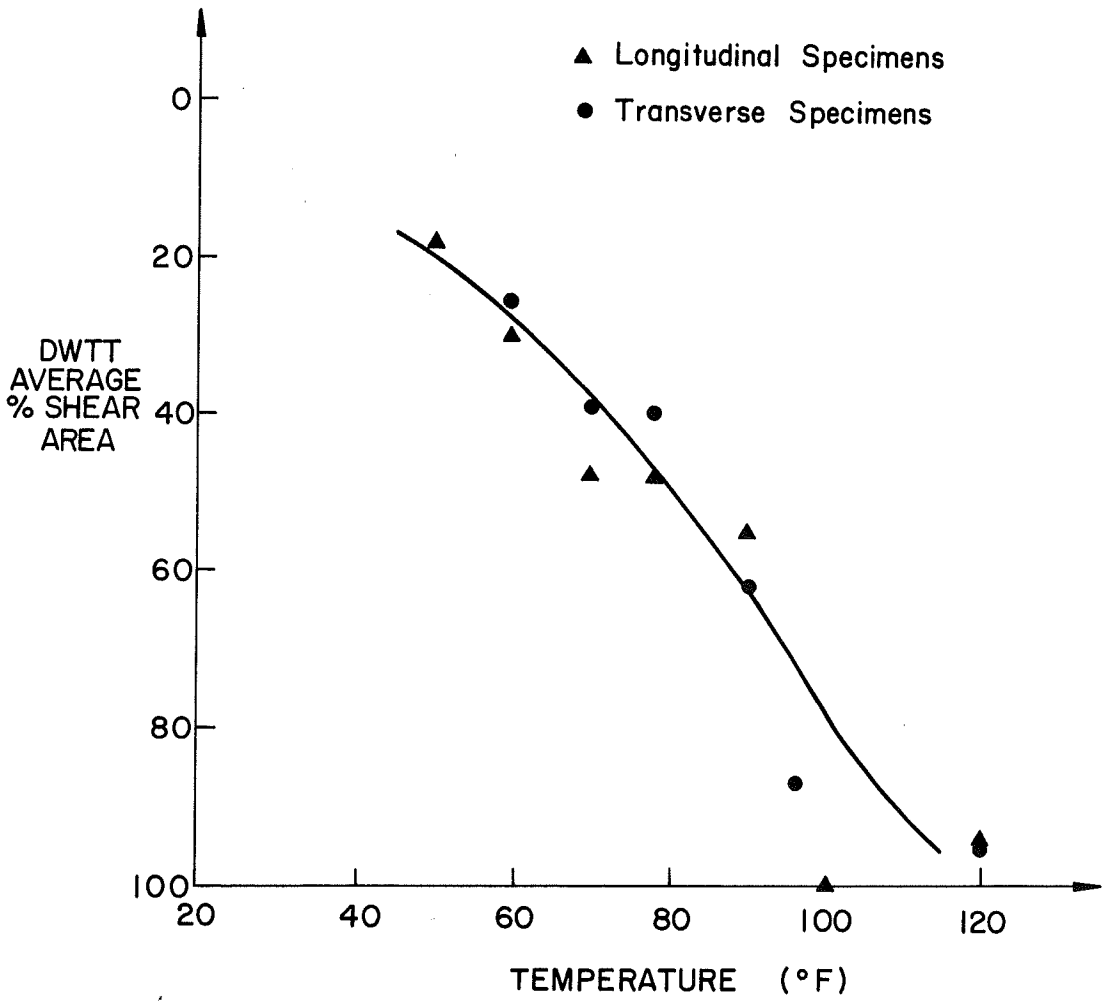

Fig. 31 1/2" PLATE

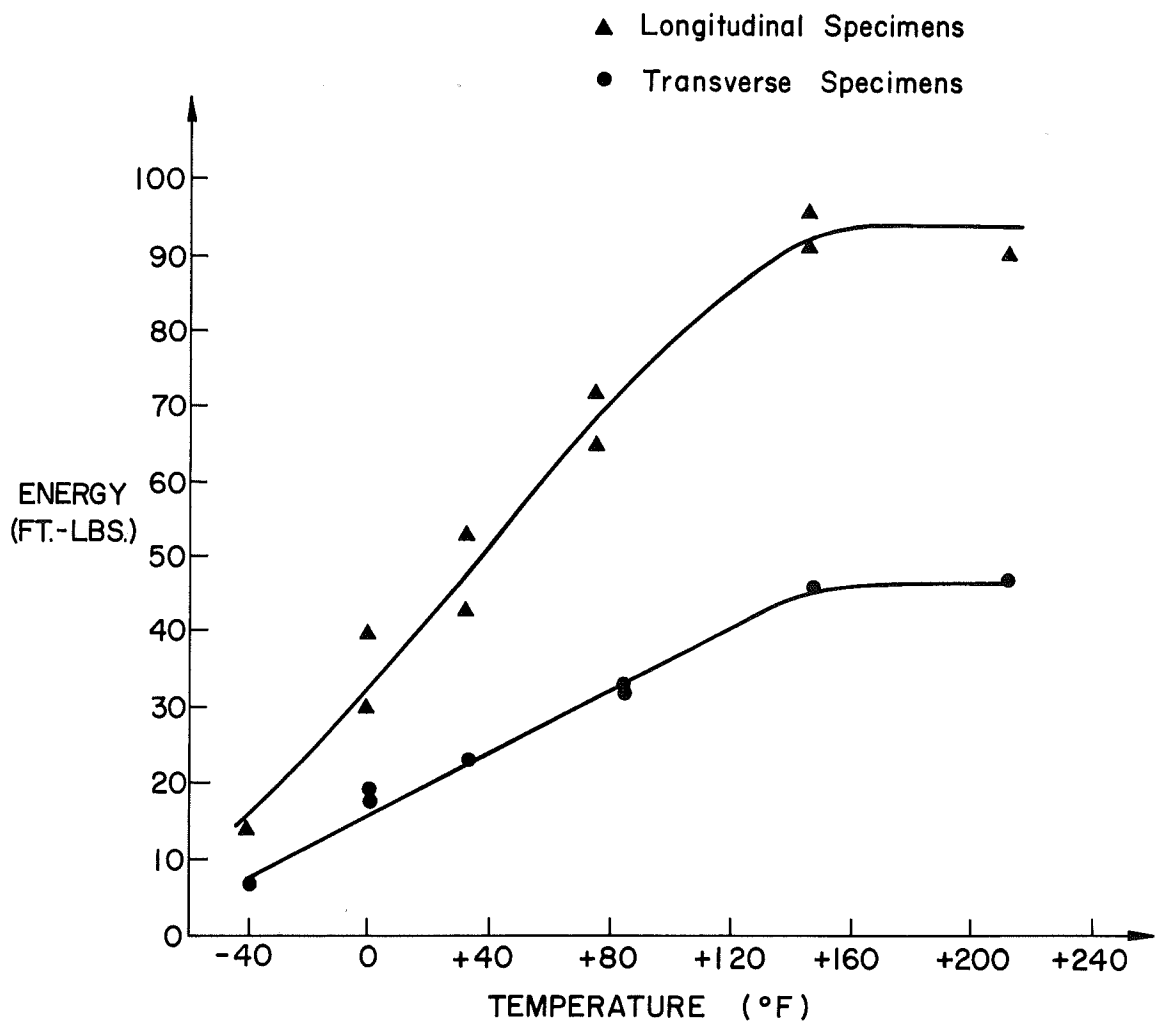

Fig. 32 1/2" PLATE

Longitudinal

Ferritic ASTM Grain Size: 8

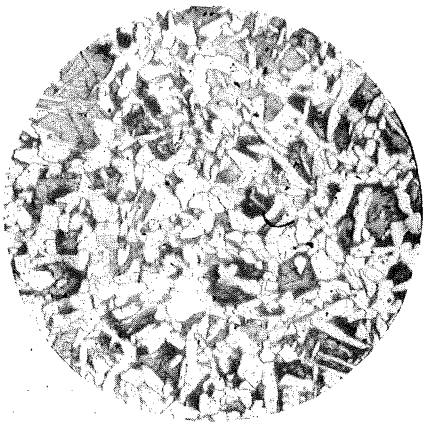

Transverse

Ferritic ASTM Grain Size: 8

(a) 1/2" THICK PLATE

Fig. 33 PHOTOMICROGRAPHS OF THE TEST STEEL

Center of Plate

7*

Edge of Plate

7-1/2*

Longitudinal

*Ferritic ASTM Grain Size

Transverse

Ferritic ASTM Grain Size: 7

(b) 1" THICK PLATE

Fig. 33 PHOTOMICROGRAPHS OF THE TEST STEEL

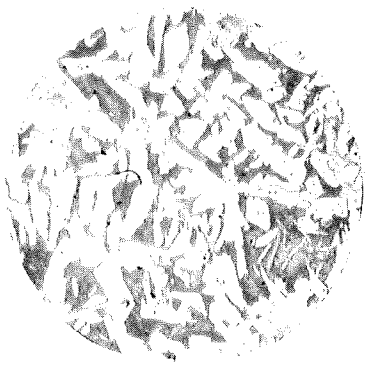

Longitudinal

Ferritic ASTM Grain Size: 6-1/2

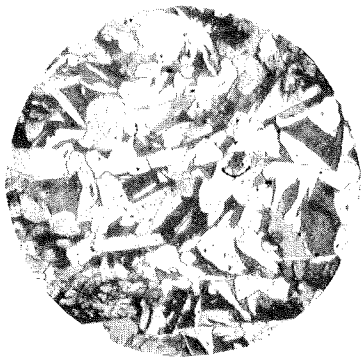

Transverse

Ferritic ASTM Grain Size: 6-1/2

(b) 2" THICK PLATE

Fig. 33 PHOTOMICROGRAPHS OF THE TEST STEEL

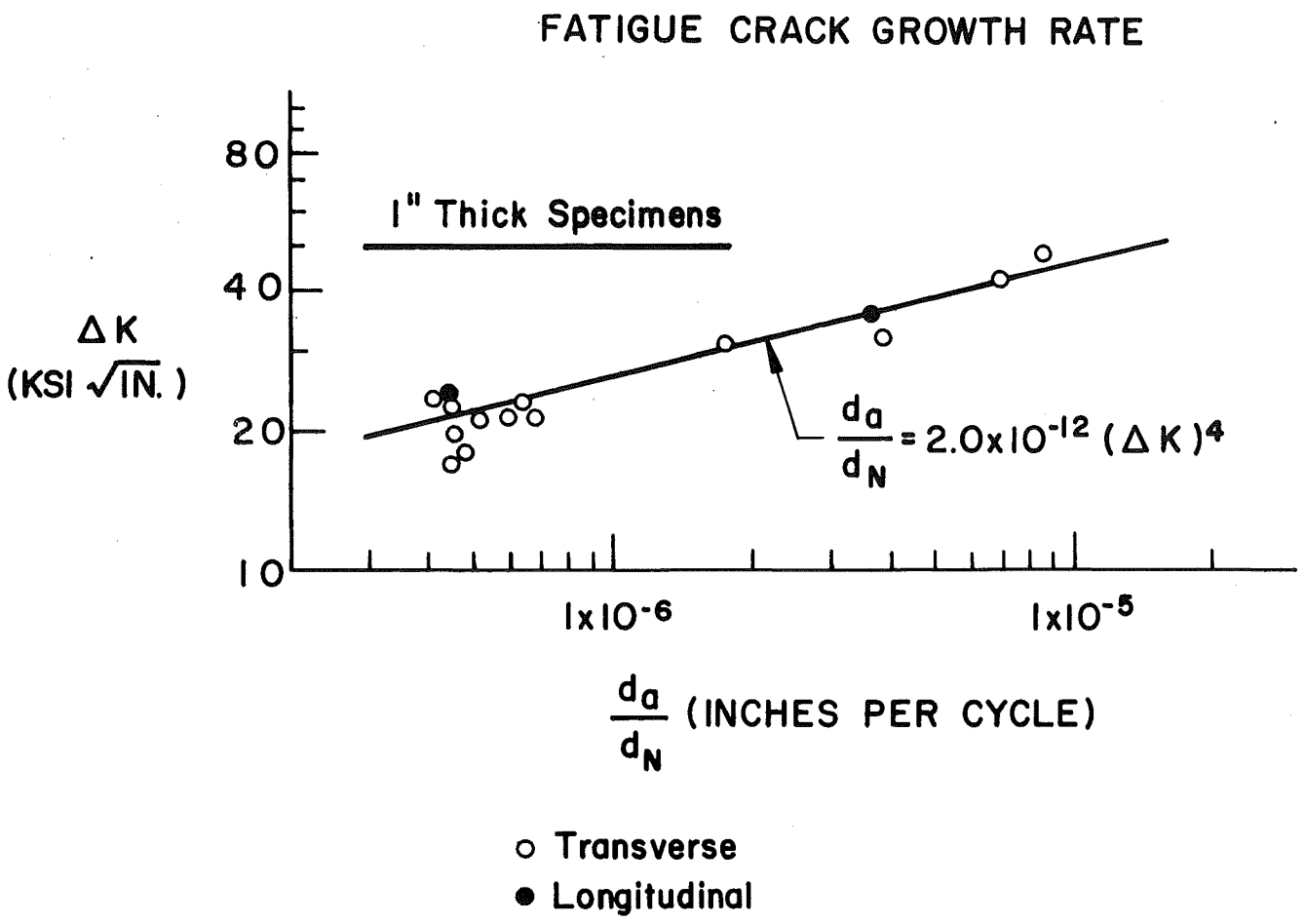

Fig. 34 FATIGUE CRACK GROWTH RATE - 1" SPECIMENS

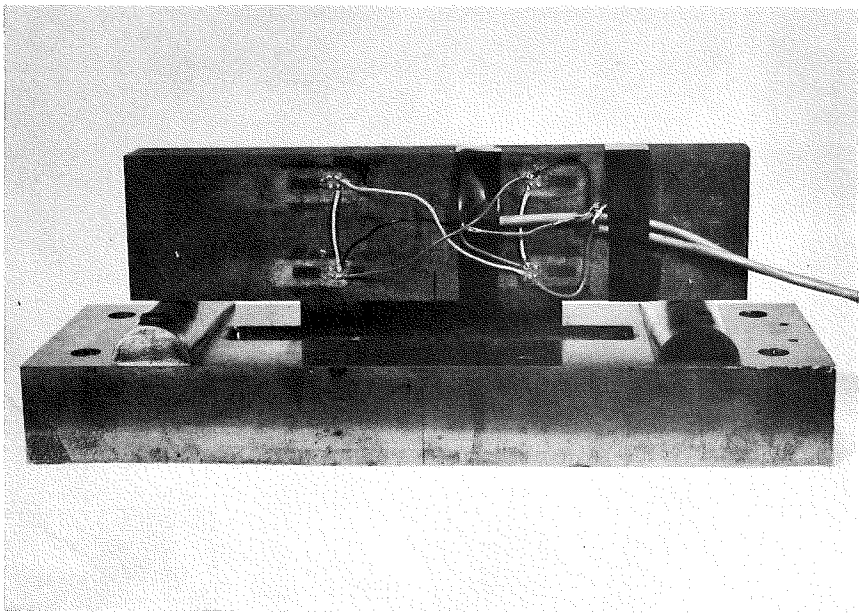

Fig. 35 A GAGED SPECIMEN

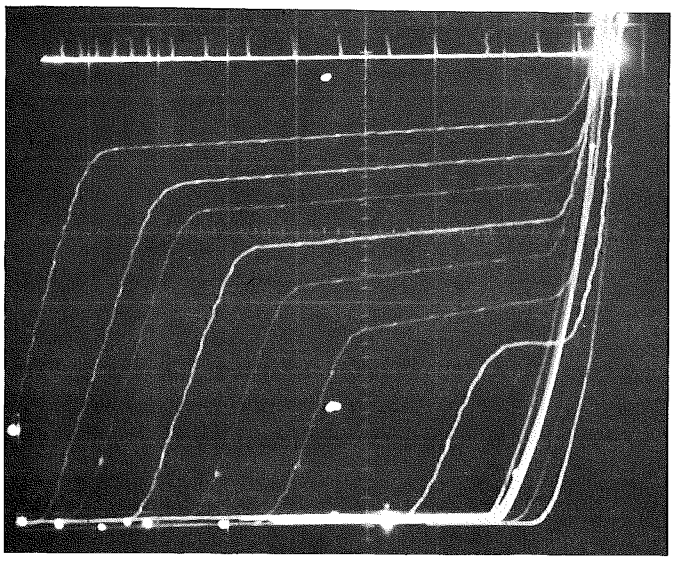

0.01 Sec
Time Marks

Loading Rate:

$\dot{\varepsilon}$ = 0.435 in/in per sec.

Total Strain = 23%

Temp. = -40°F

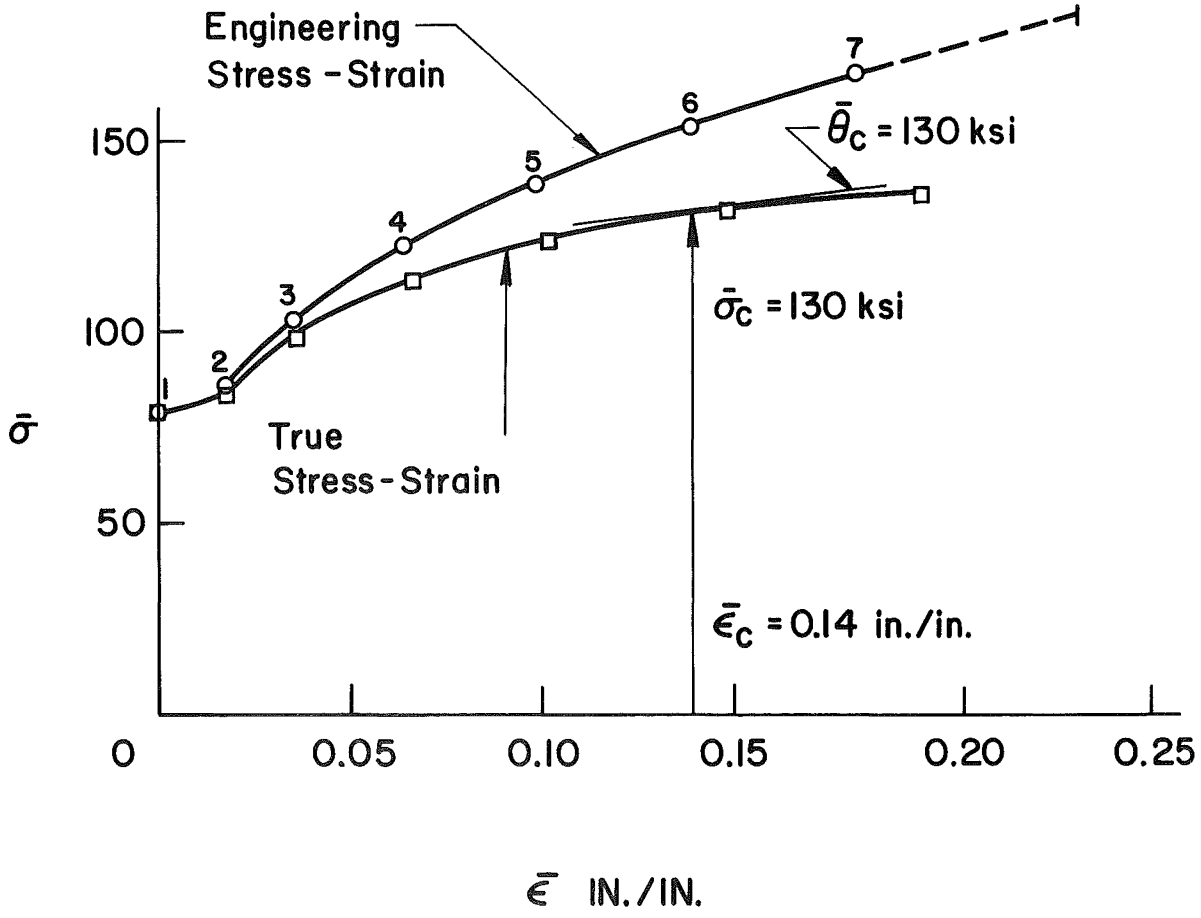

Fig. 36 A TYPICAL NRL COMPRESSION TEST RECORD AND COMPUTATION

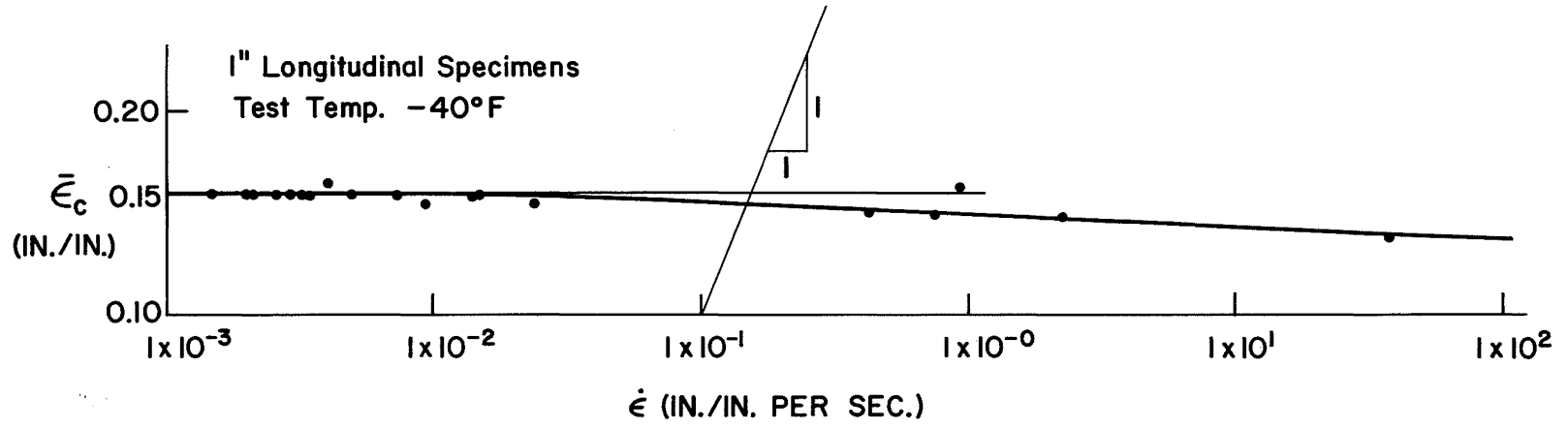

Fig. 37 CRITICAL STRAIN VERSUS STRAIN RATE: NRL COMPRESSION TESTS

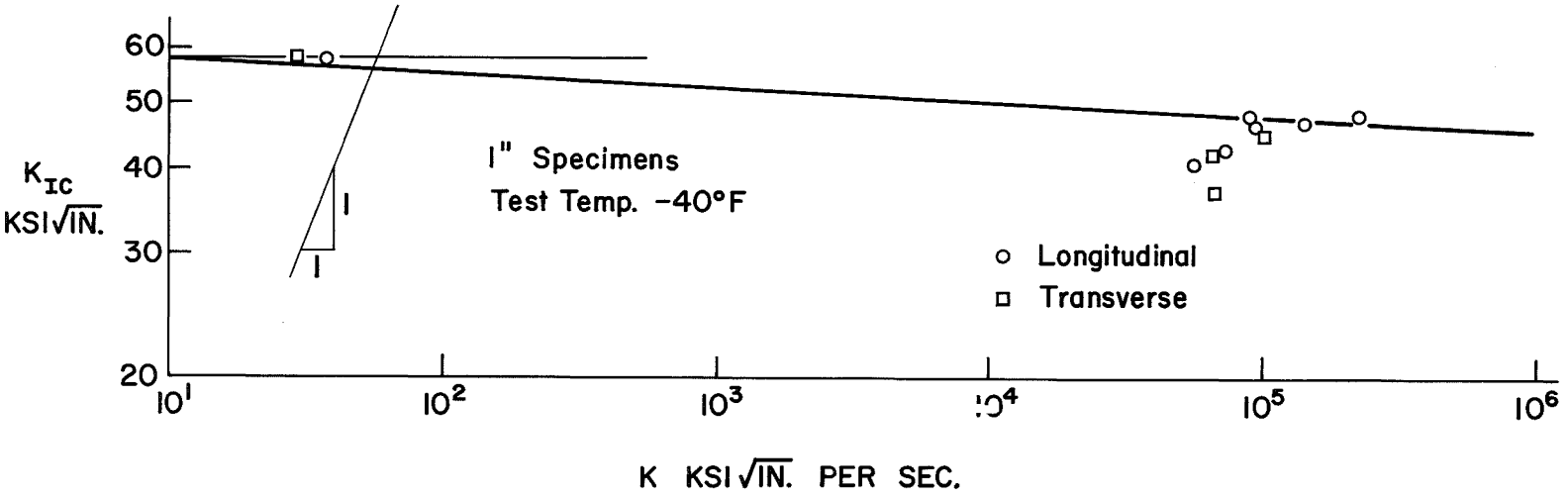

Fig. 38 K_{Ic} VERSUS $\dot{K}$: LEHIGH K_c TESTS

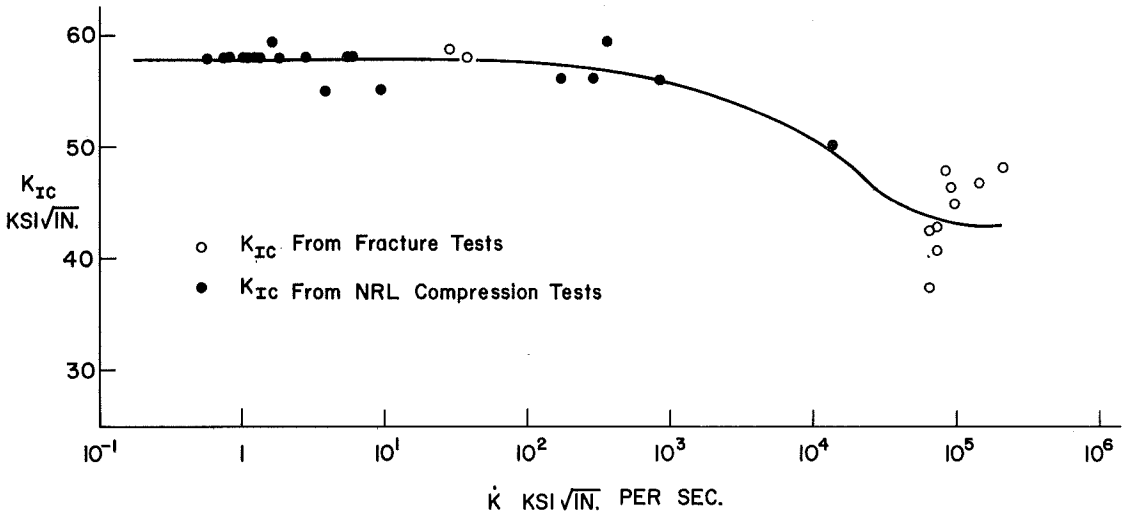

Fig. 39 K_{Ic} VERSUS $\dot{K}$ AT -40° F - 1" THICK PLATE

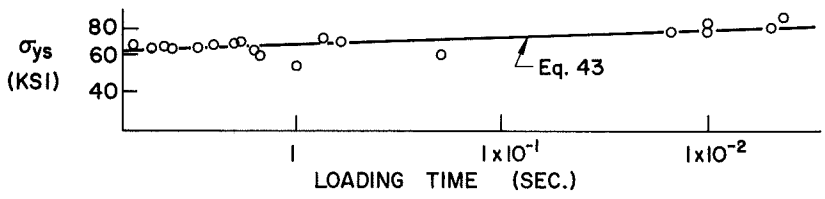

Eq. 43:

$$\sigma_{ys} = 55.9 + \frac{174{,}000}{\log (2 \times 10^{10} t)(-40 + 459)} - 27.4$$

Fig. 40 YIELD STRESS FROM COMPRESSION TESTS AT -40° F - 1" THICK PLATE

1/2" SPECIMENS - STATIC TEST

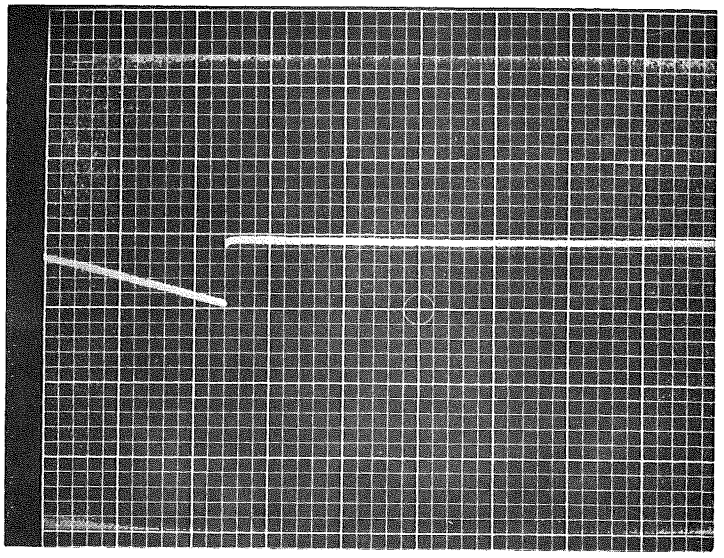

Temp.: -85^{o} F

Spec. No.: L334-4

Time Scale: 0.5 sec/cm

Load Scale: 10.0 kip/cm

r_Y = .128 in.

K_c = 66.09 ksi $\sqrt{in}$

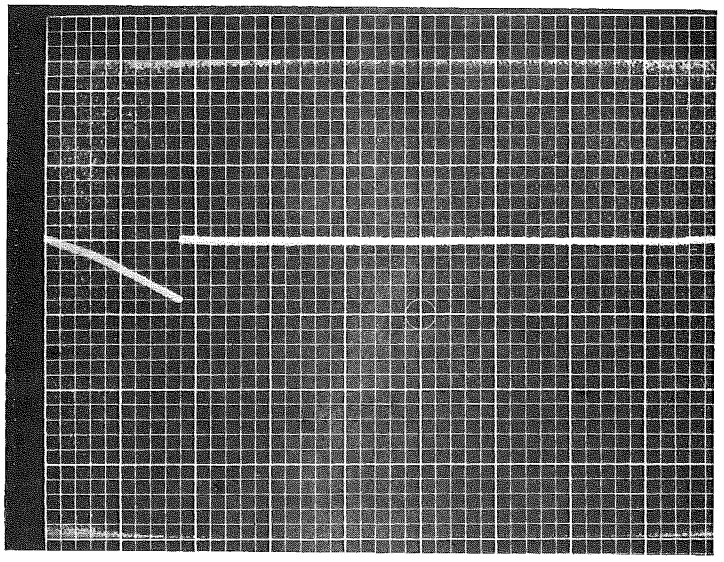

Temp.: -61^{o} F

Spec. No.: L114-4

Time Scale: 1.0 sec/cm

Load Scale: 10.0 kip/cm

r_Y = 0.152 in.

K_c = 69.15 ksi $\sqrt{in}$

Fig. 41 OSCILLOSCOPE RECORDS

1/2" SPECIMENS - IMPACT TESTS

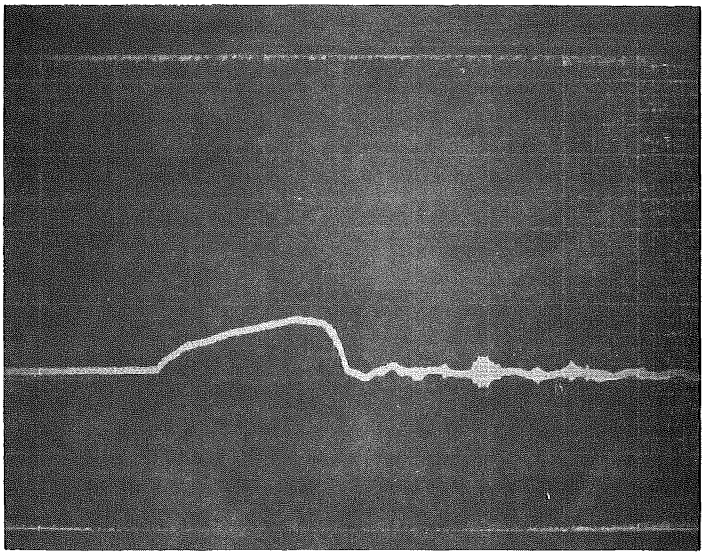

Temp.: -112^{o} F

Spec. No.: T121-4

Time Scale: 0.2 ms/cm

Load Scale: 10.0 kip/cm

r_Y = .0272 in.

K_c = 42.33 ksi $\sqrt{in}$

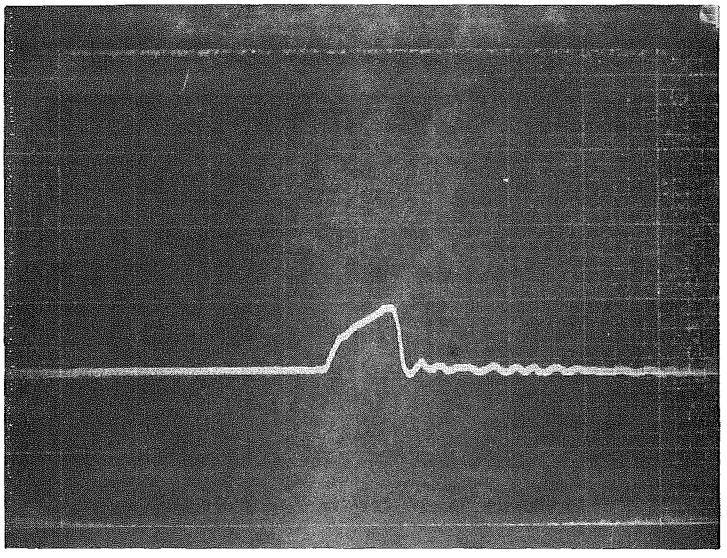

Temp.: -92^{o} F

Spec. No.: L622-3

Time Scale: 0.5 ms/cm

Load Scale: 10.0 kip/cm

r_Y = .0369 in.

K_c = 47.14 ksi $\sqrt{in}$

Fig. 41 OSCILLOSCOPE RECORDS

1/2" SPECIMENS - IMPACT TESTS

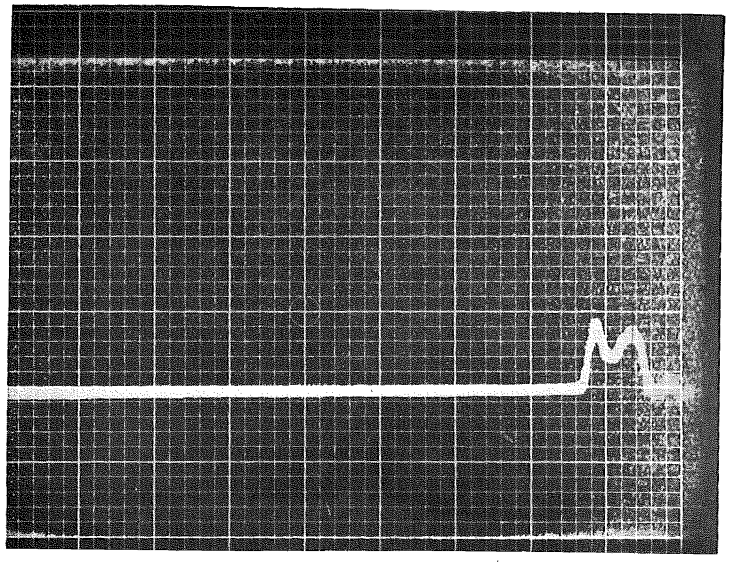

Temp.: -90^{o} F

Spec. No.: L211-4

Time Scale: 0.5 ms/cm

Load Scale: 10.0 kip/cm

r_Y = .0382 in.

K_c = 48.35 ksi $\sqrt{in}$

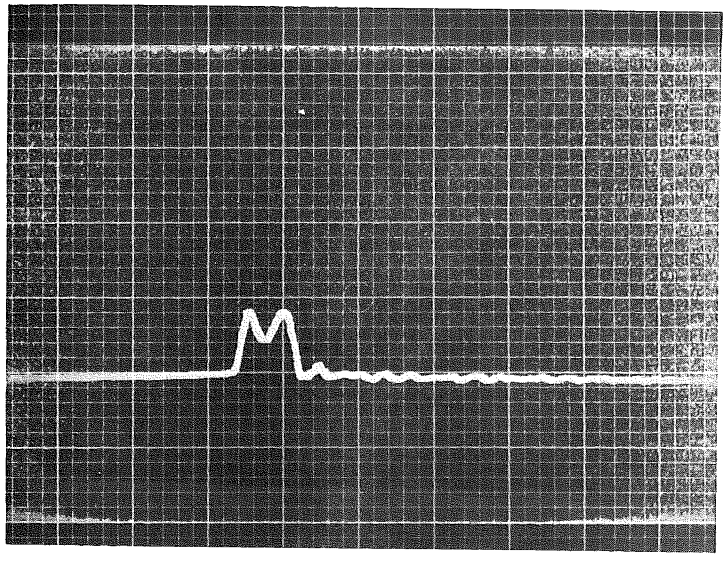

Temp.: -85^{o} F

Spec. No. T611-3

Time Scale: 0.5 ms/cm

Load Scale: 10.0 kip/cm

r_Y = .0452 in.

K_c = 52.11 ksi $\sqrt{in}$

Fig. 41 OSCILLOSCOPE RECORDS

1/2" SPECIMENS - IMPACT TESTS

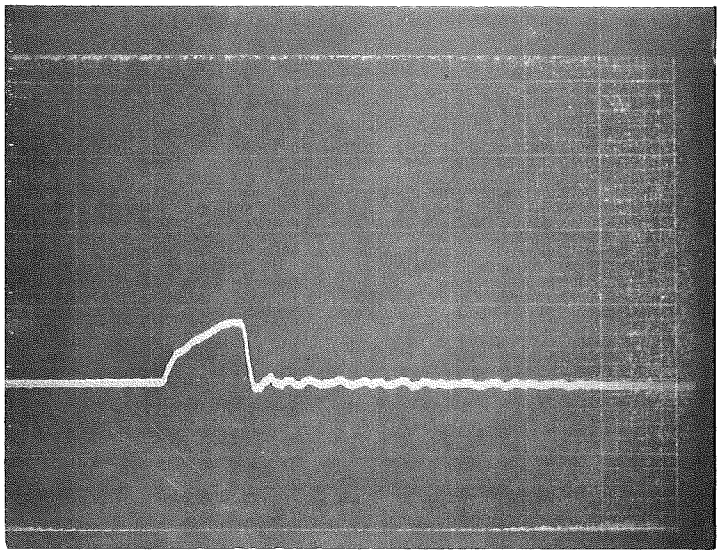

Temp.: -40^{o} F

Spec. No.: L112-4

Time Scale: 0.5 ms/cm

Load Scale: 10.0 kip/cm

r_Y = .0645 in.

K_c = 56.32 ksi $\sqrt{in}$

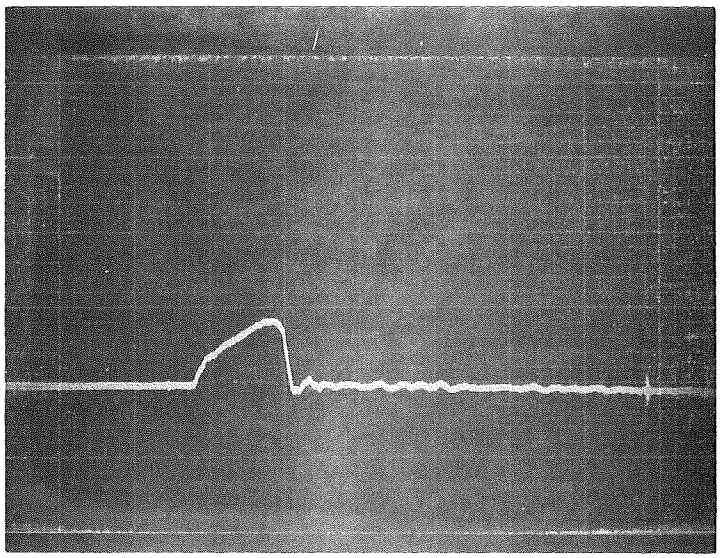

Temp.: -39^{o} F

Spec. No.: L113-4

Time Scale: 0.5 ms/cm

Load Scale: 10.0 kip/cm

r_Y = .046 in.

K_c = 47.97 ksi $\sqrt{in}$

Fig. 41 OSCILLOSCOPE RECORDS

1/2" SPECIMENS - IMPACT TESTS

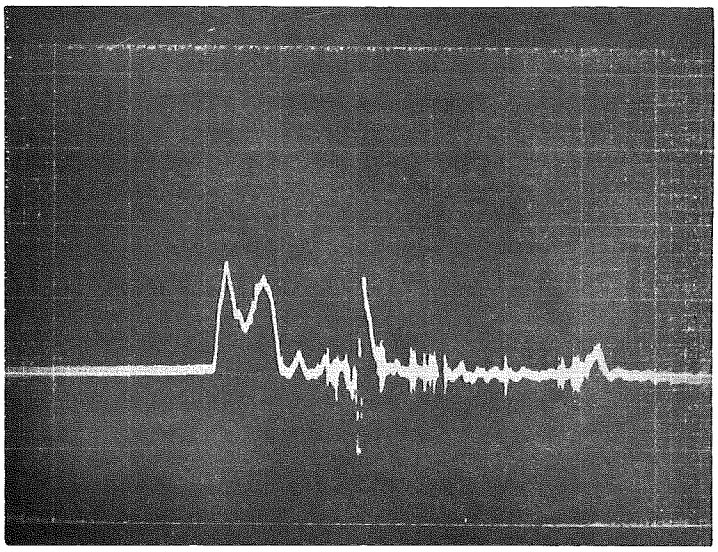

Temp.: -39^{o} F

Spec. No.: L533-4

Time Scale: 0.5 ms/cm

Load Scale: 10.0 kip/cm

r_Y = .103 in.

K_c = 72.62 ksi $\sqrt{in}$

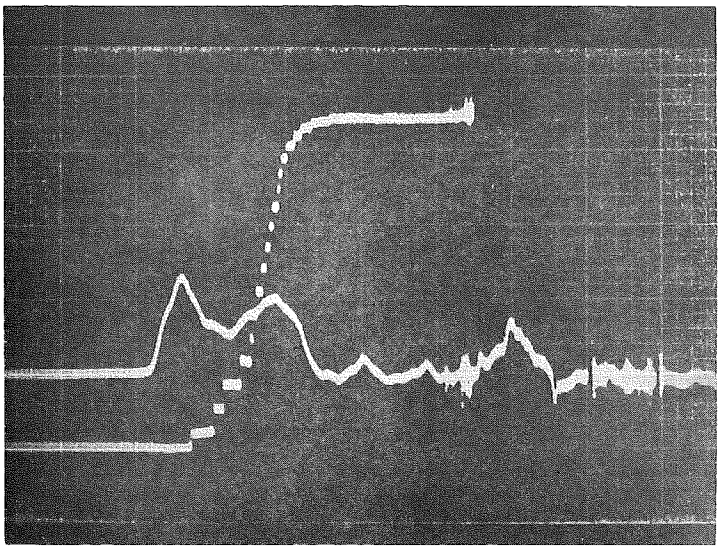

Temp.: -34^{o} F

Spec. No.: T123-4

Time Scale: 0.2 ms/cm

Load Scale: 10.0 kip/cm

r_Y = .058 in.

K_c = 54.03 ksi $\sqrt{in}$

Note: Lower trace (on left) is a crack wire trace, see Ref. 13

Fig. 41 OSCILLOSCOPE RECORDS

1/2 SPECIMENS - IMPACT TESTS

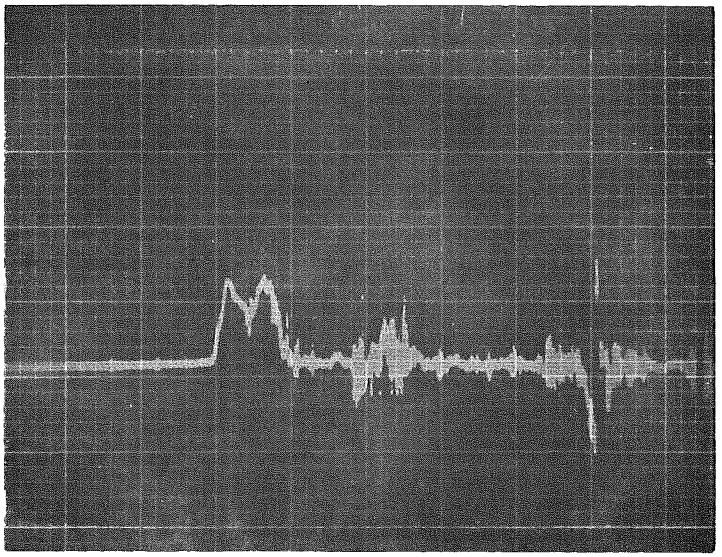

Temp.: -33^{o} F

Spec. No.: T223-4

Time Scale: 0.5 ms/cm

Load Scale: 10.2 kip/cm

r_Y = .064 in.

K_c = 56.19 ksi $\sqrt{in}$

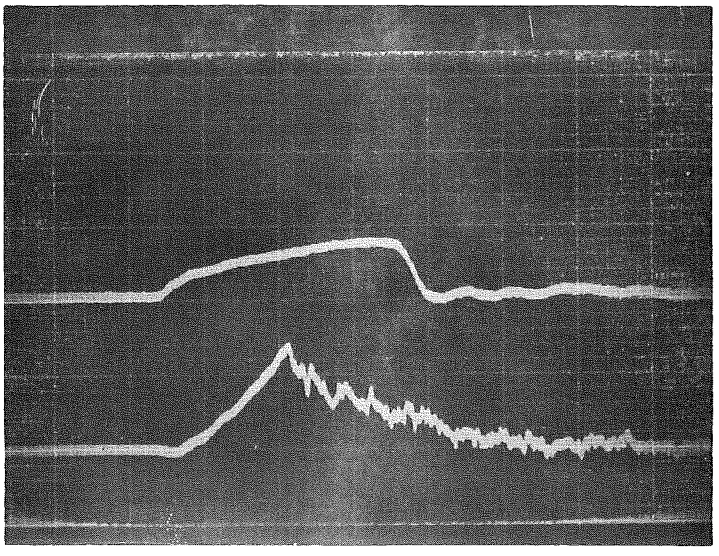

Temp.: -32^{o} F

Spec. No.: L334-3

Time Scale: 0.2 ms/cm

Tup Record:

Load Scale: 10.0 kip/cm

r_Y = .0514 in.

K_c = 49.63 ksi $\sqrt{in}$

Beam Record:

Load Scale: 5.92 kip/cm

r_Y = .0559 in.

K_c = 53.16 ksi $\sqrt{in}$

Note: Lower record is from gages mounted on specimen.

Fig. 41 OSCILLOSCOPE RECORDS

1/2" SPECIMENS - IMPACT TESTS

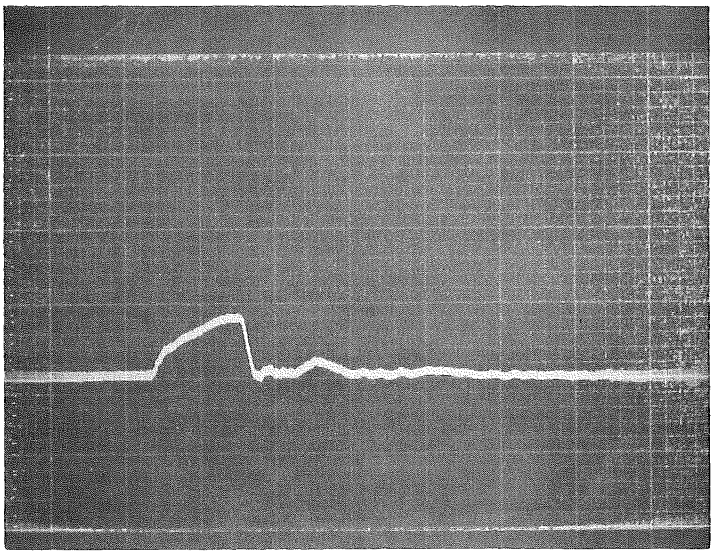

Temp.: -26^{o} F

Spec. No.: T411-4

Time Scale: 0.5 ms/cm

Load Scale: 10.0 kip/cm

r_Y = .0580 in.

K_c = 52.14 ksi $\sqrt{in}$

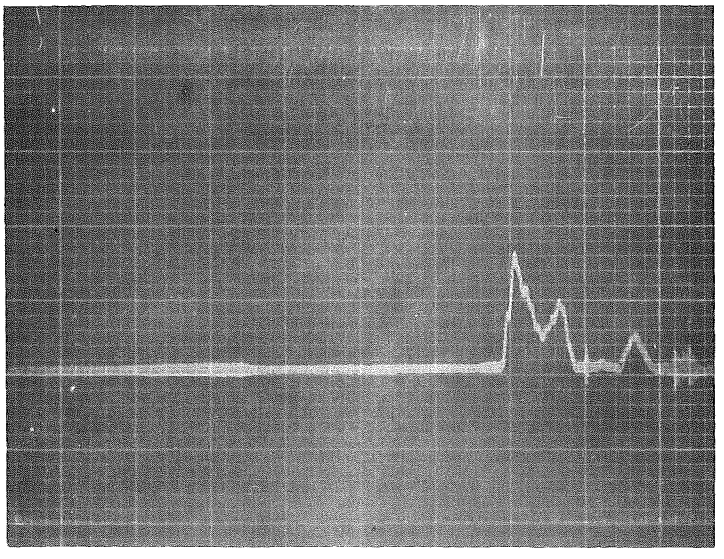

Temp.: -25^{o} F

Spec. No.: T213-4

Time Scale: 0.5 ms/cm

Load Scale: 10.2 kip/cm

r_Y = .0451 in.

K_c = 46.64 ksi $\sqrt{in}$

Fig. 41 OSCOLLOSCOPE RECORDS

1/2" SPECIMENS - IMPACT TESTS

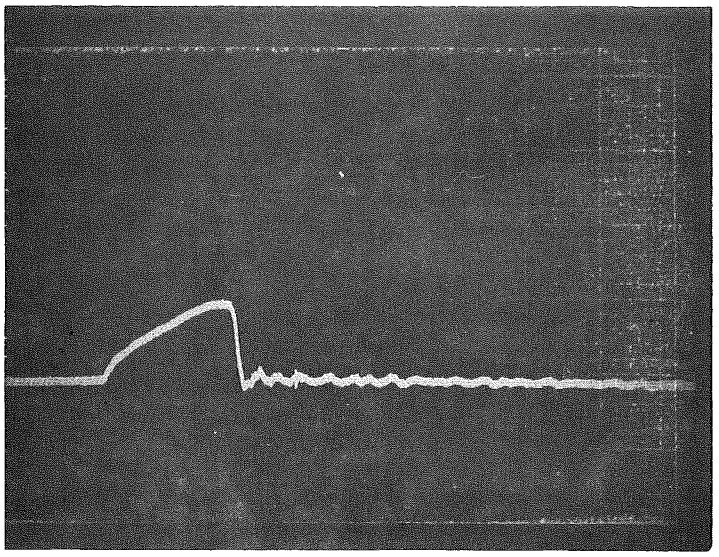

Temp.: -25^{o} F

Spec. No.: T612-3

Time Scale: 0.5 ms/cm

Load Scale: 10.0 kip/cm

r_Y = .0828 in.

K_c = 61.36 ksi $\sqrt{in}$

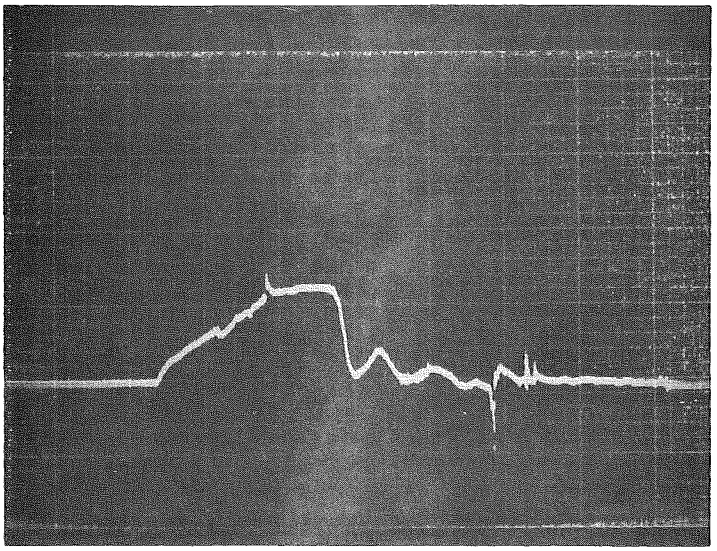

Temp.: 0^{o} F

Spec. No.: L333-4

Time Scale: 0.5 ms/cm

Load Scale: 10.0 kip/cm

r_Y = .1465 in.

K_c = 77.91 ksi $\sqrt{in}$

Fig. 41 OSCILLOSCOPE RECORDS

1/2" SPECIMENS - IMPACT TESTS

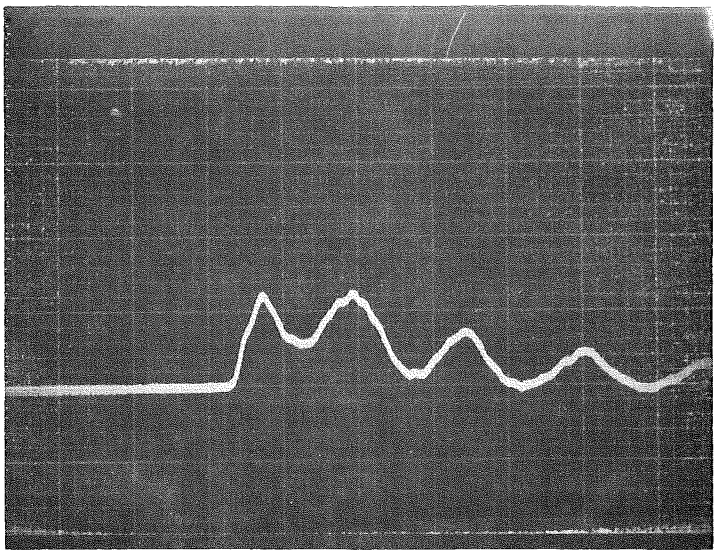

Temp.: 0^{o} F

Spec. No.: T423-4

Time Scale: 0.2 ms/cm

Load Scale: 10.0 kip/cm

r_Y = .1678 in.

K_c = 87.46 ksi $\sqrt{in}$

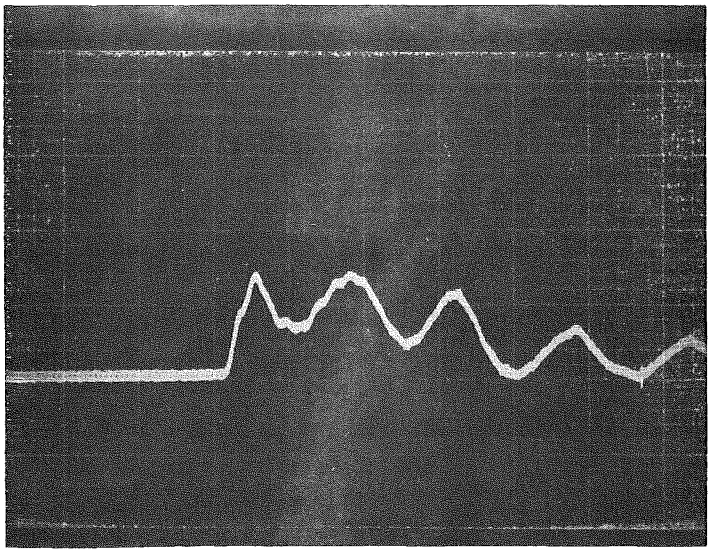

Temp.: 0^{o} F

Spec. No.: L331-4

Time Scale: 0.2 ms/cm

Load Scale: 10.0 kip/cm

r_Y = .1457 in.

K_c = 81.53 ksi $\sqrt{in}$

Fig. 41 OSCOLLOSCOPE RECORDS

1/2" SPECIMENS - IMPACT TESTS

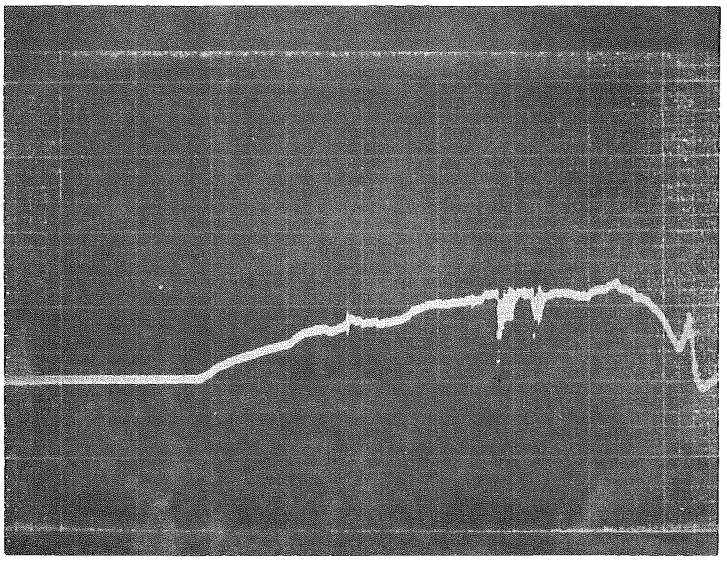

Temp.: 2^{o} F

Spec. No.: T613-3

Time Scale: 0.2 ms/cm

Load Scale: 10.0 kip/cm

r_Y = .172 in.

K_c = 84.16 ksi $\sqrt{in}$

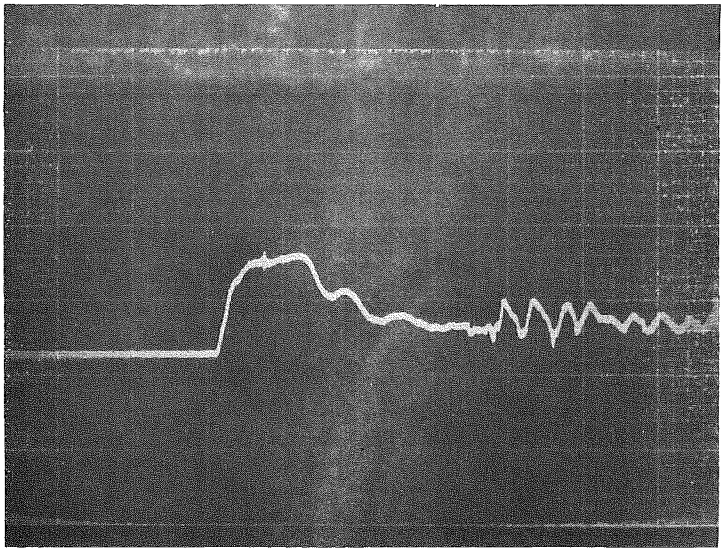

Temp.: 30^{o} F

Spec. No.: L511-4

Time Scale: 0.5 ms/cm

Load Scale: 10.0 kip/cm

r_Y = .249 in.

K_c = 100.2 ksi $\sqrt{in}$

Fig. 41 OSCILLOSCOPE RECORDS

1/2" SPECIMENS - IMPACT TESTS

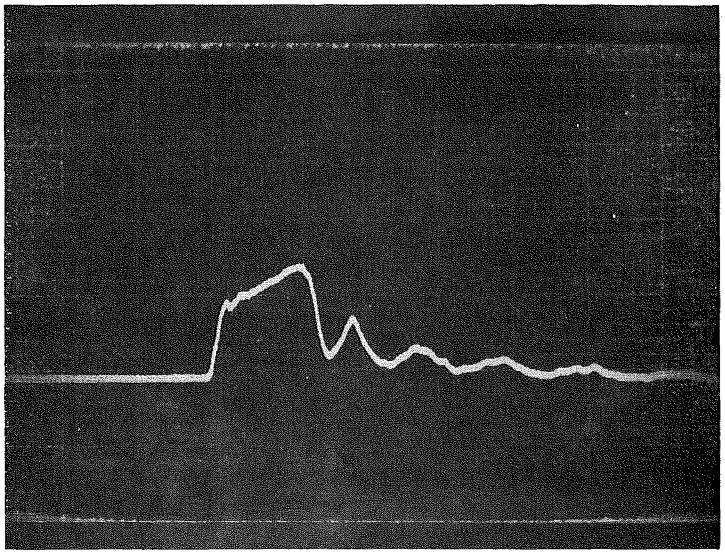

Temp.: 32^{o} F

Spec. No. T433-4

Time Scale: 0.5 ms/cm

Load Scale: 10.0 kip/cm

r_Y = .315 in.

K_c = 111.7 ksi $\sqrt{in}$

Fig. 41 OSCILLOSCOPE RECORDS

1" SPECIMENS - STATIC TESTS

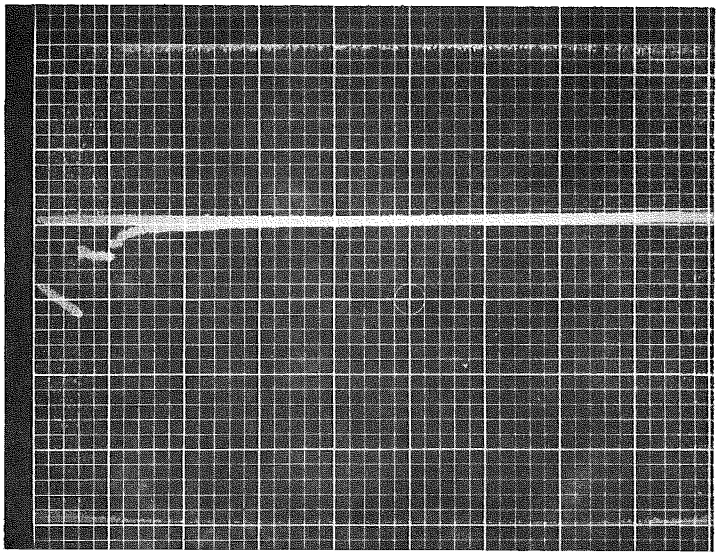

Temp.: -112^{o} F

Spec. No.: T224-2

Time Scale: 0.5 sec/cm

Load Scale: 10.0 kip/cm

r_Y = .055 in.

K_c = 46.45 ksi $\sqrt{in}$

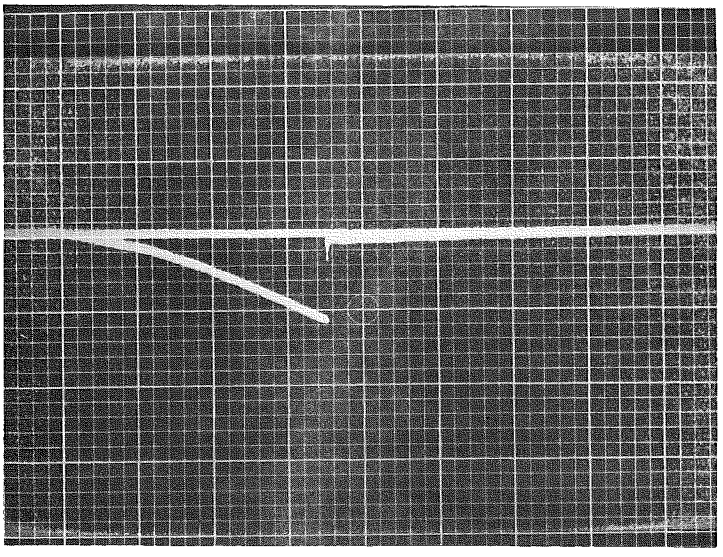

Temp.: -107^{o} F

Spec. No.: L512-3

Time Scale: 0.5 sec/cm

Load Scale: 10.0 kip/cm

r_Y = .0506 in.

K_c = 42.3 ksi $\sqrt{in}$.

Fig. 41 OSCILLOSCOPE RECORDS

1" SPECIMENS - STATIC TESTS

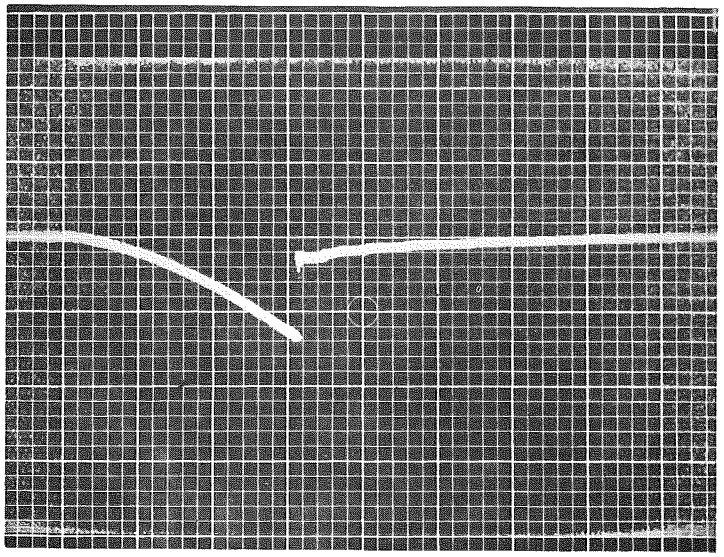

Temp.: -90° F

Spec. No.: L523-2

Time Scale: 0.5 sec/cm

Load Scale: 10.0 kip/cm

r_Y = .0852 in.

K_c = 53.65 ksi $\sqrt{in}$

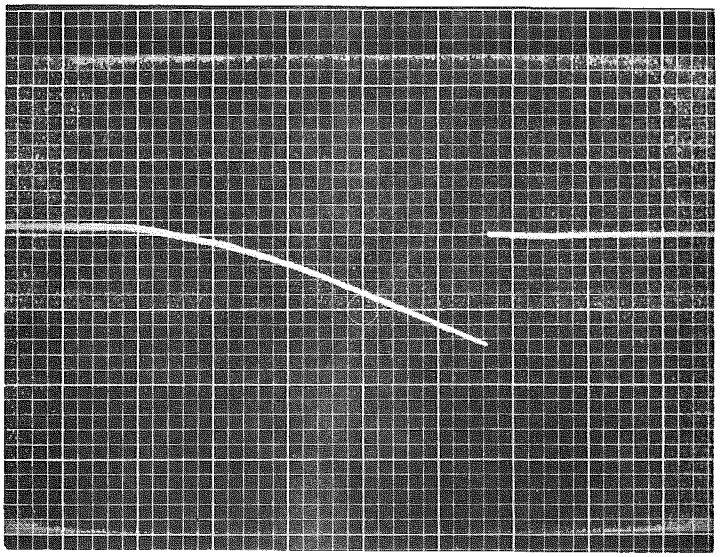

Temp.: -60° F

Spec. No.: L414-3

Time Scale: 0.5 sec/cm

Load Scale: 10.0 kip/cm

r_Y = .1316 in.

K_c = 62.78 ksi $\sqrt{in}$

Fig. 41 OSCILLOSCOPE RECORDS

1" SPECIMENS - STATIC TESTS

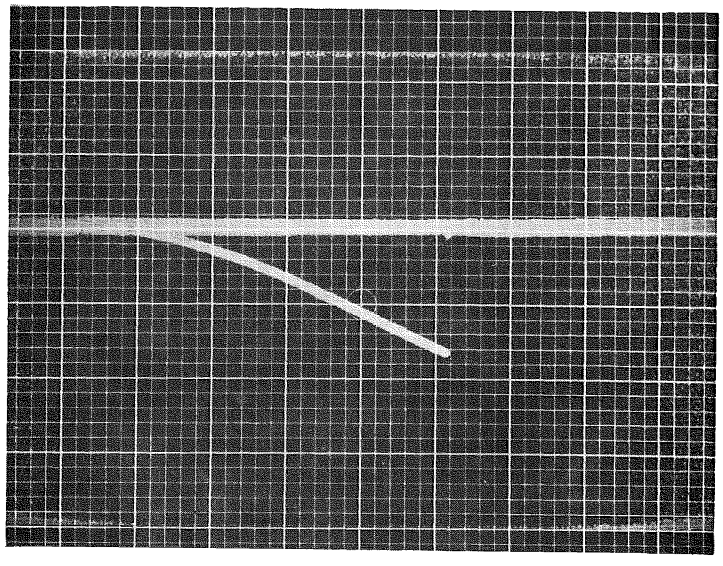

Temp.: -40^{o} F

Spec. No.: T232-2

Time Scale: 0.5 sec/cm

Load Scale: 10.0 kip/cm

r_Y = .1946 in.

K_c = 74.56 ksi $\sqrt{in}$

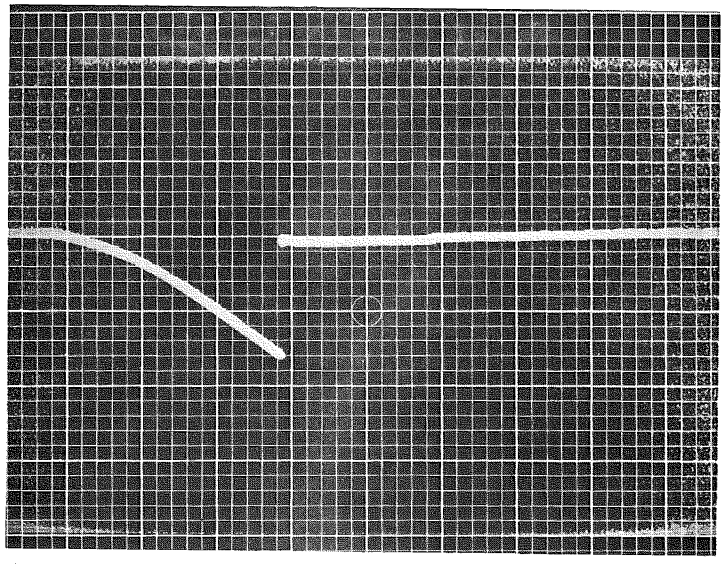

Temp.: -39^{o} F

Spec. No.: L622-2

Time Scale: 0.5 sec/cm

Load Scale: 10.0 kip/cm

r_Y = .1810 in.

K_c = 72.21 ksi $\sqrt{in}$

Fig. 41 OSCILLOSCOPE RECORDS

1" SPECIMENS - STATIC TESTS

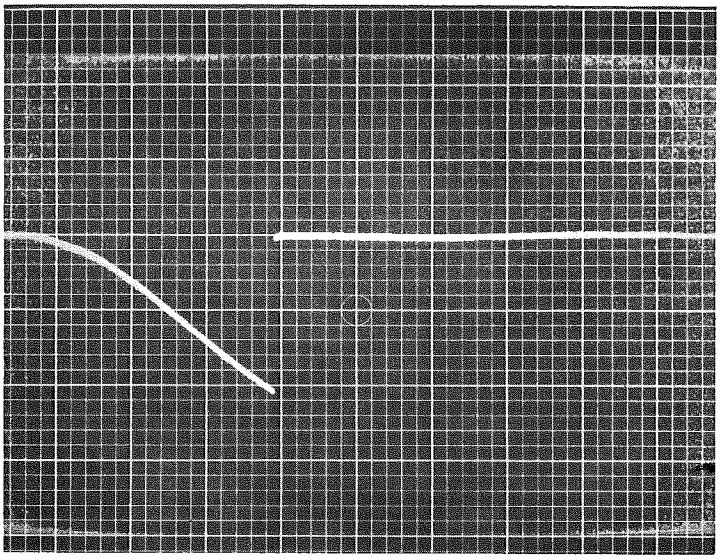

Temp.: -20^{o} F

Spec. No.: L624-3

Time Scale: 1 sec/cm

Load Scale: 10.0 kip/cm

r_Y = .449 in.

K_c = 109.0 ksi $\sqrt{in}$

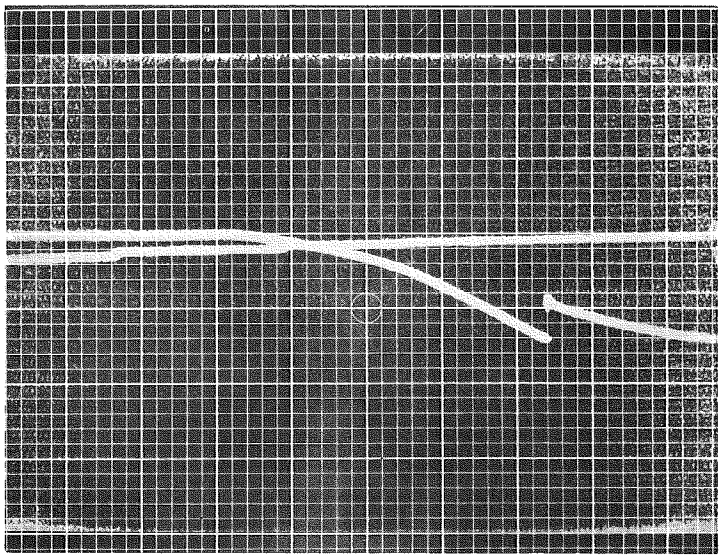

Temp.: 0^{o} F

Spec. No. T214-2

Time Scale: 0.5 sec/cm

Load Scale: 10.0 kip/cm

r_Y = .1451 in.

K_c = 60.32 ksi $\sqrt{in}$

Fig. 41 OSCILLOSCOPE RECORDS

1" SPECIMENS - STATIC TESTS

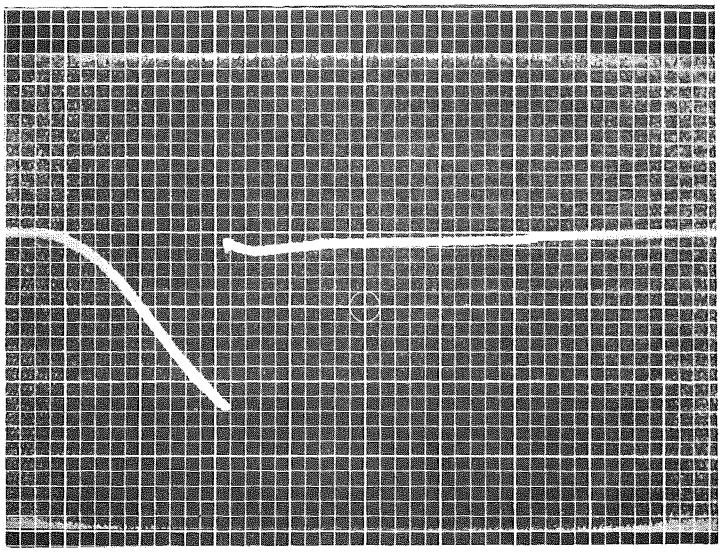

Temp.: 1^{o} F

Spec. No.: L512-2

Time Scale: 1 sec/cm

Load Scale: 10.0 kip/cm

$r_Y >$ .47 in.

$K_c >$ 109.0 ksi $\sqrt{in}$

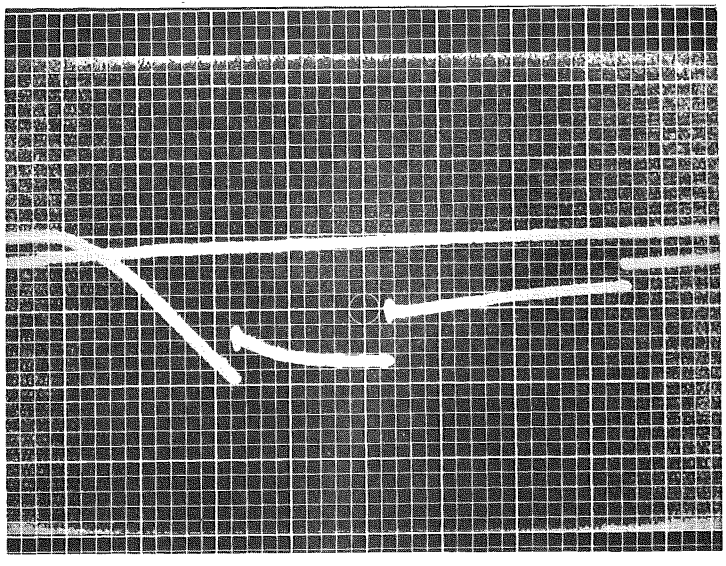

Temp.: 40^{o} F

Spec. No. T614-2

Time Scale: 1 sec/cm

Load Scale: 10.0 kip/cm

$r_Y >$ .437 in.

$K_c >$ 105.0 ksi $\sqrt{in}$

Fig. 41 OSCILLOSCOPE RECORDS

1" SPECIMENS - STATIC TESTS

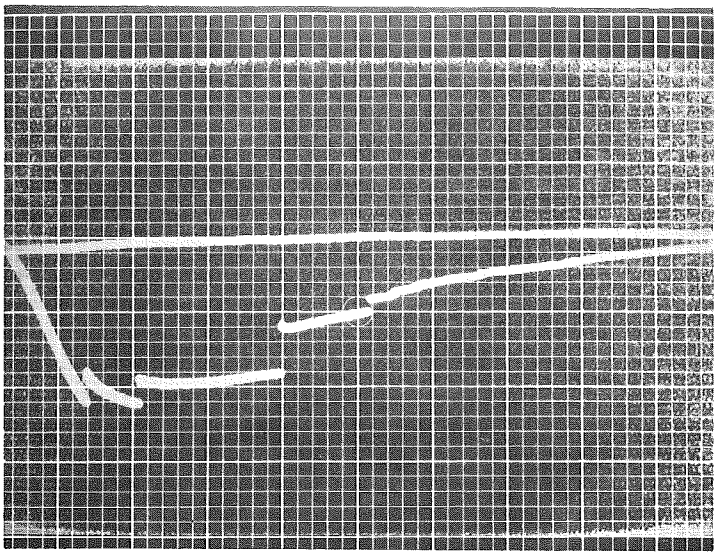

Temp.: 76° F

Spec. No. T434-2

Time Scale: 2 sec/cm

Load Scale: 10.0 kip/cm

r_Y > .491 in.

K_c > 103.0 ksi $\sqrt{in}$

1" SPECIMENS - IMPACT TESTS

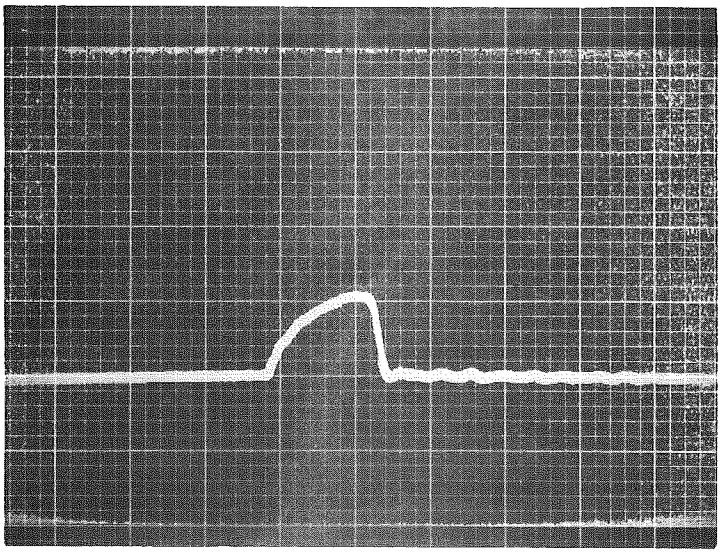

Temp.: -102° F

Spec. No. L623-2

Time Scale: 0.5 ms/cm

Load Scale: 10.0 kip/cm

r_Y = .0258 in.

K_c = 38.96 ksi $\sqrt{in}$

Fig. 41 OSCILLOSCOPE RECORDS

1" SPECIMENS - IMPACT TESTS

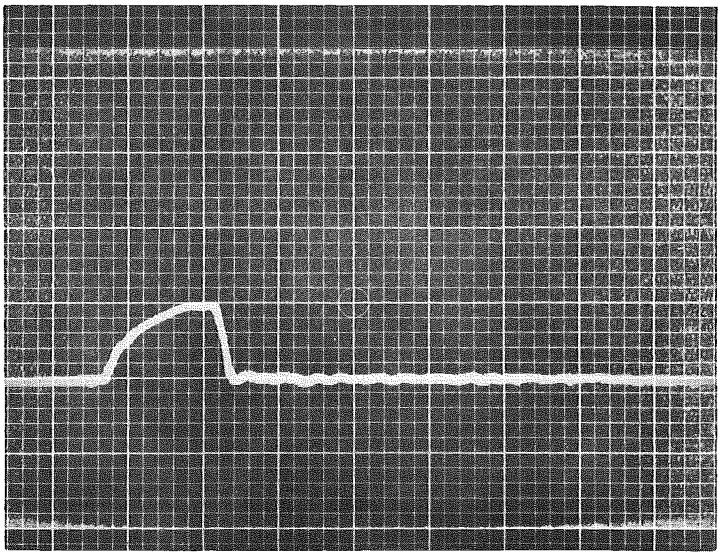

Temp.: -99^{o} F

Spec. No. L313-2

Time Scale: 0.5 ms/cm

Load Scale: 10.0 kip/cm

r_Y = .0249 in.

K_c = 37.95 ksi $\sqrt{in}$

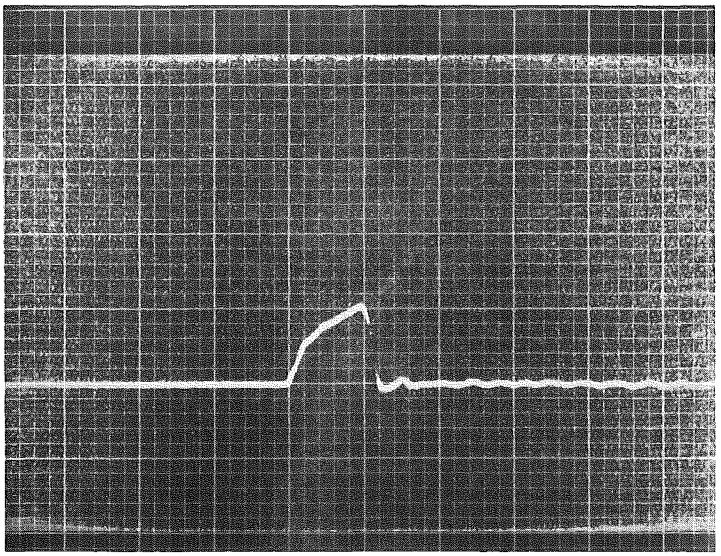

Temp.: -98^{o} F

Spec. No. L532-2

Time Scale: 0.5 ms/cm

Load Scale: 10.0 kip/cm

r_Y = .0271 in.

K_c = 40.07 ksi $\sqrt{in}$

Fig. 41 OSCILLOSCOPE RECORDS

1" SPECIMENS - IMPACT TESTS

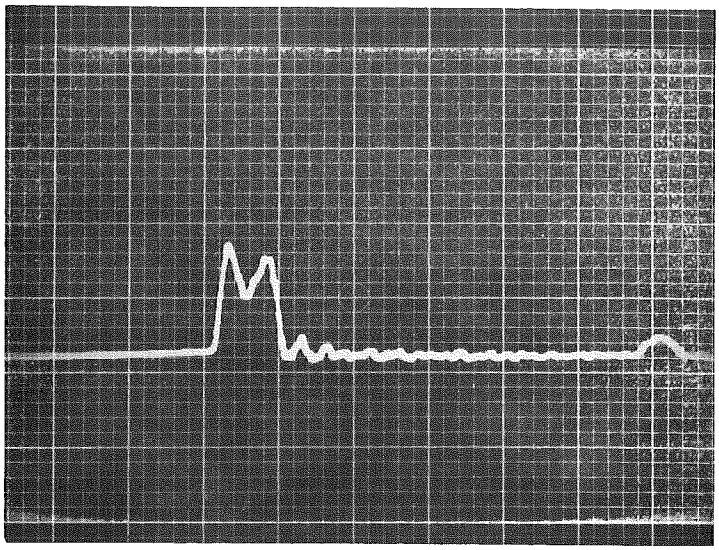

Temp.: -88^{o} F

Spec. No.: L131-2

Time Scale: 0.5 ms/cm

Load Scale: 10.0 kip/cm

r_Y = .0362 in.

K_c = 46.22 ksi $\sqrt{in}$

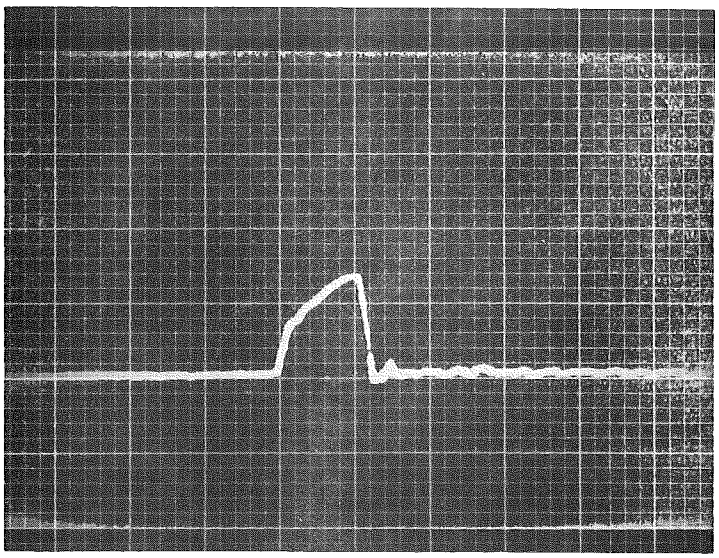

Temp.: -42^{o} F

Spec. No.: L112-2

Time Scale: 0.5 ms/cm

Load Scale: 10.0 kip/cm

r_Y = .0562 in.

K_c = 52.07 ksi $\sqrt{in}$

Fig. 41 OSCILLOSCOPE RECORDS

1" SPECIMENS - IMPACT TESTS

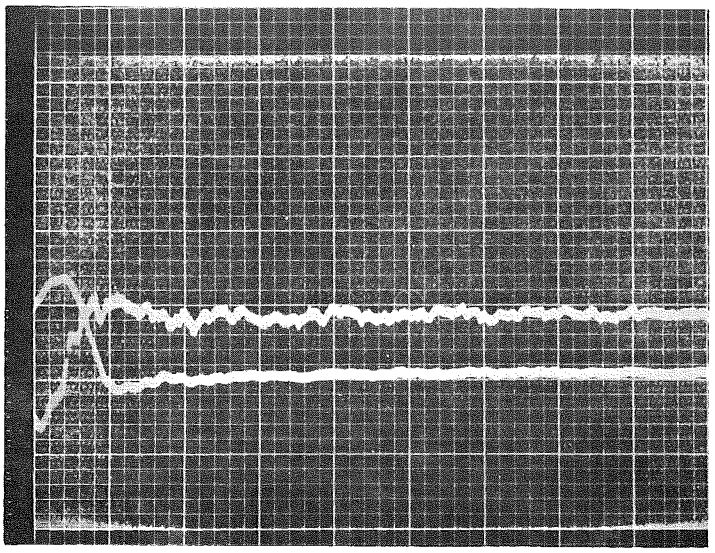

Temp.: -41^{o} F

Spec. No. L332-2

Time Scale: 0.2 ms/cm

Tup Record:

Load Scale: 10.0 kip/cm

r_Y = .0558 in.

K_c = 52.22 ksi $\sqrt{in}$

Beam Record:

Load Scale: 5.28 kip/cm

Note: Upper record (top record on right of picture) is from gages mounted on specimen. These gages failed prematurely because of poor bond to specimen.

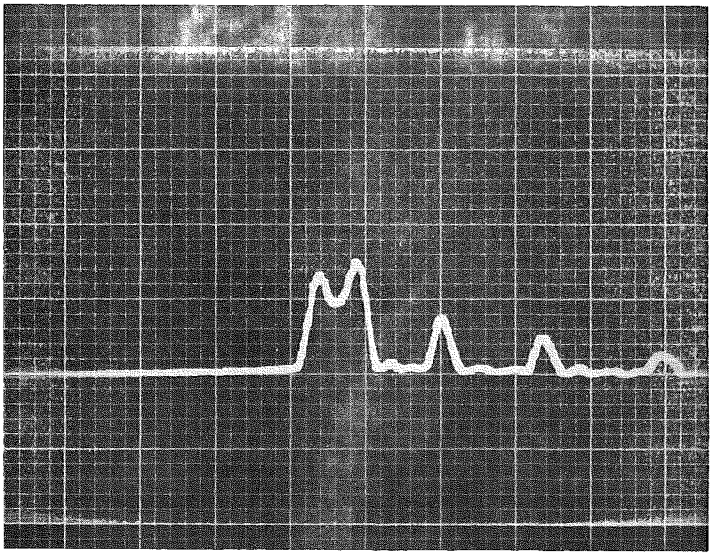

Temp.: -40^{o} F

Spec. No.: L534-2

Time Scale: 0.5 ms/cm

Load Scale: 10.0 kip/cm

r_Y = .0517 in.

K_c = 50.42 ksi $\sqrt{in}$

Fig. 41 OSCILLOSCOPE RECORDS

1" SPECIMENS - IMPACT TESTS

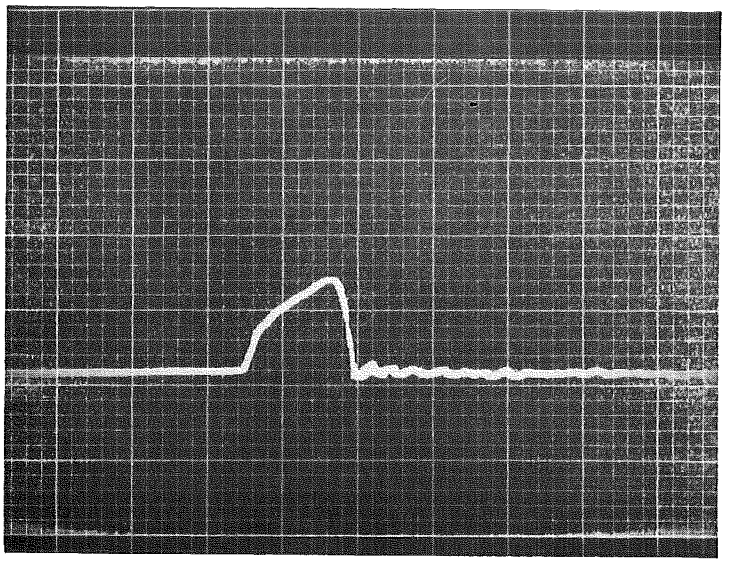

Temp.: -40^{o} F

Spec. No.: L312-2

Time Scale: 0.5 ms/cm

Load Scale: 10.0 kip/cm

r_Y = .0437 in.

K_c = 45.65 ksi $\sqrt{in}$

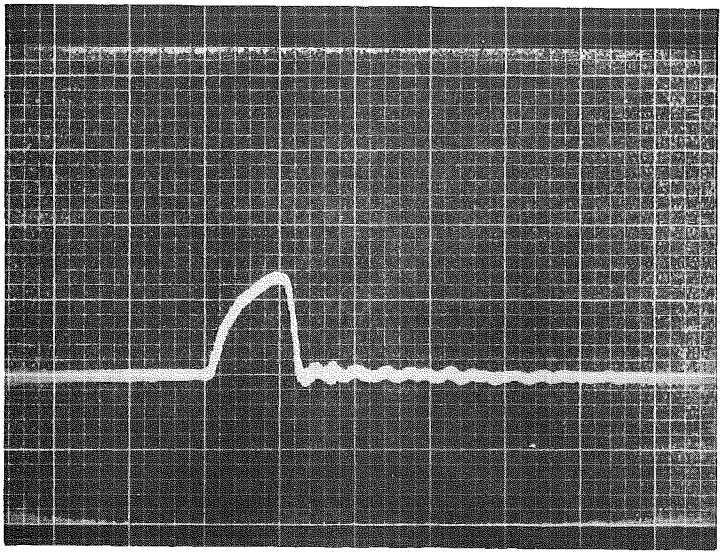

Temp.: -39^{o} F

Spec. No.: L134-2

Time Scale: 0.5 ms/cm

Load Scale: 10.0 kip/cm

r_Y = .0516 in.

K_c = 50.15 ksi $\sqrt{in}$

Fig. 41 OSCILLOSCOPE RECORDS

1" SPECIMENS - IMPACT TESTS

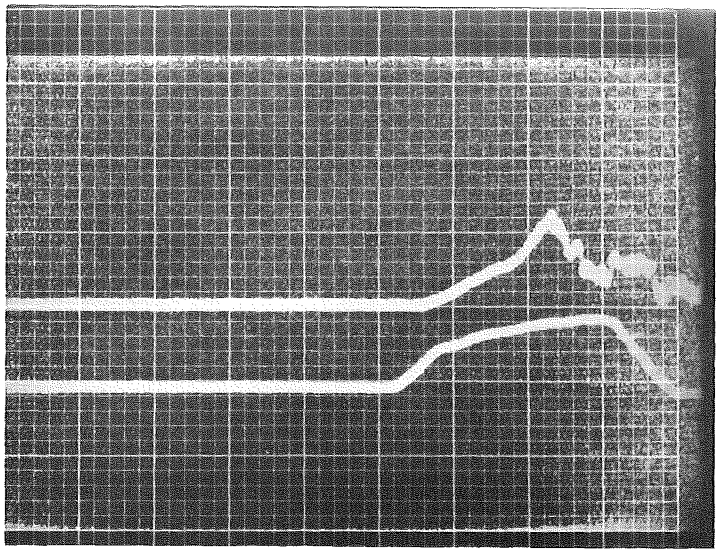

Temp.: -39^{o} F

Spec. No.: T211-2

Time Scale: 0.2 ms/cm

Tup Record:

Load Scale: 10.0 kip/cm

r_Y = .0320 in.

K_c = 30.09 ksi $\sqrt{in}$

Beam Record:

Load Scale: 5.8 kip/cm

Note: Upper record is from gages mounted on specimen. These gages failed prematurely because of poor bond to specimen.

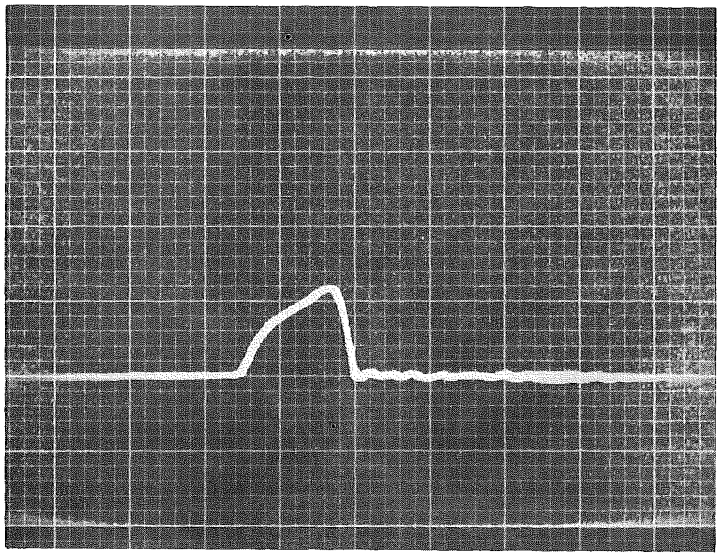

Temp.: -38^{o} F

Spec. No.: T233-2

Time Scale: 0.5 ms/cm

Load Scale: 10.0 kip/cm

r_Y = .0437 in.

K_c = 45.41 ksi $\sqrt{in}$

Fig. 41 OSCILLOSCOPE RECORDS

1" SPECIMENS - IMPACT TESTS

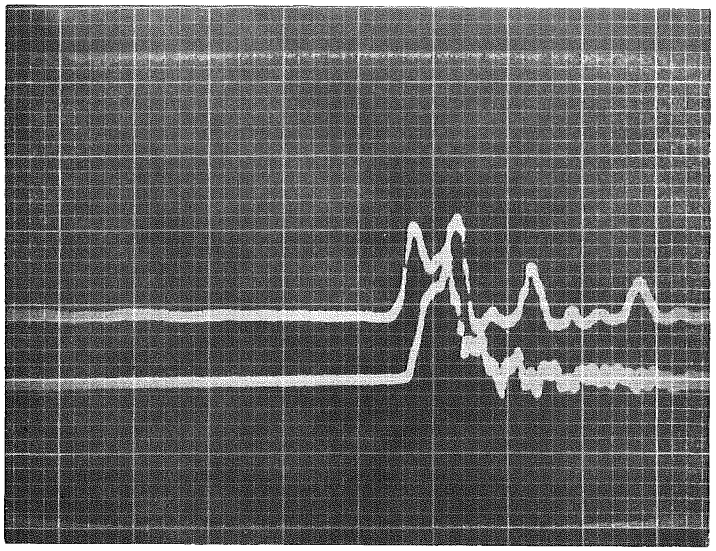

Temp.: -38^{o} F

Spec. No. T612-2

Time Scale: 0.5 ms/cm

Tup Record:

Load Scale: 10.0 kip/cm

r_Y = .0477 in.

K_c = 48.12 ksi $\sqrt{in}$

Beam Record:

Load Scale: 10.3 kip/cm

Note: Lower record is from gages mounted on specimen.
The record is illegible at fracture.

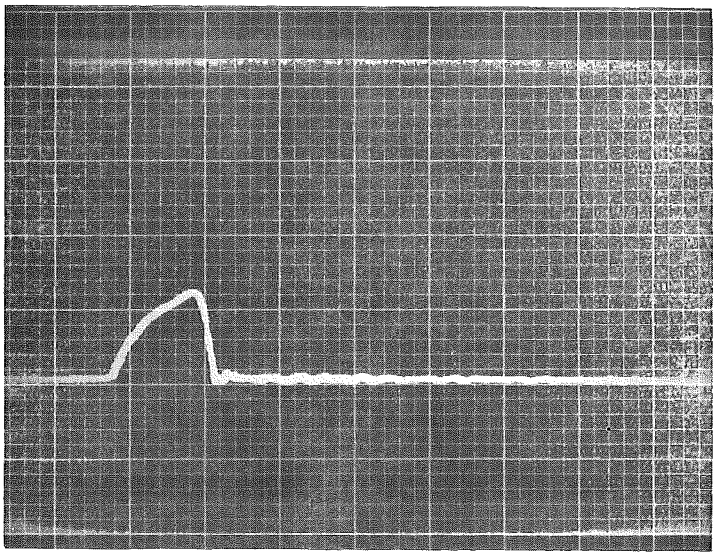

Temp.: -37^{o} F

Spec. No.: L514-2

Time Scale: 0.5 ms/cm

Load Scale: 10.0 kip/cm

r_Y = .0394 in.

K_c = 43.25 ksi $\sqrt{in}$

Fig. 41 OSCILLOSCOPE RECORDS

1" SPECIMENS - IMPACT TESTS

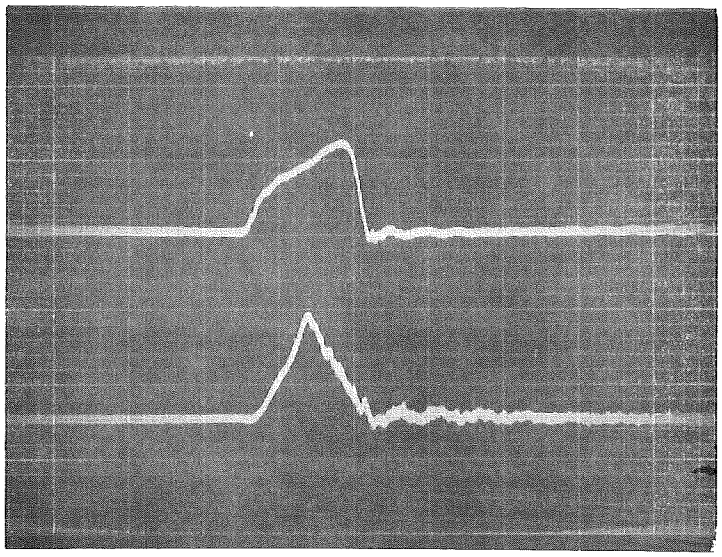

Temp.: -30^{o} F

Spec. No.: T422-2

Time Scale: 0.5 ms/cm

Tup Record:

Load Scale: 10.0 kip/cm

r_Y = .046 in.

K_c = 45.89 ksi $\sqrt{in}$

Beam Record:

Load Scale: 10.25 kip/cm

r_Y = .058 in.

K_c = 53.09 ksi $\sqrt{in}$

Note: Lower trace is from gages mounted on the specimen.

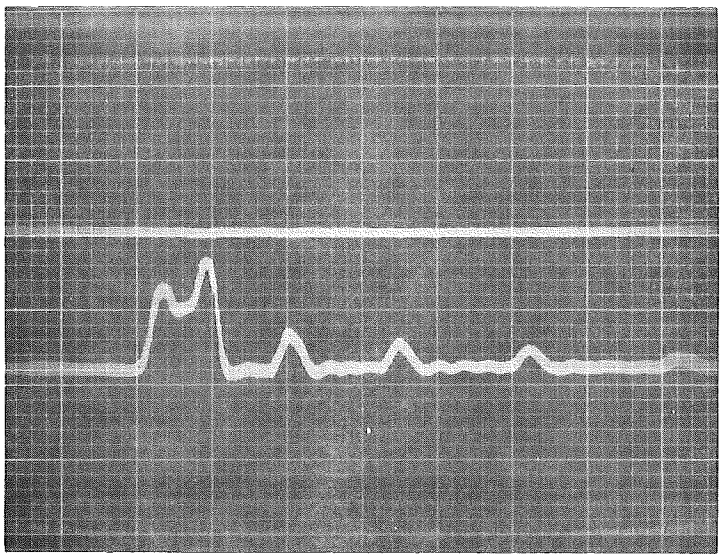

Temp.: -19^{o} F

Spec. No.: T632-2

Time Scale: 0.5 ms/cm

Load Scale: 10.0 kip/cm

r_Y = .065 in.

K_c = 54.39 ksi $\sqrt{in}$

Note: Upper trace means nothing.

Fig. 41 OSCILLOSCOPE RECORDS

1" SPECIMENS - IMPACT TESTS

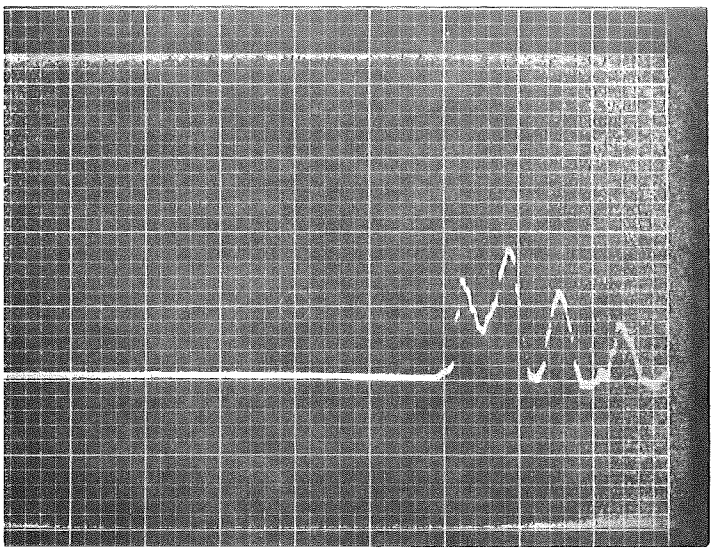

Temp.: 0^{o} F

Spec. No.: L524-2

Time Scale: 0.5 ms/cm

Load Scale: 10.0 kip/cm

r_Y = .109 in.

K_c = 68.53 ksi $\sqrt{in}$

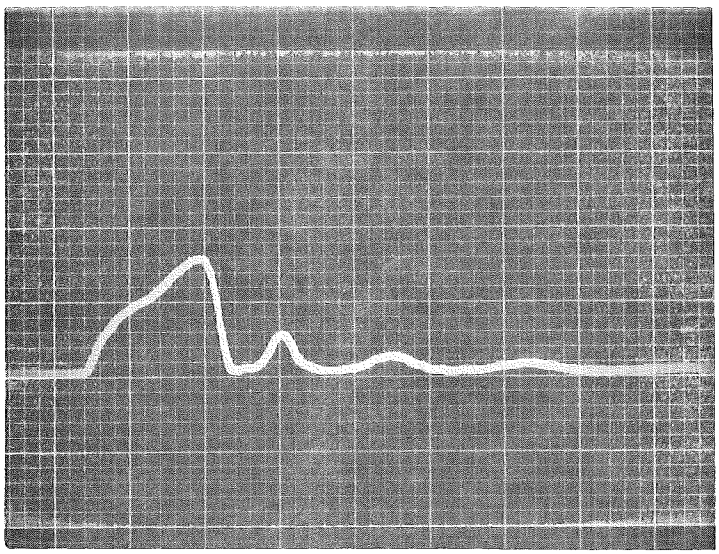

Temp.: 0^{o} F

Spec. No.: L624-2

Time Scale: 0.5 ms/cm

Load Scale: 10.0 kip/cm

r_Y = .0842 in.

K_c = 58.90 ksi $\sqrt{in}$

Fig. 41 OSCILLOSCOPE RECORDS

1" SPECIMENS - IMPACT TESTS

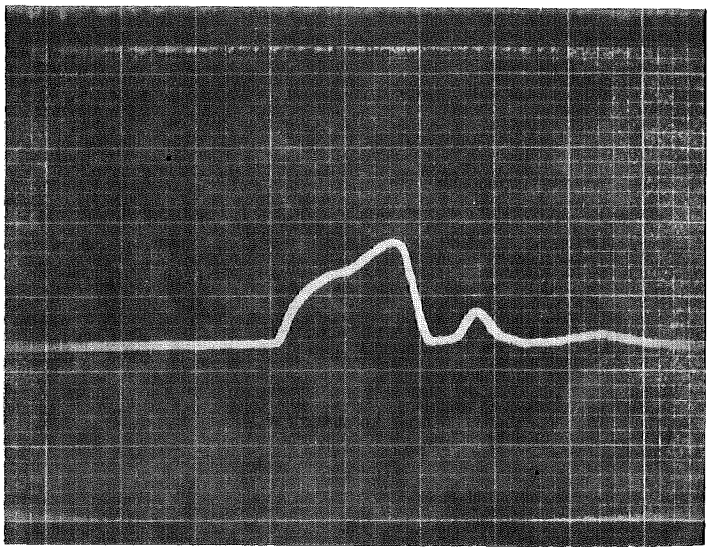

Temp.: 1° F

Spec. No.: L314-2

Time Scale: 0.5 ms/cm

Load Scale: 10.0 kip/cm

r_Y = .0643 in.

K_c = 50.91 ksi $\sqrt{in}$

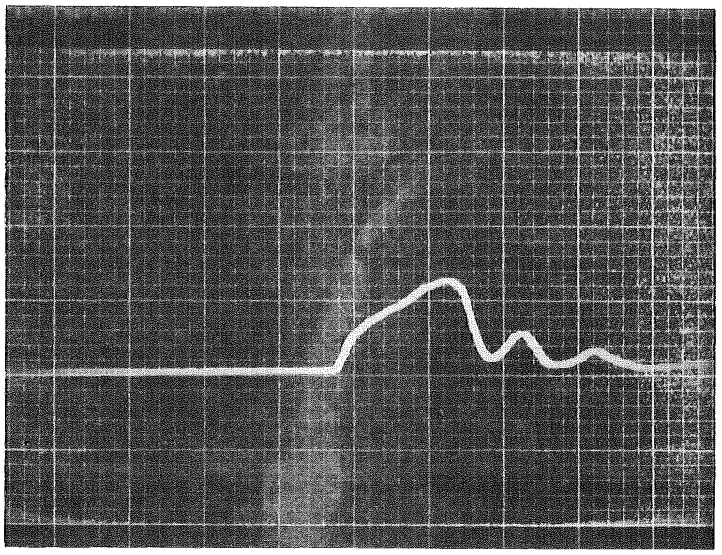

Temp.: 1° F

Spec. No.: T234-2

Time Scale: 0.5 ms/cm

Load Scale: 10.0 kip/cm

r_Y = .0521 in.

K_c = 46.39 ksi $\sqrt{in}$

Fig. 41 OSCILLOSCOPE RECORDS

1" SPECIMENS - IMPACT TESTS

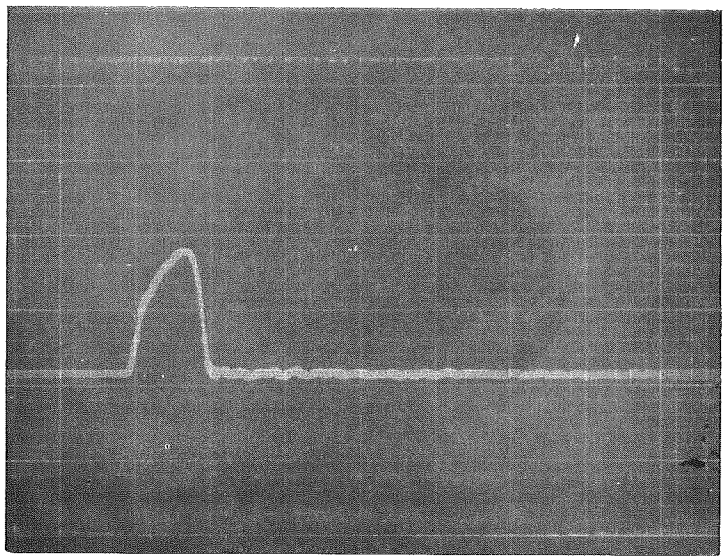

Temp.: 10^{o} F

Spec. No. T121-2

Time Scale: 0.5 ms/cm

Load Scale: 10.0 kip/cm

r_Y = .1192 in.

K_c = 70.92 ksi $\sqrt{in}$

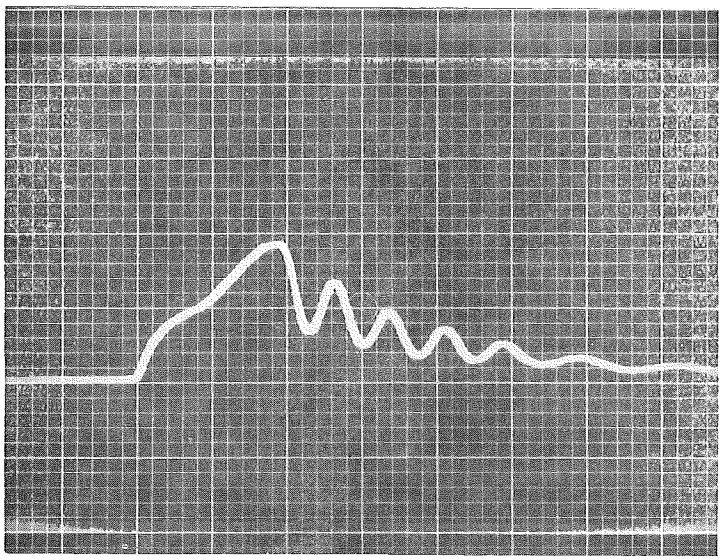

Temp.: 30^{o} F

Spec. No.: L521-2

Time Scale: 0.5 ms/cm

Load Scale: 10.0 kip/cm

r_Y = .1515 in.

K_c = 75.09 ksi $\sqrt{in}$

Fig. 41 OSCILLOSCOPE RECORDS

1" SPECIMENS - IMPACT TESTS

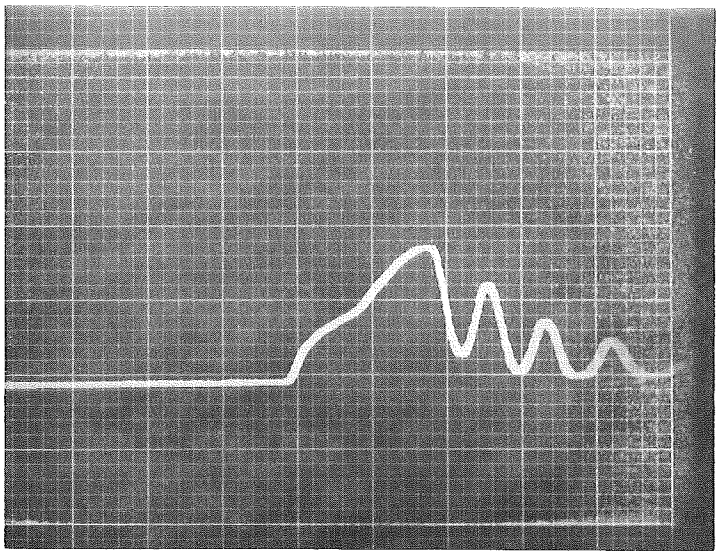

Temp.: 30^{o} F

Spec. No.: L324-2

Time Scale: 0.5 ms/cm

Load Scale: 10.0 kip/cm

r_Y = .1672 in.

K_c = 79.10 ksi $\sqrt{in}$

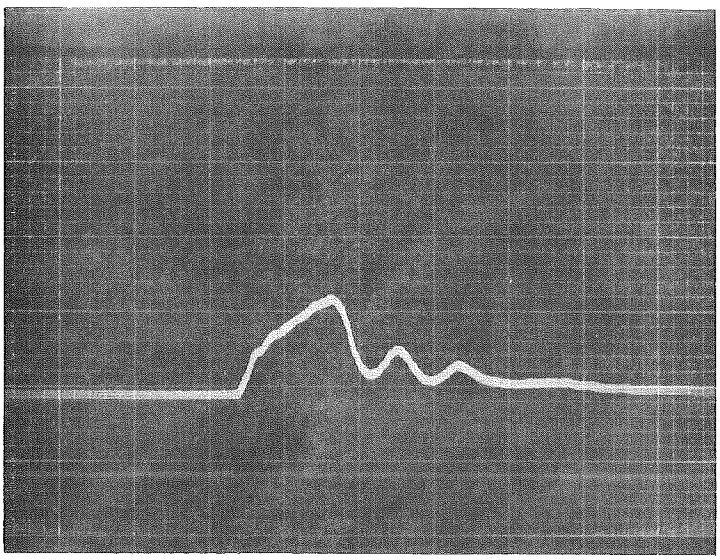

Temp.: 38^{o} F

Spec. No.: L522-2

Time Scale: 0.5 ms/cm

Load Scale: 10.0 kip/cm

r_Y = .1142 in.

K_c = 65.57 ksi $\sqrt{in}$

Fig. 41 OSCILLOSCOPE RECORDS

1" SPECIMENS - IMPACT TESTS

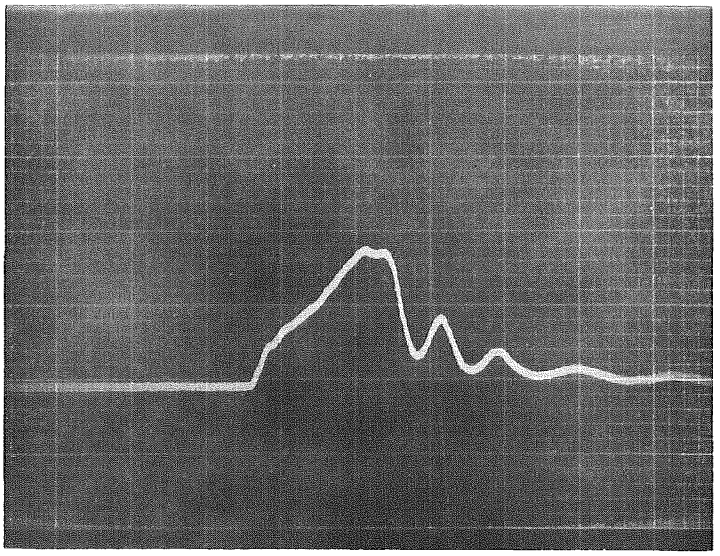

Temp.: 39° F

Spec. No.: T613-2

Time Scale: 0.5 ms/cm

Load Scale: 10.0 kip/cm

r_Y = .1459 in.

K_c = 73.05 ksi $\sqrt{in}$

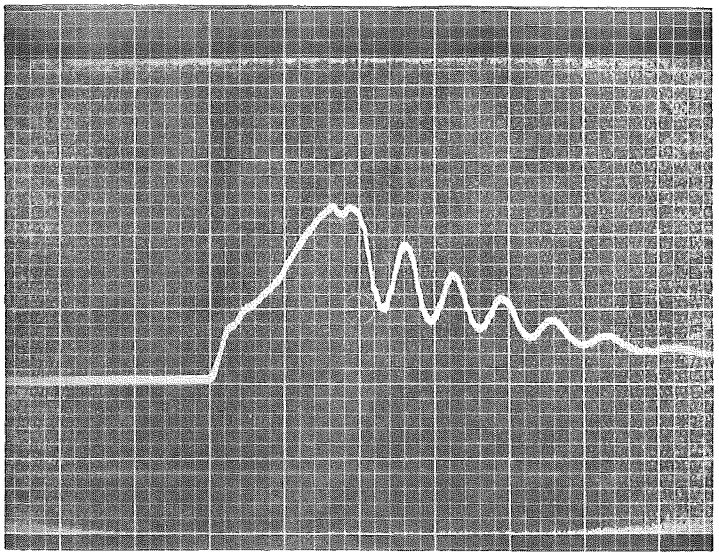

Temp.: 57° F

Spec. No.: L531-2

Time Scale: 0.5 ms/cm

Load Scale: 10.0 kip/cm

r_Y > .446 in.

K_c > 125.3 ksi $\sqrt{in}$

Fig. 41 OSCILLOSCOPE RECORDS

1" SPECIMENS - IMPACT TESTS

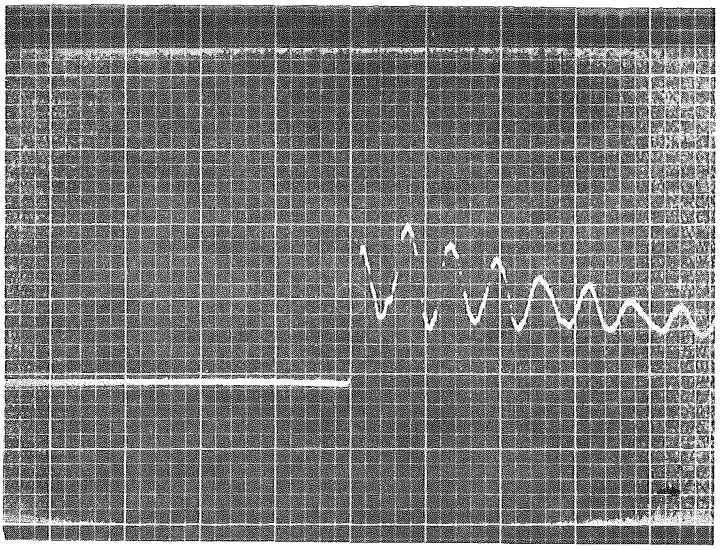

Temp.: 58^{o} F

Spec. No.: L513-2

Time Scale: 0.5 ms/cm

Load Scale: 10.0 kip/cm

r_Y = .2193 in.

K_c = 90.51 ksi $\sqrt{in}$

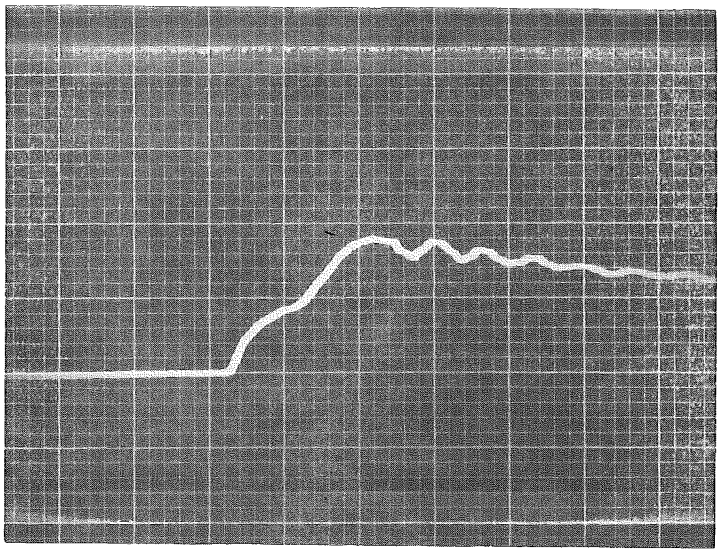

Temp.: 80^{o} F

Spec. No.: T231-2

Time Scale: 0.5 ms/cm

Load Scale: 10.0 kip/cm

r_Y > .2087

K_c > 83.02 ksi $\sqrt{in}$

Fig. 41 OSCILLOSCOPE RECORDS

2" SPECIMENS - STATIC TESTS

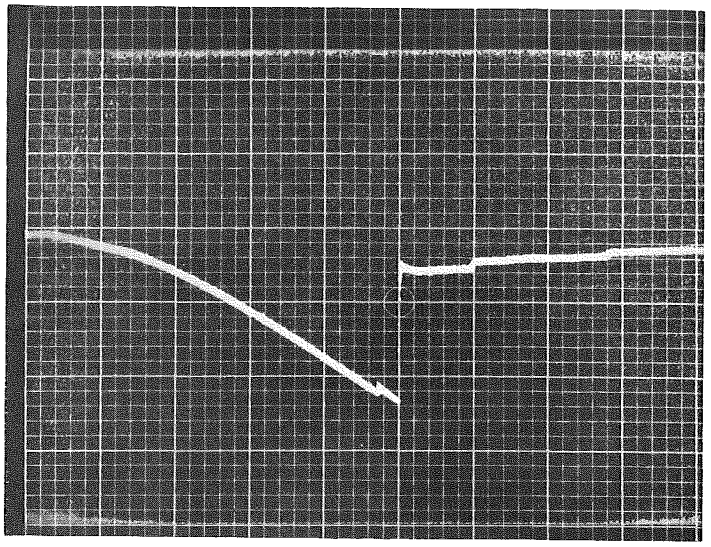

Temp.: -112° F

Spec. No.: L622-3

Time Scale: 0.5 sec/cm

Load Scale: 10.0 kip/cm

r_Y = .0496 in.

K_c = 41.22 ksi $\sqrt{in}$

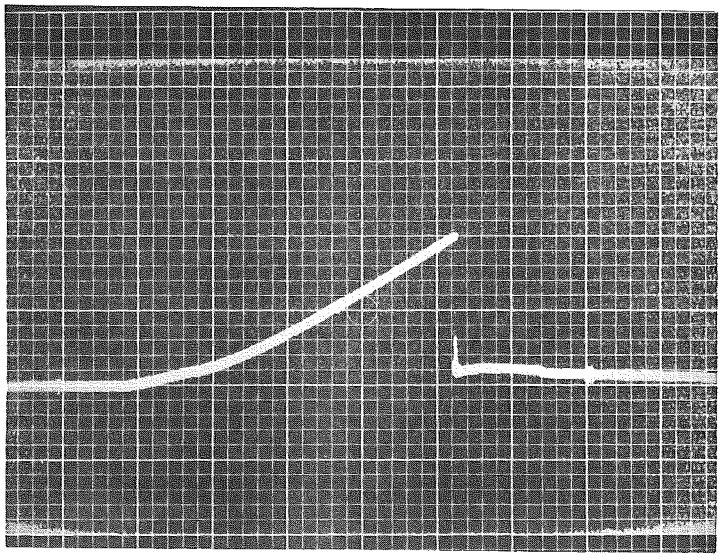

Temp.: -90° F

Spec. No.: L531-3

Time Scale: 0.5 sec/cm

Load Scale: 10.0 kip/cm

r_Y = .0714 in.

K_c = 47.61 ksi $\sqrt{in}$

Fig. 41 OSCILLOSCOPE RECORDS

2" SPECIMENS - STATIC TESTS

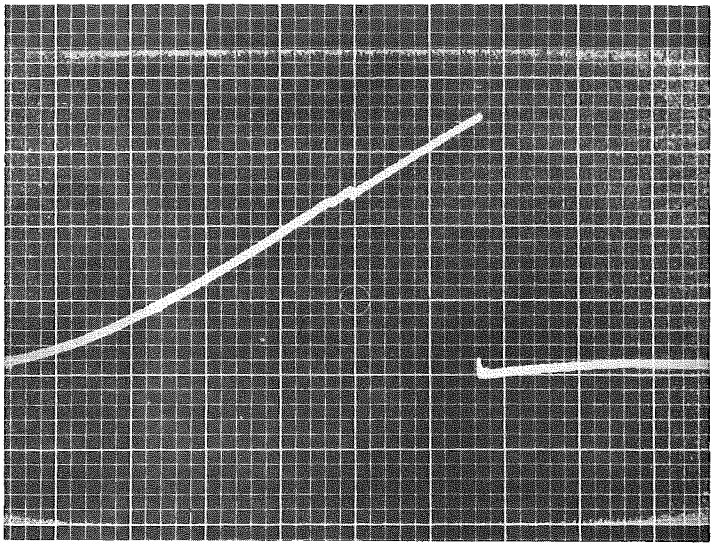

Temp.: -40^{o} F

Spec. No.: L522-3

Time Scale: 0.5 sec/cm

Load Scale: 10.0 kip/cm

r_Y = .1653 in.

K_c = 66.25 ksi $\sqrt{in}$

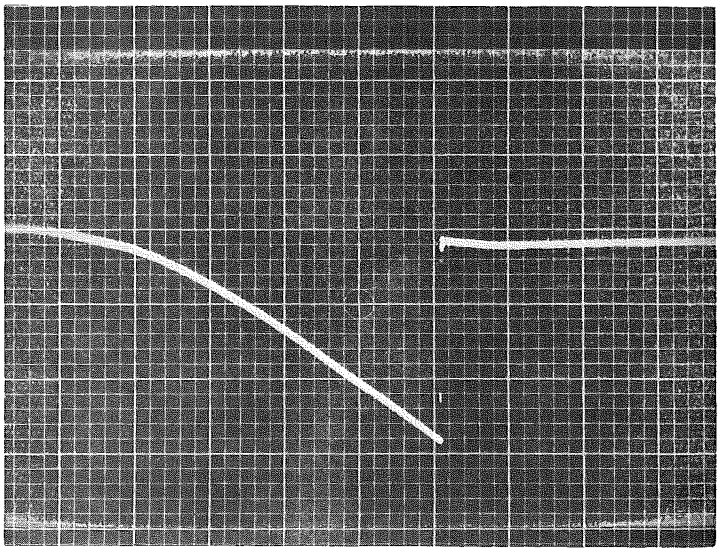

Temp.: -40^{o} F

Spec. No.: T632-3

Time Scale: 0.5 sec/cm

Load Scale: 10.0 kip/cm

r_Y = .1015 in.

K_c = 52.26 ksi $\sqrt{in}$

Fig. 41 OSCILLOSCOPE RECORDS

2" SPECIMENS - STATIC TESTS

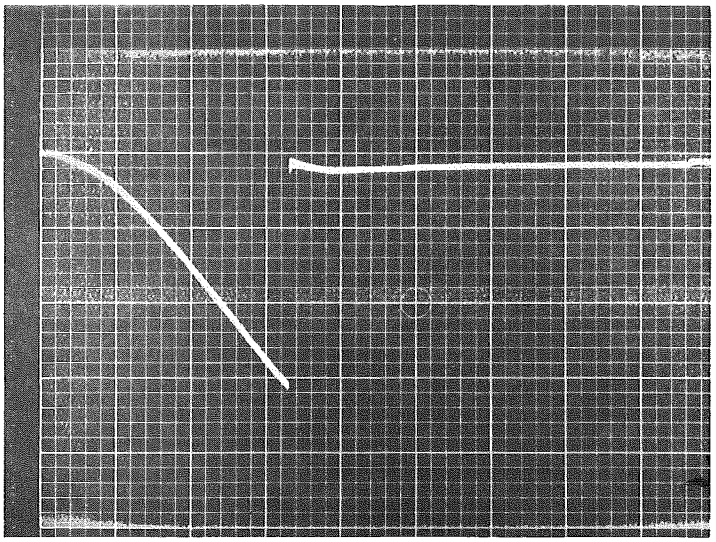

Temp.: -4^{o} F

Spec. No.: L513-3

Time Scale: 1.0 sec/cm

Load Scale: 10.0 kip/cm

r_Y = .1922 in.

K_c = 68.15 ksi $\sqrt{in}$

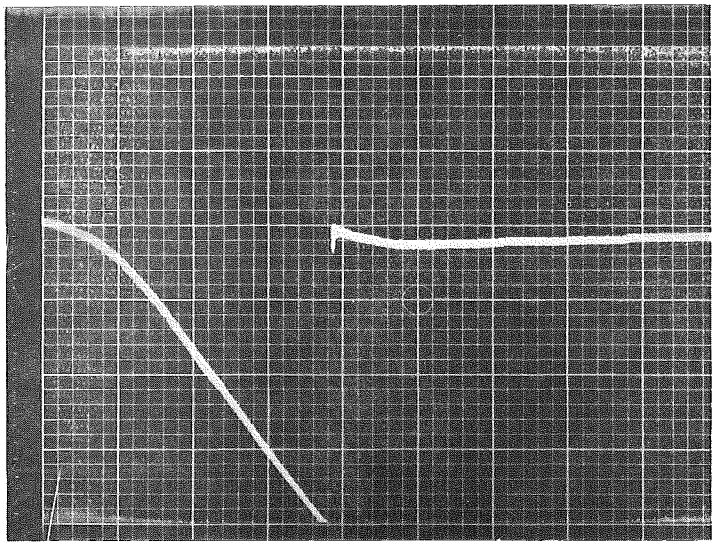

Temp.: 20^{o} F

Spec. No.: L623-3

Time Scale: 1.0 sec/cm

Load Scale: 10.0 kip/cm

r_Y = .347 in.

K_c = 88.6 ksi $\sqrt{in}$

Fig. 41 OSCILLOSCOPE RECORDS

2" SPECIMENS - STATIC TESTS

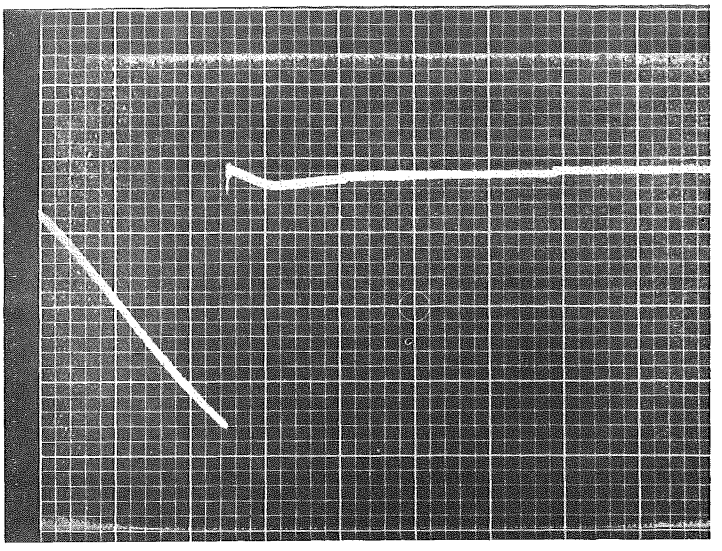

Temp.: 40^{o} F

Spec. No.: L532-3

Time Scale: 1 sec/cm

Load Scale: 10.0 kip/cm

$r_Y >$ .454 in.

$K_c > 99.2$ ksi $\sqrt{in}$

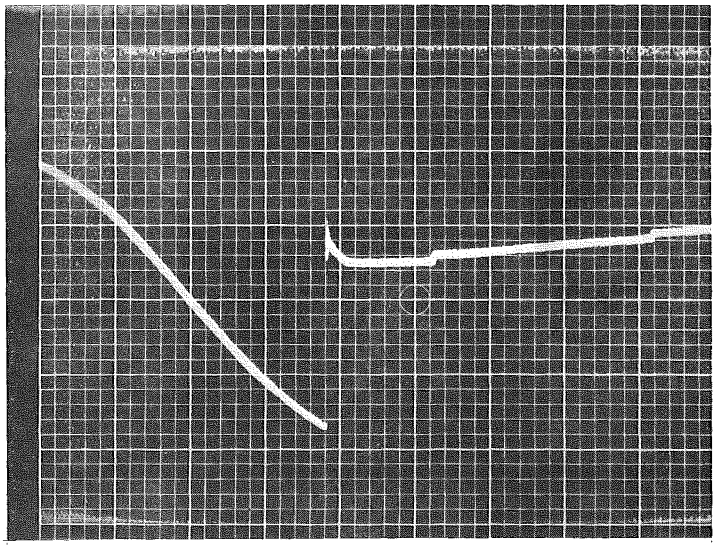

Temp.: 82^{o} F

Spec. No.: L624-3

Time Scale: 1 sec/cm

Load Scale: 10.0 kip/cm

$r_Y >$ .435 in.

$K_c > 93.1$ ksi $\sqrt{in}$

Fig. 41 OSCILLOSCOPE RECORDS

2" SPECIMENS - IMPACT TESTS

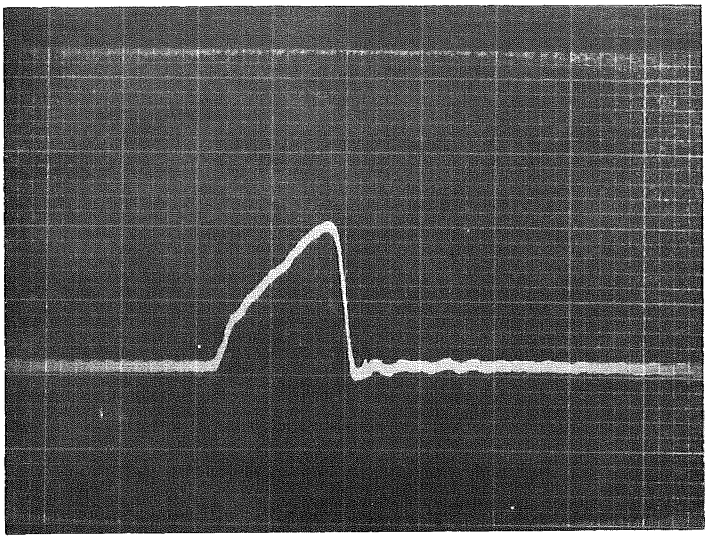

Temp.: -43° F

Spec. No.: T634-3

Time Scale: 0.5 ms/cm

Load Scale: 10.0 kip/cm

r_Y = .039 in.

K_c = 42.18 ksi $\sqrt{in}$

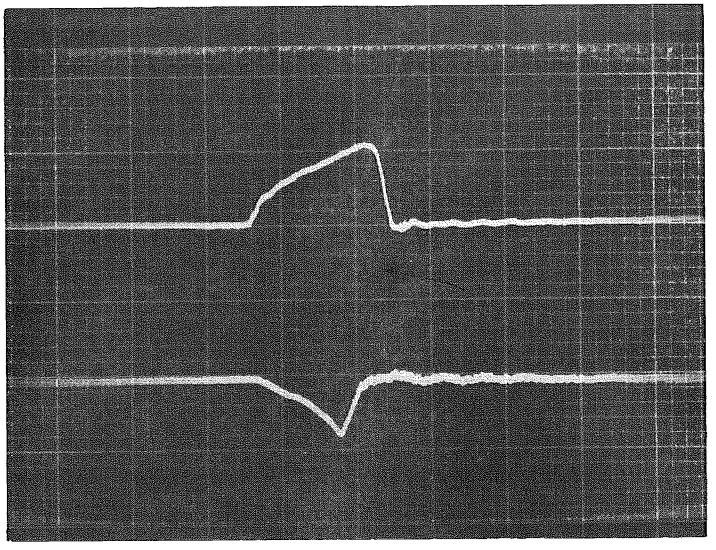

Temp.: -38° F

Spec. No.: L533-3

Time Scale: 0.5 ms/cm

Tup Record:

Load Scale: 20.0 kip/cm

r_Y = .039 in.

K_c = 41.55 ksi $\sqrt{in}$

Beam Record:

Load Scale: 41.0 kip/cm

r_Y = .085 in.

K_c = 62.27 ksi $\sqrt{in}$

Note: Lower record is from gages mounted on specimen.

Fig. 41 OSCILLOSCOPE RECORDS

2" SPECIMENS - IMPACT TESTS

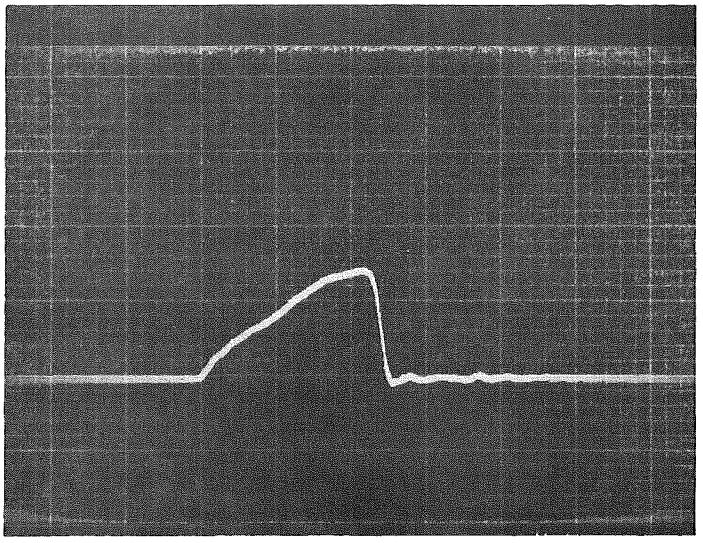

Temp.: 0^{o} F

Spec. No.: T612-3

Time Scale: 0.5 ms/cm

Load Scale: 20.0 kip/cm

r_Y = .075 in.

K_c = 53.80 ksi $\sqrt{in}$

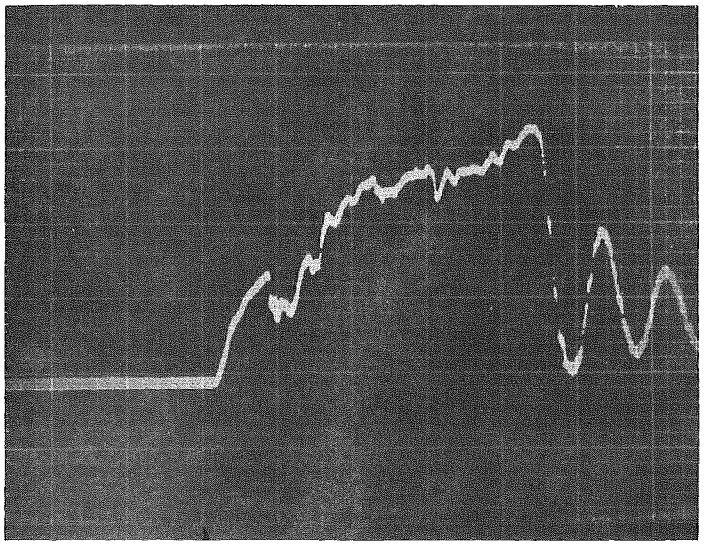

Temp.: 39^{o} F

Spec. No.: L511-3

Time Scale: 0.5 ms/cm

Load Scale: 10.0 kip/cm

r_Y = .0913 in.

K_c = 54.87 ksi $\sqrt{in}$

Fig. 41 OSCILLOSCOPE RECORDS

2" SPECIMENS - IMPACT TESTS

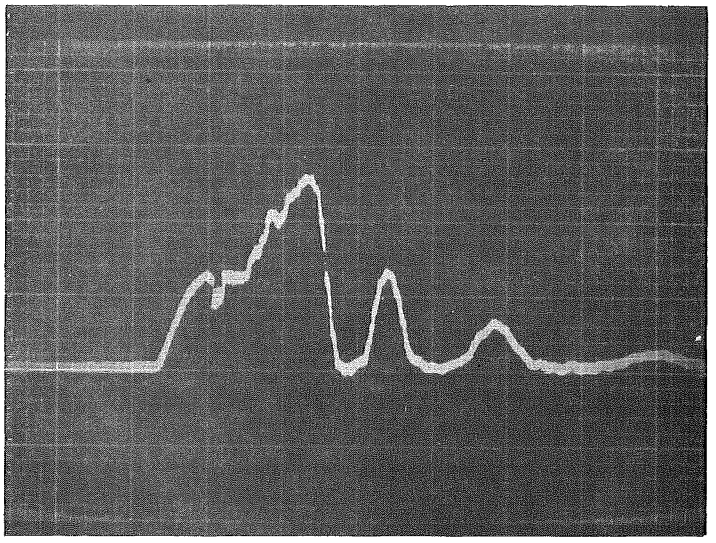

Temp.: 39^{o} F

Spec. No.: T611-3

Time Scale: 0.5 ms/cm

Load Scale: 10.0 kip/cm

r_Y = .2525 in.

K_c = 93.87 ksi $\sqrt{in}$

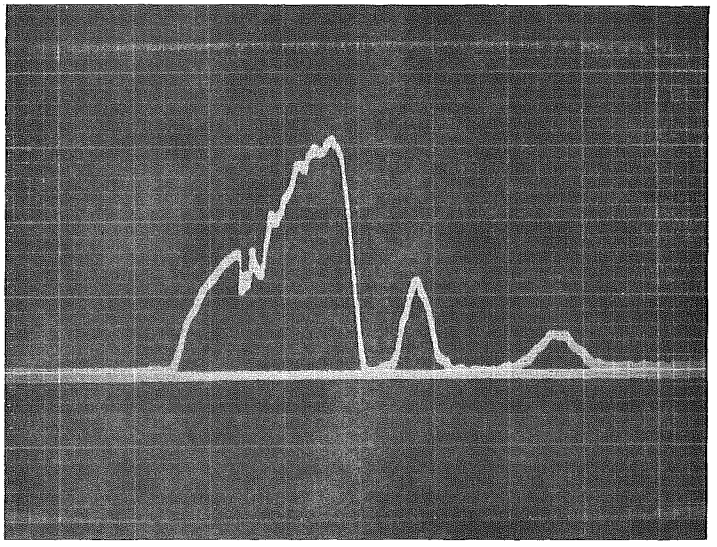

Temp.: 40^{o} F

Spec. No.: T613-3

Time Scale: 0.5 ms/cm

Load Scale: 10.0 kip/cm

r_Y = .0916 in.

K_c = 56.41 ksi $\sqrt{in}$

Fig. 41 OSCILLOSCOPE RECORDS

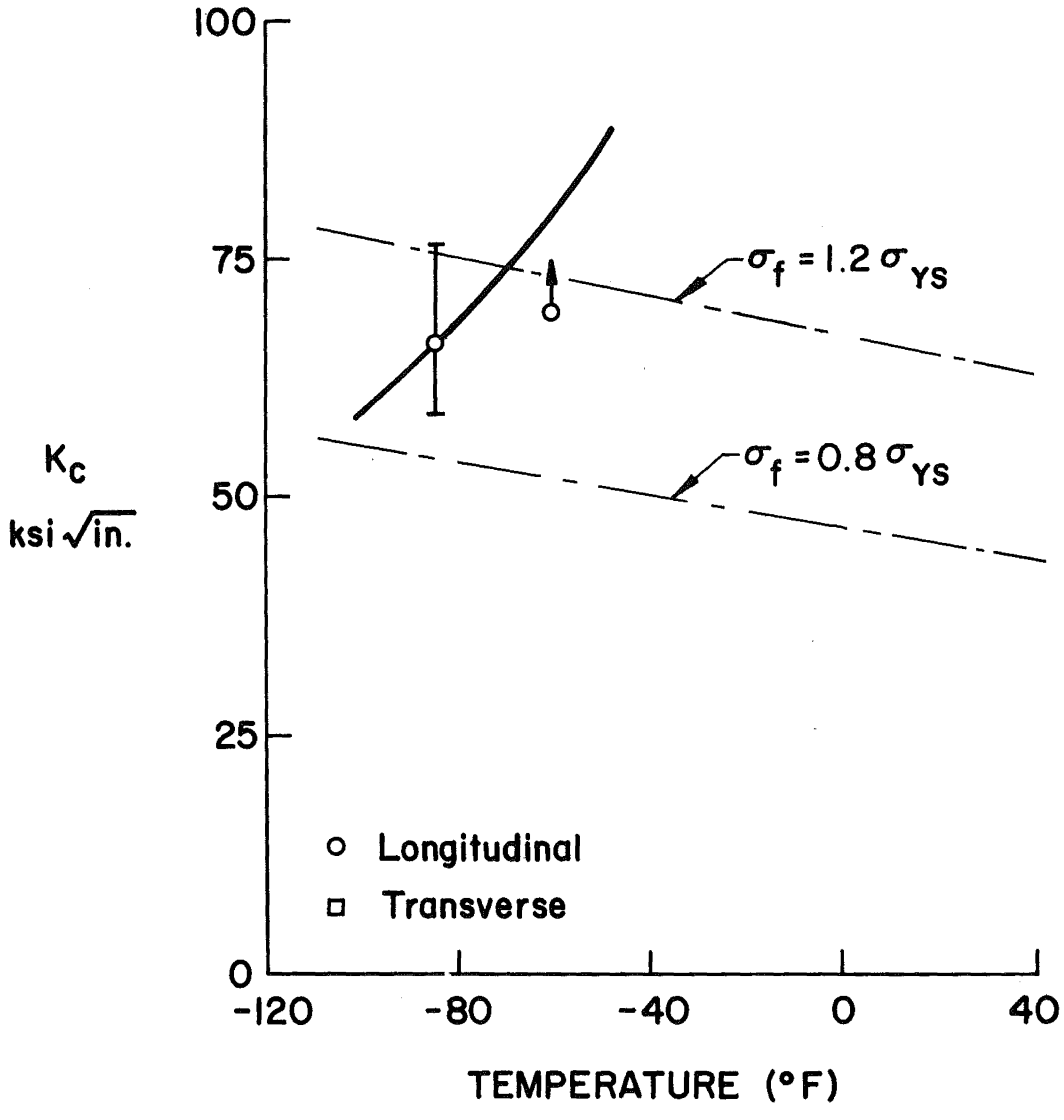

Fig. 42 K_c VERSUS TEMPERATURE: STATIC TESTS OF 1/2" PLATE

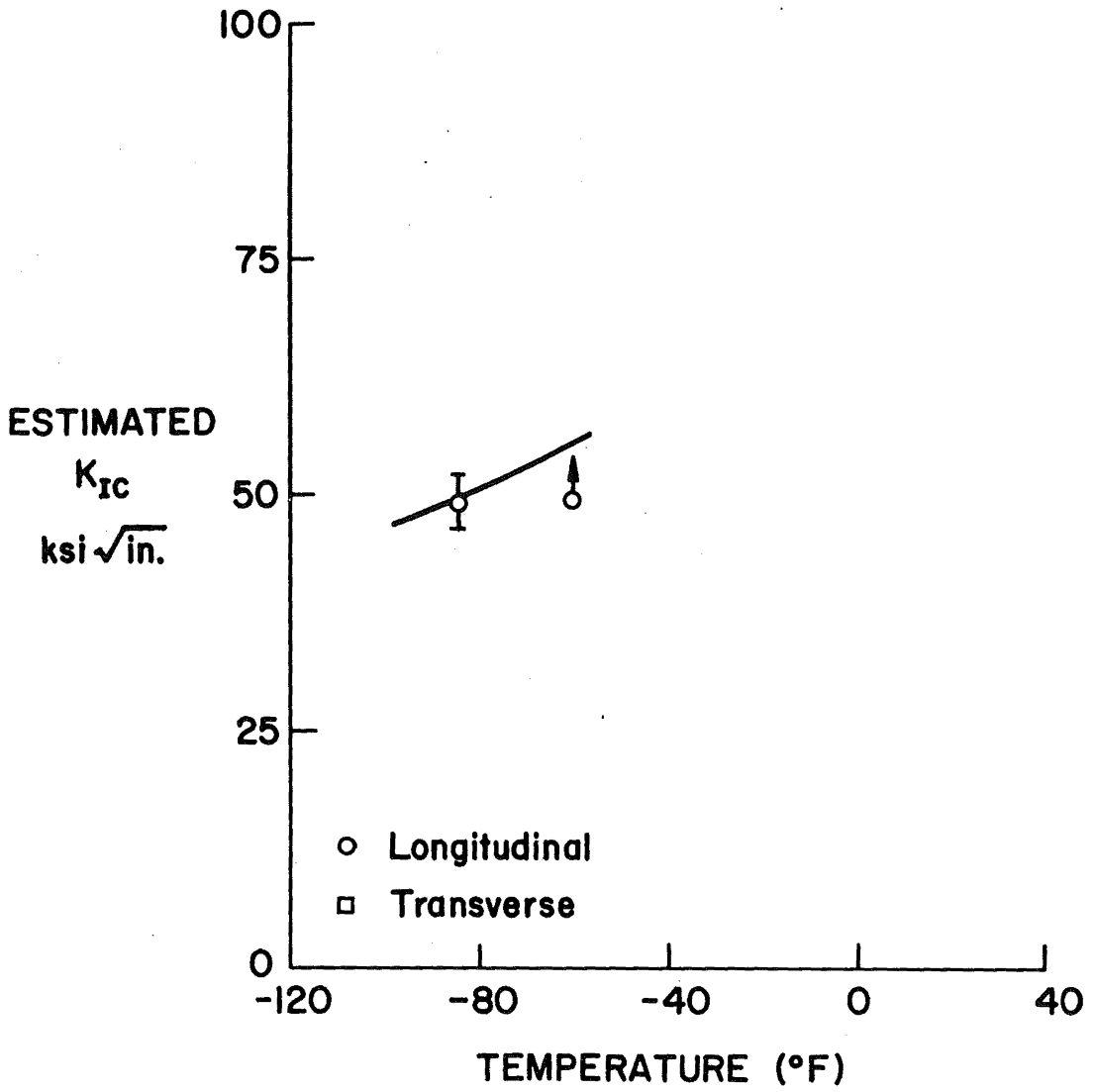

Fig. 43 K_{Ic} VERSUS TEMPERATURE: STATIC TEST OF 1/2" PLATE

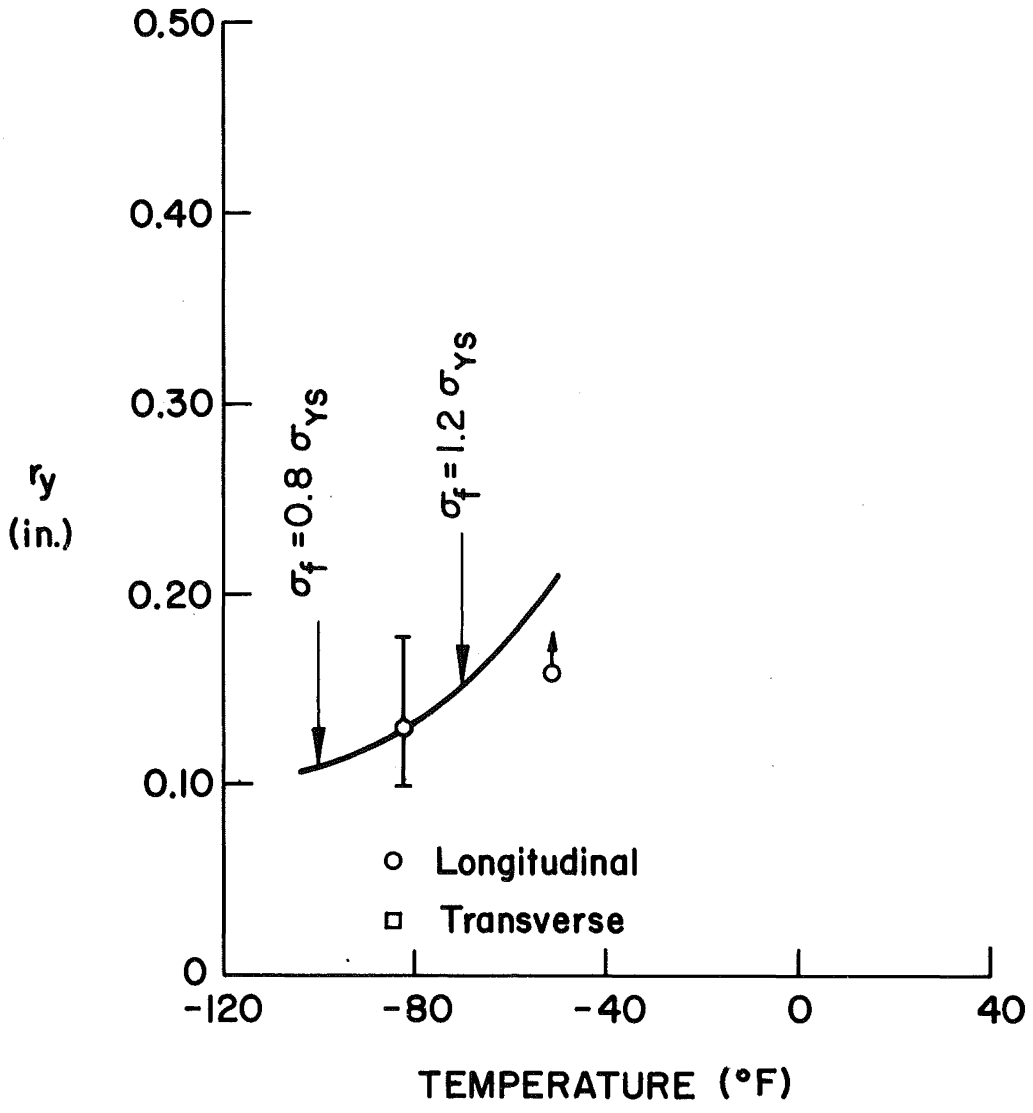

Fig. 44 r_Y VERSUS TEMPERATURE: STATIC TESTS OF 1/2" PLATE

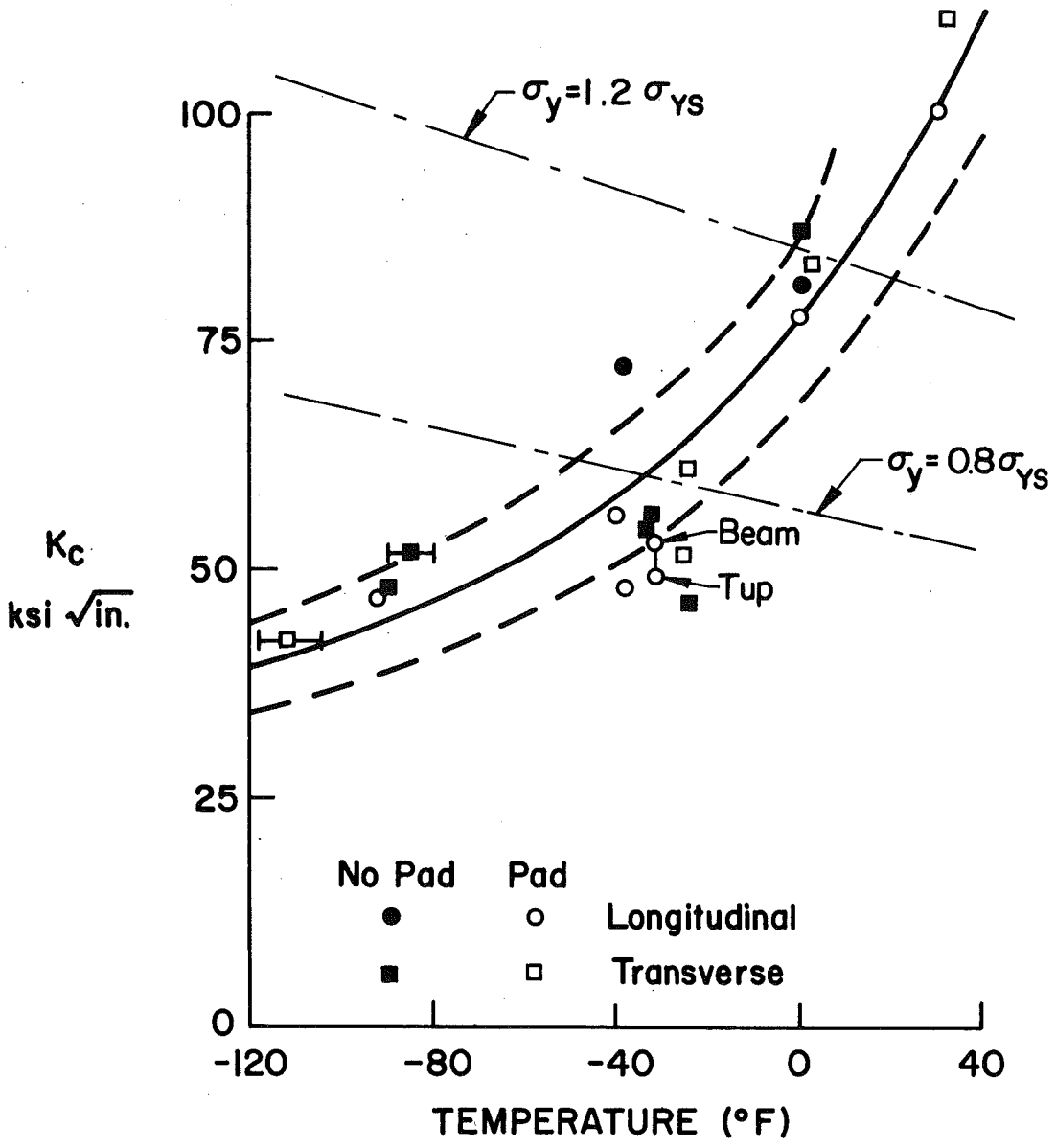

Fig. 45 K_c VERSUS TEMPERATURE: IMPACT TESTS OF 1/2" PLATE

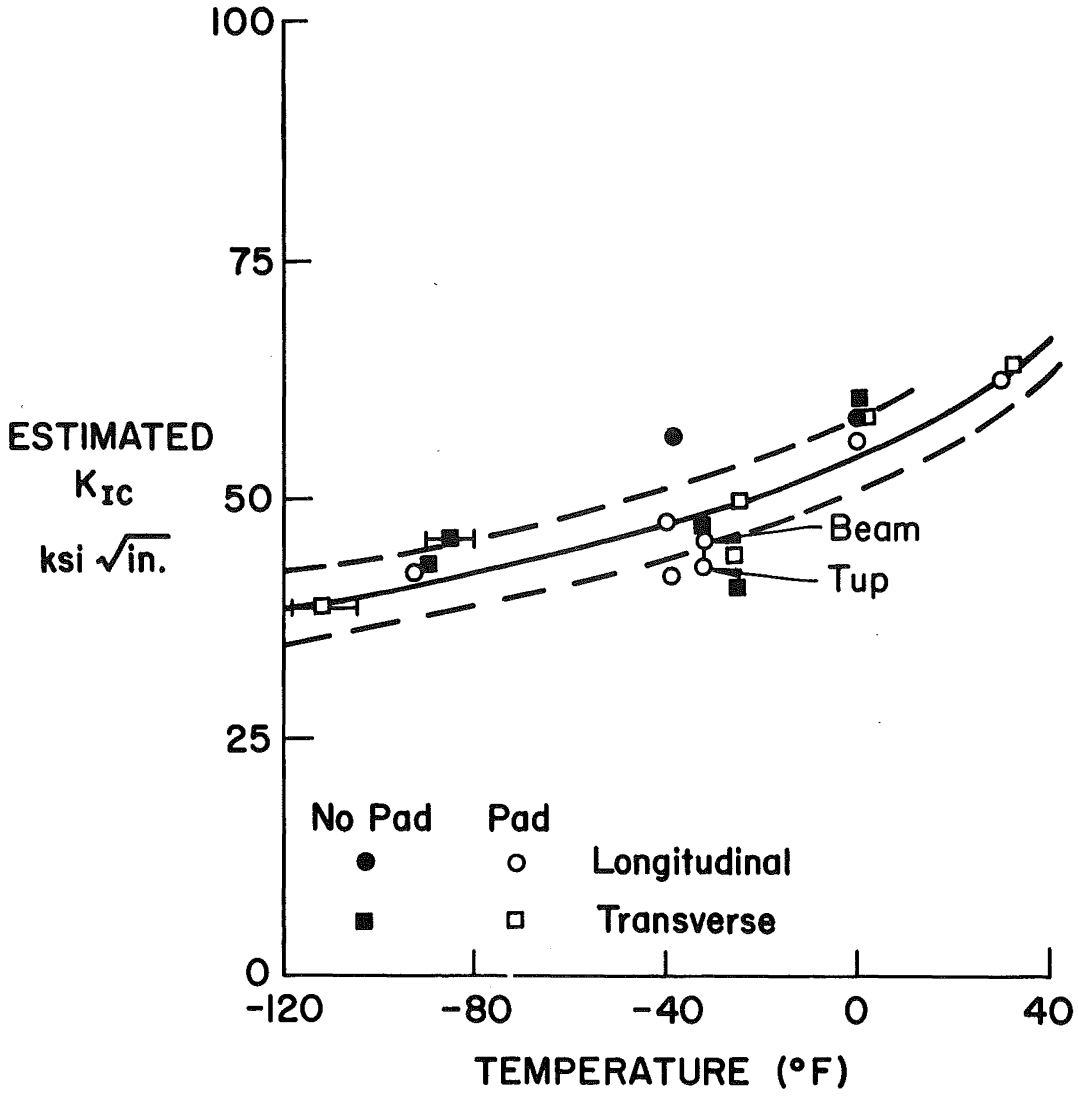

Fig. 46 K_{Ic} VERSUS TEMPERATURE: IMPACT TESTS OF 1/2" PLATE

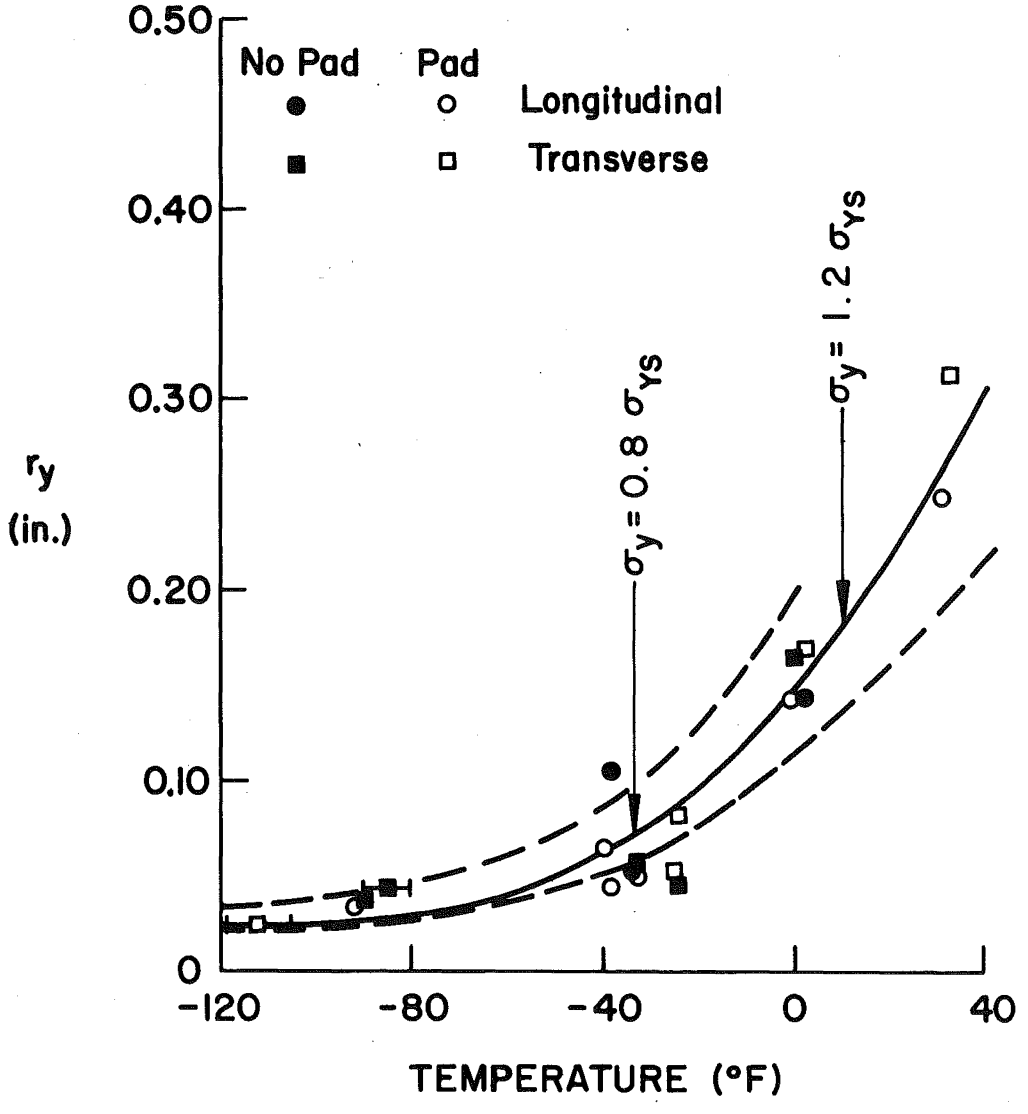

Fig. 47 r_y VERSUS TEMPERATURE: IMPACT TESTS OF 1/2" PLATE

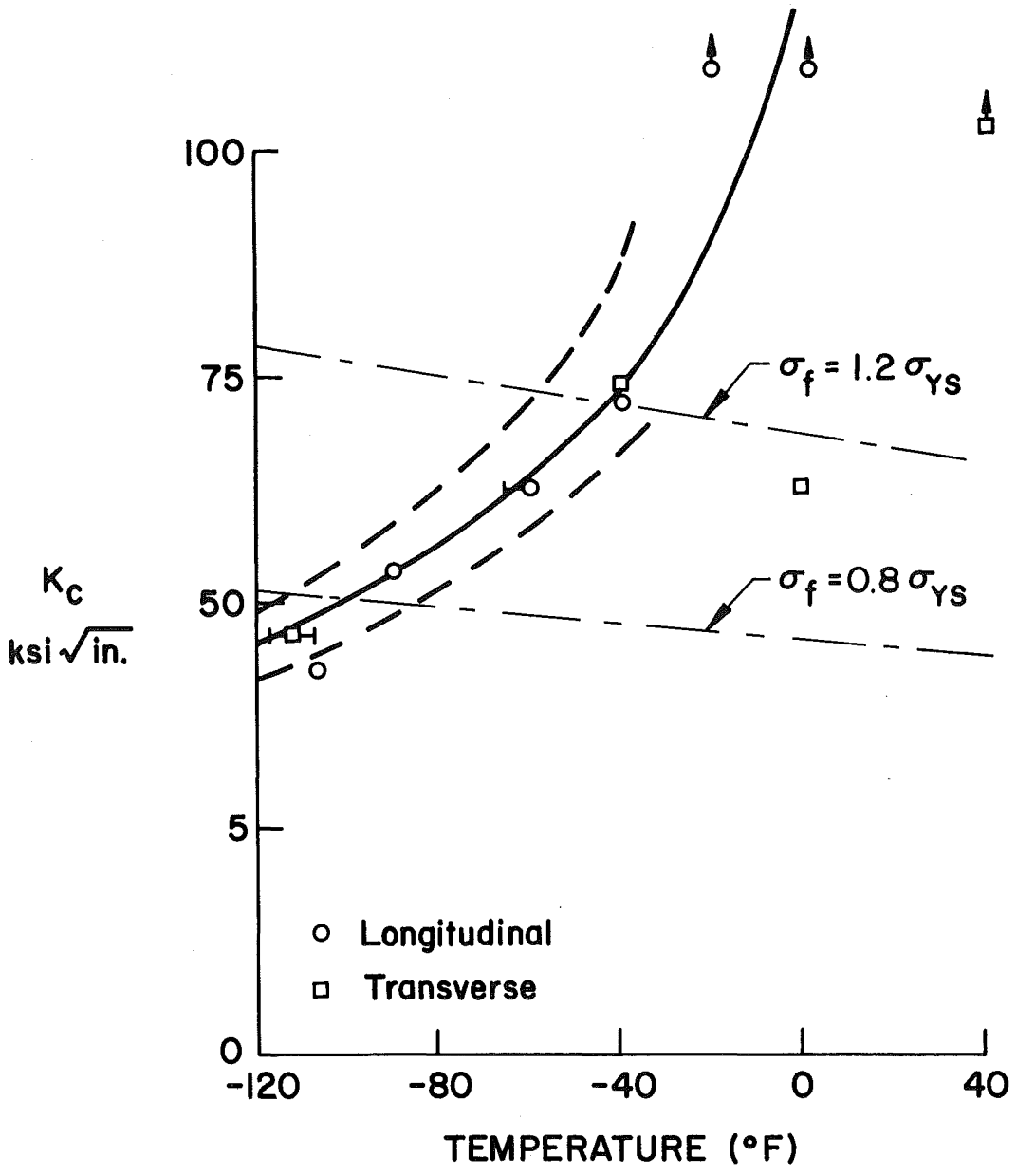

Fig. 48 K_c VERSUS TEMPERATURE: STATIC TESTS OF 1" PLATE

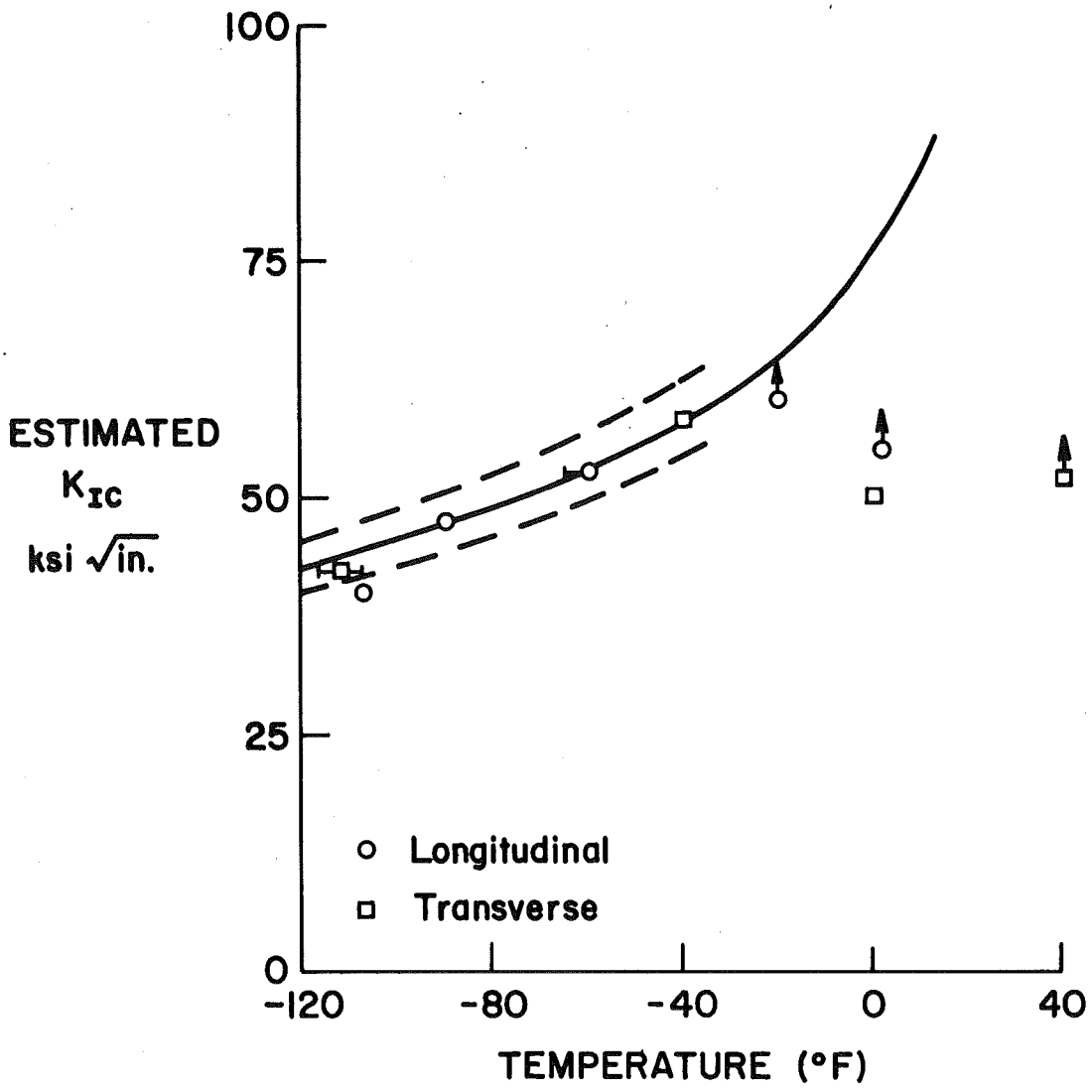

Fig. 49 K_{Ic} VERSUS TEMPERATURE: STATIC TESTS OF 1" PLATE

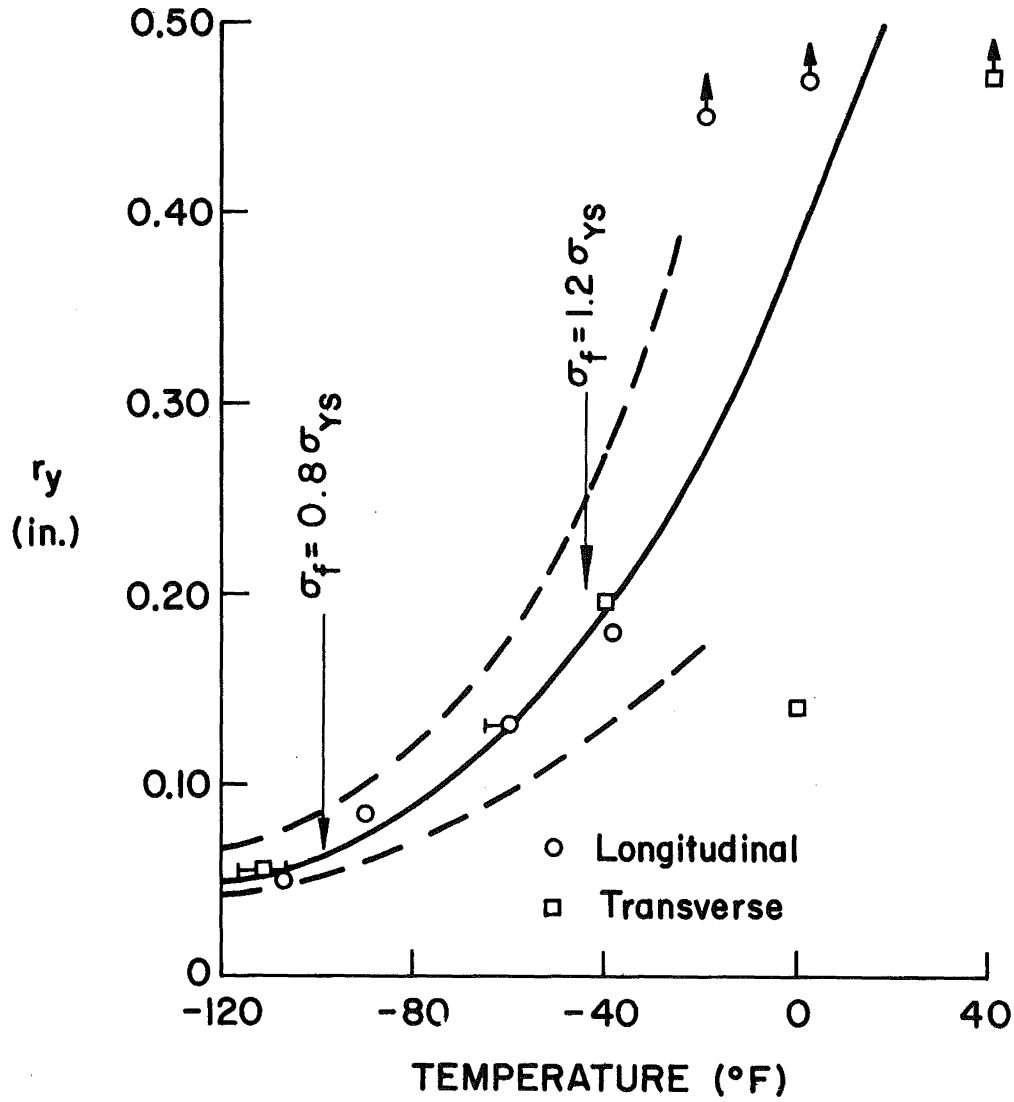

Fig. 50 r_y VERSUS TEMPERATURE: STATIC TESTS OF 1" PLATE

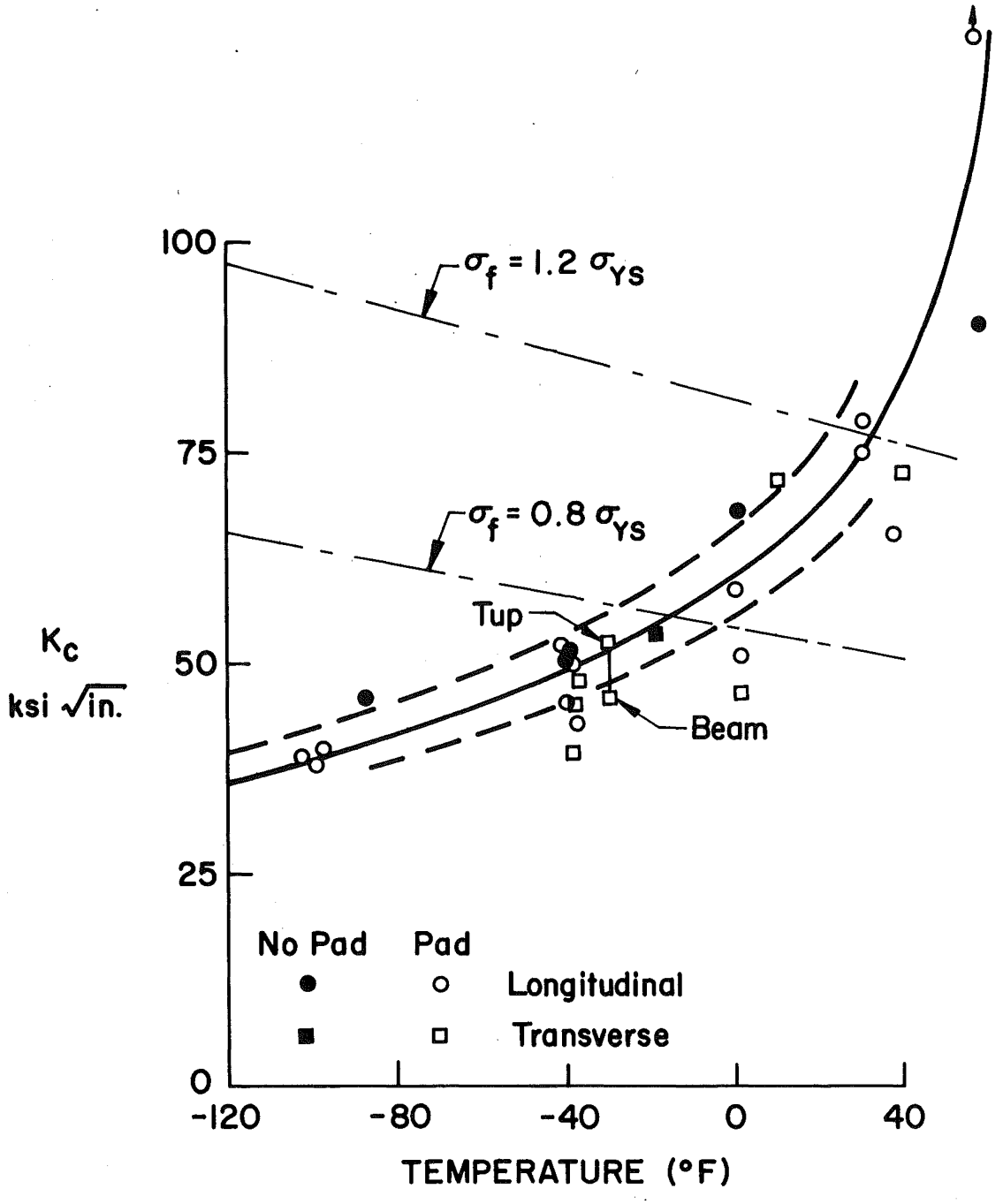

Fig. 51 K_c VERSUS TEMPERATURE: IMPACT TESTS OF 1" PLATE

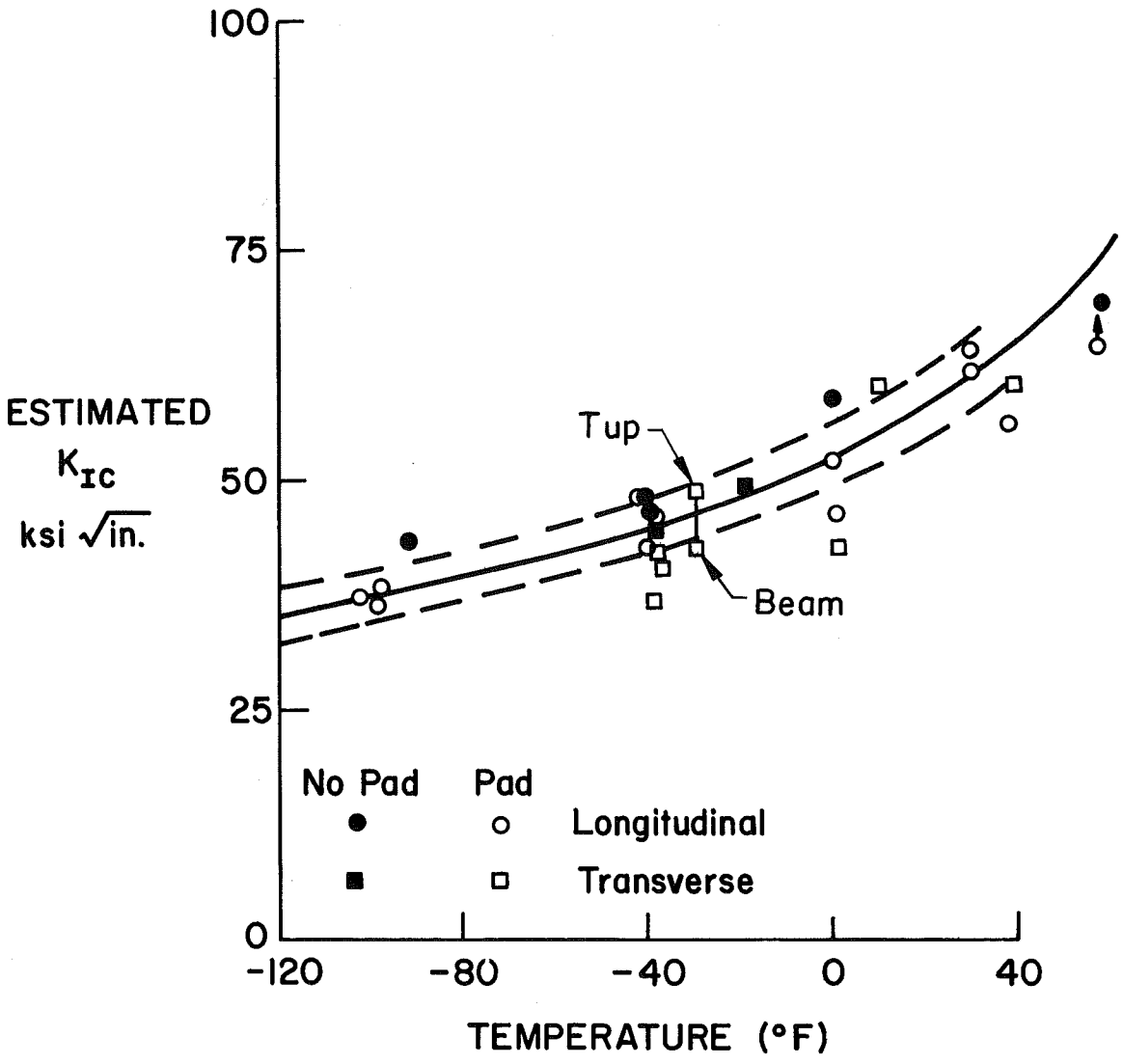

Fig. 52 K_{Ic} VERSUS TEMPERATURE: IMPACT TESTS OF 1" PLATE

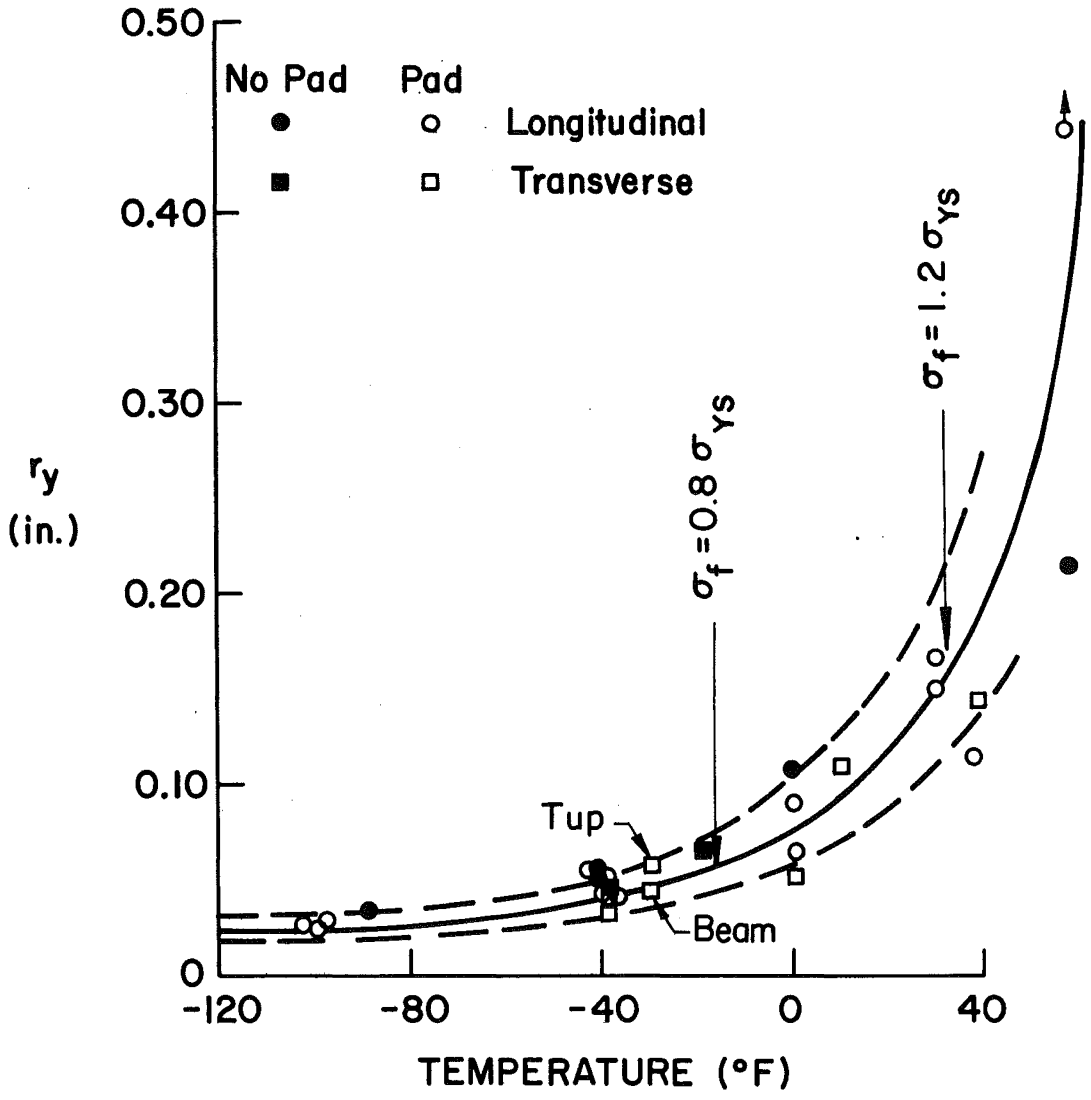

Fig. 53 r_Y VERSUS TEMPERATURE: IMPACT TESTS OF 1" PLATE

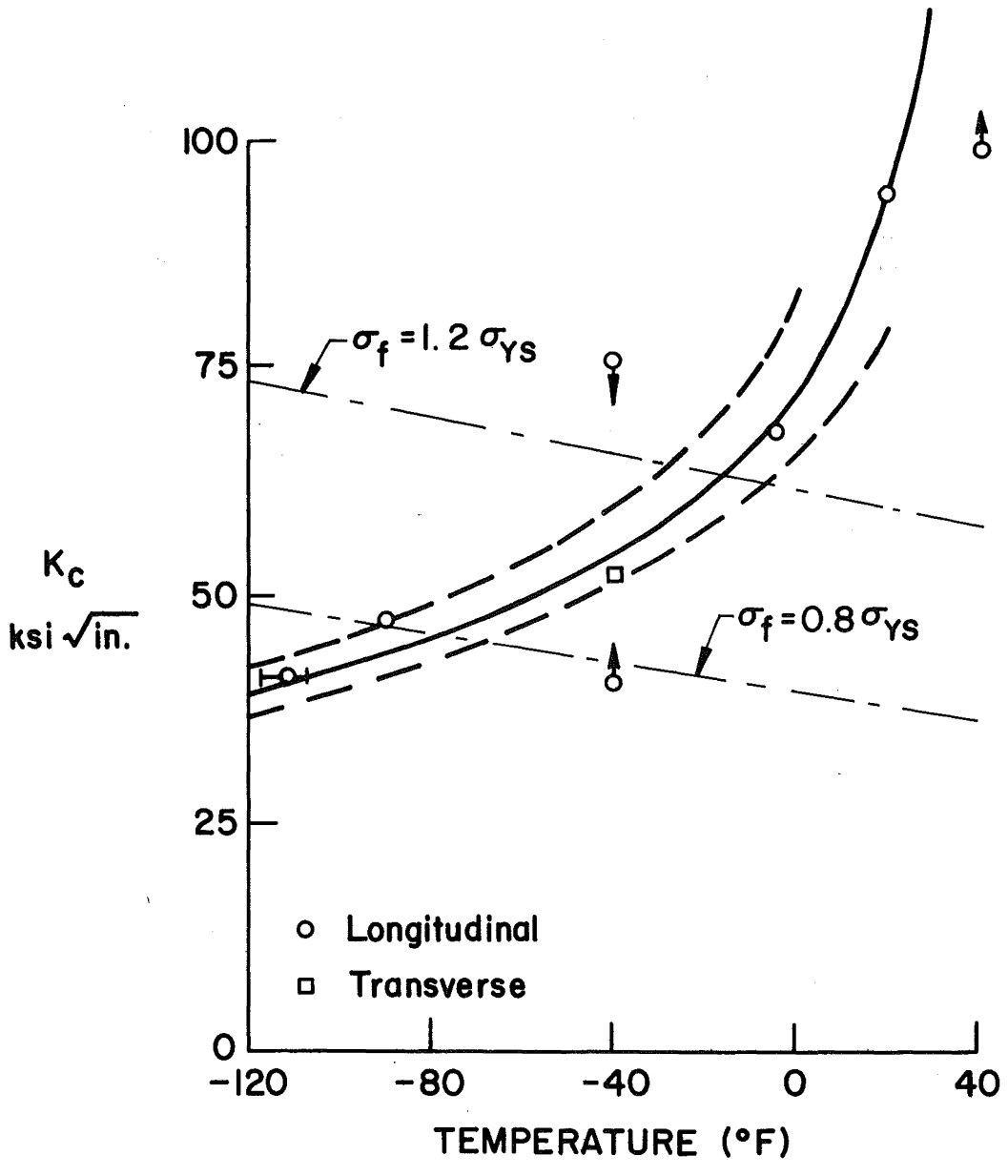

Fig. 54 K_c VERSUS TEMPERATURE: STATIC TESTS OF 2" PLATE

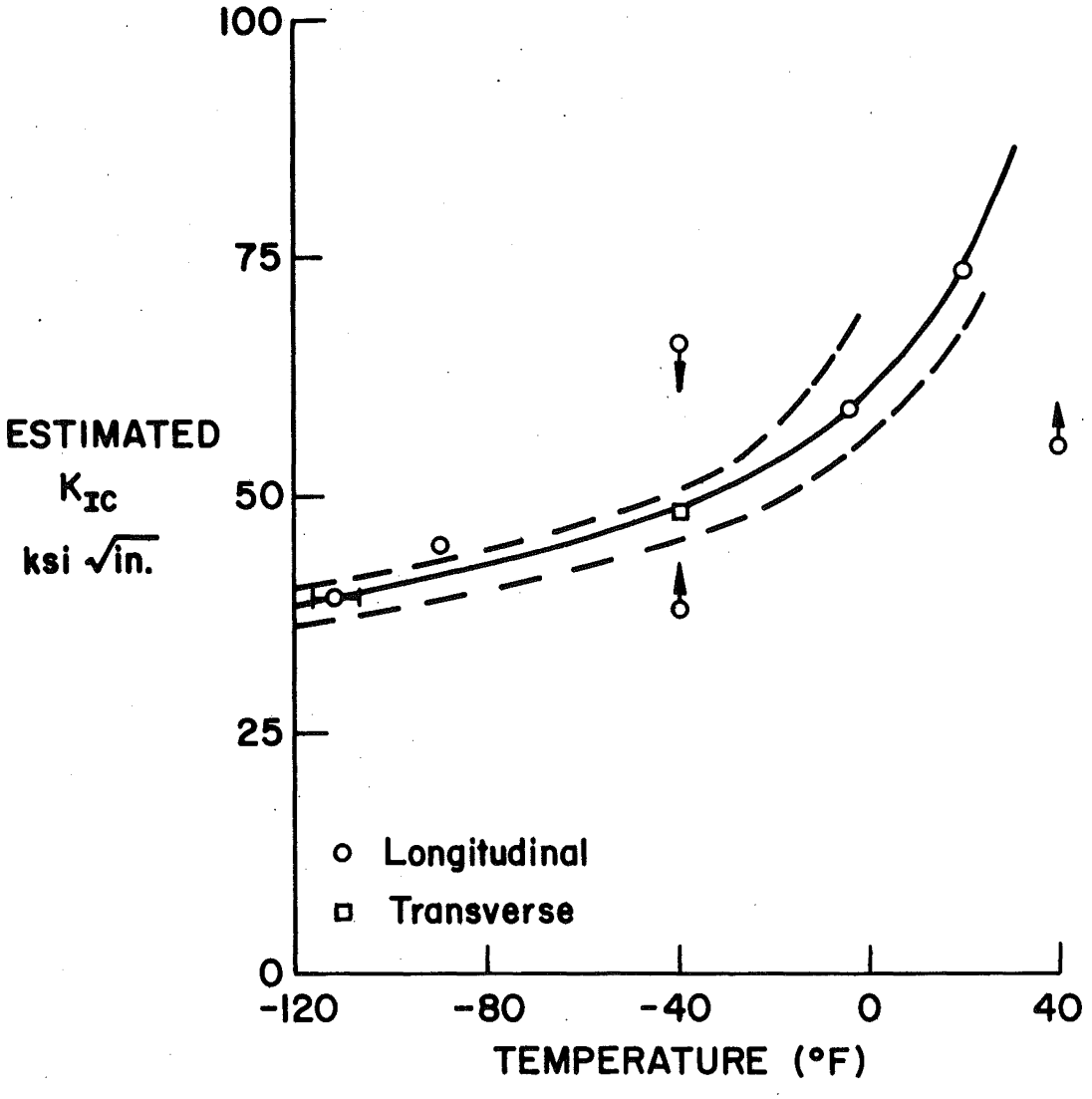

Fig. 55 K_{Ic} VERSUS TEMPERATURE: STATIC TESTS OF 2" PLATE

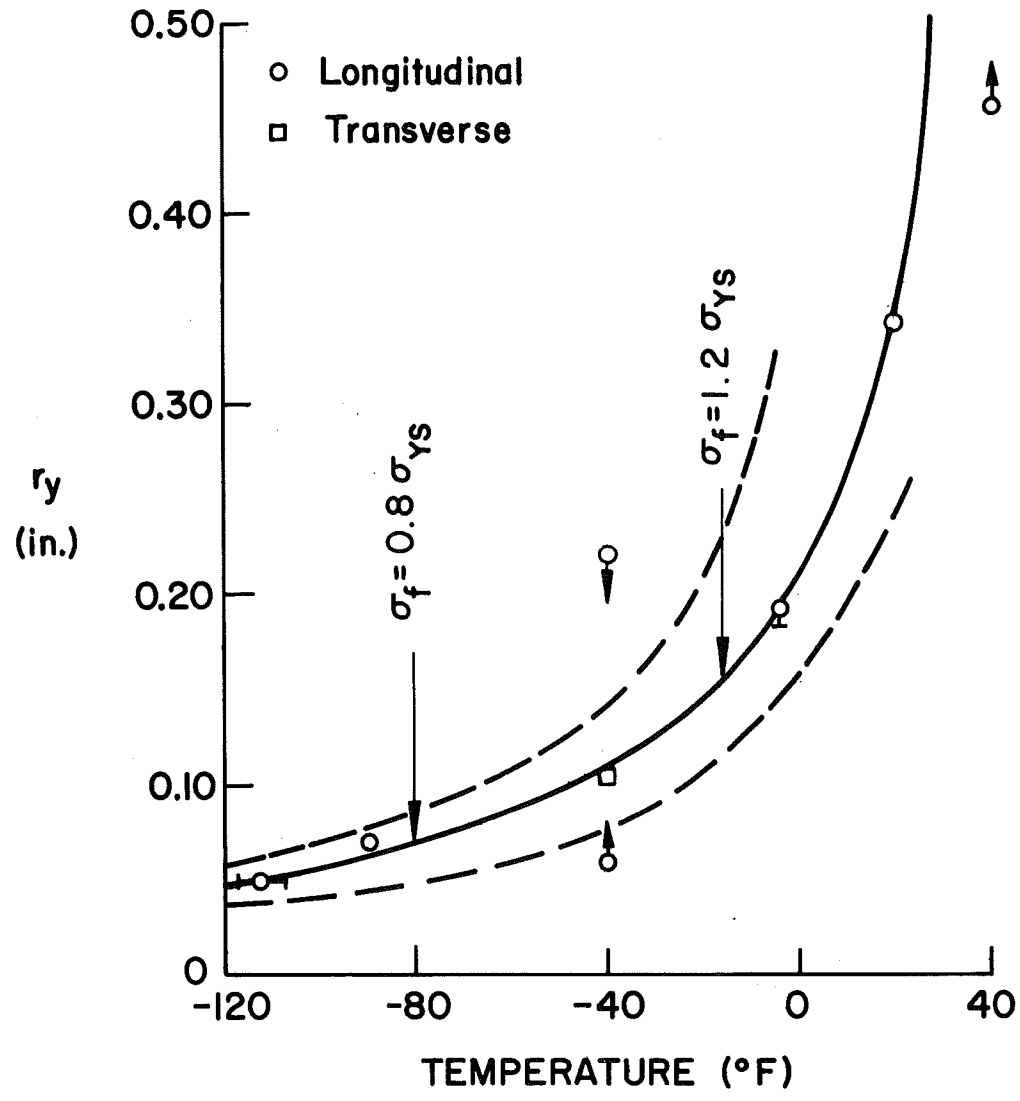

Fig. 56 r_Y VERSUS TEMPERATURE: STATIC TESTS OF 2" PLATE

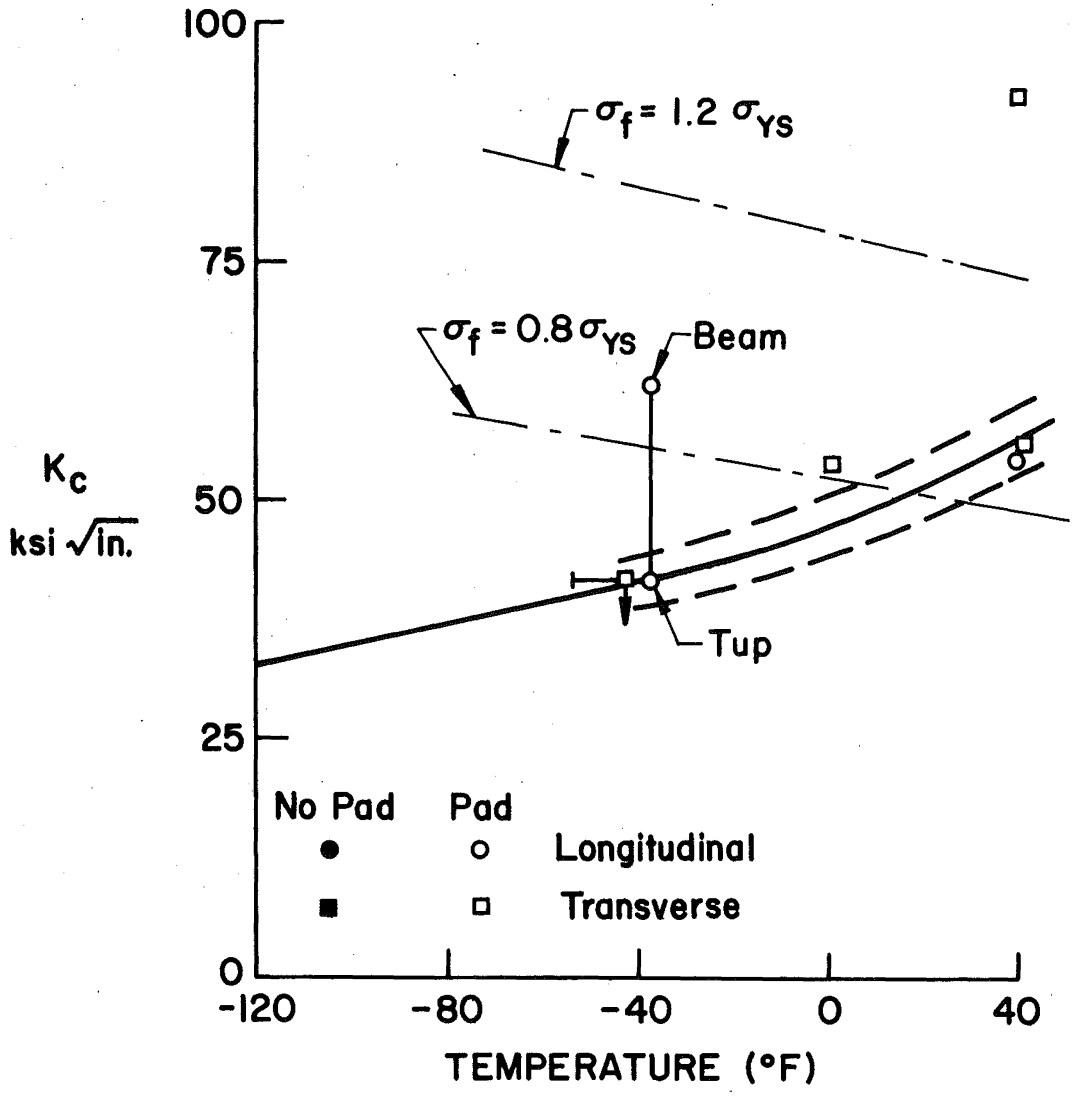

Fig. 57 K_c VERSUS TEMPERATURE: IMPACT TESTS OF 2" PLATE

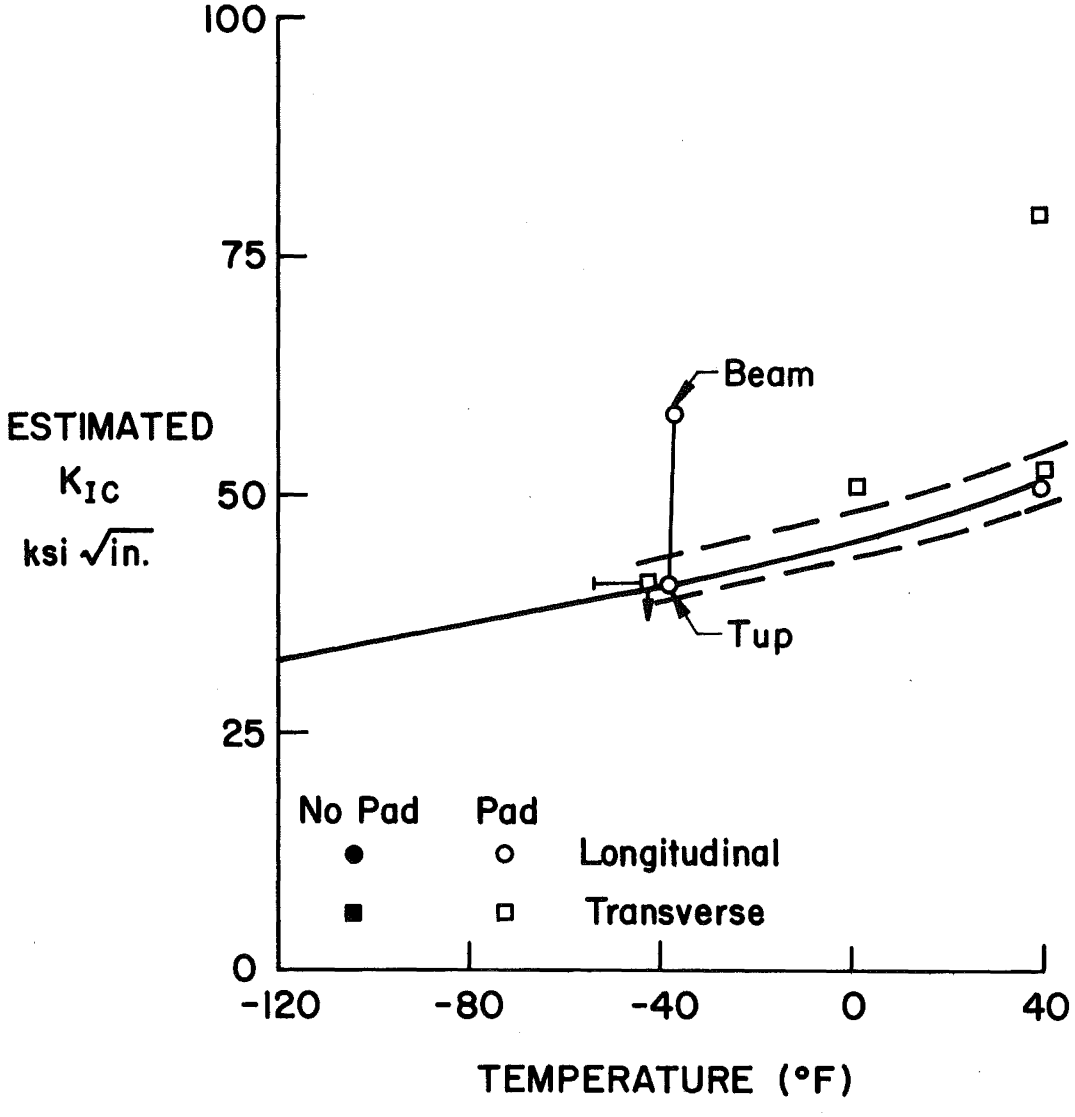

Fig. 58 K_{Ic} VERSUS TEMPERATURE: IMPACT TESTS OF 2" PLATE

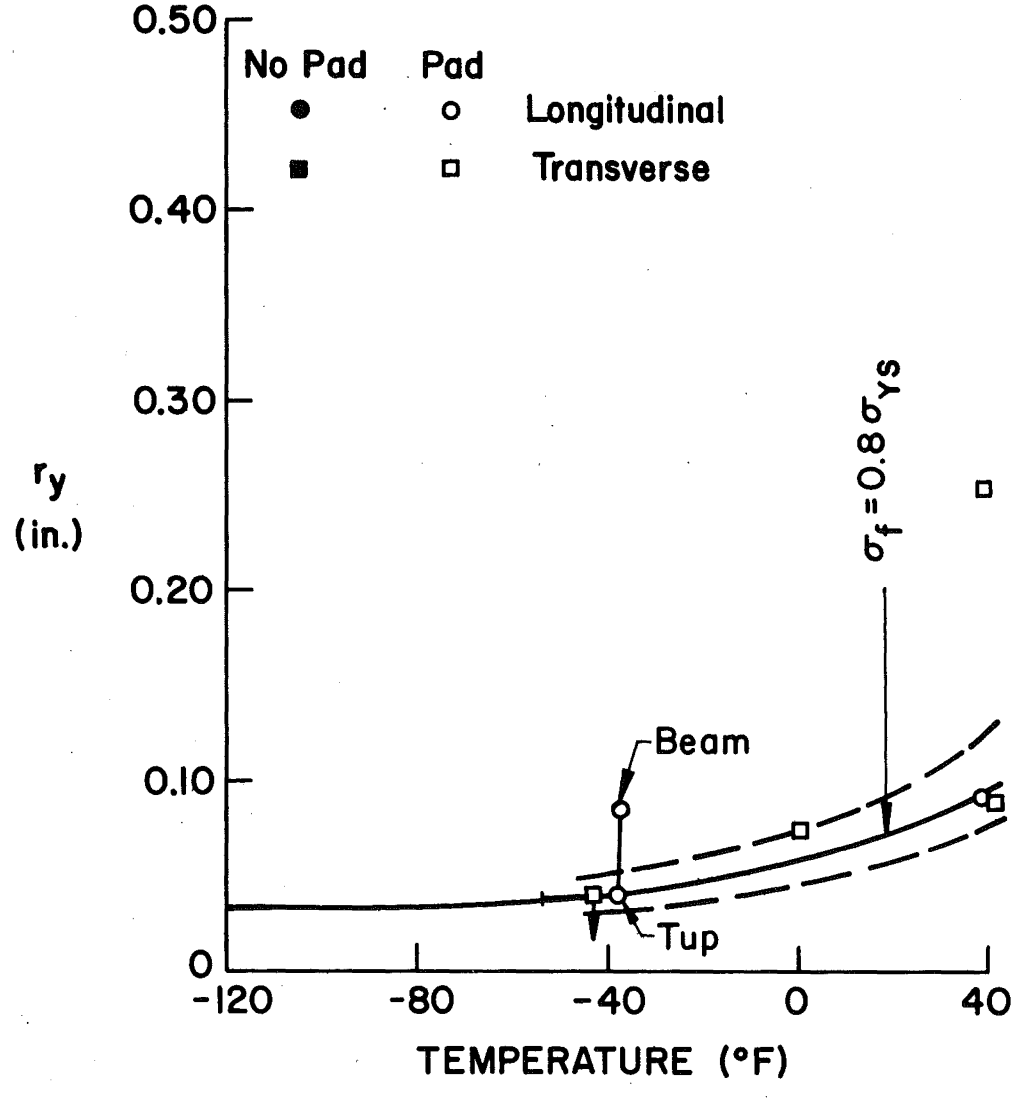

Fig. 59 r_Y VERSUS TEMPERATURE: IMPACT TESTS OF 2" PLATE

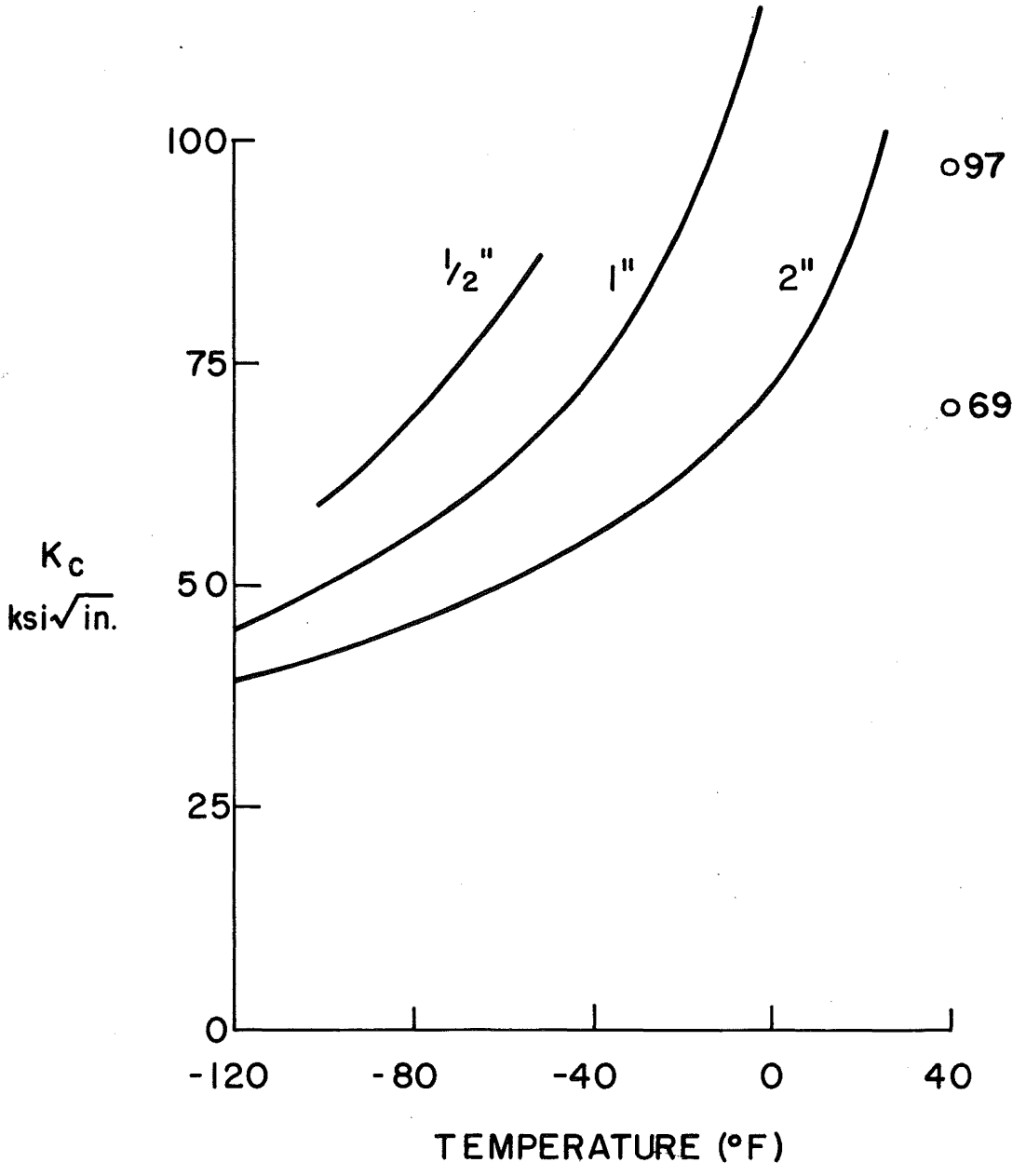

Fig. 60 K_c VERSUS TEMPERATURE: SUMMARY OF STATIC TESTS

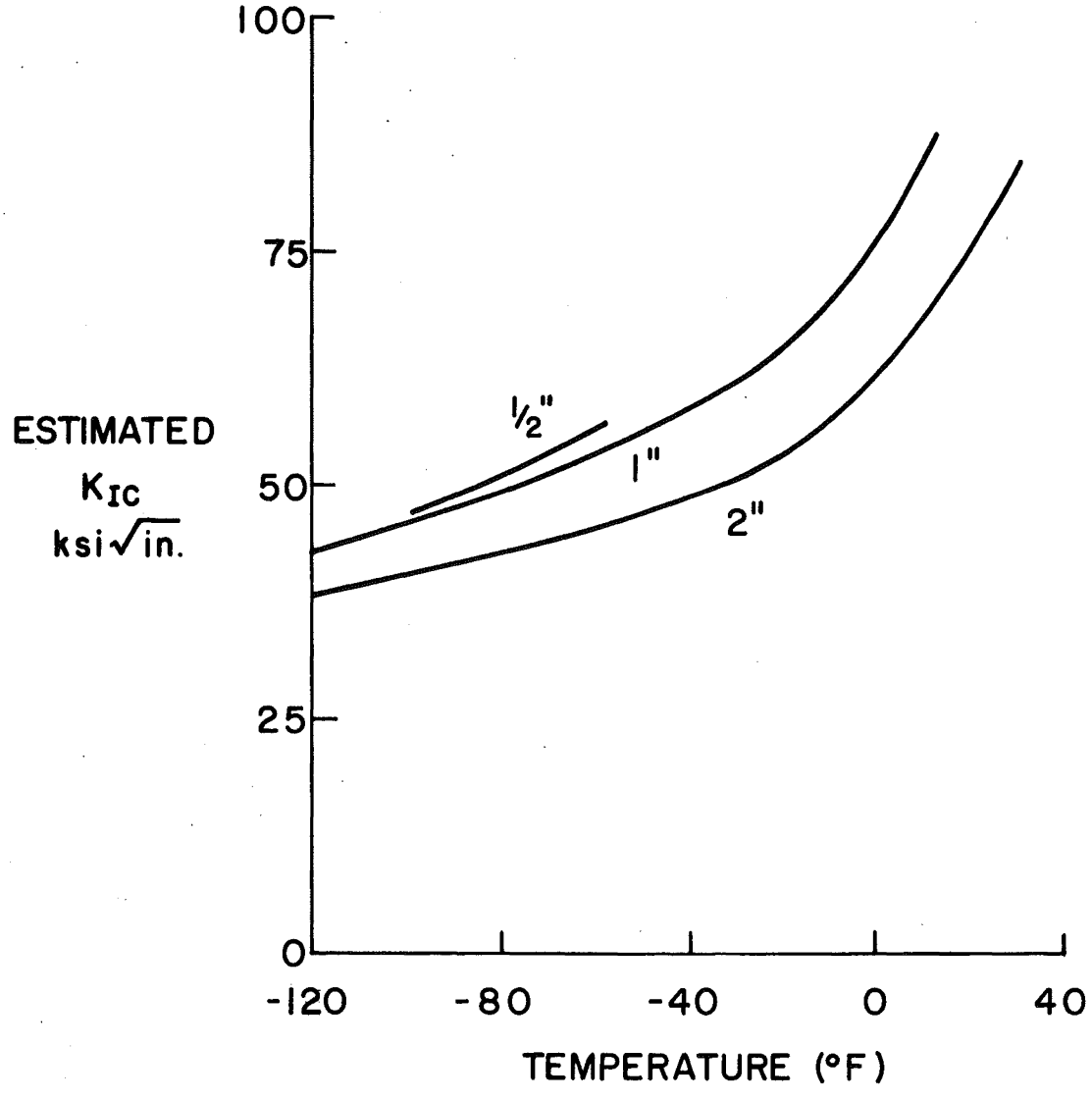

Fig. 61 K_{Ic} VERSUS TEMPERATURE: SUMMARY OF STATIC TESTS

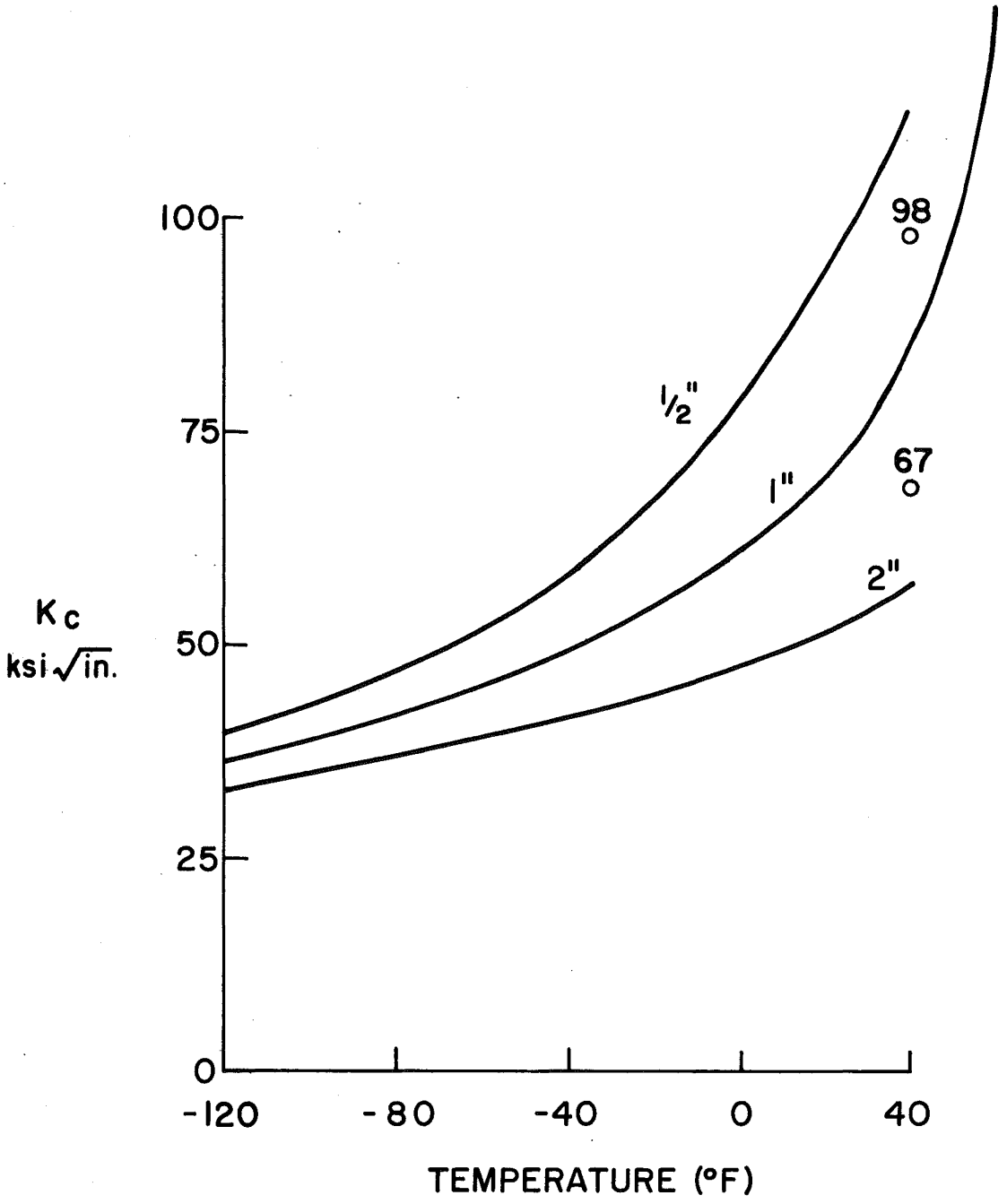

Fig. 62 K_c VERSUS TEMPERATURE: SUMMARY OF IMPACT TESTS

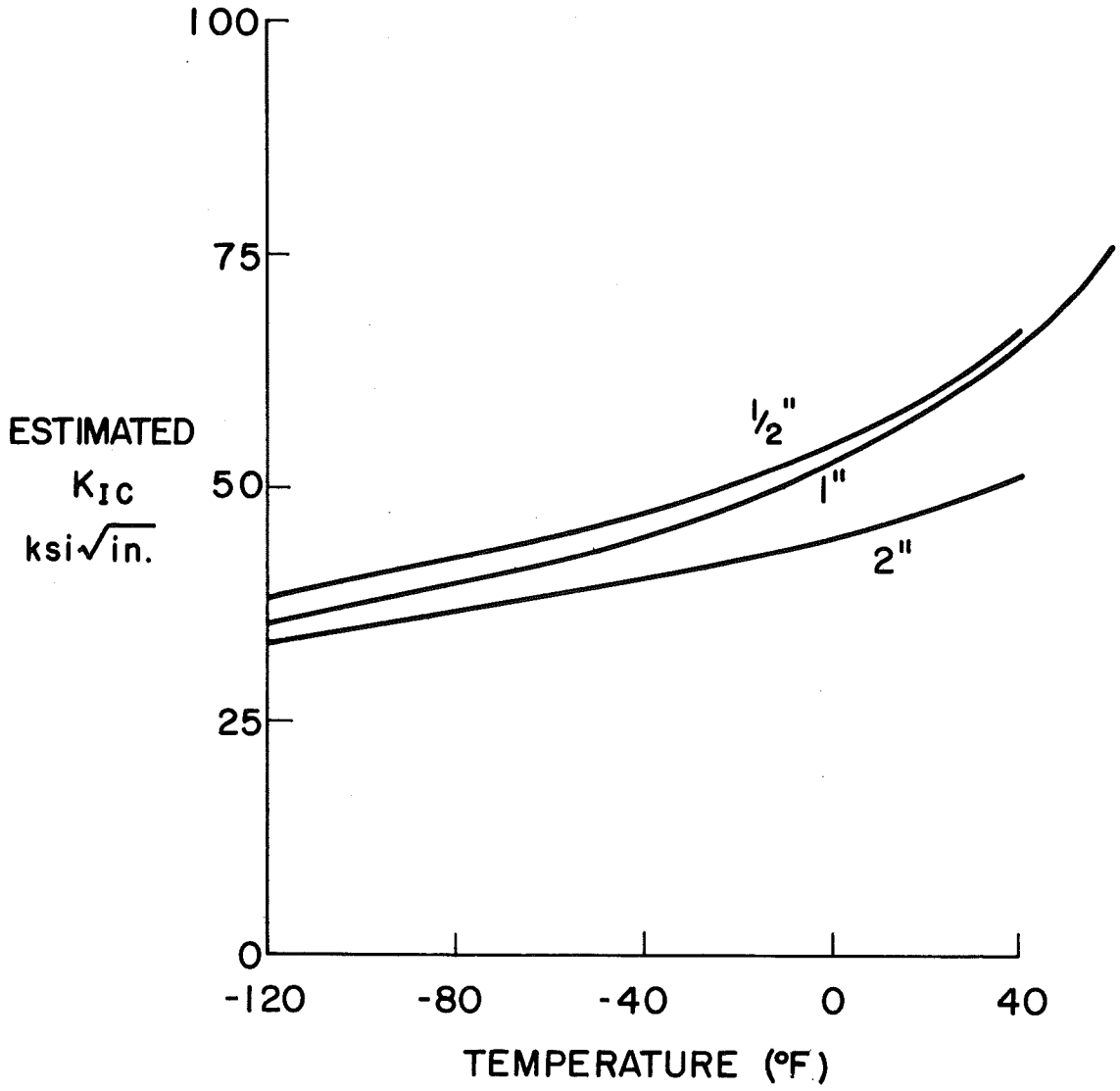

Fig. 63 K_{Ic} VERSUS TEMPERATURE: SUMMARY OF IMPACT TESTS

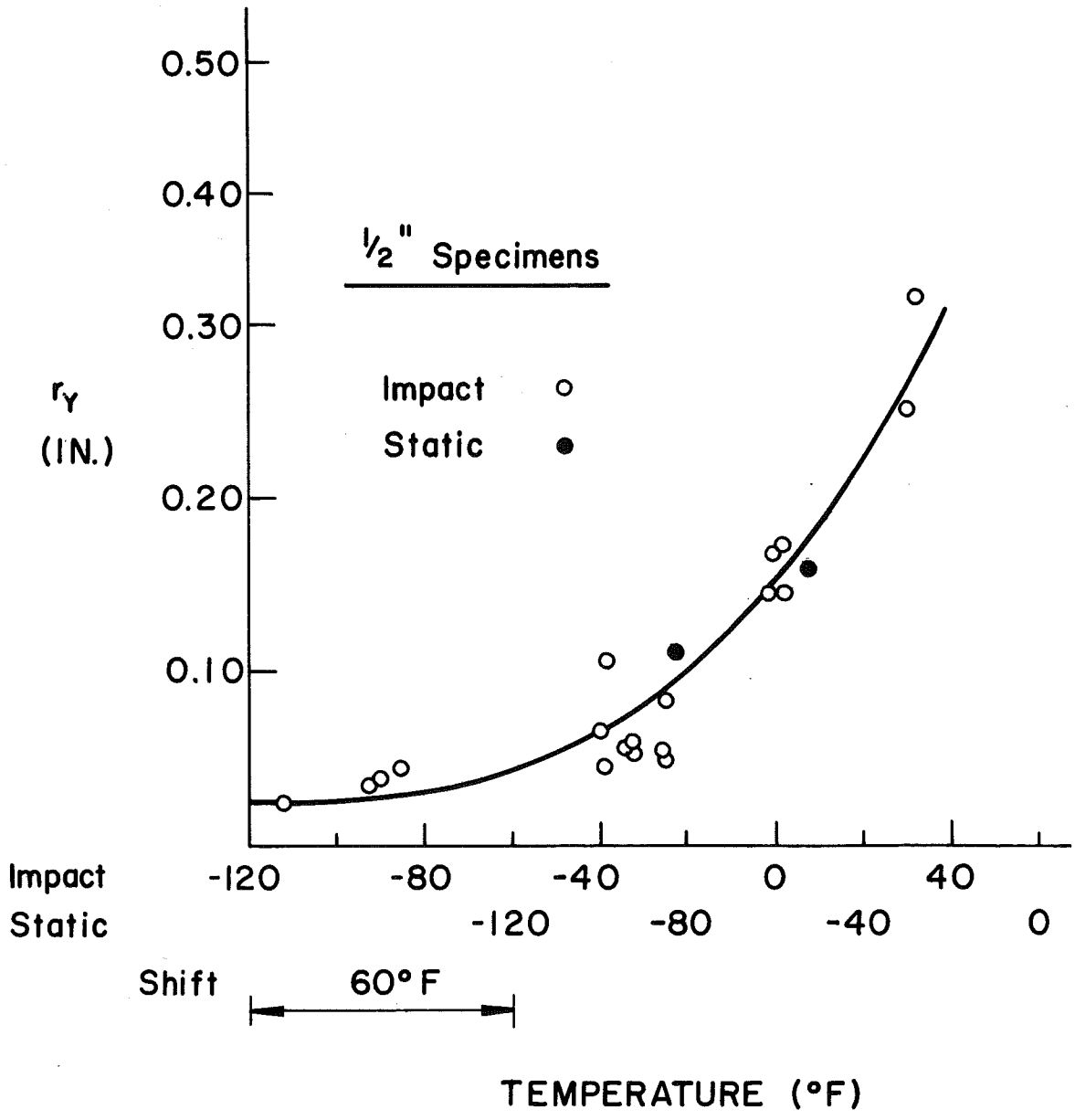

Fig. 64 TEMPERATURE DISPLACEMENT FOR 1/2" PLATE

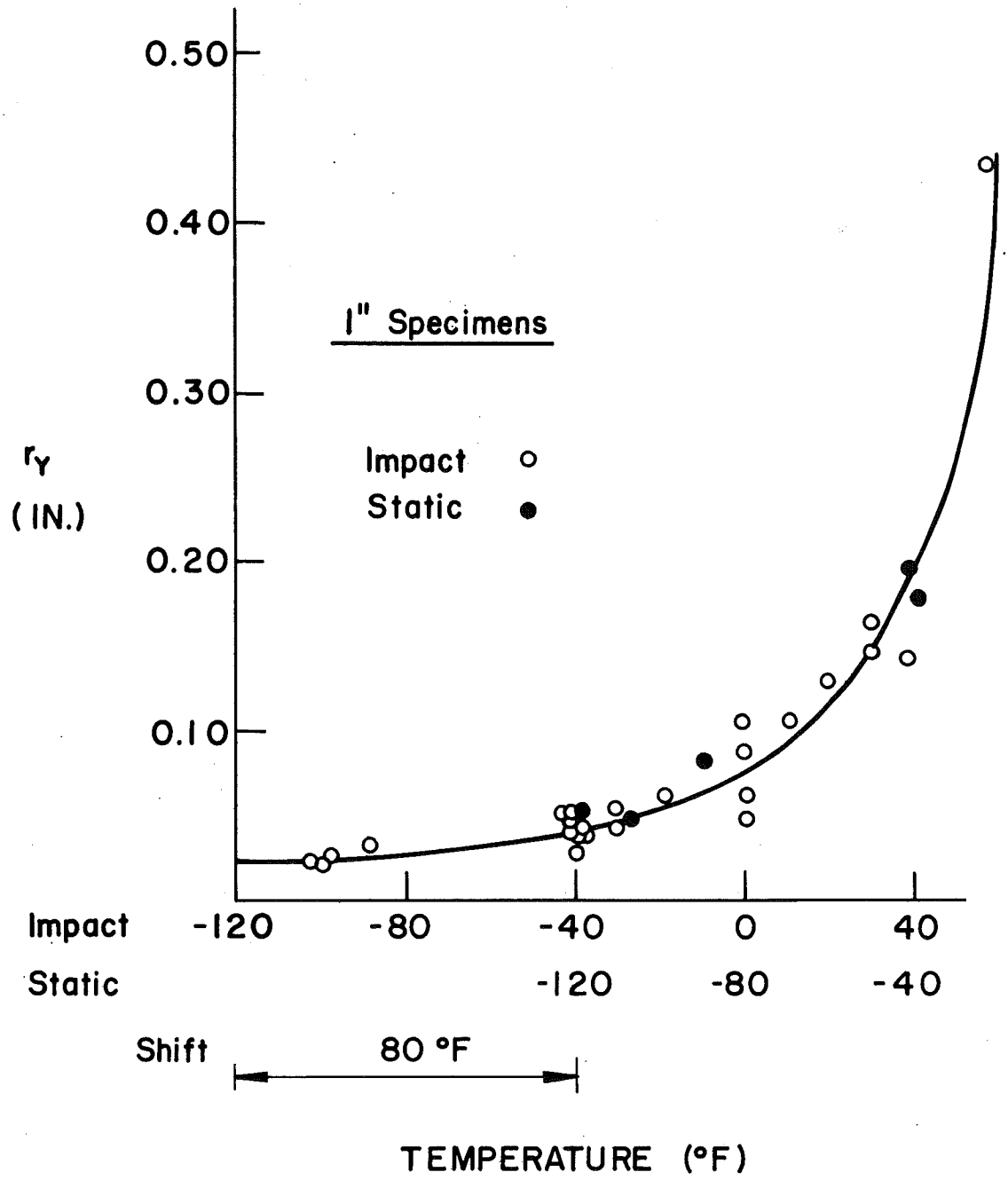

Fig. 65 TEMPERATURE DISPLACEMENT FOR 1" PLATE

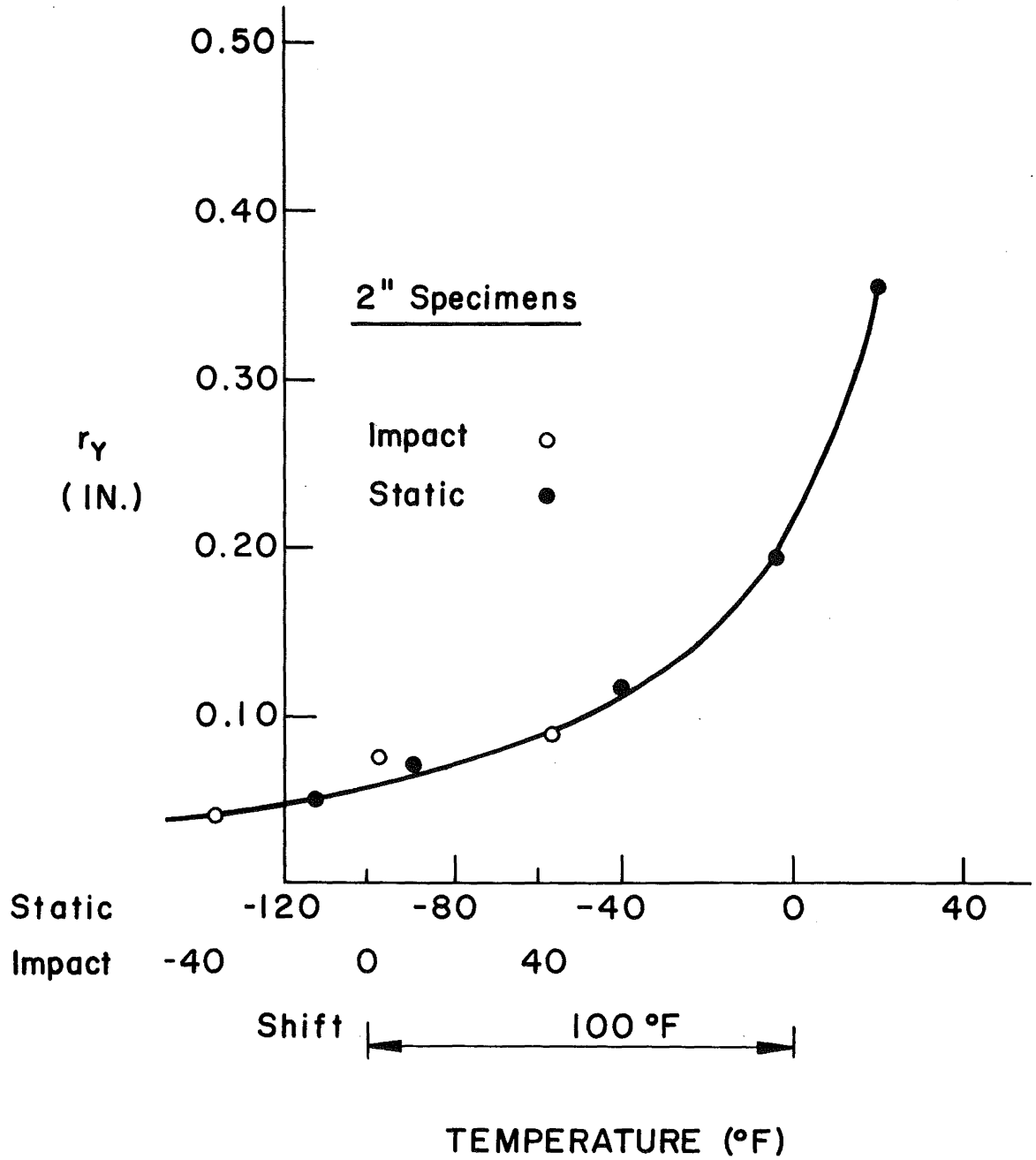

Fig. 66 TEMPERATURE DISPLACEMENT FOR 2" PLATE

1/2" SPECIMENS - STATIC TESTS

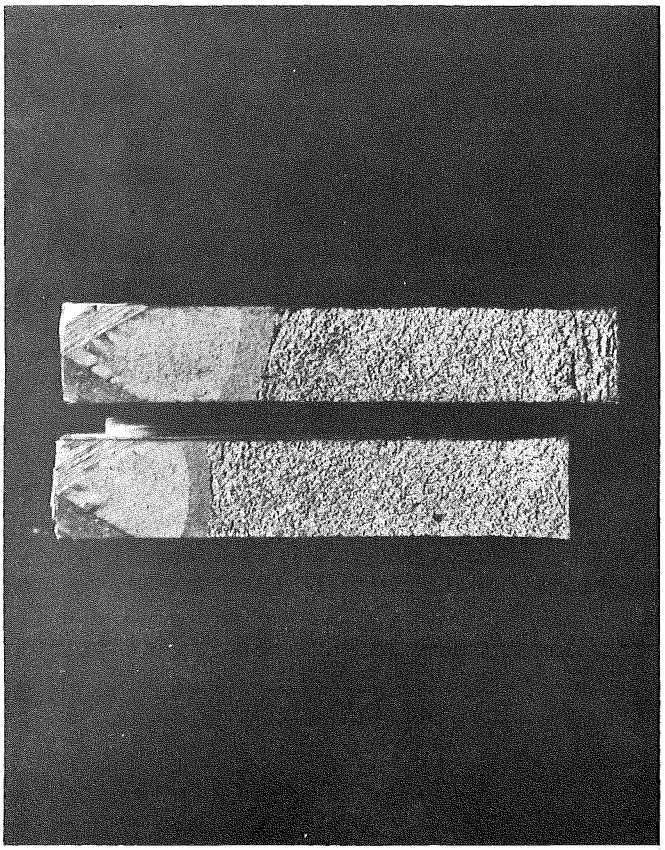

Temp.: -61^{o} F

Spec. No.: L114-4

K_c = 69.15 ksi $\sqrt{in}$

Temp.: -85^{o} F

Spec. No.: L334-4

K_c = 66.09 ksi $\sqrt{in}$

Fig. 67 PHOTOGRAPHS OF THE FRACTURE SURFACES

1/2" SPECIMENS - IMPACT TESTS

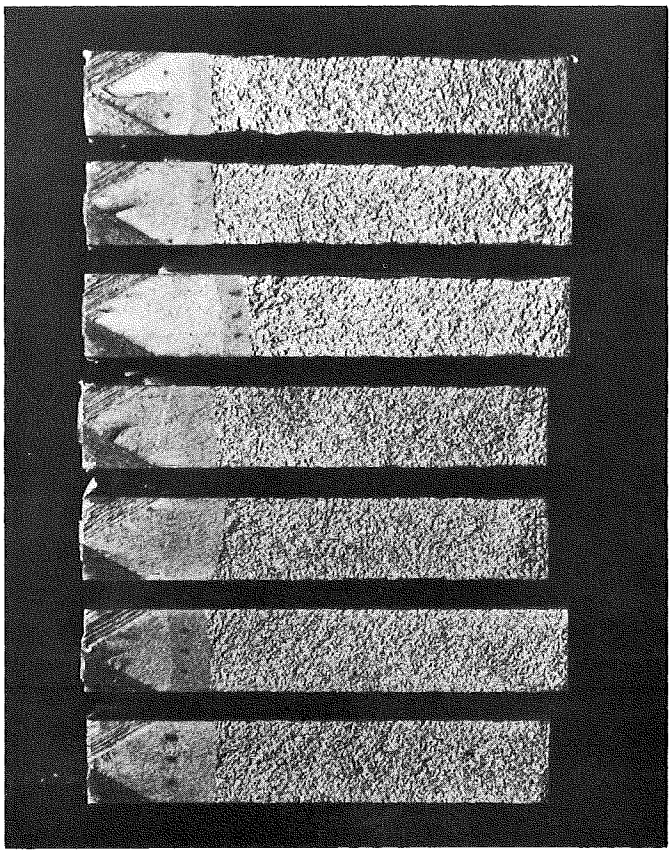

Temp.: -39° F

Spec. No.: L533-4

K_c = 72.62 ksi $\sqrt{in}$

Temp.: -39° F

Spec. No.: L113-4

K_c = 47.97 ksi $\sqrt{in}$

Temp.: -40° F

Spec. No.: L112-4

K_c = 56.32 ksi $\sqrt{in}$

Temp.: -85° F

Spec. No.: T611-3

K_c = 52.11 ksi $\sqrt{in}$

Temp.: -90° F

Spec. No.: T211-4

K_c = 48.35 ksi $\sqrt{in}$

Temp.: -92° F

Spec. No.: L622-3

K_c = 47.14 ksi $\sqrt{in}$

Temp.: -112° F

Spec. No.: T121-4

K_c = 42.33 ksi $\sqrt{in}$

Fig. 67 PHOTOGRAPHS OF THE FRACTURE SURFACES

1/2" SPECIMENS - IMPACT TESTS

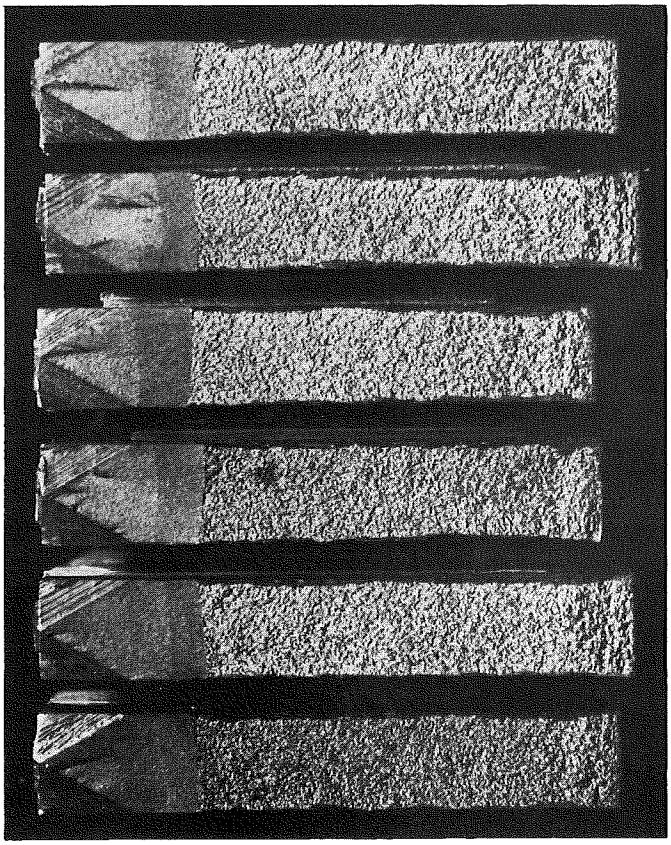

Temp.: -25^{o} F

Spec. No.: T612-3

K_c = 61.36 ksi $\sqrt{in}$

Temp.: -25^{o} F

Spec. No.: T213-4

K_c = 46.65 ksi $\sqrt{in}$

Temp.: -26^{o} F

Spec. No.: T411-4

K_c = 52.14 ksi $\sqrt{in}$

Temp.: -32^{o} F

Spec. No.: L334-3

K_c = 49.63 ksi $\sqrt{in}$

Temp.: -33^{o} F

Spec. No.: T223-4

K_c = 56.19 ksi $\sqrt{in}$

Temp.: -34^{o} F

Spec. No.: T123-4

K_c = 54.03 ksi $\sqrt{in}$

Fig. 67 PHOTOGRAPHS OF THE FRACTURE SURFACES

1/2" SPECIMENS - IMPACT TESTS

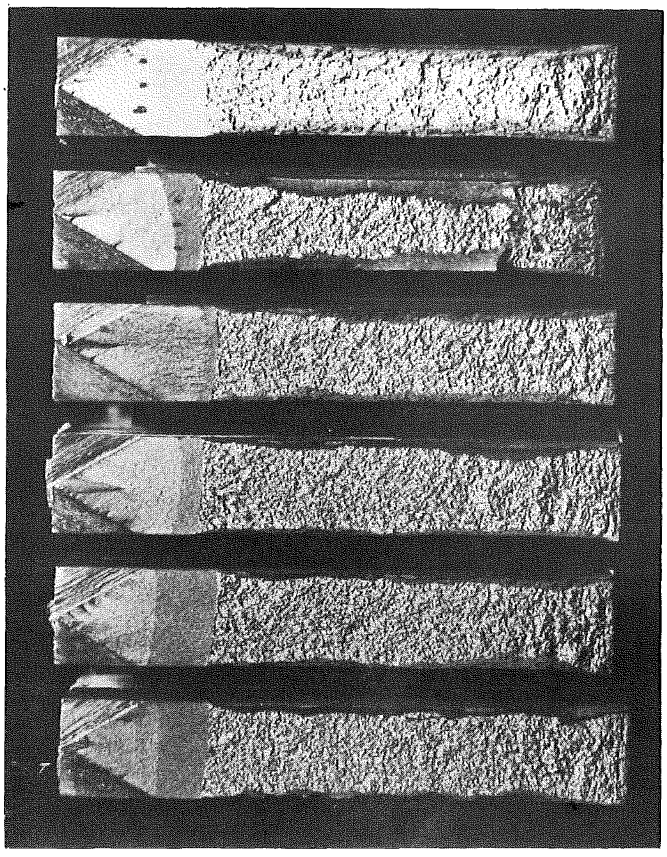

Temp.: 32^{o} F

Spec. No.: T433-4

K_c = 111.7 ksi $\sqrt{in}$

Temp.: 30^{o} F

Spec. No.: L511-4

K_c = 100.2 ksi $\sqrt{in}$

Temp.: 2^{o} F

Spec. No.: T613-3

K_c 84.16 ksi $\sqrt{in}$

Temp.: 0^{o} F

Spec. No.: L331-4

K_c = 81.53 ksi $\sqrt{in}$

Temp.: 0^{o} F

Spec. No.: T423-4

K_c 87.46 ksi $\sqrt{in}$

Temp.: 0^{o} F

Spec. No.: L333-4

K_c 77.91 ksi $\sqrt{in}$

Fig. 67 PHOTOGRAPHS OF THE FRACTURE SURFACES

1" SPECIMENS - STATIC TESTS

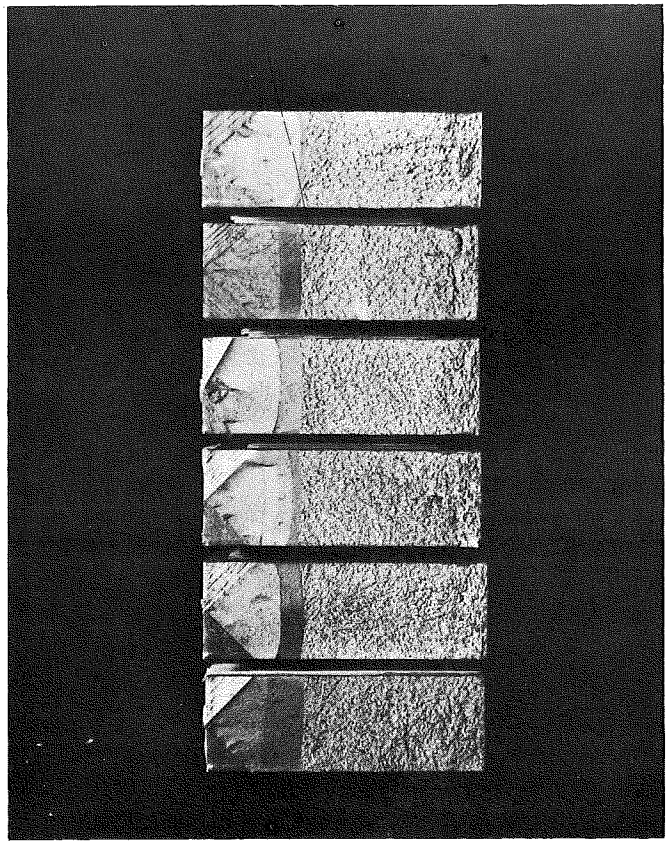

Temp.: -39^{o} F

Spec. No.: L622-2

K_c = 72.21 ksi $\sqrt{in}$

Temp.: -40^{o} F

Spec. No.: T232-2

K_c = 74.56 ksi $\sqrt{in}$

Temp.: -60^{o} F

Spec. No.: L414-3

K_c = 62.78 ksi $\sqrt{in}$

Temp.: -90^{o} F

Spec. No.: L523-2

K_c = 53.65 ksi $\sqrt{in}$

Temp.: -107^{o} F

Spec. No.: L512-3

K_c = 42.3 ksi $\sqrt{in}$

Temp.: -112^{o} F

Spec. No.: T224-2

K_c = 46.45 ksi $\sqrt{in}$

Fig. 67 PHOTOGRAPHS OF THE FRACTURE SURFACES

1" SPECIMENS - STATIC TESTS

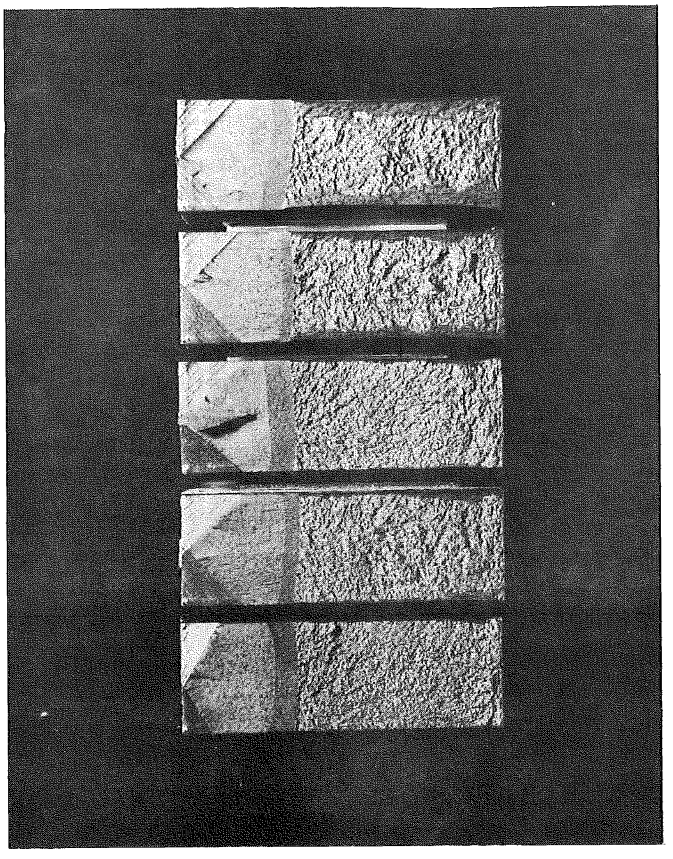

Temp.: 76° F

Spec. No.: T434-2

K_c > 103 ksi $\sqrt{in}$

Temp.: 40° F

Spec. No.: T614-2

K_c > 105 ksi $\sqrt{in}$

Temp.: 1° F

Spec. No.: L512-2

K_c > 109 ksi $\sqrt{in}$

Temp.: 0° F

Spec. No.: T214-2

K_c > 60.32 ksi $\sqrt{in}$

Temp.: -20° F

Spec. No.: L624-3

K_c > 109 ksi $\sqrt{in}$

Fig. 67 PHOTOGRAPHS OF THE FRACTURE SURFACES

1" SPECIMENS - IMPACT TESTS

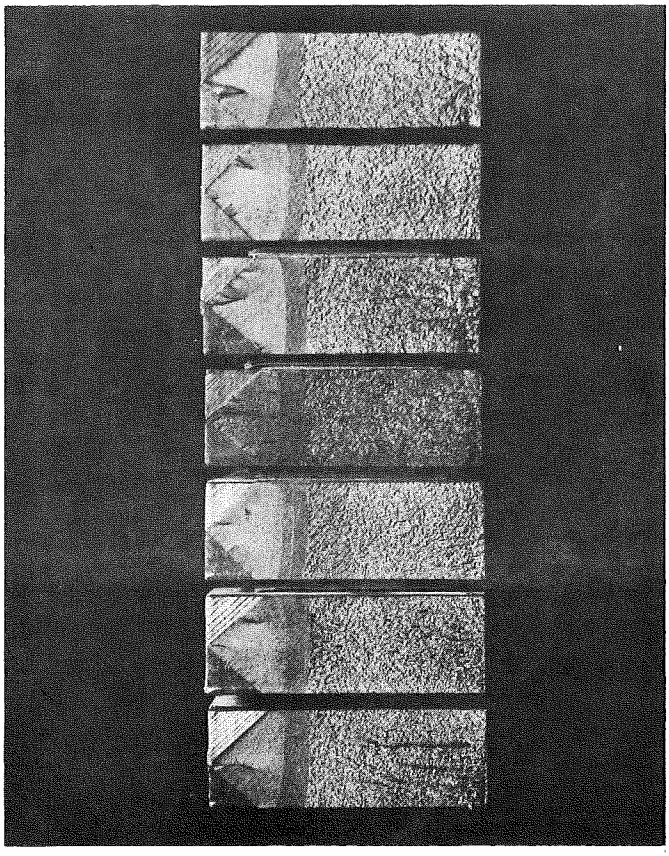

Temp.: -40° F

Spec. No.: L534-2

K_c = 50.42 ksi $\sqrt{in}$

Temp.: -41° F

Spec. No.: L322-2

K_c = 52.22 ksi $\sqrt{in}$

Temp.: -42° F

Spec. No.: L112-2

K_c = 52.07 ksi $\sqrt{in}$

Temp.: -88° F

Spec. No.: L131-2

K_c = 46.22 ksi $\sqrt{in}$

Temp.: -98° F

Spec. No.: L532-2

K_c = 40.07 ksi $\sqrt{in}$

Temp.: -99° F

Spec. No.: L313-2

K_c = 37.95 ksi $\sqrt{in}$

Temp.: -102° F

Spec. No.: L623-2

K_c = 38.96 ksi $\sqrt{in}$

Fig. 67 PHOTOGRAPHS OF THE FRACTURE SURFACES

1" SPECIMENS - IMPACT TESTS

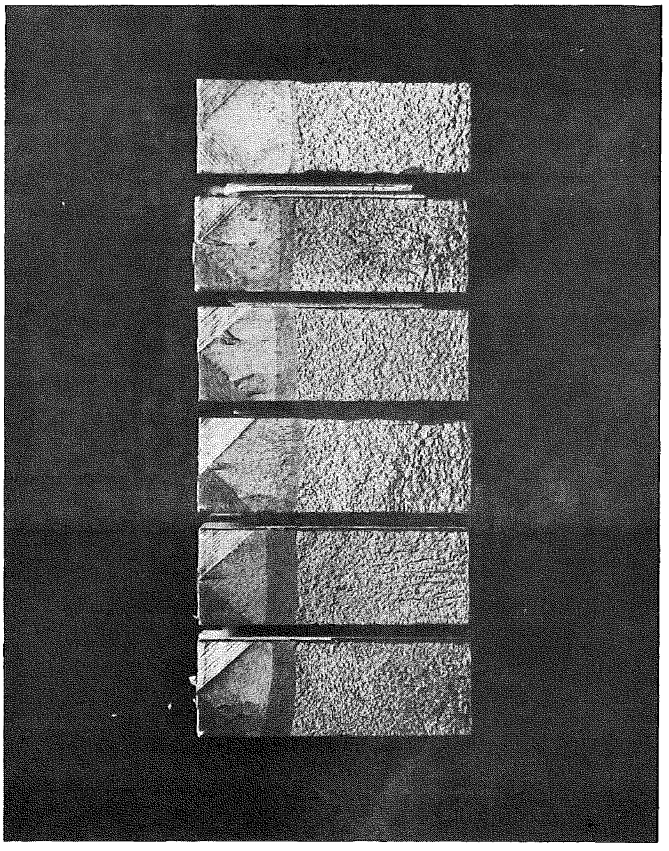

Temp.: -30^{o} F

Spec. No.: T422-2

K_c = 45.89 ksi $\sqrt{in}$

Temp.: -38^{o} F

Spec. No.: T612-2

K_c = 48.12 ksi $\sqrt{in}$

Temp.: -38^{o} F

Spec. No.: T233-2

K_c = 45.41 ksi $\sqrt{in}$

Temp.: -39^{o} F

Spec. No.: T211-2

K_c = 49.09 ksi $\sqrt{in}$

Temp.: -39^{o} F

Spec. No.: L134-2

K_c = 50.15 ksi $\sqrt{in}$

Temp.: -40^{o} F

Spec. No.: L312-2

K_c = 45.65 ksi $\sqrt{in}$

Fig. 67 PHOTOGRAPHS OF THE FRACTURE SURFACES

1" SPECIMENS - IMPACT TESTS

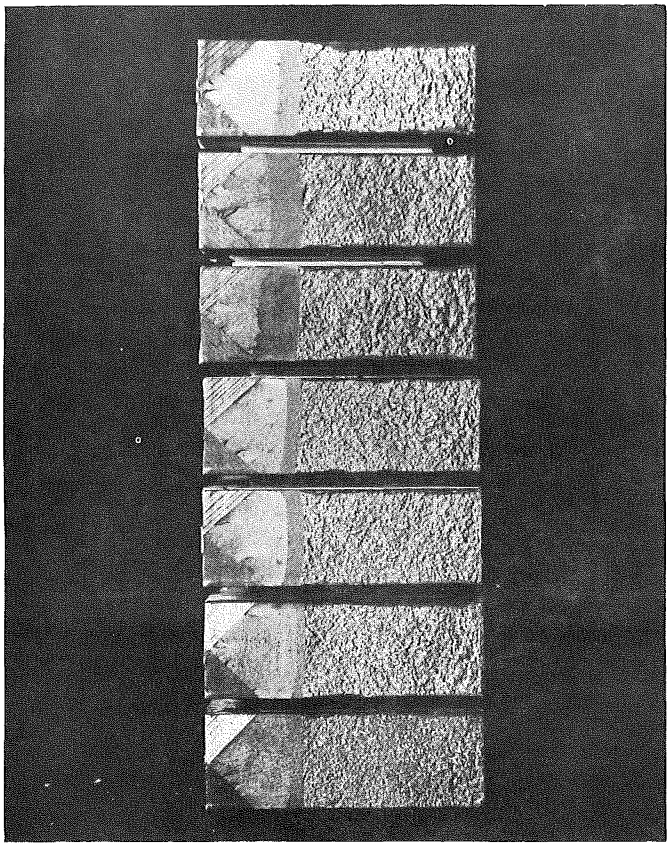

Temp.: 30^{o} F

Spec. No.: L521-2

$K_c > 75.09$ ksi $\sqrt{in}$

Temp.: 10^{o} F

Spec. No.: T121-2

$K_c = 70.92$ ksi $\sqrt{in}$

Temp.: 1^{o} F

Spec. No.: T234-2

$K_c = 46.39$ ksi $\sqrt{in}$

Temp.: 1^{o} F

Spec. No.: L304-2

$K_c = 50.91$ ksi $\sqrt{in}$

Temp.: 0^{o} F

Spec. No.: L624-2

$K_c = 58.90$ ksi $\sqrt{in}$

Temp.: 0^{o} F

Spec. No.: L524-2

$K_c = 68.53$ ksi $\sqrt{in}$

Temp.: -19^{o} F

Spec. No.: T632-2

$K_c = 54.39$ ksi $\sqrt{in}$

Fig. 67 PHOTOGRAPHS OF THE FRACTURE SURFACES

1" SPECIMENS - IMPACT TESTS

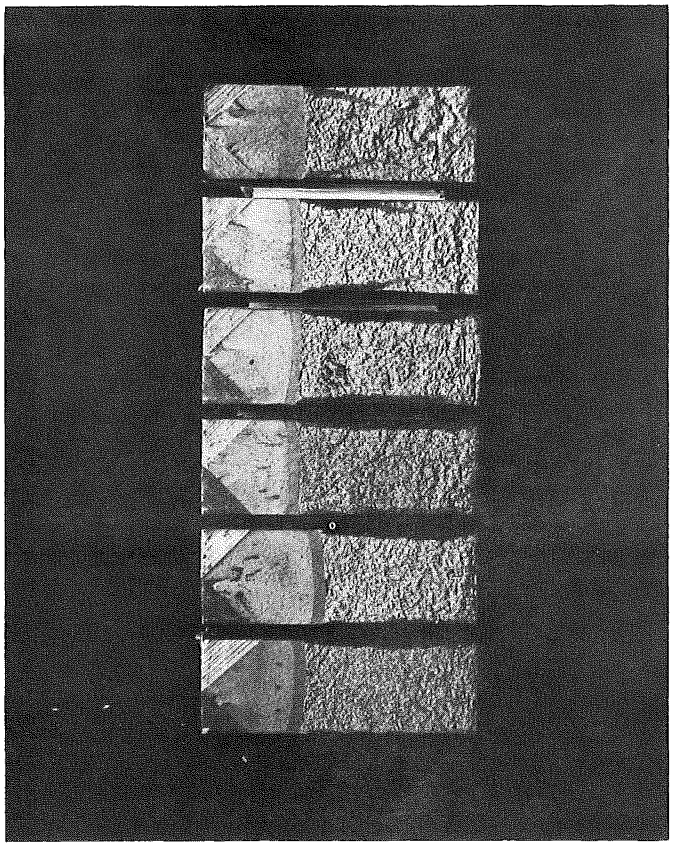

Temp.: 80^{o} F

Spec. No.: T231-2

$K_c > 83.02$ ksi $\sqrt{in}$

Temp.: 58^{o} F

Spec. No.: L513-2

$K_c > 90.51$ ksi $\sqrt{in}$

Temp.: 57^{o} F

Spec. No.: L531-2

$K_c > 125.3$ ksi $\sqrt{in}$

Temp.: 39^{o} F

Spec. No.: T613-2

$K_c = 73.05$ ksi $\sqrt{in}$

Temp.: 38^{o} F

Spec. No.: L522-2

$K_c = 65.57$ ksi $\sqrt{in}$

Temp.: 30^{o} F

Spec. No.: L324-2

K_c 79.10 ksi $\sqrt{in}$

Fig. 67 PHOTOGRAPHS OF THE FRACTURE SURFACES

2" SPECIMENS - STATIC TESTS

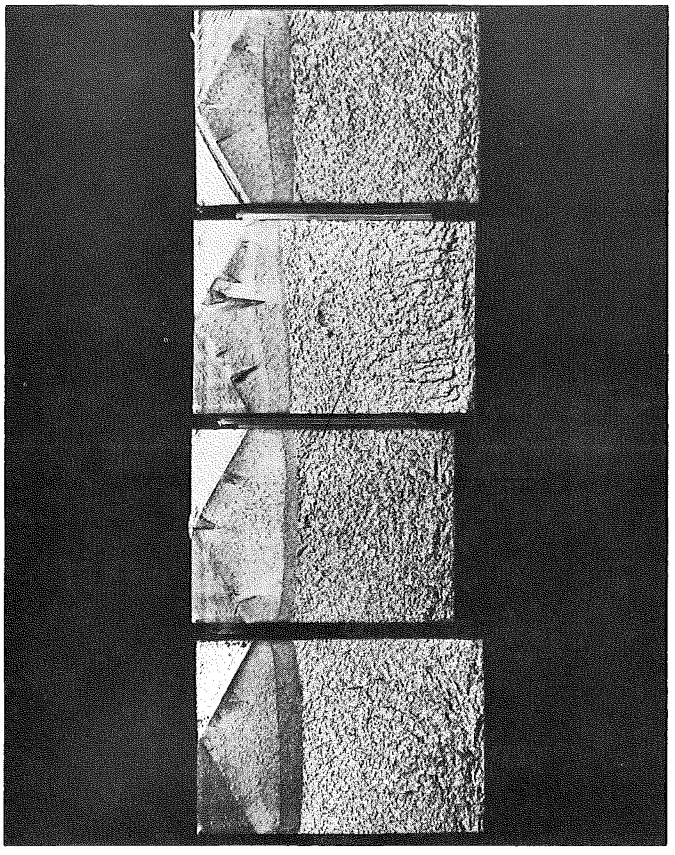

Temp.: -40^{o} F

Spec. No.: T632-3

K_c = 52.26 ksi $\sqrt{in}$

Temp.: -40^{o} F

Spec. No.: L522-3

K_c = 38.54 ksi $\sqrt{in}$

Temp.: -90^{o} F

Spec. No.: L531-3

K_c = 47.61 ksi $\sqrt{in}$

Temp.: -112^{o} F

Spec. No.: L622-3

K_c = 41.22 ksi $\sqrt{in}$

Fig. 67 PHOTOGRAPHS OF THE FRACTURE SURFACES

2" SPECIMENS - STATIC TESTS

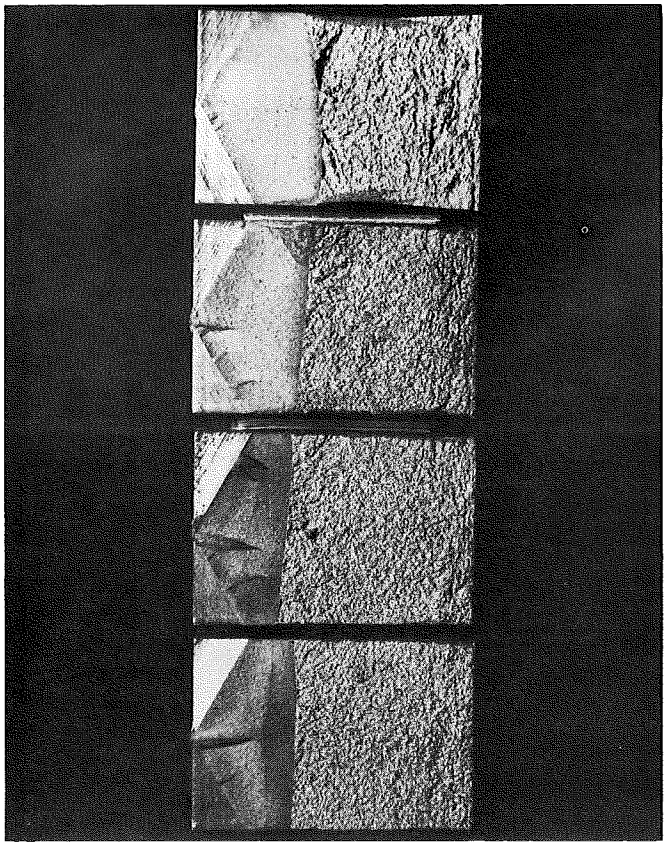

Temp.: 82^{o} F

Spec. No.: L624-3

$K_c > 93.1$ ksi $\sqrt{in}$

Temp.: 40^{o} F

Spec. No.: L532-3

$K_c > 50.6$ ksi $\sqrt{in}$

Temp.: 20^{o} F

Spec. No.: L623-3

$K_c = 49.7$ ksi $\sqrt{in}$

Temp.: -4^{o} F

Spec. No.: L531-3

$K_c = 68.15$ ksi $\sqrt{in}$

Fig. 67 PHOTOGRAPHS OF THE FRACTURE SURFACES

2" SPECIMENS - IMPACT TESTS

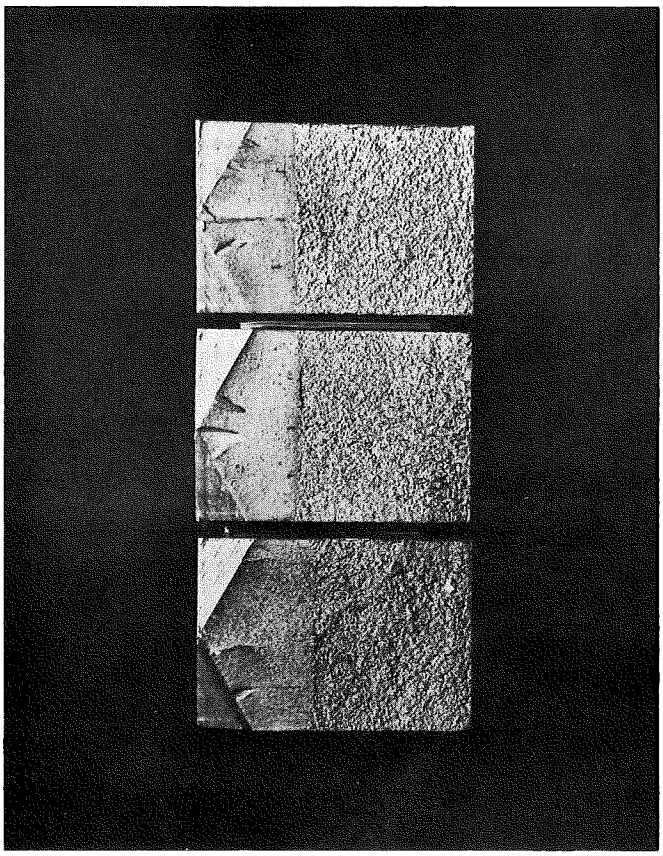

Temp.: 0^{o} F

Spec. No.: T612-3

K_c = 53.80 ksi $\sqrt{in}$

Temp.: -38^{o} F

Spec. No.: L533-3

K_c = 41.55 ksi $\sqrt{in}$

Temp.: -43^{o} F

Spec. No.: T634-2

K_c = 42.18 ksi $\sqrt{in}$

Fig. 67 PHOTOGRAPHS OF THE FRACTURE SURFACES

2" SPECIMENS - IMPACT TESTS

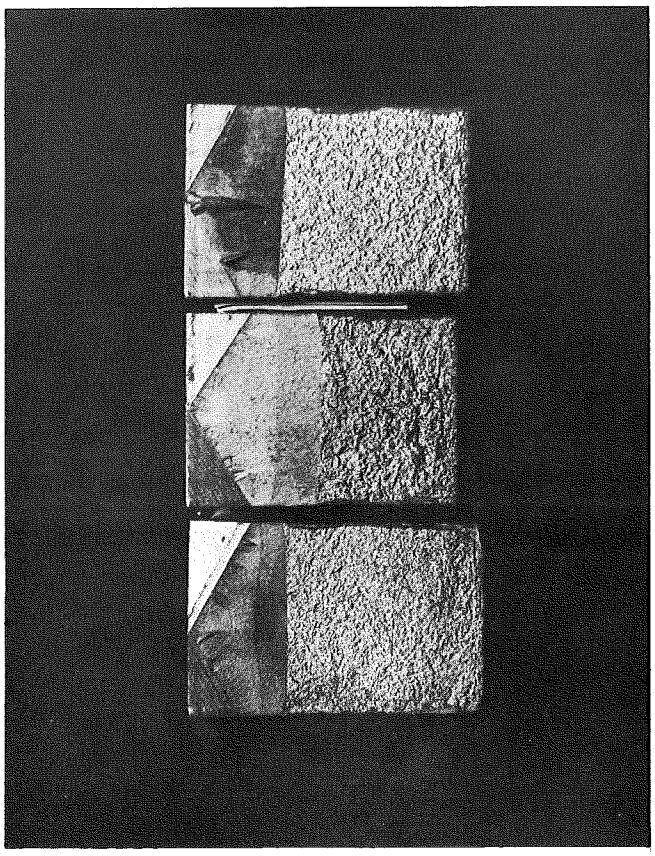

Temp.: 40^{o} F

Spec. No.: T613-3

K_c 56.41 ksi $\sqrt{in}$

Temp.: 39^{o} F

Spec. No.: T611-3

K_c 93.87 ksi $\sqrt{in}$

Temp.: 39^{o} F

Spec. No.: L511-3

K_c 54.87 ksi $\sqrt{in}$

Fig. 67 PHOTOGRAPHS OF THE FRACTURE SURFACES

APPENDIX A

STRESS ANALYSIS OF KINGS BRIDGE

THE CRITICAL GIRDER

The complete analysis of Kings Bridge indicates that Girder W14-3, the interior girder, was the girder that fractured first at the time of the failure of the bridge on July 11, 1962. Only the analysis of Girder W14-3 will be presented here.

SECTION PROPERTIES

The section properties at the end of the cover plate must be computed. Since the cover plate narrows at this point to only 3", the position of the neutral axis will be the same as for the non-cover-plated section.

Non-Composite

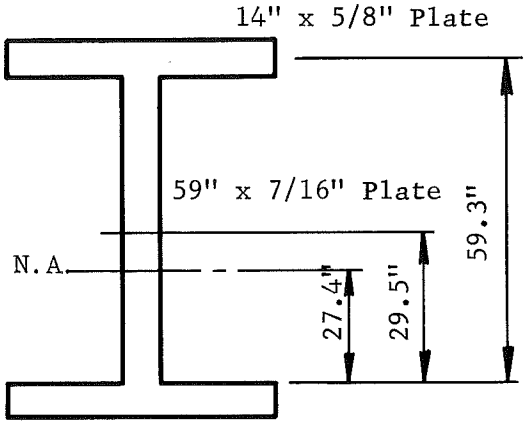

$I = 25,781 \text{ in.}^4$

$S_b = 930 \text{ in.}^3$

Note:

S_b is the section modulus to the $\mathbb{C}$ of the bottom flange.

Composite

On page 130, Section 1.7.99 of the AASHO Specification, "The effective width shall not exceed 12 times the least thickness of the slab". For Kings Bridge, this would be 84". This is in good agreement with Hulsbos (43), page 74, where an effective width of 75" was measured in the field on an actual bridge with similar slab thickness and load, but with only 30" girders.

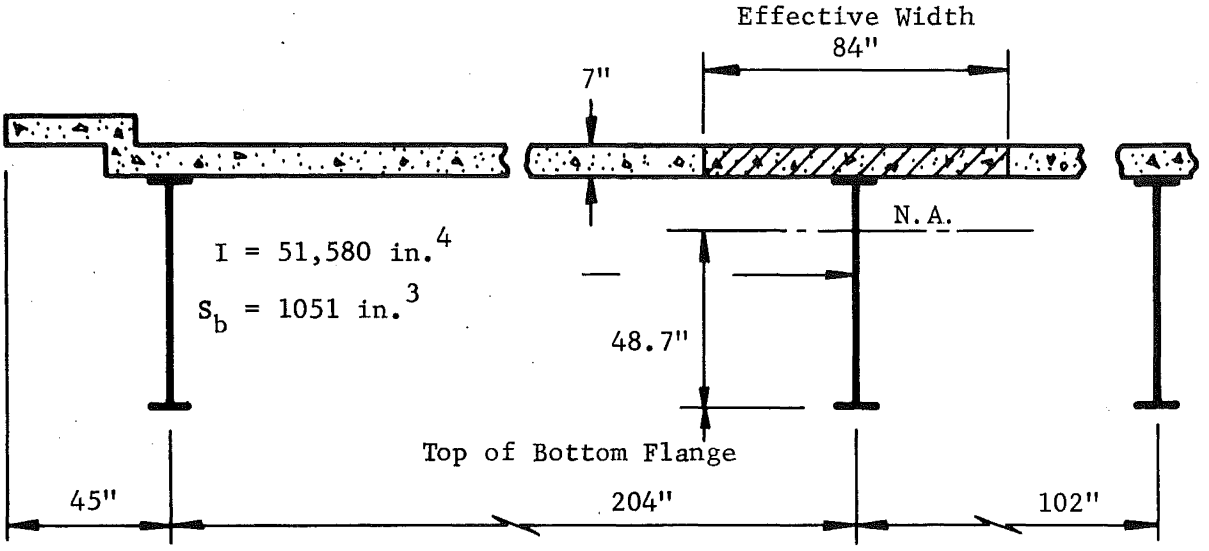

Note: S_b is the Section Modulus to the ℄ of the bottom flange.

THE TRANSVERSE DISTRIBUTION OF BRIDGE MOMENT TO EACH GIRDER

The following procedure was used to estimate the percent of the total bridge moment carried by each girder.

1. A model of a 4-beam concrete box girder bridge was tested with a standard truck load, and the load distribution determined.(44)
2. An analysis for the transverse load distribution of Kings Bridge, all four girders acting, was made using the method of Guyon-Massonnet (45).
3. A check on the analysis of Part 2 was made by comparing the results with those of a 4-girder steel bridge instrumented and tested in the field (43).
4. Influence lines for the transverse load distribution were constructed for the concrete bridge model, for the Kings Bridge, and for the steel bridge tested in the field.

5. "Lower Bound" influence lines were constructed for the Kings Bridge, three girders acting, by assuming the bridge stiffness was unchanged by the presence of a crack in Girder W14-2. The load in Girder W14-2 was distributed to the remaining three girders in the same proportion as when four girders were acting.
6. One interior girder of the concrete bridge model was removed and the model was retested.
7. "Upper Bound" influence lines were constructed for the Kings Bridge, three girders acting, by assuming the cracked girder offered no stiffening to the bridge. The distribution obtained in Part 6 was used, but with an allowance for the greater flexibility of the steel bridge.
8. The probable transverse distribution to each girder of the bending moment at the time of failure was determined from the average of the "Upper" and "Lower" bounds. The difference between the "Upper" and "Lower" Bounds was small at the location of the live load and of the fractured girder.

THE CONCRETE BRIDGE MODEL (42)

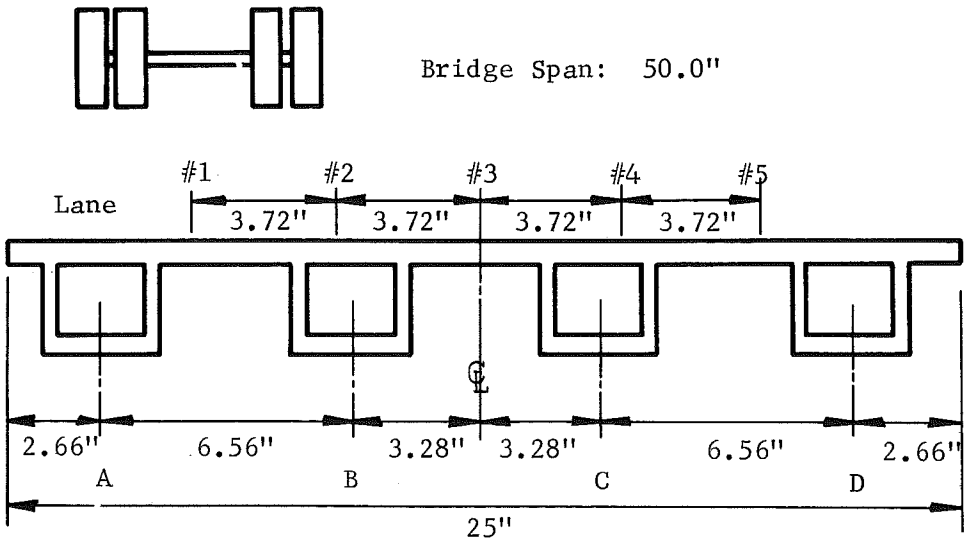

A CONTINUOUS COMPOSITE STEEL BRIDGE (43)

The following continuous composite steel bridge was the subject of extensive field investigation and will be used as a check on the work presented here.

The difference between static and dynamic load distribution was found to be small. The static values are used here.

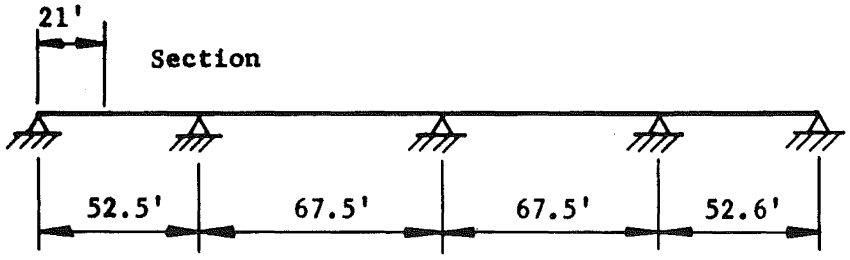

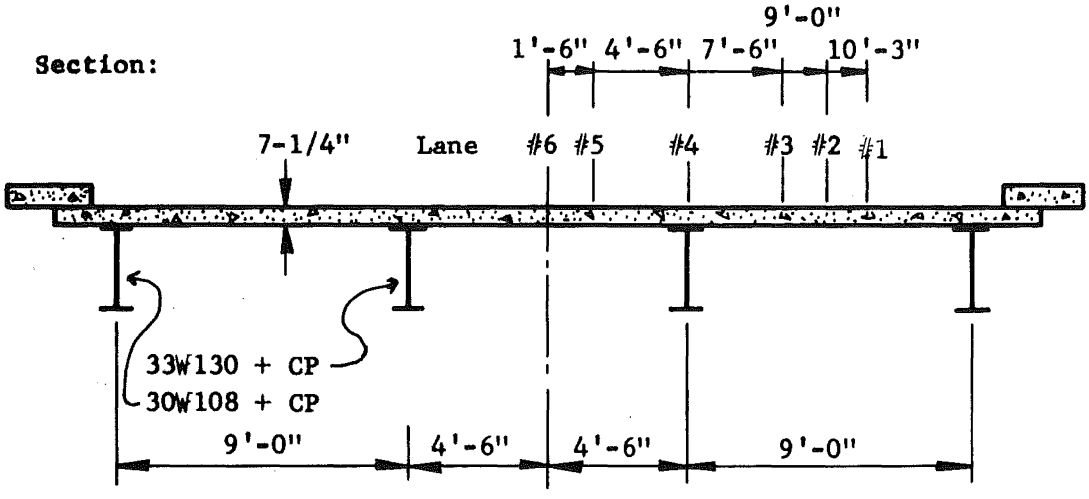

THE KINGS BRIDGE - GUYON-MASSONNET ANALYSIS

The Guyon-Massonnet Load Distribution Theory (45) was used to estimate the transverse distribution of bending moment to each girder, all four girders acting. The girders were assumed to be all of the same section, and of constant cross-section along the length of the bridge.

INFLUENCE LINES - 4 GIRDERS ACTING

INFLUENCE LINE - Girder W14-1 Scale" 1" = 6.0'

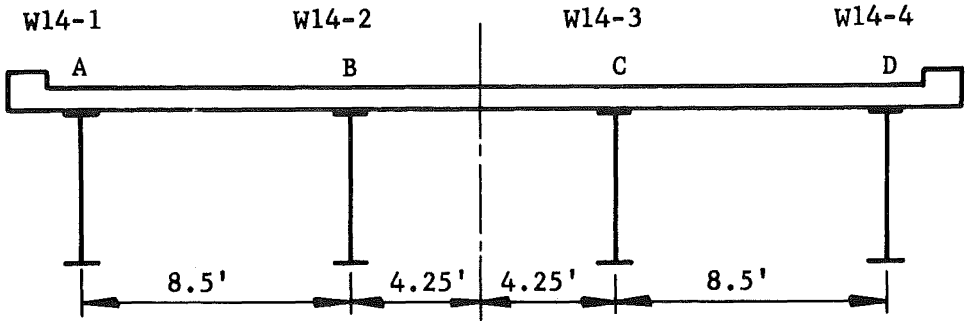

Concrete Bridge Model

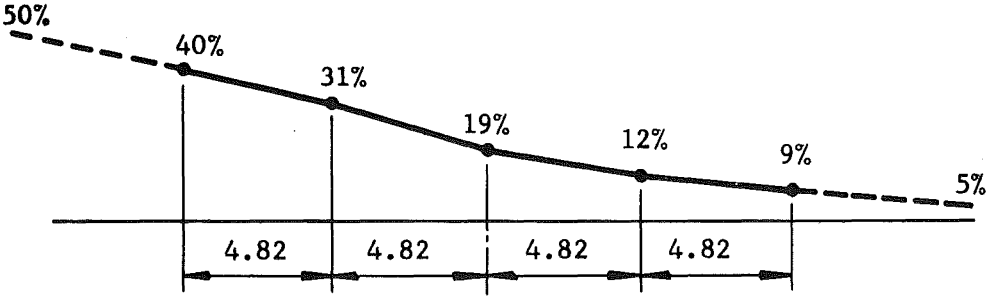

Hulsbos's Bridge

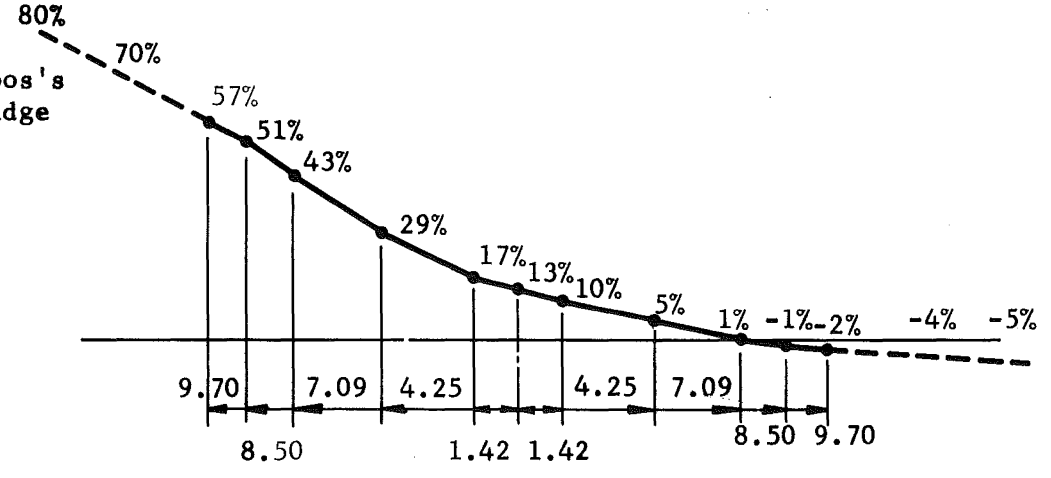

Kings Bridge - Guyon-Massonnet Theory:

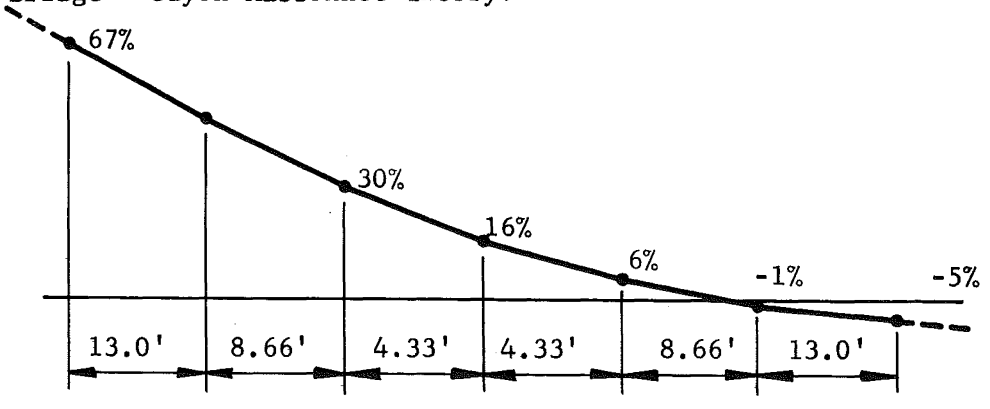

INFLUENCE LINE - GIRDER W14-3 Scale: 1" = 6.0'

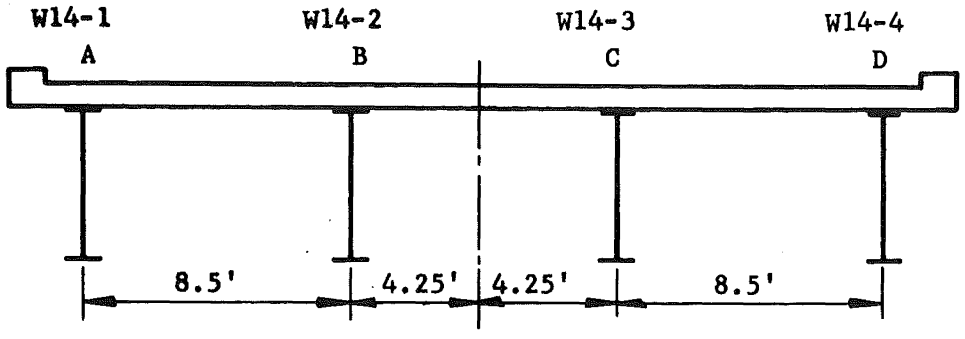

Concrete Bridge Model:

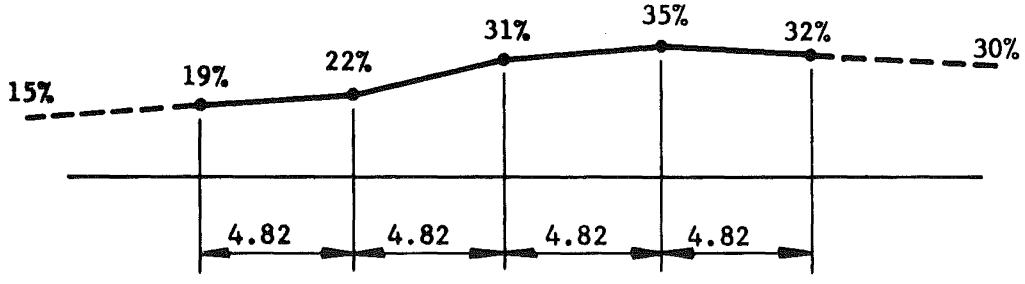

Hulsbos's Bridge:

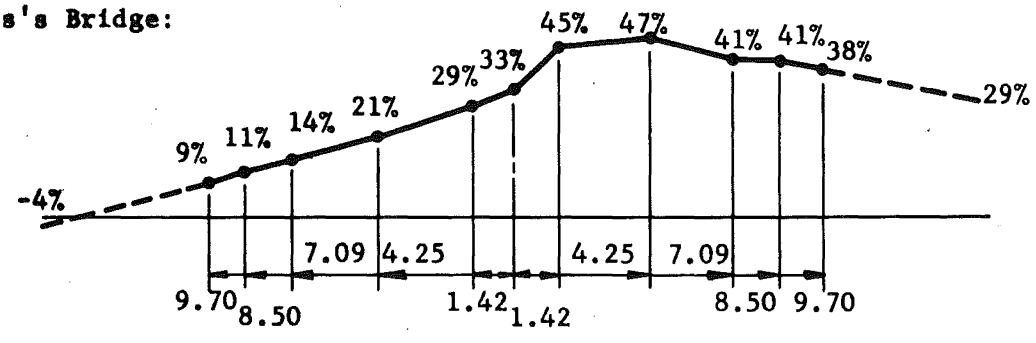

Kings Bridge - Guyon-Massonnet Theory:

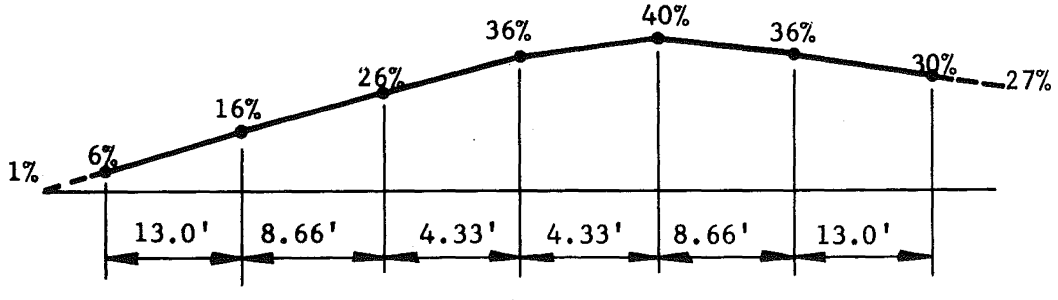

INFLUENCE LINES - 3 GIRDERS ACTING

Concrete Bridge Model

The following method was used to find a lower and an upper bound for the transverse distribution of moment with Girder W14-2 cracked.

Lower Bound - Assume Girder W14-2 when cracked contributes as much to the stiffness of the bridge as when it is not cracked. The transverse distribution of moment can be found from the results of the model study with four girders acting. The moment in Girder W14-2 was distributed successively to the other three girders until the moment in Girder W14-2 was reduced to zero.

Upper Bound - Assume Girder W14-2 when cracked contributed nothing to the stiffness of the bridge. The transverse distribution of moment was found from the model with Girder W14-2 removed. A new set of measurements were taken with Girder W14-2 removed and the influence lines were determined.

Kings Bridge

The following method was used to estimate a lower and an upper bound for the transverse distribution of moment with Girder W14-2 cracked.

Lower Bound - Assume Girder W14-2 when cracked contributes as much to the stiffness of the bridge as when it is not cracked. The transverse distribution of moment was found from the results of the Guyon-Massonnet analysis with four girders acting. The moment in Girder W14-2 was distributed successively to the other three girders until the moment in Girder W14-2 was reduced to zero.

Upper Bound - Assume Girder W14-2 when cracked contributes nothing to the stiffness of the bridge. The transverse distribution of moment was estimated from the upper bound for the concrete bridge model. The moment in Girder W14-2 was distributed to the other three girders in the same manner as the concrete model, but proportioned according to the relative stiffness determined from the lower bound solutions.

INFLUENCE LINE - GIRDER W14-1

Scale: 1" = 6.0'

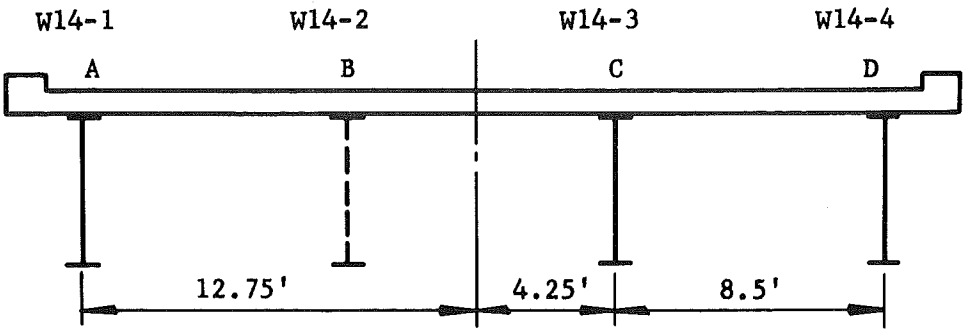

Concrete Bridge Model

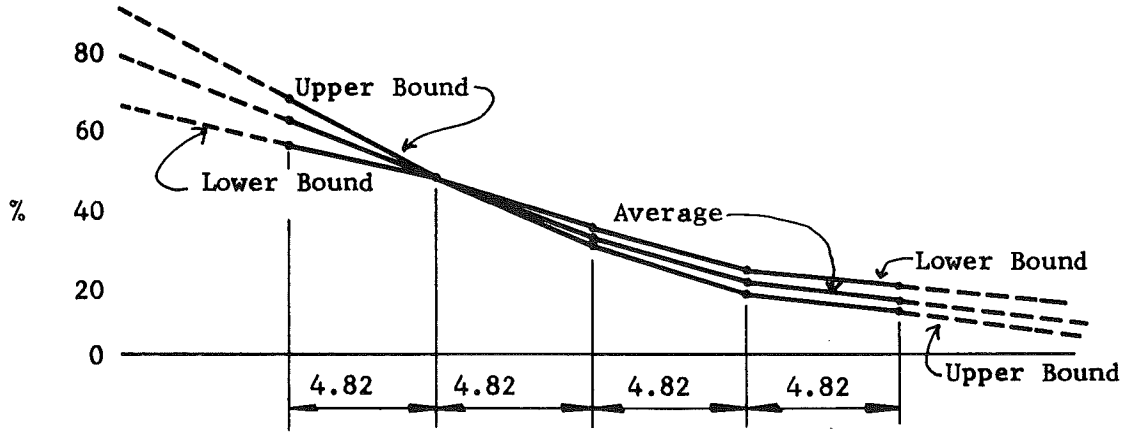

Kings Bridge:

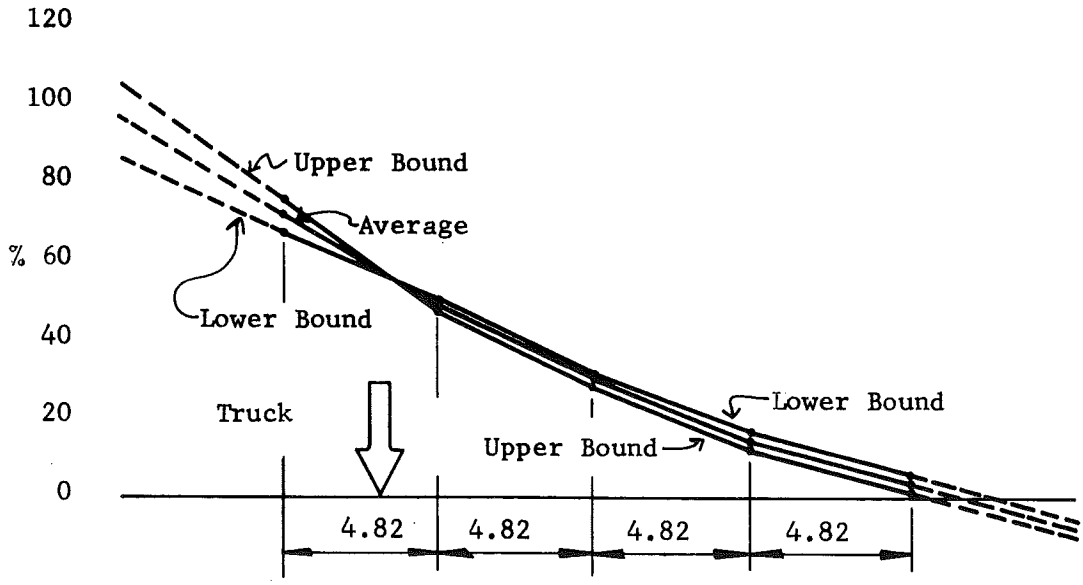

INFLUENCE LINE - GIRDER W14-3

Scale: 1" = 6.0'

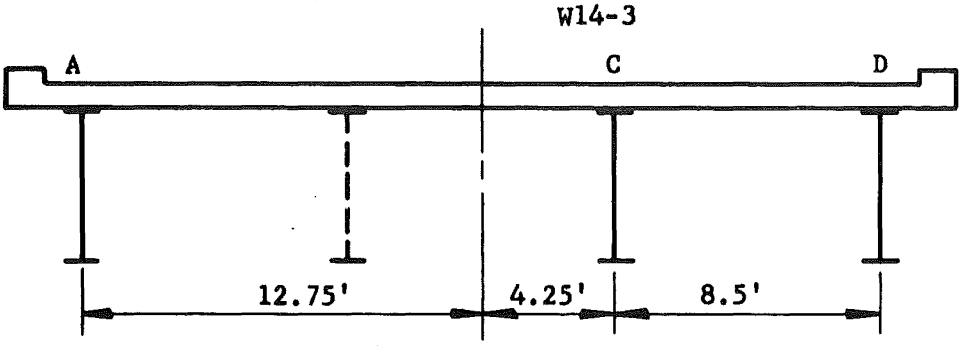

Concrete Bridge Model

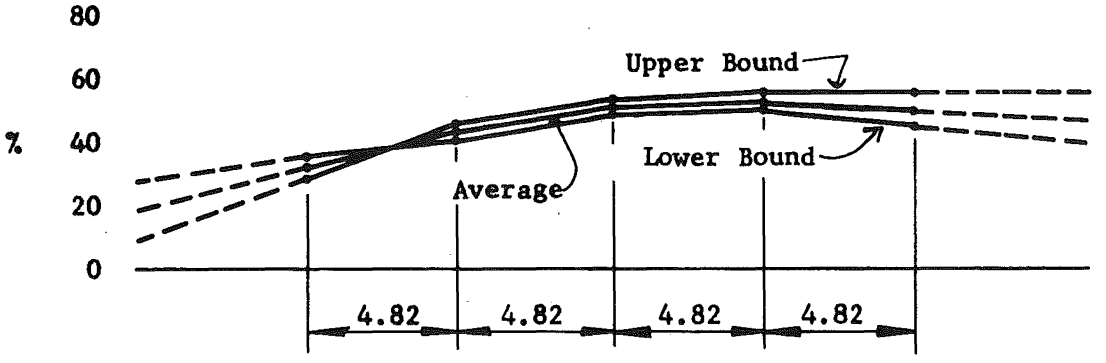

Kings Bridge

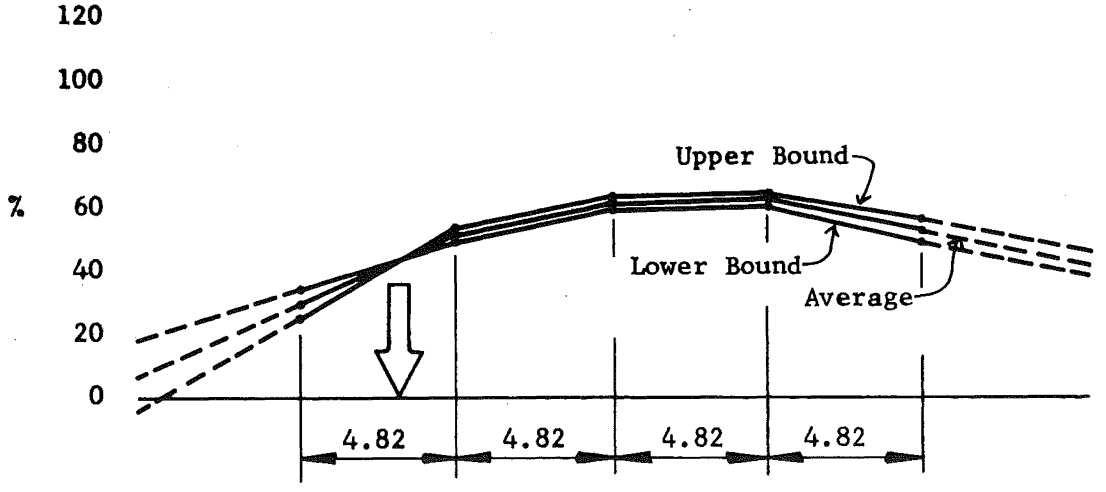

INFLUENCE LINE - GIRDER W14-4

Scale: 1" = 6.0'

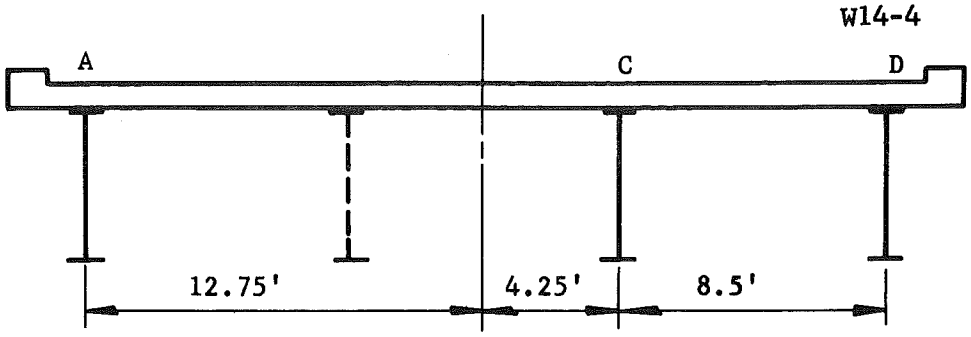

Concrete Bridge Model

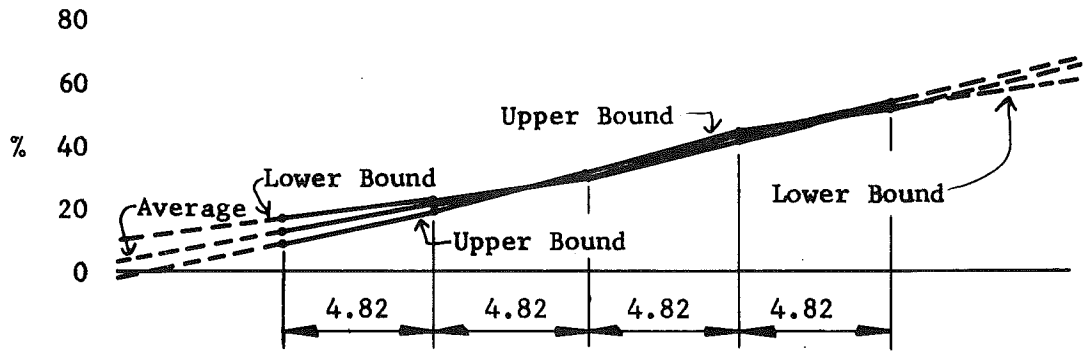

Kings Bridge

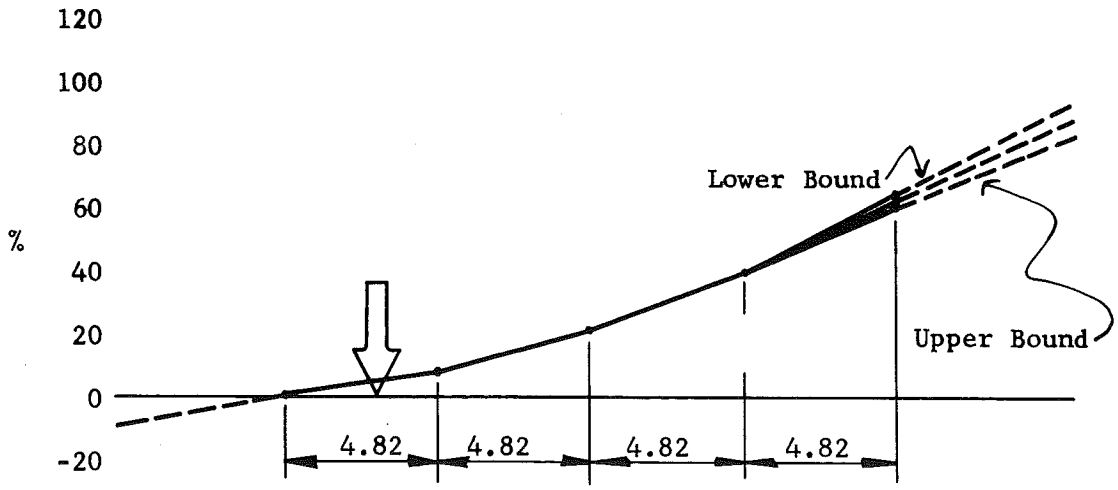

LOADS

DEAD LOAD MOMENT IN GIRDER W14-3

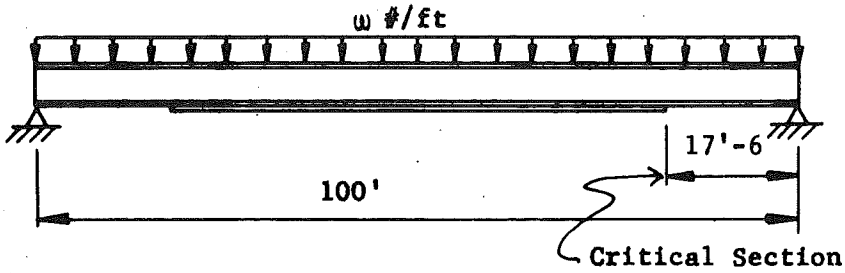

Dead Load Moment at the critical section:

$$M = (\omega \times 50)(17.5) - (\omega \times 17.5)(8.75) = 730.6\omega$$

SLAB:

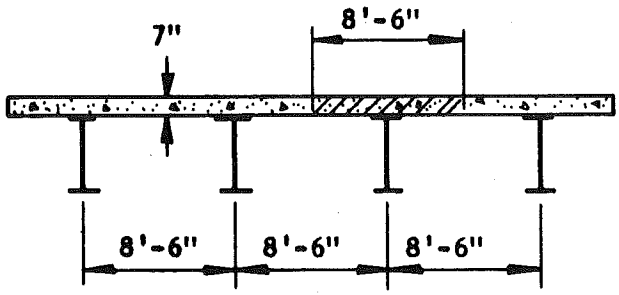

$\omega = \frac{7'}{12} \times 8.5' \times 150\#/ft.^3 = 744\#/ft.$

$M = 730.6 \times 744 = 545^{k\text{-}ft.}$

GIRDER: $\omega = 188.2\#/ft.$ $M = 730.6 \times 188.2 = 138^{k\text{-}ft}$

WEARING SURFACE:

Assume a wearing surface weighing $20\#/ft.^2$

$\omega = 20\#/ft.^2 \times 8.5' = 170\#/ft.$ $M = 730.6 \times 170 = 125^{k\text{-}ft}$

RAILING:

Assume a wt. of rail of 100#/ft. From the influence lines, the % to each girder is:

W14-1	99%
W14-2	7%
W14-3	-6%
	100%

$7\% \times 730.6 \times 0.1 = 5^{k\text{-}ft}$

LOAD FROM GIRDER W14-2

Slab	$545^{k\text{-}ft}$	W14-1	47%
Girder	138	W14-2	45%
Wearing Surface	$\frac{125}{808}^{kl}$	W14-3	8%
			100%

$45\% \times 808 = 364^{k\text{-}ft}$

LIVE LOAD MOMENT IN GIRDER W14-3

THE VEHICLE:

Page 9 of Report: "... a low loader weighing unloaded about 17^T - carrying a load of approximately 28^T..."[15]

Page 108 of Report: "... a semi-trailer vehicle having a total length of about 49 feet. The total weight was approximately 47 tons."[15]

Assume the total weight of the vehicle was 47 long tons or 47^T x 2240 lbs/T = 105,000 lbs.

Compare this with the Type 4 design loading shown on Page 13 of The AASHO Report.[35] Assume a similar distribution:

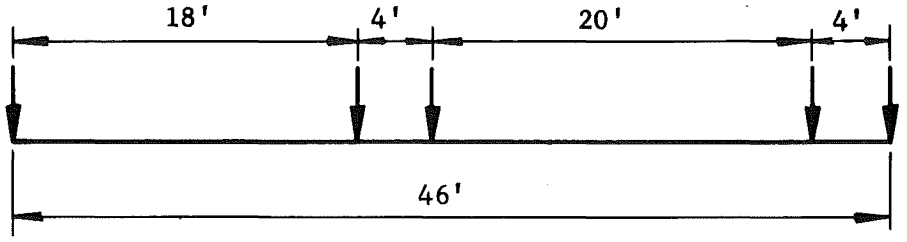

							Total
AASHO Design	11^k		25^k	25^k		25^k 25^k	111^k
Assumed Vehicle	10.4^k		23.6^k	23.6^k		23.6^k 23.6^k	105^k

According to the newspaper reports, it was foggy the morning of the failure and the fog did not lift until late in the morning. Also, the truck had just left a city street and was on an upgrade. Assume truck speed of 20 to 30 mph.

From Page 59 of the AASHO Report,[35] impact varied from 11 to 29% at 30 mph.

From Pages 61, 62, and 63 of the Iowa Report,[43] impact varied from 2 to 20% for velocities in the 10 to 30 mph range, but there is a resonance phenomenon. Could be as high as 100%

From Biggs[47] impact was a maximum of 20% for speeds from 19 to 25 mph.

From Wen,[48] impact was probably 20% but could be as high as 100%.

Assume a 20% increase in load due to impact.

Impact	2.08	4.72	4.72	4.72	4.72	21.0^{k}
Probable Total Load	12.4	28.4	28.4	28.4	28.4	126.0^{k}

COMMENTS ON IMPACT LOAD:

According to theory (Refs. 43, 47, and 28) a resonance phenomenon can occur even at speeds as slow as 20 mph. This could cause an impact factor of as much as 80% and possibly 100%.

However, actual test records seldom show an impact factor as high as 40% and 20% is usually the case. The AASHO Specifications require an impact factor of:

$$I = \frac{50}{L + 225} = \frac{50}{225} = 22\%$$

An impact factor of 20% seems to be a logical assumption for the Kings Bridge.

If a total live plus impact load 50% higher than that used were considered (corresponding to an impact of 80%), it would increase the K_c by less than 20%.

MAXIMUM LIVE LOAD MOMENT AT 17'-6" FROM SUPPORT

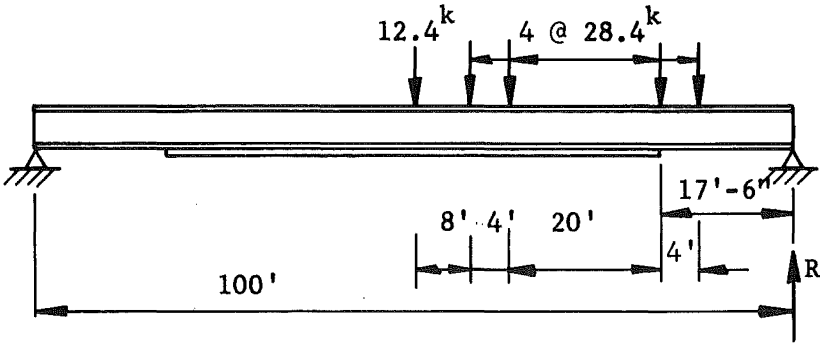

$$R = \frac{1}{100}\,[12.4 \times 50.5 + 28.4(58.5 + 62.5 + 82.5 + 86.5)]$$

$$R = 88.622^{k}$$

$$M = 88.622 \times 17.5 - 28.4 \times 4$$

$$M = 1437.3^{k\text{-ft.}}$$

TRANSVERSE LOCATION OF THE TRUCK AT FAILURE

Scale: 1" = 6.0'

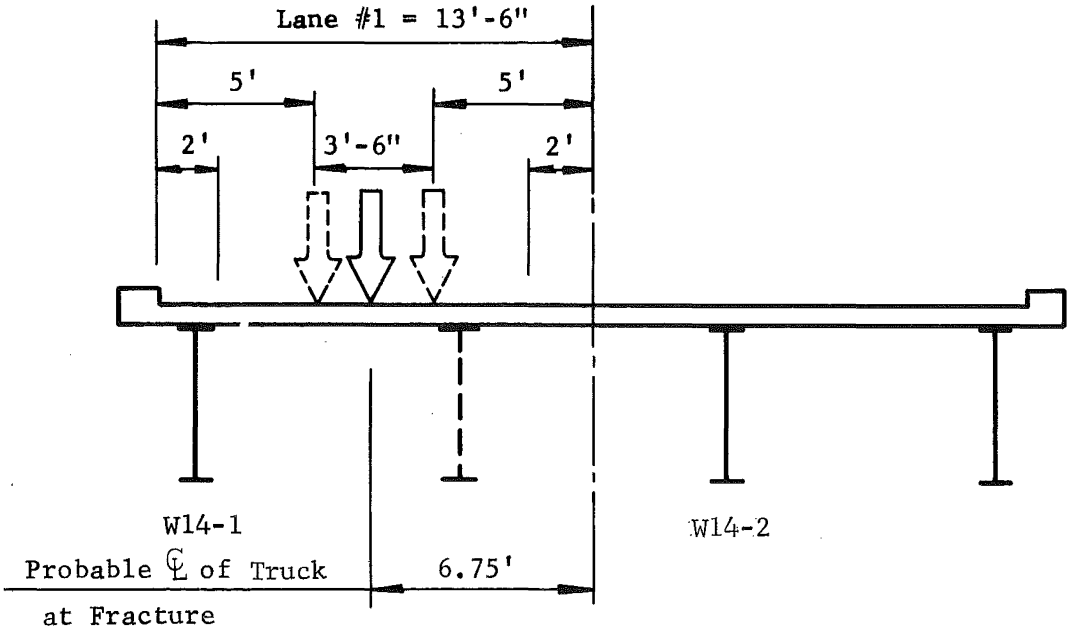

It was a foggy morning with little traffic and the truck was on an upgrade.

He was probably in the left lane, the slow lane.

Considering the standard H truck, page 14 of the AASHO Specification,[49] the ℄ of the truck would not be any closer than 5' from the curb or 5' from ℄ of roadway.

Assume the ℄ of the truck was in the ℄ of the lane, this is within an error of ± 1'-9" either way.

The portion of the Live Load Moment carried by each girder is found from the influence lines:

W14-1	58%	
W14-3	37% x 1437. $^{k\text{-}ft}$	= 531$^{k\text{-}ft}$
W14-4	5%	
	100%	

STRESSES

The following stresses are computed for the center of the bottom flange at the end of the cover plate of Girder W14-3.

Dead Load Stress

Concrete and Steel (Carried by Steel Section)

σ = (545 k-ft + 138 k-ft) x 12 in.ft. ÷ 930 in.^{3} = 8.82 ksi

Wearing Surface and Railing (Carried by Composite Section)

σ = (125 k-ft + 5 k-ft) x 12 in.ft. ÷ 1051 in.^{3} = 1.48 ksi

Girder W14-2 (Carried by Composite Section)

σ = 364 k-ft x 12 in.ft. ÷ 1051 in.^{3}	4.14	ksi
Total Dead Load Stress	14	ksi

Live Load Stress (Carried by Composite Section)

σ = 531 k-ft x 12 in.ft. ÷ 1051 in.^{3} =	6	ksi
Total Stress	20	ksi

RESIDUAL STRESS

This is an attempt to estimate the probable residual stress pattern at the time of failure. The girder will be followed through fabrication and service to estimate the effect of each event on the stress pattern.

The Tensile Flange

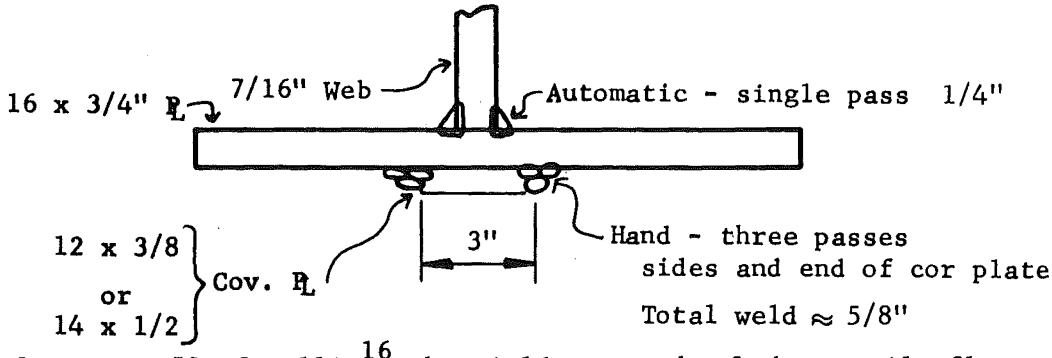

from page 52 of Ballie[16] the yield strength of the tensile flange was 53 ksi.

A theoretical analysis of the residual stresses is not possible. However, by comparing the section to the residual stresses measured in a similar welded section we shall make an estimate.

From page 37 of Rao[50]

1" plates, 5/8" welds

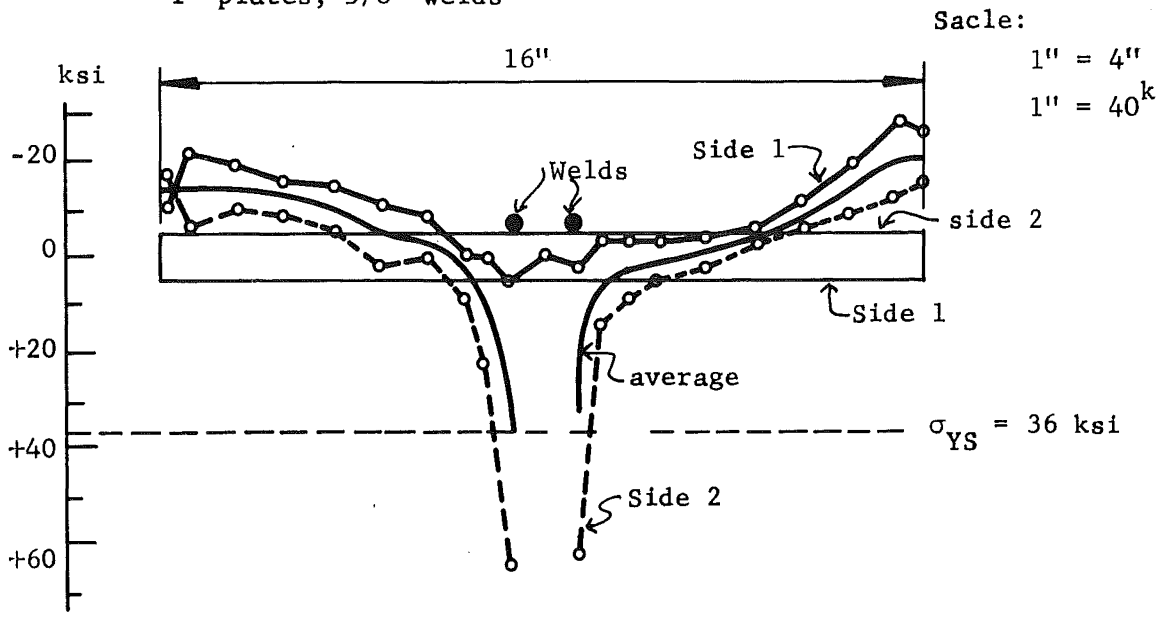

WEB TO FLANGE WELD

Assume the probable average stress across the flange of the Kings Bridge was the same as above, except the welds are 1/2" apart instead of 1".

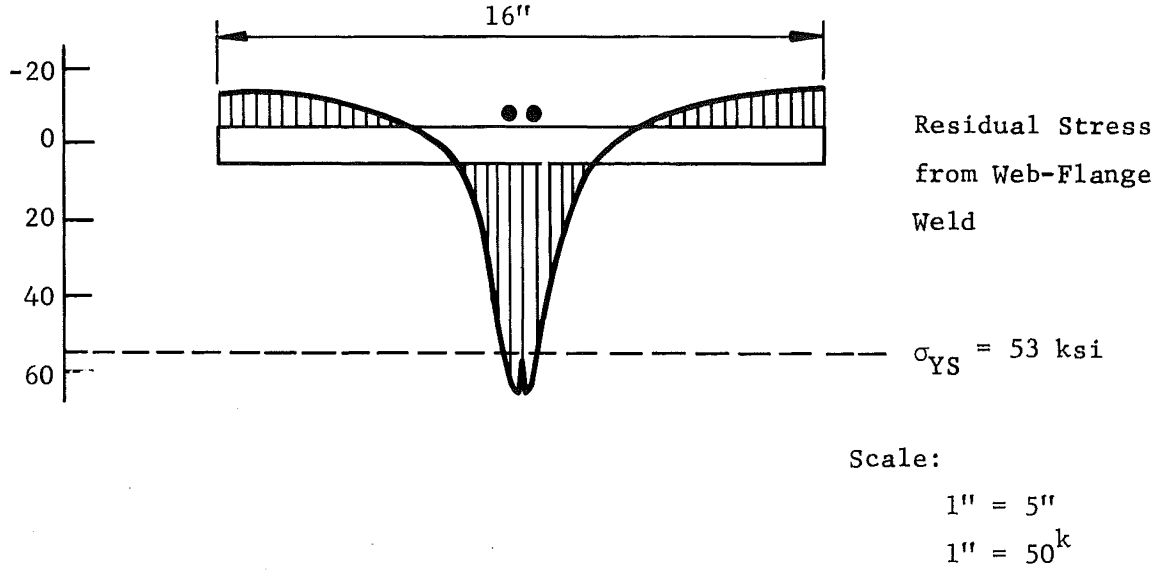

COVER PLATE TO FLANGE WELD

Assume a residual stress pattern similar to Rao's, but with welds 3" apart.

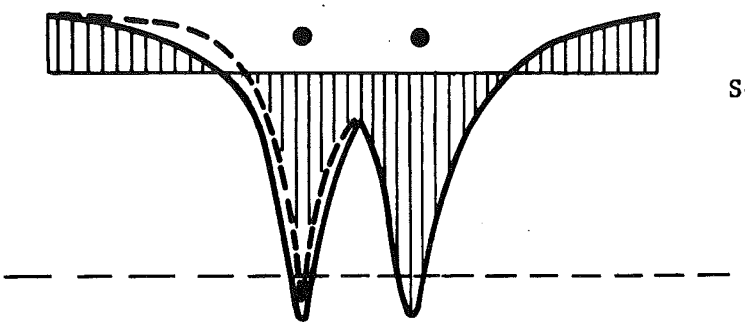

Scale:
1" = 5"
1" = 50^{k}

σ_{YS} = 53 ksi

Adjust the areas to balance tens and comp. (dotted)

Combine above with step #1:

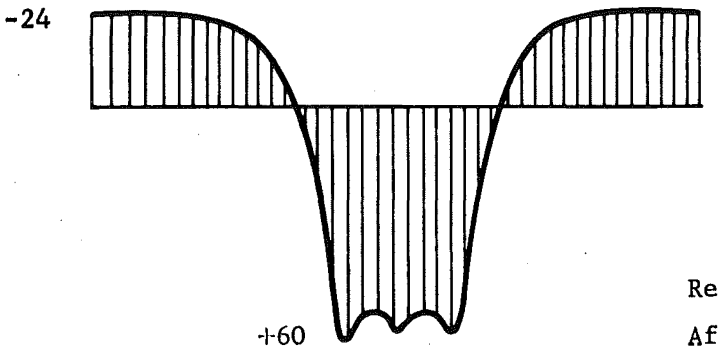

Scale:
1" = 5"
1" = 50^{k}

Residual Stresses
After Welding

Assumed the weld on the end of the cover plate does not further change the pattern.

APPLICATION OF DEAD LOAD

Apply the dead load. Except for the weld metal itself (a localized effect), the stress can not be greater than the yield stress, 53 ksi.

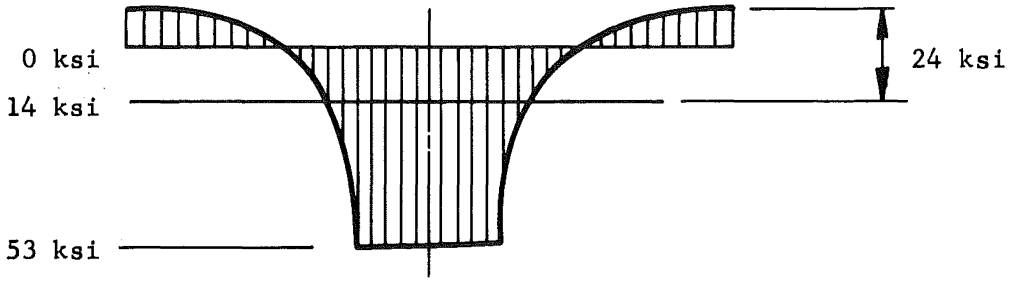

Since yielding has removed a portion of the tensile residual stress, the compressive residual stress must also be relaxed somewhat.

Remove the dead load and re-balance the stresses.

Set area $A_1 = A_2$

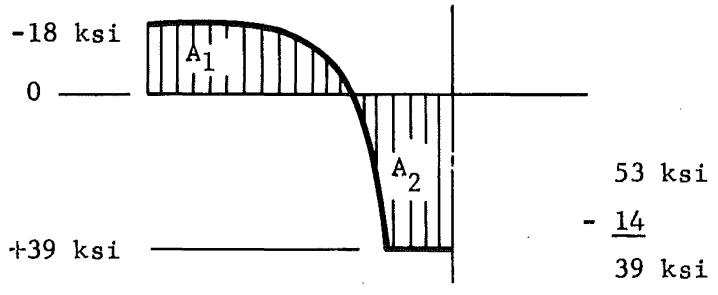

Residual Stress after

application of Dead Load

APPLICATION OF THE MAXIMUM LIVE LOAD

The next step is to estimate the maximum live load applied to Girder W14-3 prior to failure. Assume a loading condition equivalent to the 50^T crawler in the left lane and a 20^T truck (with the wheel spacing as the 50^T crawler) passing in the right lane.

From page 16, the live load moment is:

50^T Truck	$1437^{k\text{-}ft}$
20^T Truck	$575^{k\text{-}ft}$

From the Influence Lines, the moment in Girder W14-3 is:

$$37\% \times 1437^{k\text{-}ft} = 531^{k\text{-}ft}$$
$$48\% \times 575^{k\text{-}ft} = 276^{k\text{-}ft}$$
$$807^{k\text{-}ft}$$

The stress is:

Live Load $\sigma = 807^{k\text{-}ft} \times 12^{in\text{-}ft} \div 1051\ in.^3 = 9$ ksi

Dead Load 14

Total 23 ksi

Apply this live load plus the dead load:

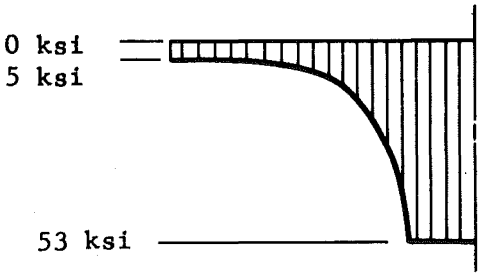

-18 ksi
+23 ksi
5 ksi

Since part of the tensile stress has been relieved by yielding, the compressive stress must be relaxed accordingly. Remove the dead and live load and rebalance the residual stress.

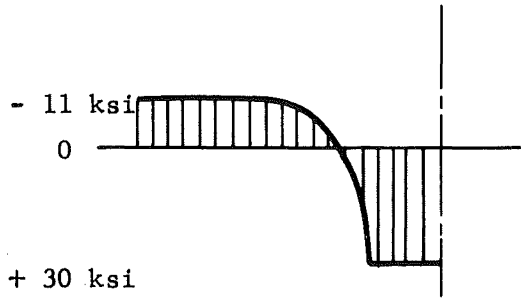

Net Residual Stress
at Failure

TOTAL STRESS AT FAILURE

Adding the dead load, live load, and residual stress:

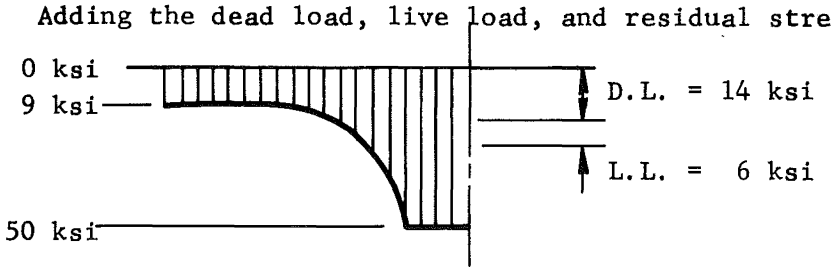

Idealized Stress Pattern:

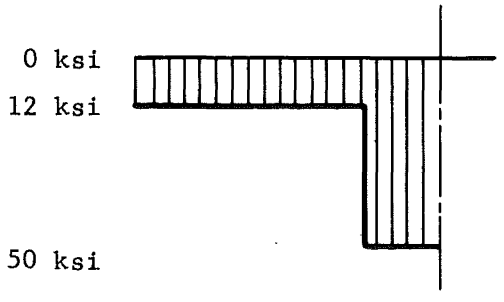

APPENDIX B

FRACTURE ANALYSIS OF KINGS BRIDGE

THE THREE-ENDED CRACK

THE FLANGE CRACK

THE WEB CRACK

COMPUTATION PROCEDURE

IMPACT DATA - KINGS BRIDGE

RESULTS

THE THREE ENDED CRACK

The three ended crack, shown in Fig. 19 was analyzed using the basic theory described in Part II, Section 7.

THE FLANGE CRACK

For the uniform stress across the flange, see Fig. 29a, the stress intensity factor and the center crack displacement are, from Eqs. 7 and 34:

$$K_{11} = \sigma_{11}\sqrt{\pi\, a_1}\ \sqrt{\sec\frac{\pi a_1}{W}}$$

$$v_{11} = \frac{2}{E}\,\sigma_{11}\,a_1$$

where σ_{11} is the uniform stress across the flange and a_1 is the effective length of the flange crack.

For the welding residual stress, see Fig. 29b, the stress intensity factor and the center crack displacement are, from Eqs. 42 and 41:

$$K_{12} = \sigma_{12}\sqrt{\pi\, a_1}\ \left[\frac{2}{\pi}\left(\sin^{-1}\frac{C_{12}}{a_1}\right)\right]$$

$$v_{12} = \frac{4\,\sigma_{12}}{E\,\pi}\left\{a_1 \sin^{-1}\frac{C_{12}}{a_1} + C_{12}\coth^{-1}\left[1 - \left(\frac{C_{12}}{a_1}\right)^2\right]^{-1/2}\right\}$$

where σ_{12} is the uniform stress over part of the crack from $-C_{12}$ to $+C_{12}$.

For the stress transferred from the end of the cover plate at the crack:

$$K_{13} = \sigma_{13}\sqrt{\pi\, a_1}\left[\frac{1}{\pi}\left(\sin^{-1}\frac{C_{13}}{a_1}\right) - \frac{C_{13}}{W}\sec\frac{\pi\, a_1}{W}\right]$$

$$v_{13} = \frac{2\,\sigma_{13}}{E\,\pi}\left\{a_1 \sin^{-1}\frac{C_{13}}{a_1} + C_{13}\coth^{-1}\left[1 - \left(\frac{C_{13}}{a_1}\right)^2\right]^{-1/2} - \frac{C_{13}}{W}\,\pi\, a_1\right\}$$

where σ_{13} is the uniform stress over part of one side of the crack from $- C_{13}$ to $+ C_{13}$.

For the restraining effect of the web on the flange crack:

$$K_{14} = \sigma_{14}\sqrt{\pi\, a_1}\left[\frac{2}{\pi}\left(\sin^{-1}\frac{C_{14}}{\quad}\right)\right]$$

$$v_{14} = \frac{4\,\sigma_{14}}{E\,\pi}\left\{a_1 \sin^{-1}\frac{C_{14}}{a_1} + C_{14}\coth^{-1}\left[1 - \left(\frac{C_{14}}{a_1}\right)^2\right]^{-1/2}\right\}$$

where σ_{14} is the uniform stress over part of the crack from $- C_{14}$ to $+ C_{14}$. The uniform stress is found from

$$\sigma_{14} = \frac{P_1}{2\, t_1\, C_{14}}$$

where P_1 is the restraining force from the web, and t_1 is the thickness of the flange.

The total stress intensity factor and center crack displacement of the flange crack are:

$$K_1 = K_{11} + K_{12} + K_{13} + K_{14}$$

$$v_1 = v_{11} + v_{12} + v_{13} + v_{14}$$

THE WEB CRACK

Since the depth of the web crack is small compared to the distance to the neutral axis, and since the residual stress in the web is small, the web crack loading can be approximated as a uniform stress on a semi-infinite plate with an edge crack. The opening force from the flange crack must also be considered.

These loading conditions are shown in the following sketches.

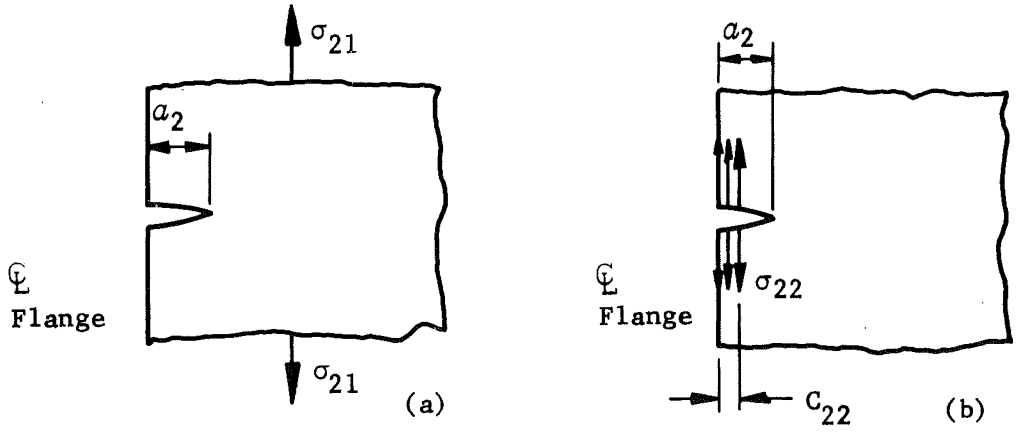

For the uniform stress across the web, see Sketch a, the stress intensity factor and the crack displacement are:

$$K_{21} = \sigma_{21}\sqrt{\pi\, a_2}$$

$$v_{21} = \frac{2}{E}\,\sigma_{21}\, a_2$$

where σ_{12} is the effective uniform stress over the crack and a_2 is the effective length of the web crack.

For the opening effect of the flange crack on the web crack:

$$K_{22} = \sigma_{22}\sqrt{\pi\, a_2}\ [\frac{2}{\pi}\ (\sin^{-1}\frac{C_{22}}{a_2})]$$

$$v_{22} = \frac{4\ \sigma_{22}}{E\ \pi}\left\{ a_2\ \sin^{-1}\frac{C_{22}}{a_2} + C_{22}\ \coth^{-1}\ [1 - (\frac{C_{22}}{a_2})^2]^{-1/2} \right\}$$

where σ_{22} is tge uniform stress over the distance C_{22}.

$$\sigma_{22} = \frac{P_2}{2t_2\ C_{22}}$$

where P_2 is the restraining force from the flange, and t_2 is the thickness of the web.

COMPUTATION PROCEDURE

The following computations were done in an iterative manner using a computer.

1. Set $P_1 = - P_2 = 0$
2. Solve for v_1 and v_2
3. Check $v_1 = v_2$
4. If $v_1 \neq v_2$, increase P_1 by 1.0 kip
5. Repeat steps 1 through 4 until $v_1 = v_2$
6. Compute K_1 and K_2
7. Compute r_{Y1} and r_{Y2} from

$$r_Y = \frac{1}{2\pi}\ (\frac{K}{\sigma_{YS}})^2$$

8. Set $a_1 = a_1 + r_{Y1}$ and $a_2 = a_2 + r_{Y2}$

9. Repeat steps 1 through 8 until the change in a in step 8 is negligible from one iteration to the next.

10. Print out the final values of K_1 and K_2

IMPUT DATA - KINGS BRIDGE

1. No Residual Stress

a_1 = 2.5"	σ_{11} = 20 ksi	
t_1 = 0.75"	σ_{12} = 0	C_{12} = 2.0"
	σ_{13} = 0 (see note)	C_{13} = 2.0
	$\sigma_{14} = \sigma_{14}$	C_{14} = 0.5
a_2 = 4.6"	σ_{12} = 20 ksi	
t_2 = 0.4375"	$\sigma_{22} = \sigma_{22}$	C_{22} = 0.5

For static mode fracture, σ_{YS} = 53 ksi

For impact mode fracture, σ_{YS} = 80 ksi

2. With Residual Stress

a_1 = 2.5"	σ_{11} = 12 ksi	
t_1 = 0.75"	σ_{12} = 38	C_{12} = 2.0
	σ_{13} = 0 (see note)	C_{13} = 2.0
	$\sigma_{14} = \sigma_{14}$	C_{14} = 0.5
a_2 = 4.6"	σ_{12} = 20 ksi	
t_2 = 0.4375"	$\sigma_{22} = \sigma_{22}$	C_{22} = 0.5

For static mode fracture, σ_{YS} = 53 ksi

For impact mode fracture, σ_{YS} = 80 ksi

RESULTS

The program converged on the following values of K and r_Y.

	Flange		Web	
	K_1	r_{Y1}	K_2	r_{Y2}
	ksi $\sqrt{in}$	inch	ksi $\sqrt{in}$	inch
No Residual Stress				
Static Mode	65.6	0.24	71.1	0.29
Impact Mode	63.5	0.10	71.1	0.125
With Residual Stress				
Static Mode	92.8	0.48	83.9	0.39
Impact Mode	94.4	0.22	82.1	0.16

Note: The analysis presented in Section 15, Part II, indicates that the net effect of σ_{13} is very small. It was neglected in the above computations. For comparison with the flange crack values of K from the finite plate analysis 3.4 ksi $\sqrt{in}$ was added to the flange crack K values shown above to obtain the results discussed in Part II.

REFERENCES

1. Irwin, G. R.
   ANALYSIS OF STRESSES AND STRAINS NEAR THE END OF A CRACK TRANSVERSING A PLATE, Transactions, ASME, Journal of Applied Mechanics, 1957.

2. Irwin, G. R.
   FRACTURE MECHANICS, Structural Mechanics, Pergamon Press, New York, N. Y., 1960.

3. Paris, P. C. and Sih, G. C.
   STRESS ANALYSIS OF CRACKS, pp. 30-83, Fracture Toughness Testing and Its Applications, ASTM Spec. Tech. Publ. 381, 1965.

4. Irwin, G. R.
   ONSET OF FAST CRACK PROPAGATION IN HIGH STRENGTH STEEL AND ALUMINUM ALLOYS, NRL Report 4763, and Proceedings, 1955 Sagamore Conference on Ordinance Materials, Vol. II, Syracuse University Press, Syracuse, N. Y., 1956.

5. Beedle, L. S. and Tall, L.
   BASIC COLUMN STRENGTH, Journal of the Structural Division, ASCE, Proc. Paper 2555, Vol. 86, ST7, July, 1960.

6. McClintock, F. A. and Irwin, G. R.
   PLASTICITY ASPECTS OF FRACTURE MECHANICS, pp. 84-113, Fracture Toughness Testing and Its Applications, ASTM Spec. Tech. Publ, 381, 1965.

7. Irwin, G. R.
   RELATION OF CRACK TOUGHNESS MEASUREMENTS TO PRACTICAL APPLICATIONS, Welding Journal Research Suppliment, Nov., 1962.

8. Paris, P. C.
   THE FRACTURE MECHANICS APPROACH TO FATIGUE, Fatigue - An Interdisciplinary Approach, Syracuse University Press, p. 107, 1965.

9. Carman, C. and Katlin, J.
   LOW CYCLE FATIGUE CHARACTERISTICS OF HIGH STRENGTH STEELS, Transactions, ASCE, Journal of Basic Engineering, Paper No. 66-MET-2, 1966.

10. Irwin, G. R., Krafft, J. M., Paris, P. C. and Wells, A. A.
    BASIC ASPECTS OF CRACK GROWTH AND FRACTURE, Naval Research Laboratory, Report 6598, 1967.

11. Irwin, G. R.
FRACTURE MODE TRANSITION FOR A CRACK TRANSVERSING A PLATE Transactions, ASME, Vol. 82, Series D, 1960.

12. Krafft, J. M and Irwin, G. R.
CRACK-VELOCITY CONSIDERATIONS, pp. 114-129, Fracture Toughness Testing and Its Applications, ASTM Spec. Tech. Publ. 381, 1965.

13. Luft, D. E., Madison, R. B., and Irwin, G. R.
MEASUREMENT OF DYNAMIC K_c FROM THE DROP WEIGHT TEAR TEST, Fritz Engineering Laboratory Report No. 335.1, Lehigh University, 1968.

14. The Sidney Morning Herald, July 11, 1969.

15. Report of Royal Commission into the Failure of Kings Bridge, Victoria, Australia, 1963.

16. Ballie, J. G.
UNDERBEAD AND TOE CRACKS, British Welding Journal, February, 1967.

17. Irwin, G. R.
FRACTURING AND FRACTURE MECHANICS, TAM Report No. 208, University of Illinois, October, 1961.

18. Irwin, G. R.
ANALYTICAL ASPECTS OF CRACK STRESS FIELD PROBLEMS, TAM Report No. 213, University of Illinois, March, 1962.

19. Green, A. E. and Snedden, I. N.
THE STRESS DISTRIBUTION IN THE NEIGHBORHOOD OF A FLAT ELLIPTICAL CRACK IN AN ELASTIC SOLID, Proceedings, Cambridge Philosophical Society, Vol. 46, p. 159, 1950.

20. Irwin, G. R.
ANALYSIS OF STRESSES AND STRAINS NEAR THE END OF A CRACK TRAVERSING A PLATE, Journal of Applied Mechanics, Vol. 24, p. 361, September, 1957.

21. Westergaard, H. M.
BEARING PRESSURES AND CRACKS, Transactions, ASME, Journal of Applied Mechanics, Series A, Vol. 61, p. 49, 1939.

22. Griffith, A. A.
THE PHENOMENON OF RUPTURE AND FLOW IN SOLIDS, Philosophical Transactions of the Royal Society of London, Series A, Vol. 221, pp. 163-168, 1920.

23. Paris, P. C. and Erdogan, F.
A CRITICAL ANALYSIS OF CRACK PROPAGATION LAWS, Transactions, ASME, Journal of Basic Engineering, Series D, Vol. 85, No. 4, December, 1963.

24. Brothers, A.J. and Yukawa, S.
FATIGUE CRACK PROPAGATION IN LOW-ALLOY HEAT-TREATED STEELS, Transactions, ASME, Journal of Basic Engineering, Paper No. 66-MET-2, 1966.

25. Clark, W. and Wessel, E., private communication to Paris, data on A302B steel.

26. Crooker, T. W. and Lange, E. A.
FATIGUE CRACK PROPAGATION IN A HIGH STRENGTH STEEL UNDER CONSTANT CYCLIC LOAD WITH VARIABLE MEAN LOADS, NRL Report 6805, Naval Research Lab., Wash., D. C., Nov. 29, 1968.

27. Rice, J. R.
MECHANICS OF CRACK TIP DEFORMATION AND EXTENSION BY FATIGUE, Fatigue Crack Propagation, ASTM STP 415, ASTM, 1967, p. 247.

28. Johnston, H. H. and Willner, A. M.
MOISTURE AND STABLE CRACK GROWTH IN A HIGH STRENGTH STEEL, Appl. Mater, Res. 4 (No. 1): 34, Jan., 1965.

29. Krafft, J. M.
DYNAMIC MECHANICAL BEHAVIOR OF METAL AT THE TIP OF A PLANE STRAIN CRACK, Southwest Research Institute Symposium on the Mechanical Behavior of Materials under Dynamic Loads, San Antonio, Texas, Sept. 6, 1967.

30. Gross, B. and Srawley, J. E.
STRESS-INTENSITY FACTORS FOR THREE-POINT BEND SPECIMENS BY BOUNDARY COLLOCATIONS, Technical Note D3092, NASA, Dec., 1965.

31. Brown, H., Jr., and Srawley, J. E.
PLANE STRAIN CRACK TOUGHNESS TESTING OF HIGH STRENGTH METALLIC MATERIALS, ASTM Spec. Tech. Publ, No. 410.

32. Nash, G.E.
AN ANALYSIS OF THE FORCES AND BENDING MOMENTS GENERATED DURING THE NRL DYNAMIC TEAR TEST, NRL Report 6864, Naval Research Lab., Wash., D. C., Jan. 30, 1969.

33. Goldsmith, W.
IMPACT, THE THEORY AND PHYSICAL BEHAVIOR OF COLLIDING SOLIDS, Edward Arnold Ltd., London, 1960.

34. Gurlin, M. E.
VARIATIONAL PRINCIPLES FOR LINEAR ELASTODYNAMICS, Archive for Rational Mechanics and Analysis, Vol. 16, 1964.

35. Highway Research Board of the NAS-NRC Division of Engineering and Industrial Research, the AASHO Road Test, Report 4, Bridge Research, Special Report CID, Publication No. 953, National Academy of Science - National Research Council, Washington, D. C., 1962.

36. Eiber, R. J. and McClure, G. M.
LABORATORY FRACTURE TESTS - THEIR RELATION TO FULL-SCALE PROPERTIES, Oil & Gas Journal, September 23, 1963.

37. Puzak, P. P. and Pellini, W. S.
STANDARD METHOD FOR NRL DROP-WEIGHT TEST, NRL Report 5831, Naval Research Laboratory, Washington, D. C., August, 1962.

38. Crosley, P. B. and Ripling, E. J.
DYNAMIC FRACTURE TOUGHNESS OF A533 STEEL, ASME Journal of Basic Engineering, presented at the AWS-ASME Metals Engineering Conference, Chicago, Illinois, April 1-5, 1968.

39. Shoemaker, A. K. and Rolfe, S. T.
STATIC AND DYNAMIC LOW TEMPERATURE K_{Ic} BEHAVIOR OF STEELS, (forthcoming in Journal of Basic Engineering with Reference 38).

40. Jackson, L. R.
WORK HARDENING AND RUPTURE IN METALS, Transactions, Institute of Metals Division of the AIME, Vol. 171, 1947.

41. Krafft, J. M.
A RATE "SPECTRUM" OF STRAIN HARDENABILITY AND OF FRACTURE TOUGHNESS, Report of NRL Progress, January, 1966.

42. Ripling, E. J., private communication.

43. Linger, D. A. and Hulsbos, C. L.
DYNAMICS OF HIGHWAY BRIDGES, The Iowa Engineering Experiment Station, Bulletin No. 188, November, 1960.

44. Macias Rendon, M. A.
A STRUCTURAL MODEL STUDY OF LEAD DISTRIBUTION IN BOX-BEAM BRIDGES, Ph. D. Dissertation, Lehigh University, 1968.

45. Mattock, A. H. and Kaar, P. H.
PRECAST-PRESTRESSED CONCRETE BRIDGES - Part 6: TESTS OF HALF-SCALE HIGHWAY BRIDGE CONTINUOUS OVER TWO SPANS, Journal of the PCA Research and Development Lab., September 1961, Vol. 3, No. 3, Appendix I, "Guyon-Massonnet Load Distribution Theory".

46. Macias Rendon, M. A., private communication.

47. Biggs, J. M. and Suer, H. S.
THE VIBRATION OF SIMPLE SPAN HIGHWAY BRIDGES, Journal of the Structural Division, Proceedings of the ASEC, ST2, March, 1957.

48. Wen, R. K. and Veletson, A. S.
BEHAVIOR OF SIMPLE-SPAN HIGHWAY BRIDGES, HRB Bulletin 315, NAS-NRC, 1962.

49. AASHO Standard Specifications for Highway Bridges, 1965.

50. Rao, N. R. Nagaraja, Estuar, F. R. and Tall, L. RESIDUAL STRESSES IN WELDED SHAPES, Fritz Engineering Laboratory Report No. 249.18, Lehigh University, 1963.